Title

Development of Polymeric Materials for the Stabilization and Delivery of Biological Therapeutics

Author

Yang, Jane

Publication Date

2023

Peer reviewed|Thesis/dissertation

UNIVERSITY OF CALIFORNIA

Los Angeles

Development of Polymeric Materials for the Stabilization and Delivery of Biological Therapeutics

A dissertation submitted in partial satisfaction of the requirements for the degree Doctor of Philosophy in Chemistry

by

Jane Yang

2023

ABSTRACT OF THE DISSERTATION

Development of Polymeric Materials for the Stabilization
and Delivery of Biological Therapeutics

by

Jane Yang
Doctor of Philosophy in Chemistry
University of California, Los Angeles, 2023
Professor Heather D. Maynard, Chair

Peptide and protein therapeutics are highly effective for the treatment and management of numerous diseases. Despite this, their clinical potential is underutilized mainly due to drawbacks inherent to many native proteins such as poor stability, immunogenicity, and short pharmacokinetics. These issues cause a multitude of challenges in manufacturing, formulation, transportation, and administration. Ideally, peptide and protein therapeutics are shelf stable and are able to be administered in its native state through a minimally invasive method. My research focuses on 1) the exploration of different polymeric models in response to various stimuli to elucidate mechanisms behind certain drug delivery vehicles, 2) the sustained release of therapeutic peptide glucagon through a glucose-responsive hydrogel for the prevention of hypoglycemia, 3) the site-selective conjugation of a degradable, zwitterionic polymer to a model protein, and 4) the investigation of how polymer tacticity affects biological function through the conjugation of regio-

and sequence-defined macromolecules to a model protein. Chapter 1 discusses three different strategies

Stimuli-responsive nanoparticles, particularly those that respond to two different environmental cues, are useful materials in drug delivery. In chapter 2, the size-response of nanogels based on two different polymers, poly(N-isopropylacrylamide) p(NIPAM) and poly(oligo(ethylene glycol) methyl ether methacrylate) (PEGMA), to temperature and glucose concentration changes was investigated. The nanogels were prepared by precipitation polymerization, 114 nm and 169 nm for pNIPAM and PEGMA at 37 °C, respectively, and characterized by proton nuclear magnetic resonance and infrared spectroscopies. Both nanogels underwent a volume phase transition in biologically relevant ranges upon heating. Incorporation of 2-aminophenylboronic acid enabled glucose-binding, resulting in a shift of the volume phase transition temperature (VPTT) of both nanogels as assessed by differential scanning calorimetry (DSC) and turbidity measurements. P(NIPAM) nanogel demonstrated a predictable decrease in size in response to both increase of temperature and glucose. PEGMA nanogel showed a predictable decrease in size to increasing temperature and but exhibited a surprising increase then decease in size to increasing concentrations of glucose.

Glucagon is a peptide hormone used in the treatment of hypoglycemia. Unlike its counterpart insulin, glucagon has only started garnering interest in the past few decades. While recent advances have introduced user friendly formulations for glucagon administration, there remain no glucagon formulations on the market intended for combating nocturnal hypoglycemia. Chapter 3 details the sustained release of native glucagon using a glucose- and thermo-responsive

hydrogel. RAFT polymerization was used to create PEG-*b*-p(NIPAM-*co*-2-APBA) polymers which were subsequently crosslinked using glucose. Polymer size, PEG length, boronic acid incorporation, and polymer wt % were varied to optimize hydrogel sensitivity to 1 mg/mL glucose at 37 ºC, which correspond to normoglycemia. Glucagon release was tested over 48 hours in which the hydrogel released up to 80% of the payload, 40% more than its control. Rheological measurements demonstrate the shear-thinning property of the hydrogel. Finally, viscosity measurements in conjunction with injectability calculations show that the hydrogel can be formulated as an injectable.

Chapter 4 describes the exploration of a degradable zwitterionic polymer as a PEG-alternative. Zwitterionic polymers have gained rising interest for their ability to stabilize proteins, increase circulation time, and retain bioactivity. While polyethylene glycol (PEG) still exists as the gold standard polymer used to mitigate challenges associated with native proteins, there are merits to investigating alternative polymers for this purpose. In this work, we report the site-selective conjugation of degradable zwitterionic poly(caprolactone-carboxybetaine) (pCLZ) to growth hormone receptor antagonist (GHA) B2036-alkyne and study bioactivity, pharmacokinetics, and immunogenicity. Azide-containing pCLZs of 5, 20, and 60 kDa are conjugated to GHA B2036-Alkyne *via* copper-catalyzed click reaction and their *in vitro* bioactivity is compared to PEGylated GHA B2036 5, 10, and 20 kDa, of matching hydrodynamic radii. The ability of pCLZs to elicit IgG and IgM antibody production was tested *in vivo* and no measurable antibody production was detected. Herein, we report that pCLZs demonstrate a high retention of bioactivity, as measured by half-maximal inhibitory concentrations *in vitro*, as well as low immunogenicity *in vivo*. Using ^{18}F labeled PET/CT imaging, pharmacokinetics of our pCLZ

conjugates show a significant increase in circulation time by 23 min compared to that of GHA B2036.

Finally, in chapter five, a series of uniform, stereospecific protein-polymer conjugates were synthesized through copper-mediated click chemistry. Discrete, uniform polymers were provided by Wencong Wang from Prof. Jeremiah Johnson's lab at the Massachusetts Institute of Technology. The impact of molecular features of the conjugated polymers were evaluated through activity studies of growth hormone antagonist. Preliminary attempts at crystallizing the protein, polymer, and protein-polymer conjugates are demonstrated. Crystallization screening and crystallography model fitting was done largely with help from Genesis Falcon, Niko Vlahakis, and Dr. Michael Sawaya.

Chapter 2 is in preparation for publication as: Yang, J.; Messina, K.M.M.; Vinciguerra, D.; Maynard, H.D. "A Comparative Study of Dual Thermo- and Glucose- Responsive Nanogel Systems and Their Response to Stimuli." *In preparation*. Chapter 3 is in preparation for publication as: Yang, J.; Vinciguerra, D.; Messina, K.M.M.; Lower, H.C.; Maynard, H.D. "Sustained Release of Glucagon from an Injectable Glucose- and Thermo- responsive Hydrogel." *In preparation*. Chapter 4 is in preparation for publication as: Yang, J.; Gelb, M.B.; Tamshen, K.; Forsythe, N.L.; Puente, E.G.; Pelegri-O'Day, E.; Jamieson, S.M.F.; Perry, J.K.; Maynard, H.D. "Site-selective conjugation of degradable zwitterionic poly(caprolactone-carboxybetaine) to growth hormone receptor antagonist B2036." *In preparation.* Chapter 5 is in preparation for publication as: Yang, J.; Wang, W.; Perry, J.K.; Maynard, H.D.; Johnson, J. "Uniform polymer-protein conjugates for evaluating the impact of molecular features of conjugated polymers on the activities of growth hormone antagonist." *In preparation.*

The dissertation of Jane Yang is approved.

Timothy J. Deming

Richard B. Kaner

Ximin He

Heather D. Maynard, Committee Chair

University of California, Los Angeles

2023

This dissertation is dedicated to my husband Hanmin

and my two dogs Toby and Stella.

TABLE OF CONTENTS

LIST OF FIGURES

LIST OF TABLES

LIST OF SCHEMES

LIST OF ABBREVIATIONS

AA, Ascorbic Acid

AIBN, Azobisisobutyronitrile

2-APBA, 2-aminophenylboronic Acid

APS, Ammonium Persulfate

BCA, Bicinchoninic Acid

BTTAA, 2-(4-((Bis((1-(tert-butyl)-1H-1,2,3-triazol-4-yl)methyl)amino)methyl)-1H1,2,3-triazol 1-yl)acetic acid

CTA, Chain-Transfer Agent

CuAAC, Copper-Catalyzed Azide-Alkyne Cycloaddition

DCC, N,N-dicyclohexylcarbodiimide

DLS, Dynamic Light Scattering

DCM, Dichloromethane

DMAP, 4-dimethylaminopyridine

DMF, N,N-dimethylformamide

DMSO, Dimethyl Sulfoxide

DPBS, Dulbecco's Phosphate-buffered Saline

DSC, Differential Scanning Calorimetry

E. coli, Escherichia Coli

EtOAc, Ethyl Acetate

EDC, 1-Ethyl-3-(3-dimethylaminopropyl)carbodiimide

ELISA, Enzyme-Linked Immunosorbent Assay

FBS, Fetal Bovine Serum

FDA, Food and Drug Administration

FPLC, Fast Protein Liquid Chromatography

FT-IR, Fourier Transform Infrared Spectroscopy

GH, Growth Hormone

GHR, Growth Hormone Receptor

GPC, Gel Permeation Chromatography

HPLC, High Performance Liquid Chromatography

IEG, Iterative Exponential Growth

I.P., Intraperitoneal

IPTG, Isopropyl-β-D-thiogalactopyranoside

I.V., Intravenous

LC-MS, Liquid Chromatography Mass Spectrometry

LCST, Lower Critical Solution Temperature

MALDI-ToF, Matrix Assisted Laser Desorption/Ionization Time-of-Flight

mPEG methoxy-poly(ethylene glycol)

Native PAGE, Native Polyacrylamide Gel Electrophoresis

Ni-NTA, Nickel-Nitrilotriacetic Acid

NHS, N-hydroxysuccinimide

NIPAM, N-isopropyl Acrylamide

NMR, Nuclear Magnetic Resonance

OEGA, Oligo(ethylene glycol) Acrylate

OEGMA, Oligo(ethylene glycol) Methacrylate

OVA, Ovalbumin

PK, Pharmacokinetics

PBS, Phosphate Buffered Saline

PEG, Poly(ethylene glycol)

PCB, Poly(carboxybetaine)

PEGMA, Poly(ethylene glycol) Methacrylate

Phe, Phenylalanine

QTOF, Quadrupole-Time-of-Flight

RAFT, Reversible Addition-Fragmentation Chain-Transfer

SDS-PAGE, Sodium Dodecyl Sulfate PolyAcrylamide Gel Electrophoresis

SEC, Size Exclusion Chromatography

UV, Ultraviolet

TEA, Triethylamine

TEM, Transmission Electron Microscopy

TEV, Tobacco Etch Virus

TFA, Trifluoroacetic Acid

THF, Tetrahydrofuran

TLC, Thin-layer Chromatography

UAA, Unnatural Amino Acid

Acknowledgements

It really does take a village. The mentors that have inspired and influenced me to pursue an advanced degree, Frank Tsung and Jacob Hooker - thank you for your invaluable mentorship and opportunities that have brought me to UCLA.

At UCLA, I've had the pleasure of meeting many great scientists and personalities that have helped me improve both as a scientist and as a human. I would particularly like to thank Kathryn Messina, Daniele Vinciguerra, Kyle Tamshen, and Douglas Rose for their guidance and encouragement I relied on heavily as a young scientist. I would also like to thank my co-authors and collaborators Madeline Gelb and Wencong Wang for two key chapters of my thesis. I am also extremely grateful to Priera Panescu, Ellie Puente, and Haillie Lower for listening to me drone on about my trials and tribulations. I thank the remaining members of the Maynard lab, past and present, for watching me with empathy as I tried my best to wrestle with the problems of my professional and personal life throughout this journey. And of course, I thank my advisor, Heather Maynard, for allowing me the space and freedom to grow as a scientist in her lab. Some particularly outstanding staff members I'd like to thank are Mark Arbing, Genesis Falcon, and Ricky Ruiz for helping me reach the finish line.

Vita

Education:

University of California, Los Angeles, Department of Chemistry, Los Angeles, CA

Ph. D. in Chemistry, Expected Fall 2022

MS in Chemistry, June 2020

Boston College, Chestnut Hill, MA

Bachelor of Science in Chemistry, May 2016

Publications (*Denotes equal contribution):

1. Yang, J. *****; Messina, K.M. *****; Vinciguerra, D; Maynard, H.D. "Choice of Polymer in Dual Thermo- and Glucose- Responsive Nanogel Affects Response to Stimuli." In Preparation
2. Yang, J. *****; Vinciguerra, D. *****; Messina, K.M.; Maynard, H.D. "Glucose- and Thermoresponsive- Hydrogel for Sustained Glucagon Release for the Management of Type 1 Diabetes." In Preparation
3. Vinciguerra, D.**;** Yang, J.; Messina, K.M.; Hevener, A.; Maynard, H.D. "micelle paper" In Preparation
4. Yang, J; Gelb, M.B.; Tamshen, K.; Forsythe, N.L.; Pelegri-O'Day, E.; Jamieson, S.M.F.; Perry, J.K.; Maynard, H.D. "Degradable Poly(caprolactone-carboxybetaine) Site-Selectively Conjugated to Growth Hormone Receptor Antagonist." In Preparation
5. Yang, J. *****; Wang, W. *****; Perry, J.K.; Maynard, H.D.; Johnson, J. "Stereo- and Sequence-Defined, Unimolecular macromolecules Site-Selectively Conjugated to Growth Hormone Antagonist." In Preparation
6. Williams BP, Young AP, Andoni I, Han Y, Lo WS, Golden M, Yang J, Lyu LM, Kuo CH, Evans JW, Huang W, Tsung CK. Strain-Enhanced Metallic Intermixing in Shape-

Controlled Multilayered Core–Shell Nanostructures: Toward Shaped Intermetallics. *Angew Chem Int Ed*. 2020;59(26):10574-10580. doi:10.1002/anie.202001067

7. Strebl MG, Yang J, Isaacs L, Hooker JM. Adamantane/Cucurbituril: A Potential Pretargeted Imaging Strategy in Immuno-PET. *Molecular Imaging*. January 2018. doi:10.1177/1536012118799838

Presentations

1. Site-Selective Conjugation of Degradable Zwitterionic Poly(caprolactone-carboxybetaine) to Growth Hormone Receptor Antagonist. UCLA Glenn T. Seaborg Symposium, Los Angeles, California, August 2022
2. Boston College Undergraduate Research Symposium, Chestnut Hill, Massachusetts, April 2016

Service and Leadership

Organization for Cultural Diversity in Sciences at UCLA

Internal Coordinator 2021-2022

Professional Development Chair 2020-2021

California NanoSystems Institute Outreach at UCLA

Member 2018-2020

Chapter 1

Polymer-mediated Delivery of Peptide and Protein Therapeutics

1.1 Introduction

Proteins and peptides are a class of therapeutic agents that are used to relieve symptoms of and treat numerous diseases. Unlike small molecule therapeutics, proteins and peptides have higher target specificity and fewer off-target effects. Though this is an immense advantage, native proteins and peptides do suffer from their own set of disadvantages including instability during transportation and storage, short *in vivo* half-lives, and cell limited permeability.[1–4] Addressing the stability of biological therapeutics during transportation and storage is important for cost-reducing measures that ultimately ease patient financial burden and environmental pollution. Having shelf stable formulations can reduce the need for cold chain transport and storage, which would also allow for more therapeutics to be available in wider geographic regions across the world. Secondly, extending the half-life of a biological therapeutic can increase the overall utility of a drug. Oftentimes, for a protein or peptide to produce its desired effect, it needs to bypass different physiological barriers safely and stably in the body such as the acidic stomach lining, tight junctions in the blood brain barrier, or more generally cell membranes. Proteins in their native form may not possess these abilities but that can be overcome by altering the lipophilicity, polar surface area, or the number of rotatable bonds. Broadly speaking, these challenges can often be ameliorated using excipients and drug delivery vesicles.

To mitigate these aforementioned challenges, various strategies have been developed. Researchers have explored numerous drug delivery models ranging from entirely inorganic nanoparticles to hybrid inorganic and organic frameworks to autologous vesicles.[5–9] Polymers are attractive materials because their physical and chemical properties can easily be tuned by varying the size and monomer composition. The downside to this versatility is that these polymers often need to be uniquely tailored for each individual application. This chapter will focus on

polymer-based delivery strategies with a particular emphasis on protein-polymer conjugates, nanogels, and hydrogels.

Regardless of delivery system and mechanism, important parameters to evaluate and tailor are encapsulation or conjugation efficiency, rate of drug release, and fate of delivery system upon administration. While proof-of-concept experiments undoubtedly advance the overall field, many reported delivery systems are not practically feasible due to manufacturing costs. One main component that can greatly affect this is the efficiency at which the drug is encapsulated or conjugated. Methods requiring large excess of protein have low yields and poor scalability that increase manufacturing costs. Next, the rate of drug release needs to match the physiological dose and timeline at which maximal therapeutic benefits are observed. For example, in the case of severe hypoglycemia a high bolus of therapeutic peptide glucagon is desired to offset the potentially fatal symptoms as fast as possible. However, in the case of nocturnal hypoglycemia, a sustained release of glucagon would be most desirable to prevent blood glucose levels from gradually falling below target ranges due to factors such as time of last meal, higher amounts of basal insulin, or changes in exercise routine. The last parameter that will be discussed here is the fate of delivery system after administration. Depending on the size and/or charge of the carrier, the system can be immediately cleared from the body by the macrophages before releasing its payload. Cationic nanoparticles are generally accepted to be more cytotoxic and inflammatory than neutral or anionic nanoparticles.[10–12] In addition, polymers above 40 kDa and nanoparticles above 200 nm in diameter have been shown to activate the lymphatic system and are removed from circulation quicker.[13–16] After the initial response and pathway, clearance of these foreign carriers is important to evaluate. Accumulation within organs is undesirable, and furthermore, accumulation in environmental waste systems should receive more attention.

Of the many polymers incorporated into therapeutics, PEG has the longest clinical track record with more than 22 FDA-approved PEG-protein conjugates on the market. As expected with a gold standard polymer, PEG and PEGylation have demonstrated increased pharmacokinetics, improved storage stability, reduced renal clearance, and/or blocking of antibody and protein binding sites depending on the particular formulation. PEG is an amphiphilic polymer that imparts these aforementioned benefits upon conjugation by increasing the hydrodynamic radius of the conjugated protein, as well as sterically shielding the protein through the immune system. Despite the broad utility of PEG and PEGylation, there has been an increased importance in discovering and studying PEG-alternatives due to reported shortcomings regarding accumulation and immuogenicity.[17–19] The overall toxicity of PEG is reported to be low, however, chronic dosing of high molecular weight PEGylated biologics has been associated with vacuolation and degeneration of renal tubular epithelial cells.[20] Accumulation of large PEG molecules (>20-30 kDa) *in vivo* with long-term exposure is a potential concern,[21–24] but regardless of PEG size, biodegradability is necessary for materials entering environmental or wastewater systems.[25] To that point, PEGs are unfortunately not degradable under physiologically or environmentally friendly conditions.[26] Furthermore, patients with pre-existing antibodies against PEG can show allergic responses to some PEGylated medicines. The greater concern here is that many individuals, naïve to PEGylated therapeutics, can have pre-existing PEG antibodies in their circulation most likely due to casual exposure through cosmetic and healthcare products.[18] While PEGs are generally regarded as safe by the United States Food and Drug Administration (FDA), the FDA updated their guidelines and implemented in 2014 a screen for anti-PEG antibodies during clinical trials of PEGylated therapeutics. For at least these reasons, PEG-alternatives are an important area of research to mediate the non-degradability and immunogenicity of PEG. There are many misconceptions

concerning the immunogenic path and nature of PEG but the bottom line is that the administration of some PEGylated drugs has resulted in anti-PEG antibodies which reduced treatment efficacy or caused adverse drug reactions.[17,20,21,23,27,28]

Many different classes of polymers have been used as PEG-alternatives in protein-polymer conjugates.[17,19,29] Our group has long been interested in studying alternative polymers to PEG both for improving the stabilization of therapeutic proteins and improving drug efficacy through prolonging blood circulation time. PEG alternatives that have been reported in literature include synthetic polymers such as poly(oxazolines) and poly(acrylamides), natural polymers such as lipids and carbohydrates, and zwitterionic polymers such as poly(carboxybetaine) and poly(sulfobetaine), among others.[19,30–33] Polyzwitterions are an interesting class of polymers. They have a net neutral charge and have been demonstrated to stabilize proteins through their ionic structuring of water. An advantage of polyzwitterions versus PEG is that in some cases, conjugation of polyzwitterions has shown to increase the binding affinity towards the receptor.[32]

1.2 Protein-Polymer Conjugates

Covalent conjugation of a polymer to a protein is a commonly used method to stabilize and deliver proteins.[32,34–36] One major disadvantage of covalent conjugation of polymer to protein is the direct chemical modification of the biomolecule and possible downstream effects stemming from it. The conjugation site on the protein needs to be carefully chosen to mitigate loss in bioactivity as well as other important parameters including solubility and stability. For example, residues that interact with the receptor should not be chosen as the conjugation site as it can directly affect bioactivity. In addition, there needs to be careful selection of the conjugation chemistry that is used to attach the polymer since, depending on the chemistry, it could require conditions that may cause protein instability. Relevant methods and techniques to prepare and characterize

protein-polymer conjugates are controlled polymerizations, bioorthogonal chemistry, size exclusion chromatography, gel electrophoresis, and fast protein liquid chromatography.

The three different methods to creating protein-polymer conjugates are listed in order of most to least utilized: grafting to, grafting from, and grafting through. In the grafting to strategy, the polymer is pre-formed and subsequently covalently conjugated to a protein. This strategy receives the most use because it introduces the protein at the last step which limits exposure to potentially harsh conditions. In addition, this strategy can take advantage of the numerous conjugation chemistries introduced by the rapidly growing field of bioorthogonal chemistry. The downsides to the grafting to approach are that with most conjugation chemistries, it requires a large molar excess of the polymer which can introduce issues for product scale up, as well as subsequent purification of the excess polymer. Next, the grafting from technique entails installing a polymerization initiation handle directly onto the protein and using the protein as an initiator. In contrast to the grafting to strategy, grafting from does not require the use of large molar excess of polymer. Polymerization strategies that have been utilized in this context are ATRP, RAFT, and ROMP.[37–39] Finally, the grafting through method requires installing a polymerizable unit, such as an acrylate, directly onto the protein and copolymerizing the protein with the other monomers. The advantages and disadvantages of grafting through are similar to those of the grafting from technique.

In this thesis, examples of protein-polymer conjugates, nanogels, and hydrogels are demonstrated. Accordingly, an example of grafting to protein-polymer conjugates further detailed in chapter four and five, growth hormone receptor antagonist and its numerous conjugates embody a wide array of combinations and scenarios that contribute to a variety of therapeutic results.[40–46] The B2036 variant of GHA, formulated as Pegvisomant, has four to six non-specifically

conjugated 5 kDa PEG molecules to nine possible amines through NHS displacement. This nonspecific multi-PEGylation extends the circulation half life from 15 min to 74 h. This major improvement is not without its drawbacks, however. UnPEGylated B2036 demonstrates a 4.5 fold greater affinity for GH binding protein in comparison to that of Pegvisomant.[42] To overcome this loss of bioactivity, a higher molar amount of Pegvisomant needs to be administered. Expanding upon this work, an alkyne moiety was incorporated into GHA B2036 using an amber code suppression method in order to examine the effects of site-specific conjugation. Azido-mPEGs of 5, 10, and 20 kDa were site-selectively conjugated to GHA B2036-Alkyne through copper mediated click chemistry and the bioactivity loss was significantly mitigated compared to Pegvisomant.[43] Using half-maximal inhibitory concentrations as a measure of bioactivity, site-specific conjugation demonstrates 12 to 23-fold retention of bioactivity compared to Pegvisomant. In this instance, circulation time in vivo was not measured so a direct comparison of half lives is not possible. A further exploration of growth hormone receptor antagonist -polymer conjugates is detailed in chapters four and five.

1.3 Nanogels

Nanogels are crosslinked, three-dimensional gels at the nanoscale. Unlike protein-polymer conjugates, nanogels encapsulate the entire therapeutic payload in a three-dimensional structure. The main advantages of nanogels include high loading capacity and versatility in design. The outer shell can provide a protective shield for the cargo. Depending on the chemical design and strategy, the outer shell can also be functionalized with targeting agents such as cell penetrating peptides or stealth agents such as PEG. This can greatly enhance the transmembrane and intracellular delivery of protein drugs. The payload can be encapsulated either through covalent linkages that will release upon exposure to a particular stimulus or noncovalent loading followed by diffusion-based release.

Varying the crosslinking density can help tune the loading and release of the cargo. Encapsulation of biological therapeutics, however, still remains a challenge for nanogels. Important techniques for analyzing nanogels include dynamic light scattering, transmission electron microscopy, scanning electron microscopy, and small angle x-ray scattering.

A common method of synthesizing nanogels is through emulsion-based polymerization of monomers and a crosslinker in aqueous conditions.[47,48] In some cases, the protein is encapsulated during this step through a microemulsion technique that targets microparticle polymerization around the protein. Another method for creating nanogels is to covalently link polymerizable motifs onto the protein and polymerize around the protein. The key difference between the two methods above is noncovalent versus covalent encapsulation of the protein. In both cases, an external stimulus is generally used to trigger the release of the cargo. Stimuli-responsive nanomedicine has received wide attention and thus a wide variety of stimuli have been examined such as temperature, pH, light, redox, magnetic field, biomolecule recognition, and more.[49–52] In addition, nanogels can be imparted with multiple stimuli and designed to release sequentially depending on the stimulus.

When the protein is attached to the nanogel covalently, the drug is often attached through bonds that can be easily broken by a specific stimulus. For example, acid sensitive linkers, such as hydrazones, are used because the intracellular environment becomes acidic upon uptake of the carrier by endocytosis. In another example, disulfide bonds are used to covalently link the protein that can be released in the presence of glutathione, which is a reduction-responsive mechanism. Covalently bound systems have greater drug stability compared to noncovalently bound systems. Having the drug tethered to the delivery vehicle reduces the opportunity for payload leakage from formulation to site of intended payload release.

For noncovalent encapsulation, nanogel systems that can swell and shrink in response to pH and temperature are commonly used. The thermoresponsive polymer pNIPAM has a cloud point at 32 ºC and shrinks and swells at temperatures above and below its cloud point, respectively. The general delivery strategy here is that upon nanogel swelling, the pores of the nanogel expand and release the payload through diffusion. For biological applications, a solely thermoresponsive nanogel is limited in usefulness because the physiological temperature is 37 ºC with little deviation. To that point, dual pH- and thermo-responsive nanogels, as well as other iterations, are used to take advantage of the swelling and contraction from the thermoresponsive moieties and the degree of swelling and contracting determined by the pH responsive segments. Polyacrylates are commonly incorporated into these nanogels. The change in pH will cause a change in the degree of ionization which then triggers a size change of the nanogel, allowing for payload release. A dual glucose- and thermo-responsive nanogel system is explored in chapter two.

1.4 Hydrogels

Hydrogels are crosslinked networks with high water content that remain insoluble in water and maintain their three-dimensional structure. Hydrogels can be crosslinked chemically or physically and can have a wide range of properties depending on their chemical composition and crosslinking density. They are advantageous drug delivery systems because of their injectability and ability to achieve sustained release. Other administration methods include surgical implantation or systemic delivery via intravenous infusion. In addition, hydrogels are prepared in generally mild conditions which help preserve protein stability. Relevant analytical methods for hydrogels include rheology, viscosity, and atomic force microscopy.

The two main mechanisms for protein delivery from hydrogels are diffusion and surface erosion.[53–55] The polymer and protein characteristics govern which release mechanism is at play.

In the case that the protein size is smaller than the pores of the hydrogel, diffusion is the primary method of release. When the relative sizes are reversed, surface erosion will need to occur for the protein to release. The release rate of this method is limited by the rate at which the hydrogel network degrades. With the invention of novel hydrogel systems, different release mechanisms are expected to be observed. In order to bias the release mechanism towards one method, the crosslinking density, which influences the hydrogel pore size, is the most logical parameter to modify. Similarly, tuning the network degradation rate and erosion mechanism will be important for achieving the desired release profile.

One method of hydrogel preparation is directly polymerizing monomers and crosslinkers to create a 3-D network, similar to nanogels.[54,56,57] Hydrophilic monomers are typically used along with an initiator and crosslinker. The protein or peptide of interest is also added at this step for drug delivery applications. In this method of hydrogel preparation, the hydrogel formation can be seen macroscopically. Upon termination, the hydrogel should be washed to remove unreacted reagents. Another method of hydrogel preparation is the polymerization of the linear polymer followed by a subsequent step of crosslinking. The crosslinking can be permanent covalent junctions or transient junctions that can break based on ionic interactions, hydrogen bonds, hydrophobic interactions, or other external interactions. This method can be advantageous when precisely synthesized polymers are needed to impart the desired functionality on the hydrogel. Precisely synthesized polymers can include properties hard to achieve in a one-step reaction such as side-chain functionalities, reactive handles, and monodispersity. The protein or peptide of interest is added at the step of crosslinking, which may reduce the exposure of the biologic to harsh chemical conditions.

Though significant progress has been made towards the discovery of hydrogels, some challenges remain. Unwanted release at inopportune times is a key shortcoming that needs to be overcome. Burst release is an initial payload release that is often attributed to the rate of gelation of the hydrogel. Particularly for injectable hydrogels, the sol-gel transition upon administration needs to be at a sufficiently high rate to minimize undesirable initial payload release. If the sol-gel transition is slower than desired, the therapeutic remains as a solution longer, which widens the window for premature leakage of protein into the surrounding tissue. Burst release is also possible.

1.5 Conclusions and Future Perspectives

Selection of the desired stimuli must be carefully decided as this will often limit the possible chemical reactions that can be used to create a delivery vehicle. For this reason, it is recommended to add the biological drug of interest at the last step possible in the formulation. While nanogels are clearly an innovative approach, more development is needed in some cases to achieve uniform particle sizes, because a wider dispersity can cause larger variations in the distribution of the nanogels in the body along with interaction with biological cells. Particle Replication in Non-Wetting Templates (PRINT) nanoparticles is a uniform nanoparticle fabrication technology that has the potential to overcome limitations from polydispersity. Nanogel morphology is another parameter to study and modify.[58] Some reports have shown ellipsoid or disc-shaped particles have demonstrated weaker phagocytosis compared to spherical particles[59,60] and it will be important to see the morphological effects of novel nanogel systems.

For polymer-mediated drug delivery systems, a recurring concern is batch to batch reproducibility and polydispersity of the polymer.[61,62] The variation often stems from the polymerization process. These resulting variations in molecular weight, crosslinking density, and monomer distribution often cause issues in reproducing desired properties. For protein-polymer

conjugates, these concerns have been addressed through the development and use of controlled polymerizations. In addition, owing to the wide use of PEG in drug formulations, PEGs of narrow dispersities are widely available commercially. Of the delivery systems described in this chapter, nanogels, for example, can suffer from issues with batch to batch reproducibility. Nanogels commonly have three or more comonomers, making it more challenging to closely study polymerization kinetics. In addition, there is a lack of methods to monitor or elucidate the distribution of monomers within the 3-D network. However, in the case the nanogels crosslinked in a separate step from the polymerization, the batch to batch reproducibility can be improved, owing to the presence of one less monomer to track. has shown to be sufficient. This can be explained through the use of commercial polymers or controlled polymerization techniques to create the linear polymer. This way, there is already a strong basis of conformity amongst the particles. Layer-by-layer delivery systems are an example of highly reproducible nanogels.[63] Finally, hydrogels have similar batch to batch reproducibility trends as nanogels meaning if the polymeric precursors are well defined, the reproducibility is higher. The development and large-scale manufacturing of monodisperse polymers will likely be instrumental in addressing reproducibility issues.

Another concern to be addressed is the degradability of polymers used in these systems. As briefly mentioned above, PEG and other commonly used polymers are not biodegradable. In general, the chemical degradation of many synthetic polymers requires the use of harsh conditions. Natural polymers based on polypeptides and polysaccharides are a good alternative. However, their use is limited by the difficulty in preparing and modifying the existing structures to impart desired functionalities.[30] Another alternative is synthetic polymers with easily degradable functional groups within the backbone. For example, polyesters, polyanhydrides, and polyamides

are promising because they are hydrolysable under acidic or basic conditions.[64–69] While these structures definitely can be hydrolyzed, most of the conditions for degradation require strong acids or bases and/or high temperatures and can take a long time in vivo. Some literature reports argue that polythioesters are degradable under milder conditions.[70] The degradability of these polymers is a delicate situation requiring the molecules to be robust enough to withstand necessary reaction conditions, but also able to degrade with relative ease and desired timeframe. Future work expanding on truly degradable polymers will be an important area.

Of the polymeric drug delivery systems detailed in this chapter, protein-polymer conjugates are the most straightforward to synthesize and characterize. One of the biggest challenges with protein-polymer conjugates is the purification of the conjugate from unreacted protein and polymer. Nanogels and hydrogels can be simple to synthesize depending on the method, but they are difficult to thoroughly analyze and characterize the 3D network, which contributes to batch to batch irreproducibility. Nonetheless, all three delivery systems have shown high levels of promise with regards to translational nanomedicine. Synergistic collaboration amongst chemists, material scientists, biologists, and process engineers will greatly expand the clinical use of polymeric drug delivery systems for protein and peptide therapeutics.

1.6 References

(1) Onoue, S.; Ohshima, K.; Debari, K.; Koh, K.; Shioda, S.; Iwasa, S.; Kashimoto, K.; Yajima, T. Mishandling of the Therapeutic Peptide Glucagon Generates Cytotoxic Amyloidogenic Fibrils. *Pharm. Res.* **2004**, *21* (7), 1274–1283. https://doi.org/10.1023/b:pham.0000033016.36825.2c.

(2) Cleland, J. L.; Daugherty, A.; Mrsny, R. Emerging Protein Delivery Methods. *Curr. Opin. Biotechnol.* **2001**, *12* (2), 212–219. https://doi.org/10.1016/S0958-1669(00)00202-0.

(3) Leader, B.; Baca, Q. J.; Golan, D. E. Protein Therapeutics: A Summary and Pharmacological Classification. *Nat. Rev. Drug Discov.* **2008**, *7* (1), 21–39. https://doi.org/10.1038/nrd2399.

(4) Welch, R. P.; Lee, H.; Luzuriaga, M. A.; Brohlin, O. R.; Gassensmith, J. J. Protein–Polymer Delivery: Chemistry from the Cold Chain to the Clinic. *Bioconjug. Chem.* **2018**, *29* (9), 2867–2883. https://doi.org/10.1021/acs.bioconjchem.8b00483.

(5) Rizvi, S. A. A.; Saleh, A. M. Applications of Nanoparticle Systems in Drug Delivery Technology. *Saudi Pharm. J. SPJ* **2018**, *26* (1), 64–70. https://doi.org/10.1016/j.jsps.2017.10.012.

(6) Bhunia, S.; Deo, K. A.; Gaharwar, A. K. 2D Covalent Organic Frameworks for Biomedical Applications. *Adv. Funct. Mater.* **2020**, *30* (27), 2002046. https://doi.org/10.1002/adfm.202002046.

(7) Vargason, A. M.; Anselmo, A. C.; Mitragotri, S. The Evolution of Commercial Drug Delivery Technologies. *Nat. Biomed. Eng.* **2021**, *5* (9), 951–967. https://doi.org/10.1038/s41551-021-00698-w.

(8) Yun, Y. H.; Lee, B. K.; Park, K. Controlled Drug Delivery: Historical Perspective for the next Generation. *J. Control. Release Off. J. Control. Release Soc.* **2015**, *219*, 2–7. https://doi.org/10.1016/j.jconrel.2015.10.005.

(9) Liong, M.; Lu, J.; Kovochich, M.; Xia, T.; Ruehm, S. G.; Nel, A. E.; Tamanoi, F.; Zink, J. I. Multifunctional Inorganic Nanoparticles for Imaging, Targeting, and Drug Delivery. *ACS Nano* **2008**, *2* (5), 889–896. https://doi.org/10.1021/nn800072t.

(10) Cho, W.-S.; Thielbeer, F.; Duffin, R.; Johansson, E. M. V.; Megson, I. L.; MacNee, W.; Bradley, M.; Donaldson, K. Surface Functionalization Affects the Zeta Potential, Coronal

Stability and Membranolytic Activity of Polymeric Nanoparticles. *Nanotoxicology* **2014**, *8* (2), 202–211. https://doi.org/10.3109/17435390.2013.773465.

(11) Fröhlich, E. The Role of Surface Charge in Cellular Uptake and Cytotoxicity of Medical Nanoparticles. *Int. J. Nanomedicine* **2012**, *7*, 5577–5591. https://doi.org/10.2147/IJN.S36111.

(12) Weiss, M.; Fan, J.; Claudel, M.; Sonntag, T.; Didier, P.; Ronzani, C.; Lebeau, L.; Pons, F. Density of Surface Charge Is a More Predictive Factor of the Toxicity of Cationic Carbon Nanoparticles than Zeta Potential. *J. Nanobiotechnology* **2021**, *19* (1), 5. https://doi.org/10.1186/s12951-020-00747-7.

(13) Fox, M. E.; Szoka, F. C.; Fréchet, J. M. J. Soluble Polymer Carriers for the Treatment of Cancer: The Importance of Molecular Architecture. *Acc. Chem. Res.* **2009**, *42* (8), 1141–1151. https://doi.org/10.1021/ar900035f.

(14) Mitchell, M. J.; Billingsley, M. M.; Haley, R. M.; Wechsler, M. E.; Peppas, N. A.; Langer, R. Engineering Precision Nanoparticles for Drug Delivery. *Nat. Rev. Drug Discov.* **2021**, *20* (2), 101–124. https://doi.org/10.1038/s41573-020-0090-8.

(15) Peng, C.; Huang, Y.; Zheng, J. Renal Clearable Nanocarriers: Overcoming the Physiological Barriers for Precise Drug Delivery and Clearance. *J. Controlled Release* **2020**, *322*, 64–80. https://doi.org/10.1016/j.jconrel.2020.03.020.

(16) Karmali, P. P.; Simberg, D. Interactions of Nanoparticles with Plasma Proteins: Implication on Clearance and Toxicity of Drug Delivery Systems. *Expert Opin. Drug Deliv.* **2011**, *8* (3), 343–357. https://doi.org/10.1517/17425247.2011.554818.

(17) Verhoef, J. J. F.; Anchordoquy, T. J. Questioning the Use of PEGylation for Drug Delivery. *Drug Deliv. Transl. Res.* **2013**, *3* (6), 499–503.

(18) Kozma, G. T.; Shimizu, T.; Ishida, T.; Szebeni, J. Anti-PEG Antibodies: Properties, Formation, Testing and Role in Adverse Immune Reactions to PEGylated Nano-Biopharmaceuticals. *Adv. Drug Deliv. Rev.* **2020**, *154–155*, 163–175. https://doi.org/10.1016/j.addr.2020.07.024.

(19) Hoang Thi, T. T.; Pilkington, E. H.; Nguyen, D. H.; Lee, J. S.; Park, K. D.; Truong, N. P. The Importance of Poly(Ethylene Glycol) Alternatives for Overcoming PEG Immunogenicity in Drug Delivery and Bioconjugation. *Polymers* **2020**, *12* (2), 298. https://doi.org/10.3390/polym12020298.

(20) Rudmann, D. G.; Alston, J. T.; Hanson, J. C.; Heidel, S. High Molecular Weight Polyethylene Glycol Cellular Distribution and PEG-Associated Cytoplasmic Vacuolation Is Molecular Weight Dependent and Does Not Require Conjugation to Proteins. *Toxicol. Pathol.* **2013**, *41* (7), 970–983. https://doi.org/10.1177/0192623312474726.

(21) Ivens, I. A.; Achanzar, W.; Baumann, A.; Brändli-Baiocco, A.; Cavagnaro, J.; Dempster, M.; Depelchin, B. O.; Irizarry Rovira, A. R.; Dill-Morton, L.; Lane, J. H.; Reipert, B. M.; Salcedo, T.; Schweighardt, B.; Tsuruda, L. S.; Turecek, P. L.; Sims, J. PEGylated Biopharmaceuticals: Current Experience and Considerations for Nonclinical Development. *Toxicol. Pathol.* **2015**, *43* (7), 959–983. https://doi.org/10.1177/0192623315591171.

(22) Stidl, R.; Fuchs, S.; Bossard, M.; Siekmann, J.; Turecek, P. L.; Putz, M. Safety of PEGylated Recombinant Human Full-Length Coagulation Factor VIII (BAX 855) in the Overall Context of PEG and PEG Conjugates. *Haemophilia* **2016**, *22* (1), 54–64. https://doi.org/10.1111/hae.12762.

(23) Turecek, P. L.; Bossard, M. J.; Schoetens, F.; Ivens, I. A. PEGylation of Biopharmaceuticals: A Review of Chemistry and Nonclinical Safety Information of

Approved Drugs. *J. Pharm. Sci.* **2016**, *105* (2), 460–475. https://doi.org/10.1016/j.xphs.2015.11.015.

(24) Fang, J.-L.; Vanlandingham, M. M.; Beland, F. A.; Felton, R. P.; Maisha, M. P.; Olson, G. R.; Patton, R. E.; Rosenberg, A. S.; Gamboa da Costa, G. Toxicity of High-Molecular-Weight Polyethylene Glycols in Sprague Dawley Rats. *Toxicol. Lett.* **2022**, *359*, 22–30. https://doi.org/10.1016/j.toxlet.2022.01.011.

(25) Kawai, F. Biodegradation of Polyethers (Polyethylene Glycol, Polypropylene Glycol, Polytetramethylene Glycol, and Others). In *Biopolymers Online*; John Wiley & Sons, Ltd, 2005. https://doi.org/10.1002/3527600035.bpol9012.

(26) Giroto, J. A.; Teixeira, A. C. S. C.; Nascimento, C. A. O.; Guardani, R. Degradation of Poly(Ethylene Glycol) in Aqueous Solution by Photo-Fenton and H2O2/UV Processes. *Ind. Eng. Chem. Res.* **2010**, *49* (7), 3200–3206. https://doi.org/10.1021/ie9015792.

(27) Hershfield, M. S.; Ganson, N. J.; Kelly, S. J.; Scarlett, E. L.; Jaggers, D. A.; Sundy, J. S. Induced and Pre-Existing Anti-Polyethylene Glycol Antibody in a Trial of Every 3-Week Dosing of Pegloticase for Refractory Gout, Including in Organ Transplant Recipients. *Arthritis Res. Ther.* **2014**, *16* (2), R63. https://doi.org/10.1186/ar4500.

(28) Kozma, G. T.; Shimizu, T.; Ishida, T.; Szebeni, J. Anti-PEG Antibodies: Properties, Formation, Testing and Role in Adverse Immune Reactions to PEGylated Nano-Biopharmaceuticals. *Adv. Drug Deliv. Rev.* **2020**, *154–155*, 163–175. https://doi.org/10.1016/j.addr.2020.07.024.

(29) Qi, Y.; Chilkoti, A. Protein–Polymer Conjugation—Moving beyond PEGylation. *Curr. Opin. Chem. Biol.* **2015**, *28*, 181–193. https://doi.org/10.1016/j.cbpa.2015.08.009.

(30) Vinciguerra, D.; Gelb, M. B.; Maynard, H. D. Synthesis and Application of Trehalose Materials. *JACS Au* **2022**. https://doi.org/10.1021/jacsau.2c00309.

(31) Han, Y.; Yuan, Z.; Zhang, P.; Jiang, S. Zwitterlation Mitigates Protein Bioactivity Loss in Vitro over PEGylation. *Chem. Sci.* **2018**, *9* (45), 8561–8566. https://doi.org/10.1039/C8SC01777H.

(32) Keefe, A. J.; Jiang, S. Poly(Zwitterionic)Protein Conjugates Offer Increased Stability without Sacrificing Binding Affinity or Bioactivity. *Nat. Chem.* **2012**, *4* (1), 59–63. https://doi.org/10.1038/nchem.1213.

(33) Shao, Q.; Jiang, S. Molecular Understanding and Design of Zwitterionic Materials. *Adv. Mater.* **2015**, *27* (1), 15–26. https://doi.org/10.1002/adma.201404059.

(34) Alconcel, S. N. S.; Baas, A. S.; Maynard, H. D. FDA-Approved Poly(Ethylene Glycol)–Protein Conjugate Drugs. *Polym. Chem.* **2011**, *2* (7), 1442–1448. https://doi.org/10.1039/C1PY00034A.

(35) Hoon Ko, J.; D. Maynard, H. A Guide to Maximizing the Therapeutic Potential of Protein–Polymer Conjugates by Rational Design. *Chem. Soc. Rev.* **2018**, *47* (24), 8998–9014. https://doi.org/10.1039/C8CS00606G.

(36) Liu, X.; Gao, W. Precision Conjugation: An Emerging Tool for Generating Protein–Polymer Conjugates. *Angew. Chem. Int. Ed.* **2021**, *60* (20), 11024–11035. https://doi.org/10.1002/anie.202003708.

(37) E. Averick, S.; D. Magenau, A. J.; Simakova, A.; F. Woodman, B.; Seong, A.; A. Mehl, R.; Matyjaszewski, K. Covalently Incorporated Protein –Nanogels Using AGET ATRP in an Inverse Miniemulsion. *Polym. Chem.* **2011**, *2* (7), 1476–1478. https://doi.org/10.1039/C1PY00050K.

(38) C. Church, D.; Takiguchi, L.; K. Pokorski, J. Optimization of Ring-Opening Metathesis Polymerization (ROMP) under Physiologically Relevant Conditions. *Polym. Chem.* **2020**, *11* (27), 4492–4499. https://doi.org/10.1039/D0PY00716A.

(39) Huang, Y.; Li, X.; Zhang, Y. C.; Shi, Z.; Zeng, L.; Xie, J.; Du, Y.; Lu, D.; Hu, Z.; Cai, T.; Luo, Z. Aqueous Protein–Polymer Bioconjugation via Photoinduced RAFT Polymerization Using High Loading Heterogeneous Catalyst. *ACS Appl. Mater. Interfaces* **2021**, *13* (37), 44488–44496. https://doi.org/10.1021/acsami.1c13770.

(40) Pradhananga, S.; Wilkinson, I.; Ross, R. J. M. Pegvisomant: Structure and Function. *J. Mol. Endocrinol.* **2002**, *29* (1), 11–14. https://doi.org/10.1677/jme.0.0290011.

(41) Divisova, J.; Kuiatse, I.; Lazard, Z.; Weiss, H.; Vreeland, F.; Hadsell, D. L.; Schiff, R.; Osborne, C. K.; Lee, A. V. The Growth Hormone Receptor Antagonist Pegvisomant Blocks Both Mammary Gland Development and MCF-7 Breast Cancer Xenograft Growth. *Breast Cancer Res. Treat.* **2006**, *98* (3), 315–327. https://doi.org/10.1007/s10549-006-9168-1.

(42) Ross, R. J.; Leung, K. C.; Maamra, M.; Bennett, W.; Doyle, N.; Waters, M. J.; Ho, K. K. Binding and Functional Studies with the Growth Hormone Receptor Antagonist, B2036-PEG (Pegvisomant), Reveal Effects of Pegylation and Evidence That It Binds to a Receptor Dimer. *J. Clin. Endocrinol. Metab.* **2001**, *86* (4), 1716–1723. https://doi.org/10.1210/jcem.86.4.7403.

(43) Tamshen, K.; Wang, Y.; Jamieson, S. M. F.; Perry, J. K.; Maynard, H. D. Genetic Code Expansion Enables Site-Specific PEGylation of a Human Growth Hormone Receptor Antagonist through Click Chemistry. *Bioconjug. Chem.* **2020**, *31* (9), 2179–2190. https://doi.org/10.1021/acs.bioconjchem.0c00365.

(44) Wang, Y.; Langley, R. J.; Tamshen, K.; Jamieson, S. M.; Lu, M.; Maynard, H. D.; Perry, J. K. Long-Acting Human Growth Hormone Receptor Antagonists Produced in E. Coli and Conjugated with Polyethylene Glycol. *Bioconjug. Chem.* **2020**, *31* (6), 1651–1660. https://doi.org/10.1021/acs.bioconjchem.0c00208.

(45) Cho, H.; Daniel, T.; Buechler, Y. J.; Litzinger, D. C.; Maio, Z.; Putnam, A.-M. H.; Kraynov, V. S.; Sim, B.-C.; Bussell, S.; Javahishvili, T.; Kaphle, S.; Viramontes, G.; Ong, M.; Chu, S.; GC, B.; Lieu, R.; Knudsen, N.; Castiglioni, P.; Norman, T. C.; Axelrod, D. W.; Hoffman, A. R.; Schultz, P. G.; DiMarchi, R. D.; Kimmel, B. E. Optimized Clinical Performance of Growth Hormone with an Expanded Genetic Code. *Proc. Natl. Acad. Sci.* **2011**, *108* (22), 9060–9065. https://doi.org/10.1073/pnas.1100387108.

(46) Kopchick, J. J.; Parkinson, C.; Stevens, E. C.; Trainer, P. J. Growth Hormone Receptor Antagonists: Discovery, Development, and Use in Patients with Acromegaly. *Endocr. Rev.* **2002**, *23* (5), 623–646. https://doi.org/10.1210/er.2001-0022.

(47) Rajput, R.; Narkhede, J.; Naik, J. Nanogels as Nanocarriers for Drug Delivery: A Review. *ADMET DMPK* **2019**, *8* (1), 1–15. https://doi.org/10.5599/admet.724.

(48) Sivaram, A. J.; Rajitha, P.; Maya, S.; Jayakumar, R.; Sabitha, M. Nanogels for Delivery, Imaging and Therapy. *Wiley Interdiscip. Rev. Nanomed. Nanobiotechnol.* **2015**, *7* (4), 509–533. https://doi.org/10.1002/wnan.1328.

(49) Boularas, M.; Deniau-Lejeune, E.; Alard, V.; Tranchant, J.-F.; Billon, L.; Save, M. Dual Stimuli-Responsive Oligo(Ethylene Glycol)-Based Microgels: Insight into the Role of Internal Structure in Volume Phase Transitions and Loading of Magnetic Nanoparticles to Design Stable Thermoresponsive Hybrid Microgels. *Polym. Chem.* **2015**, *7* (2), 350–363. https://doi.org/10.1039/C5PY01078K.

(50) Tang, Z.; Guan, Y.; Zhang, Y. The Synthesis of a Contraction-Type Glucose-Sensitive Microgel Working at Physiological Temperature Guided by a New Glucose-Sensing Mechanism. *Polym. Chem.* **2018**, *9* (8), 1012–1021. https://doi.org/10.1039/C8PY00072G.

(51) Cai, T.; Marquez, M.; Hu, Z. Monodisperse Thermoresponsive Microgels of Poly(Ethylene Glycol) Analogue-Based Biopolymers. *Langmuir* **2007**, *23* (17), 8663–8666. https://doi.org/10.1021/la700923r.

(52) Xu, X.; Shen, S.; Mo, R. Bioresponsive Nanogels for Protein Delivery. *VIEW* **2022**, *3* (1), 20200136. https://doi.org/10.1002/VIW.20200136.

(53) Nguyen, Q. V.; Huynh, D. P.; Park, J. H.; Lee, D. S. Injectable Polymeric Hydrogels for the Delivery of Therapeutic Agents: A Review. *Eur. Polym. J.* **2015**, *72*, 602–619. https://doi.org/10.1016/j.eurpolymj.2015.03.016.

(54) Li, J.; Mooney, D. J. Designing Hydrogels for Controlled Drug Delivery. *Nat. Rev. Mater.* **2016**, *1* (12). https://doi.org/10.1038/natrevmats.2016.71.

(55) Correa, S.; Grosskopf, A. K.; Lopez Hernandez, H.; Chan, D.; Yu, A. C.; Stapleton, L. M.; Appel, E. A. Translational Applications of Hydrogels. *Chem. Rev.* **2021**. https://doi.org/10.1021/acs.chemrev.0c01177.

(56) Vermonden, T.; Censi, R.; Hennink, W. E. Hydrogels for Protein Delivery. *Chem. Rev.* **2012**, *112* (5), 2853–2888. https://doi.org/10.1021/cr200157d.

(57) Ahmed, E. M. Hydrogel: Preparation, Characterization, and Applications: A Review. *J. Adv. Res.* **2015**, *6* (2), 105–121. https://doi.org/10.1016/j.jare.2013.07.006.

(58) Beletskii, A.; Galloway, A.; Rele, S.; Stone, M.; Malinoski, F. Engineered PRINT® Nanoparticles for Controlled Delivery of Antigens and Immunostimulants. *Hum. Vaccines Immunother.* **2014**, *10* (7), 1908–1913. https://doi.org/10.4161/hv.28817.

(59) Trongsatitkul, T.; Budhlall, B. M. Microgels or Microcapsules? Role of Morphology on the Release Kinetics of Thermoresponsive PNIPAm-Co-PEGMa Hydrogels. *Polym. Chem.* **2013**, *4* (5), 1502–1516. https://doi.org/10.1039/C2PY20889J.

(60) Richtering, W.; Alberg, I.; Zentel, R. Nanoparticles in the Biological Context: Surface Morphology and Protein Corona Formation. *Small* **2020**, *16* (39), 2002162. https://doi.org/10.1002/smll.202002162.

(61) Leroux, J.-C. Editorial: Drug Delivery: Too Much Complexity, Not Enough Reproducibility? *Angew. Chem. Int. Ed.* **2017**, *56* (48), 15170–15171. https://doi.org/10.1002/anie.201709002.

(62) Ekladious, I.; Colson, Y. L.; Grinstaff, M. W. Polymer–Drug Conjugate Therapeutics: Advances, Insights and Prospects. *Nat. Rev. Drug Discov.* **2019**, *18* (4), 273–294. https://doi.org/10.1038/s41573-018-0005-0.

(63) Correa, S.; Choi, K. Y.; Dreaden, E. C.; Renggli, K.; Shi, A.; Gu, L.; Shopsowitz, K. E.; Quadir, M. A.; Ben-Akiva, E.; Hammond, P. T. Highly Scalable, Closed-Loop Synthesis of Drug-Loaded, Layer-by-Layer Nanoparticles. *Adv. Funct. Mater.* **2016**, *26* (7), 991–1003. https://doi.org/10.1002/adfm.201504385.

(64) Pelegri-O'Day, E. M.; Paluck, S. J.; Maynard, H. D. Substituted Polyesters by Thiol–Ene Modification: Rapid Diversification for Therapeutic Protein Stabilization. *J. Am. Chem. Soc.* **2017**, *139* (3), 1145–1154. https://doi.org/10.1021/jacs.6b10776.

(65) Pelegri-O'Day, E. M.; Bhattacharya, A.; Theopold, N.; Ko, J. H.; Maynard, H. D. Synthesis of Zwitterionic and Trehalose Polymers with Variable Degradation Rates and Stabilization of Insulin. *Biomacromolecules* **2020**, *21* (6), 2147–2154. https://doi.org/10.1021/acs.biomac.0c00133.

(66) Mueller, R.-J. Biological Degradation of Synthetic Polyesters—Enzymes as Potential Catalysts for Polyester Recycling. *Process Biochem.* **2006**, *41* (10), 2124–2128. https://doi.org/10.1016/j.procbio.2006.05.018.

(67) Rydz, J.; Sikorska, W.; Kyulavska, M.; Christova, D. Polyester-Based (Bio)Degradable Polymers as Environmentally Friendly Materials for Sustainable Development. *Int. J. Mol. Sci.* **2014**, *16* (1), 564–596. https://doi.org/10.3390/ijms16010564.

(68) Woodard, L. N.; Grunlan, M. A. Hydrolytic Degradation and Erosion of Polyester Biomaterials. *ACS Macro Lett.* **2018**, *7* (8), 976–982. https://doi.org/10.1021/acsmacrolett.8b00424.

(69) Vert, M. Aliphatic Polyesters: Great Degradable Polymers That Cannot Do Everything. *Biomacromolecules* **2005**, *6* (2), 538–546. https://doi.org/10.1021/bm0494702.

(70) Laurel, M.; MacKinnon, D.; Becker, J.; Terracciano, R.; Drain, B.; Houck, H. A.; Becer, C. R. Degradable Thioester Core-Crosslinked Star-Shaped Polymers. *Polym. Chem.* **2022**, *13* (39), 5579–5589. https://doi.org/10.1039/D2PY00901C.

Chapter 2

A Comparative Study of Dual Thermo- and Glucose- Responsive Nanogel Systems

2.1 Introduction

The glucose-binding capacity of boronic acids has been exploited for a variety of applications including sensors, separations, chromatography, and drug delivery.[1,2] Boronic acids can form dynamic covalent bonds with 1,2- and 1,3-cis-diols. For this reason, a multitude of materials bearing boronic acids have been explored for delivery of insulin in response to changes in blood glucose concentration.[3,4] Polymeric nanogels containing boronic acids are a promising approach to drug delivery, presenting the biocompatibility of hydrophilic hydrogel networks at nanometer scale diameter, therefore enabling intravenous injection and prolonged circulation in the blood, as well as the responsiveness of the boronic acid.[5] Investigation of nanogels as glucose-responsive drug delivery vehicles has been pursued by several groups in recent years.[6] The mechanism of drug release in many of these systems relies on the swelling of the network due to the change in charge of the boronic acid after complexation with glucose.

Nanogels presenting a novel mechanism of contraction upon addition of glucose were recently reported. These nanogels were synthesized by copolymerizing thermoresponsive n-isopropyl acrylamide (NIPAM) and N-isopropylmethacrylamide (NIPMAM) with acrylic acid (AA), which was modified with 2-aminophenylboronic acid (2-APBA) post-polymerization.[7,8] Unlike similar nanogels utilizing 3-aminophenylboronic acid that become more soluble and expand from the increase in effective charge after binding with glucose due to the change from neutral trigonal to negative tetrahedral form,[9] the 2-APBA-bearing nanogels became less soluble and contracted in the presence of glucose. The selected phenylboronic acid did not change charge upon binding because the B-O dative bond with the carbonyl oxygen inherently stabilizes the negative tetrahedral geometry.[10] Instead, glucose acted as an additive, structuring water in its proximity, that changed the hydration of the pNIPAM chain to shift the lower critical solution

temperature (LCST) of the polymer and volume phase transition temperature (VPTT) of nanogels.[11–13] Incorporation of boronic acid in the polymer chain effectively concentrated the

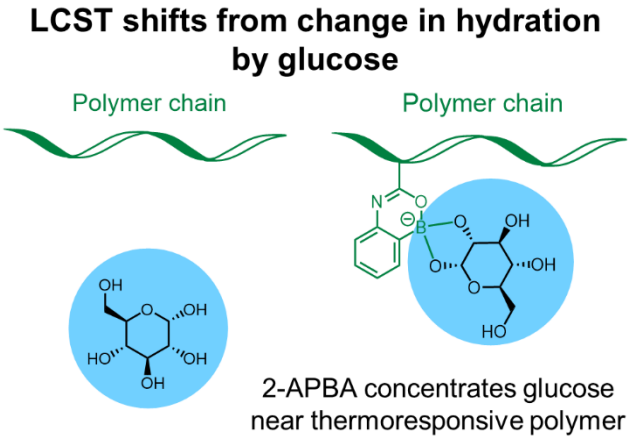

Figure 2.1 Mechanism of LCST shift for 2-APBA copolymers with glucose as additive.

saccharide near the thermoresponsive polymer, amplifying this effect (**Figure 2.1**).

Inspired by this design, we set out to explore if the contraction-type mechanism could be replicated with a different thermoresponsive polymer. Because of general concern about pNIPAM toxicity in vivo,[14] poly(ethylene glycol) methyl ether methacrylate (PEGMA) was selected as an alternative thermoresponsive component in the nanogels. These polymers have been explored for biomedical applications because they are biocompatible, with low toxicity *in vitro* and *in vivo*.[15–17] PEGMA-based nanogels have been prepared for applications in drug delivery including delivery of anticancer drugs, nucleic acids, and proteins.[18–21] Additionally, the LCST of these polymers can be readily tuned through alteration of the number of ethylene glycol units in the monomer and ratios of these monomers.[22] Thus, PEGMA is of interest to explore as a material for stimuli-responsive drug delivery. Herein, we describe the synthesis of these novel nanogels and comparison of their response to stimuli to the NIPAM nanogels reported previously.[7,8]

2.2 Results and discussion

First, the nanogels reported by Zhang and coworkers were prepared.[8] NIPAM nanogels were synthesized as previously reported (**Figure 2.2A**), with NIPMAM as a comonomer to tune the VPTT to a physiologically relevant temperature. Precipitation polymerization with NIPAM, NIPMAM, AA, and N,N′-methylenebis(acrylamide) (BIS) crosslinker at 70 °C with 20 mM sodium dodecyl sulfate (SDS) was found to give uniform nanogels with a diameter of 220 nm (polydispersity index, PDI = 0.289) at 20 °C by dynamic light scattering (DLS). A lower concentration of SDS (10 mM) resulted in larger nanogels with a diameter of 324 nm (PDI = 0.204) at 20 °C by DLS. Nanogels were functionalized post-polymerization by 1-ethyl-3-(3-dimethylaminopropyl)carbodiimide (EDC) coupling with 2-APBA as the glucose-sensing moiety.

The ^{1}H-NMR and FT-IR spectra of the NIPAM nanogels agreed with the previously reported spectra.[8] Monomer incorporation was calculated by studying kinetics via high performance liquid chromatography (HPLC) (**Figure 2.8**) using phenylalanine as a standard. Near complete conversion of each monomer was observed. Coupling of 2-APBA to AA was confirmed by the appearance of peaks from phenylboronic acid (7.6-6.7 ppm). By comparing integration of the peaks from phenylboronic acid and tertiary carbon of the isopropyl groups of NIPAM and NIPMAM (3.99-3.45 ppm) full conversion was demonstrated, showing overall 15% 2-APBA functionalization, which was consistent to the feed ratio of AA (**Figure 2.3A**). The FT-IR spectrum of NIPAM nanogels after coupling showed the presence of boronic acid (3302 cm^{-1}), amide carbonyl and amine (1634 and 1524 cm^{-1}), aromatic ring (2971 cm^{-1}), and polymer backbone alkane (2875 cm^{-1}) functional groups (**Figure 2.11**).

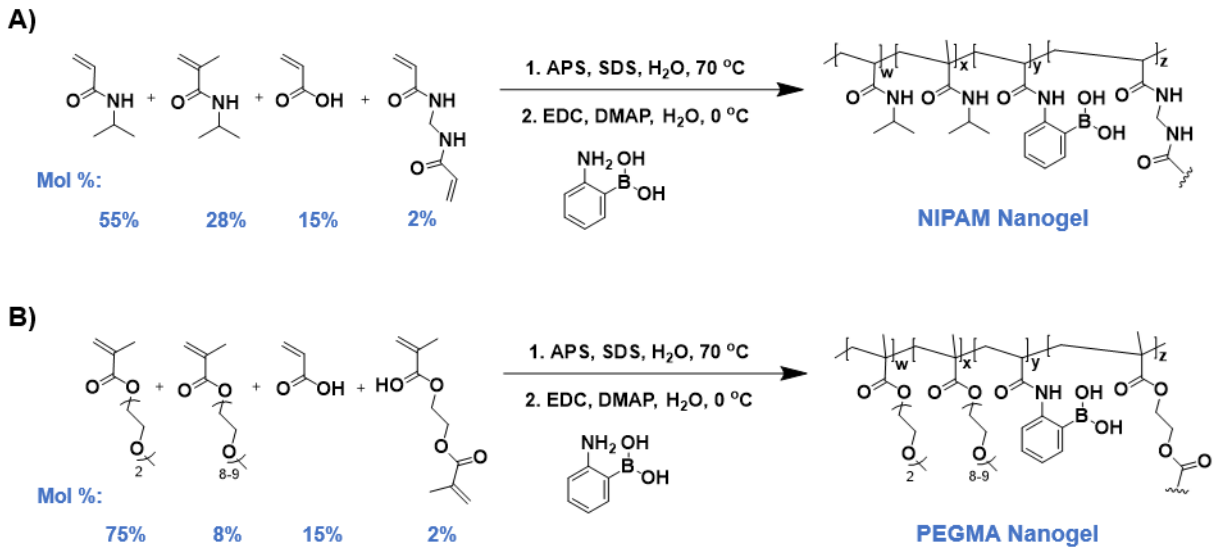

Figure 2.2 Synthesis of (A) NIPAM and (B) PEGMA nanogels by precipitation polymerization and post-polymerization coupling of boronic acid.

PEGMA nanogels were also prepared by precipitation polymerization (**Figure 2.2B**). To tune the VPTT to a physiologically relevant temperature, the feed ratio of approximately 1 to 10 of 480 Da oligo(ethylene glycol) methyl ether methacrylate ($OEGMA_{480}$) and diethylene glycol methyl ether methacrylate (DEGMA) was selected based on previous reports.[22,23] Precipitation polymerization with $OEGMA_{480}$, DEGMA, acrylic acid, and ethylene glycol dimethacrylate (EGDMA) crosslinker at 70 °C with 1.12 mM SDS was used to synthesize PEGMA nanogels with a diameter of 200 nm (PDI = 0.205) at 20 °C calculated by DLS. PEGMA nanogels were also functionalized with 2-APBA by post-polymerization EDC coupling.

Conversion of each individual monomer was not successfully studied for the PEGMA nanogel due to the difficulty of distinguishing between the various PEGMA monomers. However, incorporation of boronic acid moiety in the PEGMA nanogel was determined by ^{1}H-NMR (**Figure 2.3B**) comparing the integrations of the peak from the terminal methoxy protons of the side chains

(3.26-3.14 ppm, 3 H for each DEGMA and $OEGMA_{480}$) to the aromatic protons of the 2-APBA (7.70-6.69 ppm, 4H). The 2-APBA incorporation was calculated to be 17 mol % incorporation. The FT-IR spectrum of PEGMA nanogels after coupling confirmed the presence of boronic acid (3438 cm^{-1}), ester carbonyl (1724 cm^{-1}), aromatic ring (2966 cm^{-1}), and polymer backbone alkane

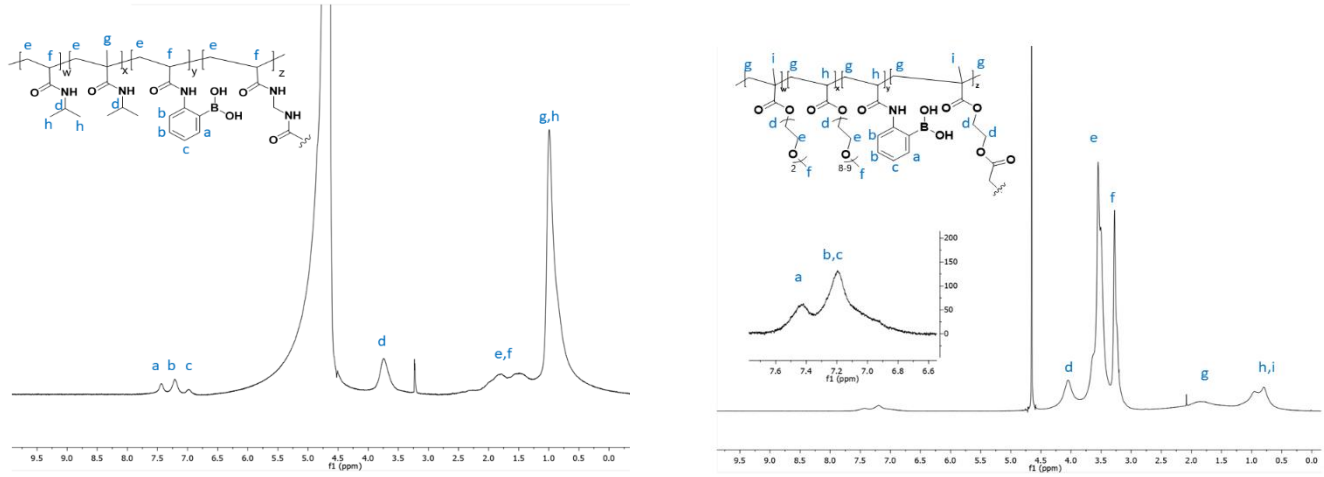

Figure 2.3 ^{1}H-NMR spectra of (A) NIPAM (D_2O) and (B) PEGMA nanogels (D_2O).

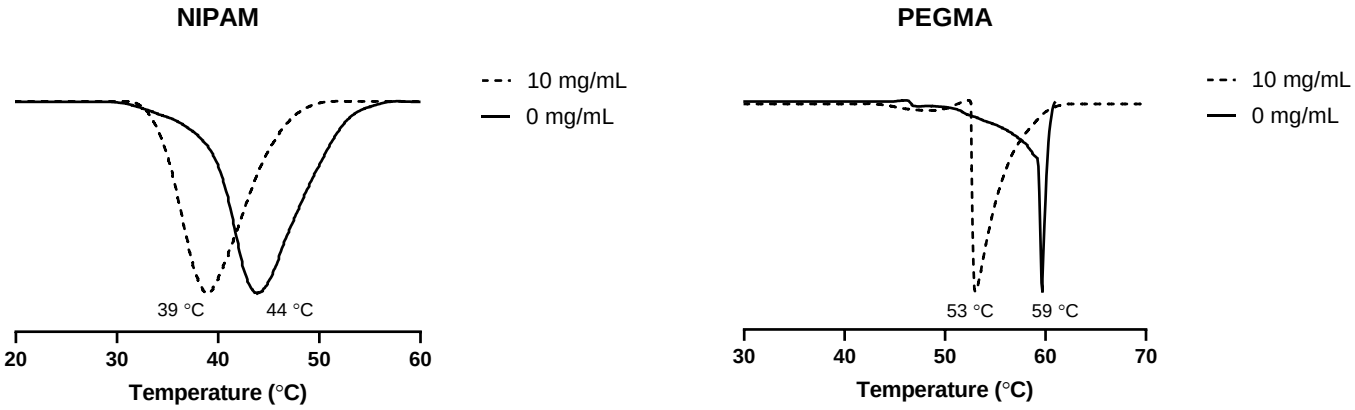

Figure 2.4 VPTT of (A) NIPAM and (B) PEGMA nanogels with and without 10 mg/mL glucose in 20 mM DPBS pH 7.4

(2878 cm^{-1}) functional groups (**Figures 2.13**).

For biological applications, temperature response at body temperatures near 37 °C is desirable. The temperature response of both NIPAM and PEGMA nanogels in 20 mM phosphate buffer pH 7.4 was tested by differential scanning calorimetry (DSC), UV-visible spectrophotometry at 600 nm, and DLS. VPTT for NIPAM and PEGMA nanogels was found to be approximately 43-45 °C and 60 °C respectively by DSC (**Figure 2.4**). The NIPAM nanogel exhibited a VPTT in the biologically relevant range due to the precise tuning of the monomers. The PEGMA nanogel, however, has a VPTT much higher than what was targeted and this was attributed to the higher incorporation of the $OEGMA_{480}$ monomer compared to the feed ratio. This is evidenced by the ^{1}H NMR (**Figure 2.3B**) that shows an approximate 5-7 to 1 ratio between the DEGMA and $OEGMA_{480.}$ Despite numerous attempts to optimize the VPTT of the PEGMA nanogels towards physiological temperature, we were unsuccessful in part due to difficulties in monitoring polymerization kinetics. NMR, HPLC, nor GC yielded clear kinetics analysis. Different length OEGMA oligomers as well as varying monomer feed ratios were explored in these attempts.. The transition profile (**Figure 2.4**) showed a sharp transition from PEGMA nanogels unlike the broad transition for NIPAM nanogels which agrees with existing literature.[24]

The change in nanogel diameter in response to temperature was measured by DLS. Nanogel diameters decreased by 106 nm and 31 nm when heating from 20 °C to 37 °C or 40 °C, temperatures close to body temperature for NIPAM and PEGMA nanogels respectively (**Table 2.1**). Gratifyingly, both nanogel compositions yielded nanogels that underwent shrinking behavior in response to temperatures in the same biologically relevant range, confirming that both polymers retain their LCST behavior with incorporation of 2-APBA and the comonomer ratios were tuned to achieve appropriate temperature response for biological applications such as drug delivery. Size and morphology of the nanogels were also assessed via transmission electron microscopy (TEM).

NIPAM nanogels averaged a diameter of 80 nm with overall spherical shape despite displaying rough edges (**Figure 2.14**). The smaller sizes, compared to DLS, are to be expected since the samples for TEM are in a dehydrated state. PEGMA nanogels could not be imaged under the same conditions likely due to low intrinsic electron-optical image contrast.[25,26]

Table 2.1. Measurement of nanogel diameter by DLS in response to temperature

Nanogel	**Diameter below 37 ºC** [a]	**PDI below 37 ºC** [a]	**Diameter near 37 ºC**	**PDI near 37 ºC**
NIPAM	220 nm	0.289	114 nm [b]	0.135 [b]
PEGMA	200 nm	0.205	169 nm [c]	0.173 [c]

[a] 20°C, [b] 37°C, [c] 40°C

Next, response of the nanogels to addition of glucose was evaluated using DSC. As expected, the addition of glucose (10 mg/mL) lowered the VPTT of NIPAM nanogels, changing the VPTT from 44 to 39 °C (**Figure 2.4**). The addition of glucose (10 mg/mL) also lowered the VPTT of the PEGMA nanogels from 59 to 53 °C. With this data, we tested the glucose concentration dependent size changes of each nanogel system using DLS. As we previously hypothesized, the NIPAM nanogel diameter decreased with increasing concentrations of glucose (**Figure 2.A-B**). The glucose-induced size changes ranged from 130 nm to 86 nm from 0 to 10 mg/mL, respectively, and displayed narrow PDIs throughout the measurements. The most noticeable shift in size change occurred at 3 mg/mL. On the other hand, the size of the PEGMA nanogels increased with the addition of glucose until 8 mg/mL glucose and subsequently decreased with higher glucose concentrations (**Figure 2.A,C**). Upon observing this trend, size changes from

additional glucose concentrations were tested. Interestingly, the size distribution at 5, 6, and 7 mg/mL glucose was bimodal with a shift towards the bigger peak with increasing glucose

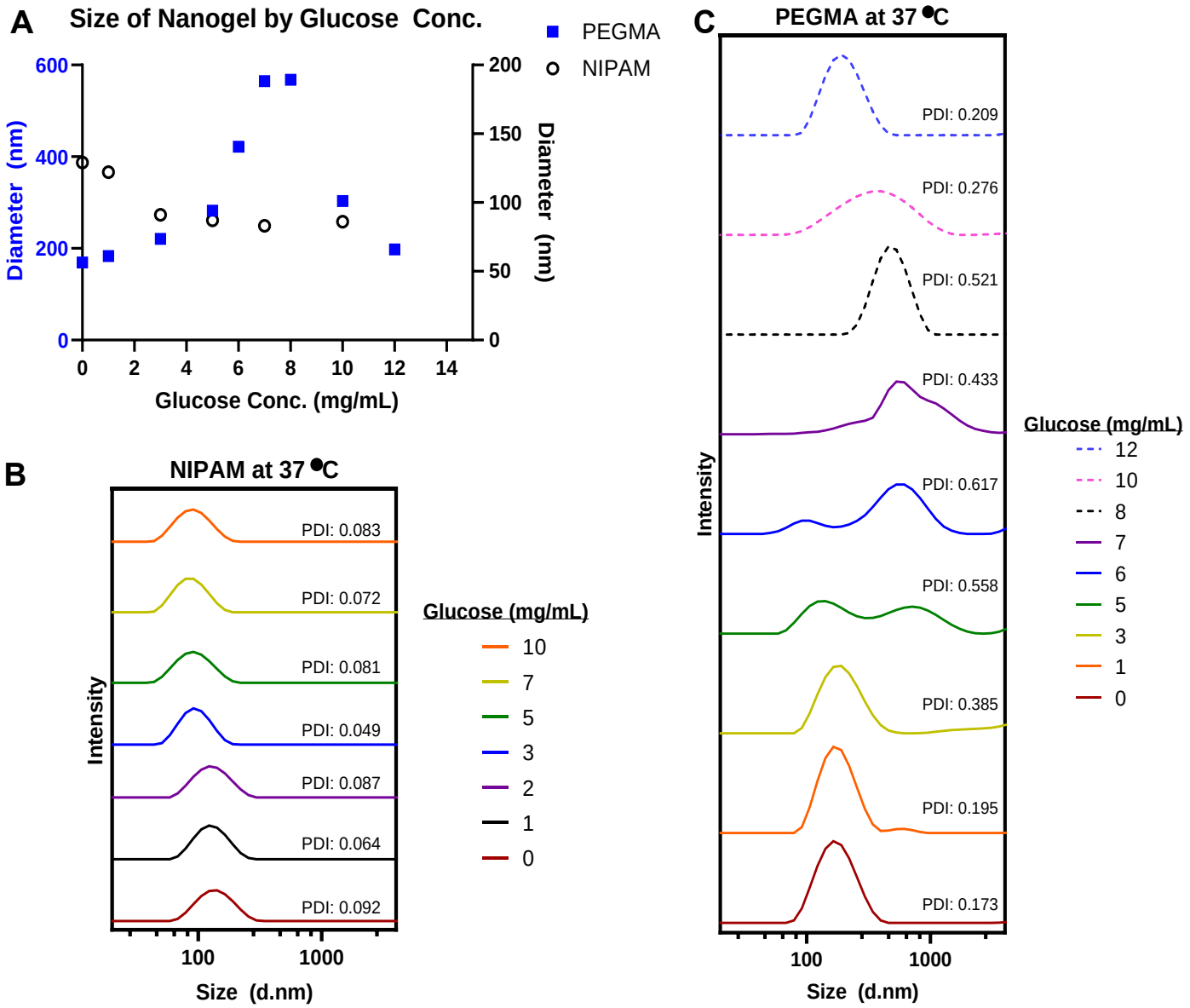

Figure 2.5 A) Measurement of PEGMA and NIPAM nanogel diameter by DLS at 37 °C in 20 mM DPBS at various glucose concentrations, (B) Measurement of NIPAM nanogel diameter and PDI by intensity at 0, 1, 2, 3, 5, 7, 10 mg/mL glucose in 20 mM DPBS, (C) Measurement of PEGMA nanogel diameter and PDI by intensity at 0, 1, 3, 5, 6, 7, 8, 10, 12 mg/mL glucose in 20 mM DPBS

concentrations. At 8 mg/mL of glucose, the PEGMA nanogel size reached its maximum of 567 nm and subsequently decreased to 304 nm and then 198 nm at 10 mg/mL and 12 mg/mL glucose, respectively.

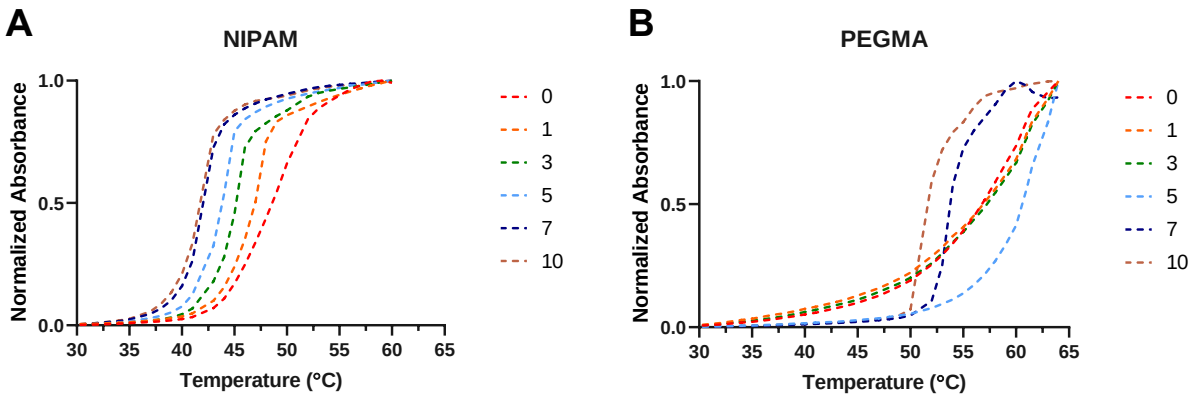

Figure 2.6. VPTT shift with addition of various glucose concentrations measured by temperature-controlled UV-visible plate reader for (A) NIPAM and (B) PEGMA nanogels

The response of the nanogels to addition of glucose was also evaluated by temperature-controlled UV-visible spectrophotometer. Turbidity measurements (**Figure 2.**) also confirmed the VPTT values measured by DSC (**Figure 2.4**). The sensitivity of the nanogels at 0, 1, 3, 5, 7, and 10 mg/mL glucose was assessed. As expected, the addition of glucose shifted the VPTT of the NIPAM nanogels to lower temperatures. At the lowest glucose concentration tested, that is 1 mg/mL, the NIPAM nanogels (**Figure 2.A**) demonstrated a VPTT shift of 0.8 °C. Moreover, in accordance to the DSC results, the total VPTT shift from 0 to 10 mg/mL of glucose was approximately 5.5 °C. In contrast, the PEGMA nanogels (**Figure 2.B**) did not show a measurable VPTT up to a glucose concentration of 3 mg/mL due to the upper limit of the instrument temperature of 65 °C. Starting from 5 mg/ml of glucose, a clear VPTT was noted. The presence of higher concentrations of glucose shifted the VPTT to lower temperatures, as expected. The total VPTT shift from 0 to 10 mg/mL is greater than 10 °C, but unfortunately due to the limitations of

the instrument, higher temperatures could not be assessed. Some discrepancy between the VPTT measurements of DSC and UV-vis can be attributed to the differences in the measured parameters which are heat loss and turbidity, respectively.

2.3 Conclusion

The different behavior of NIPAM and PEGMA in solution may lead to the observed differences in diameter and VPTT changes upon addition of glucose. The major difference between the two systems that is demonstrated here is the swelling and deswelling behaviors of PEGMA nanogels upon glucose addition. It has been reported that EGDMA-based microgels exhibit a densely crosslinked core with a loosely crosslinked shell.[24] Densely core crosslinked microgels with dangling polymer chains have been reported to show different thermoresponsive phase transitions.[27–29] Based on a kinetics study of a similar PEGMA-based nanogel,[24] both the crosslinker and glucose-responsive moieties are expected to be concentrated along the core of the particle. At the lower glucose concentrations, the interactions between the glucose and loosely crosslinked chains are thought to be dominant. The presence of ether oxygen in PEG offers various possibilities of hydrogen bond formation which has been demonstrated with sugars and poly(vinyl alcohol).[30-32] The contraction process begins as the glucose reaches the dense core of the particle and dehydrates the polymer backbone. Additionally, PEGMA lacks hydrogen bonding donors, such as the amide of NIPAM which is hypothesized to play a role in the hysteresis observed for pNIPAM upon cooling but not observed with PEGMA.[22] The mechanism of nanogel collapse is dependent upon the hydration of the polymer chains with glucose acting as an additive. Thus, we hypothesize that the increase in structured water around glucose affects the hydration of PEGMA nanogels more than NIPAM nanogels because of the differences in hydrogen bonding and amphiphilicity of OEGMA. The swelling of the PEGMA nanogels is affected by not only the

elasticity of the network but also the interplay of polymer-solvent and polymer-polymer interactions.[33]

In conclusion, dual thermo- and glucose-responsive nanogels were prepared using precipitation polymerization to incorporate glucose-binding phenylboronic acid and two different polymers exhibiting LCST behavior. Both NIPAM and PEGMA nanogels underwent a volume phase transition in response to temperature and glucose. Interestingly, PEGMA nanogels exhibited a swelling then contracting behavior in response to increased glucose concentrations while the NIPAM nanogels demonstrated a correlation of contracting in size from increased glucose concentrations. Finally, to our knowledge this is the first report of PEGMA-based nanogels that undergo a size change in response to glucose.

2.4 Appendix A

Materials

All chemicals were purchased from Sigma-Aldrich and Fisher Scientific and were used without purification unless noted otherwise. N-Isopropylacrylamide was recrystallized from n-hexane. N-Isopropylmethacrylamide was recrystallized from n-hexane. Acrylic acid was distilled under vacuum. Liquid monomers were purified by passage over basic alumina before use in polymerizations. For polymerizations, water was sparged with argon 30 min prior to initiation.

Analytical techniques

Nuclear magnetic resonance (NMR) spectra were recorded on a Bruker AV 400 MHz spectrometer. DSC for characterization of nanogel VPTT was conducted on a Mettler Toledo DSC3+ with 80 µL 10 mg/mL 20 mM DPBS pH 7.4 solution in 100 µL aluminum pans with gradient of 10 to 90 °C and a ramp rate of 5 °C/min. DLS for characterization of nanogel size and

temperature response was conducted on a Malvern Nanozetasizer at approximately 1 mg/mL in 20 mM DPBS pH 7.4. Nanogel turbidity was measured with 10 mg/mL solution in 20 mM DPBS pH 7.4 at 600 nm on a Tecan M1000 plate reader or SpectraMax iD3 plate reader. High performance liquid chromatography (HPLC) was conducted on an Agilent 1260 Infinity II HPLC system equipped with an autosampler and a UV detector using a C18 Zorbax column. Transmission electron microscopy (TEM) images were taken on a Tecnai FEI T12 microscope.

Experimental

Synthesis of NIPAM nanogel

In a 3-neck round-bottom flask under argon, NIPAM (428 mg, 3.8 mmol, 27.1 equiv.), NIPMAM (245 mg, 1.9 mmol, 13.8 equiv.), AA (75 mg, 1.0 mmol, 1 equiv.), N,N'-methylenebis(acrylamide) (21.5 mg, 0.14 mmol, 1 equiv.), SDS (58 mg, 0.2 mmol, 1.4 equiv.), water (9.5 mL), and a stir bar were added. The flask was placed in a 70 °C oil bath and stabilized under argon for 1 hour. APS (43 mg, 0.15 mmol, 1.07 equiv.) dissolved in water (0.5 mL) was added to the flask to initiate the reaction. Polymerization was ended after 7 h by exposure to oxygen and removal from the heat source. The nanogel was purified by dialysis (6-8 kDa MWCO) against water 3 days. To a round bottom flask under argon, 10 mL of NIPAM nanogel (0.12 mmol acrylic acid, 1 equiv.) was added. To the flask, 2-APBA (305 mg, 1.8 mmol, 10 equiv.), EDC (410 mg, 2.6 mmol, 15 equiv.), and DMAP (4.3 mg, 35 µmol, 0.2 equiv.) were added successively. The reaction proceeded at 0 °C in an ice bath for 4 hours under argon. The product was purified by dialysis (6-8 kDa MWCO) against water for 3 days. ^{1}H NMR (400 MHz in D_2O) δ: 7.44, 7.20, 6.97, 3.76, 1.83, 1.52, 1.01. IR: ν = 3302, 2971, 2930, 2675, 1634, 1524, 1449, 1387,

1367, 1216, 1173, 1130, 1028, 962, 885, 840, 763 cm^{-1}. Characterization results matched the protocol the synthesis is based on.[8,9]

Synthesis of PEGMA nanogel

In a 3-neck round-bottom flask under argon, DEGMA (295 µL, 1.6 mmol, 37.5 equiv.), $OEGMA_{480}$ (137 µL, 0.17 mmol, 4 equiv.), acrylic acid (22 µL, 0.32 mmol, 7.5 equiv.), ethylene glycol dimethacrylate (8 µL, 0.043 µmol, 1 equiv.), SDS (8 mg, 0.028 mmol, 0.66 equiv.), water (24.5 mL), and a stir bar were added. The flask was placed in a 70 °C oil bath and stabilized under argon for 1 hour. APS (7.3 mg, 0.032 mmol, 0.75 equiv.) dissolved in water (0.5 mL) was added to the flask and the reaction was initiated. Polymerization was ended after 20 h by exposure to oxygen. Gels were purified by dialysis (6-8 kDa MWCO) against water for 3 days. PEGMA nanogel (400 mg, 0.32 mmol acrylic acid, 1 equiv.) suspended in 25 mL water was transferred to a round bottom flask under argon in an ice bath (0 °C). To this was added EDC (255 mg, 1.6 mmol, 5 equiv.), DMAP (20.0 mg, 0.16 mmol, 0.5 equiv.) and 2-APBA (283 mg, 1.6 mmol, 5 equiv.). The mixture was stirred at 21 °C for 16 hours before being quenched by exposure to oxygen. The nanogels were purified by dialysis (6-8 kDa MWCO) against water for 3 days. ^1H NMR (400 MHz in D_2O) δ: 7.42, 7.19, 4.05, 3.63, 3.55, 3.50, 3.27, 1.86, 0.97, 0.80. IR: ν = 3438, 2966, 2878, 1724, 1450, 1388, 1352, 1246, 1104, 1028, 944, 850, 750 cm^{-1}.

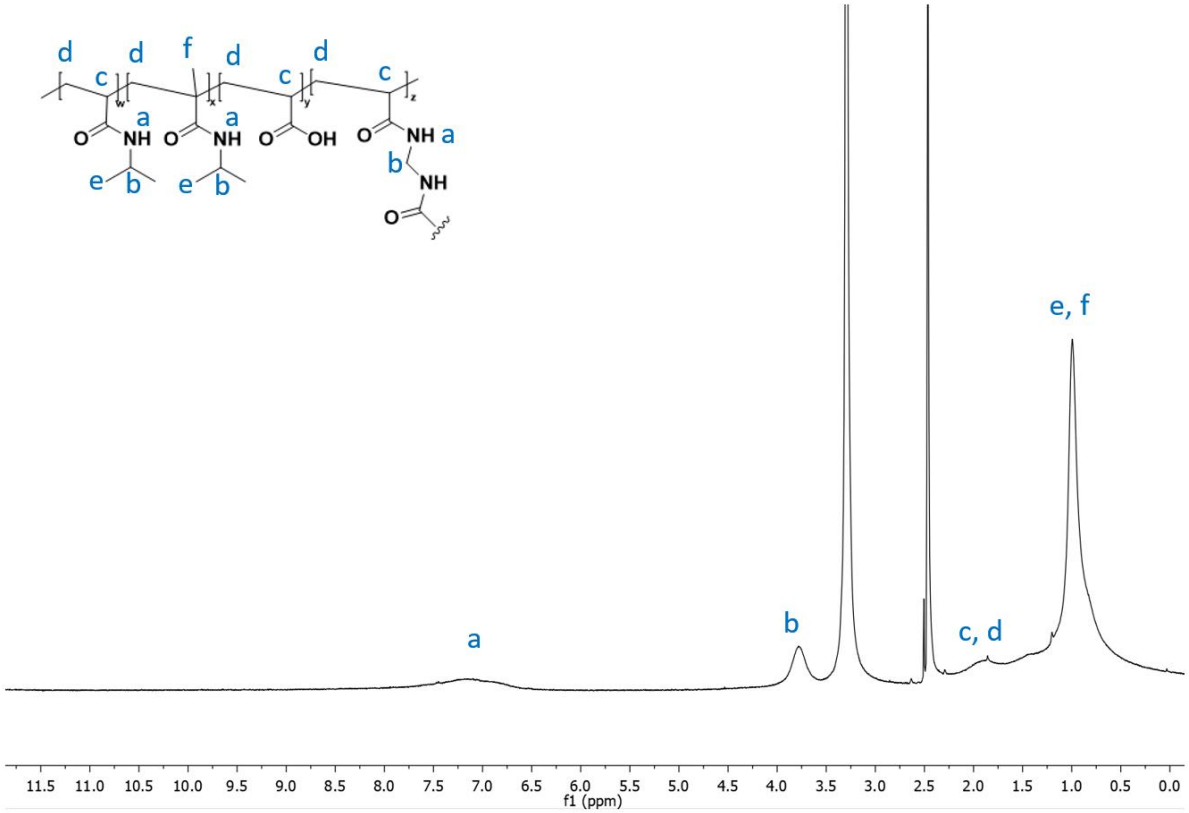

Figure 2.7. ^{1}H-NMR spectrum of NIPAM nanogels before coupling with 2-APBA (D_6DMSO)

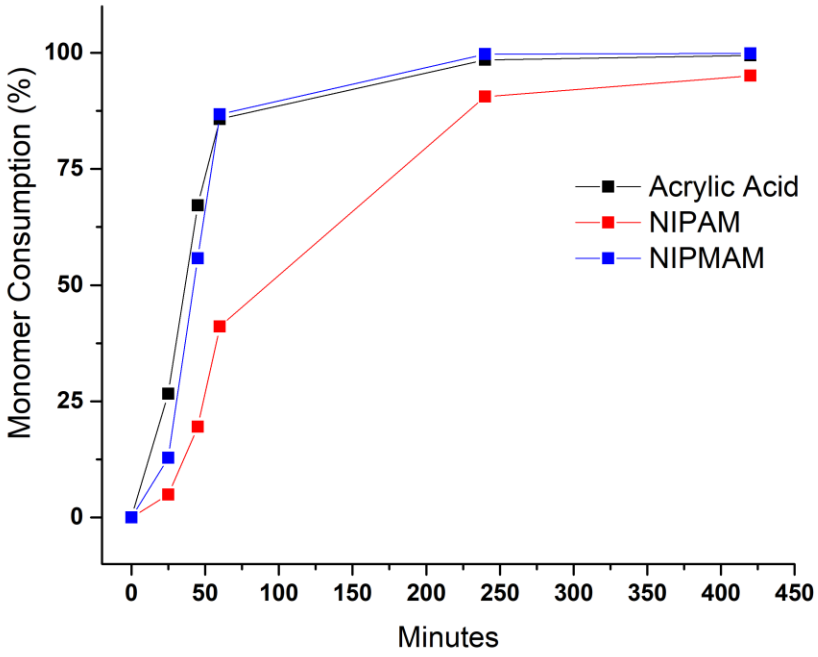

Figure 2.8. Monomer incorporation kinetics for the precipitation polymerization of NIPAM nanogel studied using HPLC C18 Zorbax 10-90% acetonitrile(0.1% TFA)/water(0.1% TFA). Phenylalanine was used as an internal standard.

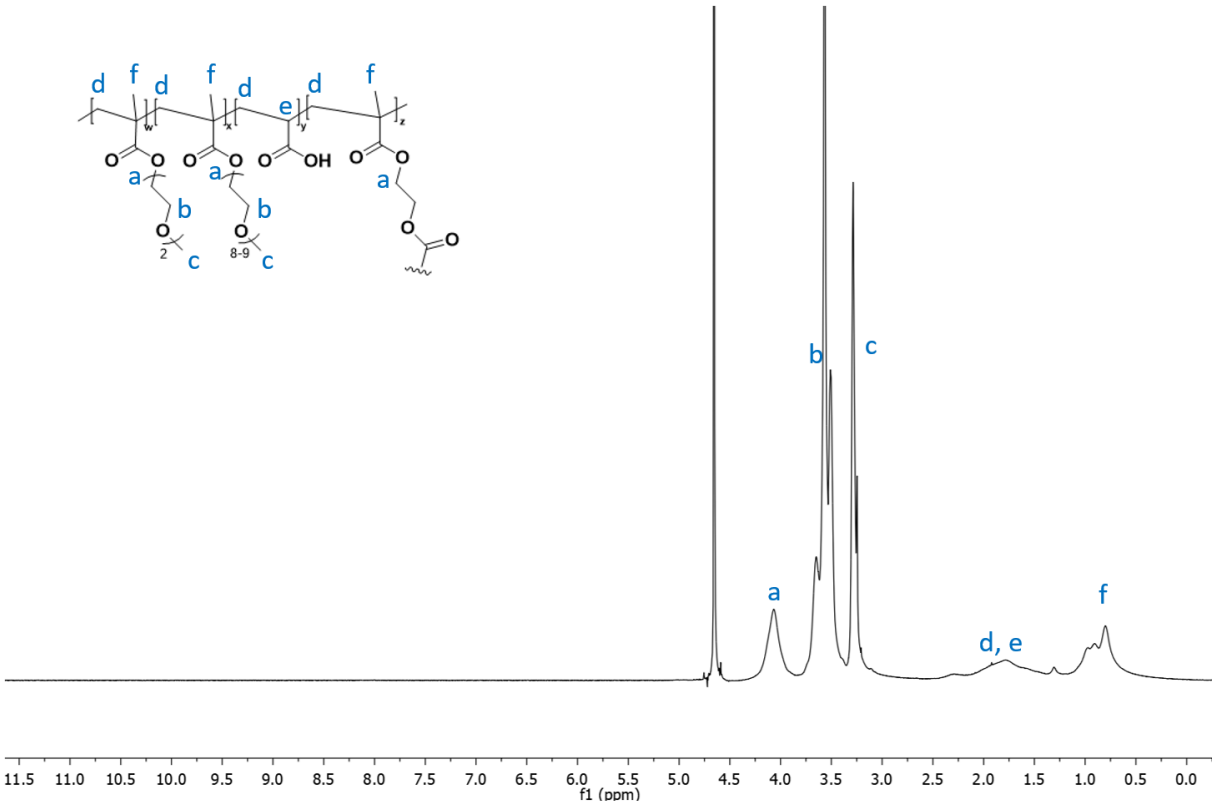

Figure 2.9. ^{1}H-NMR spectrum of PEGMA nanogels before coupling with 2-APBA (D_2O)

The mole ratio of DEGMA and $OEGMA_{480}$ was crudely calculated by setting the terminal methoxy protons of the side chains (3.33 - 2.97 ppm, 3 H for each DEGMA and $OEGMA_{480}$) to an integration of 6 and examining the integration of the side chain protons (3.84 – 3.33 ppm, 6 H for DEGMA, 58 H for $OEGMA_{480}$) which was 14.5. Subtracting the 6 protons contributed from DEGMA, $OEGMA_{480}$ becomes 8.5 which translates to an approximate ratio of 1 DEGMA for every 0.15 $OEGMA_{480}$. The same ratio can be calculated by setting alpha hydrogens of ester in DEGMA and $OEGMA_{480}$ (4.39 – 3.84 ppm, 2 H for each DEGMA and $OEGMA_{480}$) to 4 and examining the integration of the side chain protons.

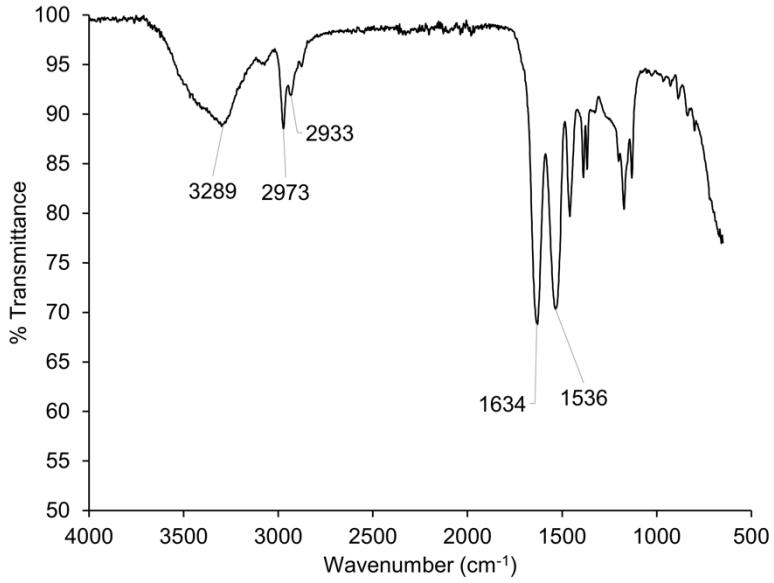

Figure 2.10. FT-IR spectrum of NIPAM nanogels before coupling with 2-APBA

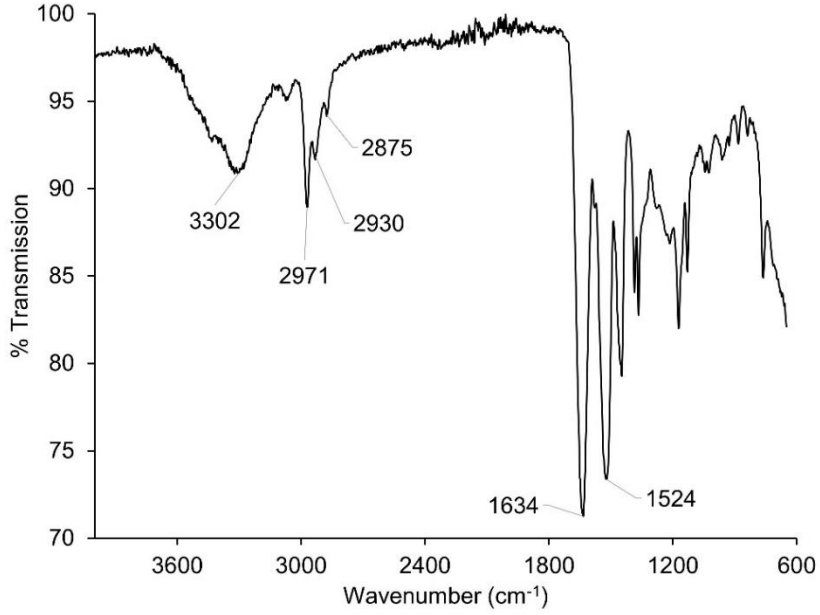

Figure 2.11. FT-IR spectrum of NIPAM nanogels after coupling with 2-APBA

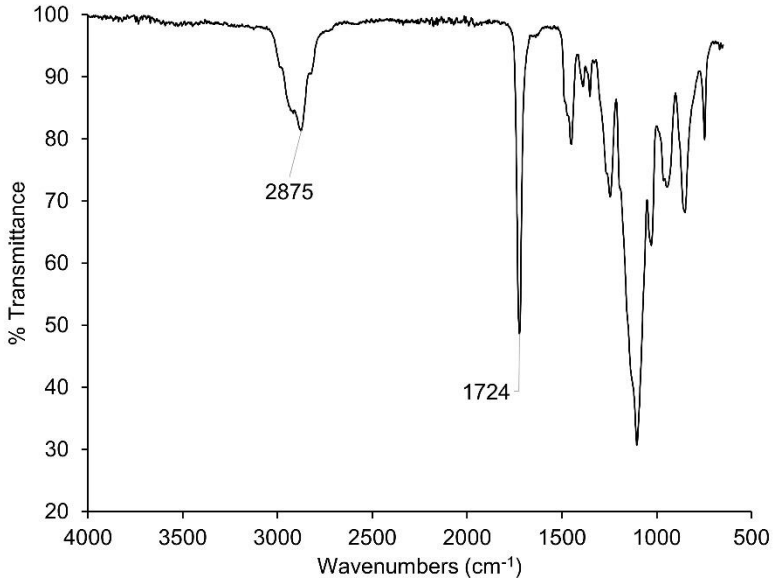

Figure 2.12. FT-IR spectrum of PEGMA nanogels before coupling with 2-APBA

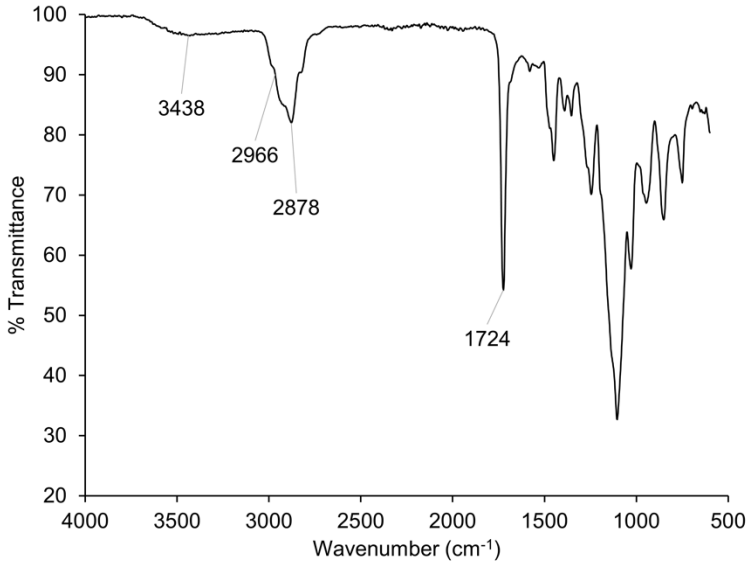

Figure 2.13. FT-IR spectrum of PEGMA nanogels after coupling with 2-APBA

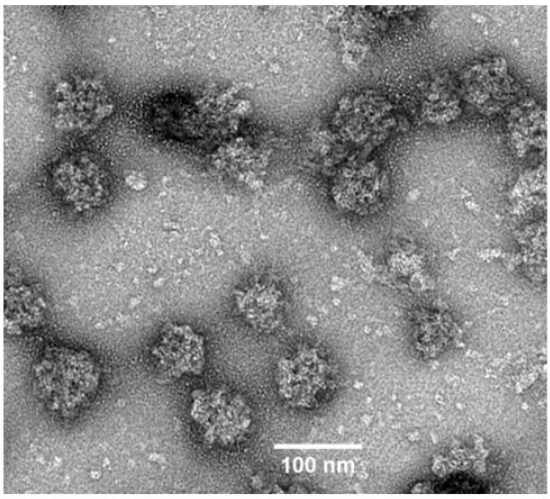

Figure 2.14 TEM image of NIPAM nanogels. 4 uL of a 5 mg/mL nanogel solution in 20 mM DPBS pH 7.4 was dropped on a glow-discharged copper/formvar grid. Uranyl acetate was used as a negative stain for visualization .

2.5 References

(1) Brooks, W. L. A.; Sumerlin, B. S. Synthesis and Applications of Boronic Acid-Containing Polymers: From Materials to Medicine. *Chem. Rev.* **2016**, *116* (3), 1375–1397. https://doi.org/10.1021/acs.chemrev.5b00300.

(2) Guan, Y.; Zhang, Y. Boronic Acid-Containing Hydrogels: Synthesis and Their Applications. *Chem. Soc. Rev.* **2013**, *42* (20), 8106–8121. https://doi.org/10.1039/C3CS60152H.

(3) Rege, N. K.; Phillips, N. F. B.; Weiss, M. A. Development of Glucose-Responsive 'Smart' Insulin Systems. *Curr. Opin. Endocrinol. Diabetes Obes.* **2017**, *24* (4), 267–278. https://doi.org/10.1097/MED.0000000000000345.

(4) Shen, D.; Yu, H.; Wang, L.; Khan, A.; Haq, F.; Chen, X.; Huang, Q.; Teng, L. Recent Progress in Design and Preparation of Glucose-Responsive Insulin Delivery Systems. *J. Controlled Release* **2020**, *321*, 236–258. https://doi.org/10.1016/j.jconrel.2020.02.014.

(5) Oh, J. K.; Drumright, R.; Siegwart, D. J.; Matyjaszewski, K. The Development of Microgels/Nanogels for Drug Delivery Applications. *Prog. Polym. Sci.* **2008**, *33* (4), 448–477. https://doi.org/10.1016/j.progpolymsci.2008.01.002.

(6) Ma, R.; Shi, L. Phenylboronic Acid-Based Glucose-Responsive Polymeric Nanoparticles: Synthesis and Applications in Drug Delivery. *Polym. Chem.* **2014**, *5* (5), 1503–1518. https://doi.org/10.1039/C3PY01202F.

(7) Tang, Z.; Guan, Y.; Zhang, Y. Contraction-Type Glucose-Sensitive Microgel Functionalized with a 2-Substituted Phenylboronic Acid Ligand. *Polym. Chem.* **2014**, *5* (5), 1782–1790. https://doi.org/10.1039/C3PY01190A.

(8) Tang, Z.; Guan, Y.; Zhang, Y. The Synthesis of a Contraction-Type Glucose-Sensitive Microgel Working at Physiological Temperature Guided by a New Glucose-Sensing Mechanism. *Polym. Chem.* **2018**, *9* (8), 1012–1021. https://doi.org/10.1039/C8PY00072G.

(9) Zhang, Y.; Guan, Y.; Zhou, S. Synthesis and Volume Phase Transitions of Glucose-Sensitive Microgels. *Biomacromolecules* **2006**, *7* (11), 3196–3201. https://doi.org/10.1021/bm060557s.

(10) Yang, X.; Lee, M.-C.; Sartain, F.; Pan, X.; Lowe, C. R. Designed Boronate Ligands for Glucose-Selective Holographic Sensors. *Chem. – Eur. J.* **2006**, *12* (33), 8491–8497. https://doi.org/10.1002/chem.200600442.

(11) Kim, Y.-H.; Kwon, I. C.; Bae, Y. H.; Kim, S. W. Saccharide Effect on the Lower Critical Solution Temperature of Thermosensitive Polymers. *Macromolecules* **1995**, *28* (4), 939–944. https://doi.org/10.1021/ma00108a022.

(12) Kawasaki, H.; Sasaki, S.; Maeda, H.; Mihara, S.; Tokita, M.; Komai, T. Saccharide-Induced Volume Phase Transition of Poly(N-Isopropylacrylamide) Gels. *J. Phys. Chem.* **1996**, *100* (40), 16282–16284. https://doi.org/10.1021/jp961219w.

(13) Shpigelman, A.; Portnaya, I.; Ramon, O.; Livney, Y. D. Saccharide-Structure Effects on Poly N-Isopropylacrylamide Phase Transition in Aqueous Media; Reflections on Protein Stability. *J. Polym. Sci. Part B Polym. Phys.* **2008**, *46* (21), 2307–2318. https://doi.org/10.1002/polb.21562.

(14) Cooperstein, M. A.; Canavan, H. E. Assessment of Cytotoxicity of (N-Isopropyl Acrylamide) and Poly(N-Isopropyl Acrylamide)-Coated Surfaces. *Biointerphases* **2013**, *8* (1), 19. https://doi.org/10.1186/1559-4106-8-19.

(15) Pissuwan, D.; Boyer, C.; Gunasekaran, K.; Davis, T. P.; Bulmus, V. In Vitro Cytotoxicity of RAFT Polymers. *Biomacromolecules* **2010**, *11* (2), 412–420. https://doi.org/10.1021/bm901129x.

(16) Lutz, J.-F.; Andrieu, J.; Üzgün, S.; Rudolph, C.; Agarwal, S. Biocompatible, Thermoresponsive, and Biodegradable: Simple Preparation of "All-in-One" Biorelevant Polymers. *Macromolecules* **2007**, *40* (24), 8540–8543. https://doi.org/10.1021/ma7021474.

(17) Ryan, S. M.; Wang, X.; Mantovani, G.; Sayers, C. T.; Haddleton, D. M.; Brayden, D. J. Conjugation of Salmon Calcitonin to a Combed-Shaped End Functionalized Poly(Poly(Ethylene Glycol) Methyl Ether Methacrylate) Yields a Bioactive Stable

Conjugate. *J. Controlled Release* **2009**, *135* (1), 51–59. https://doi.org/10.1016/j.jconrel.2008.12.014.

(18) Jiang, Z.; Cui, W.; Prasad, P.; Touve, M. A.; Gianneschi, N. C.; Mager, J.; Thayumanavan, S. Bait-and-Switch Supramolecular Strategy To Generate Noncationic RNA–Polymer Complexes for RNA Delivery. *Biomacromolecules* **2019**, *20* (1), 435–442. https://doi.org/10.1021/acs.biomac.8b01321.

(19) Oh, J. K.; Siegwart, D. J.; Lee, H.; Sherwood, G.; Peteanu, L.; Hollinger, J. O.; Kataoka, K.; Matyjaszewski, K. Biodegradable Nanogels Prepared by Atom Transfer Radical Polymerization as Potential Drug Delivery Carriers: Synthesis, Biodegradation, in Vitro Release, and Bioconjugation. *J. Am. Chem. Soc.* **2007**, *129* (18), 5939–5945. https://doi.org/10.1021/ja069150l.

(20) E. Averick, S.; D. Magenau, A. J.; Simakova, A.; F. Woodman, B.; Seong, A.; A. Mehl, R.; Matyjaszewski, K. Covalently Incorporated Protein –Nanogels Using AGET ATRP in an Inverse Miniemulsion. *Polym. Chem.* **2011**, *2* (7), 1476–1478. https://doi.org/10.1039/C1PY00050K.

(21) Tian, Y.; Bian, S.; Yang, W. A Redox-Labile Poly(Oligo(Ethylene Glycol)Methacrylate)-Based Nanogel with Tunable Thermosensitivity for Drug Delivery. *Polym. Chem.* **2016**, *7* (10), 1913–1921. https://doi.org/10.1039/C6PY00057F.

(22) Lutz, J.-F. Polymerization of Oligo(Ethylene Glycol) (Meth)Acrylates: Toward New Generations of Smart Biocompatible Materials. *J. Polym. Sci. Part Polym. Chem.* **2008**, *46* (11), 3459–3470. https://doi.org/10.1002/pola.22706.

(23) Cai, T.; Marquez, M.; Hu, Z. Monodisperse Thermoresponsive Microgels of Poly(Ethylene Glycol) Analogue-Based Biopolymers. *Langmuir* **2007**, *23* (17), 8663–8666. https://doi.org/10.1021/la700923r.

(24) Boularas, M.; Deniau-Lejeune, E.; Alard, V.; Tranchant, J.-F.; Billon, L.; Save, M. Dual Stimuli-Responsive Oligo(Ethylene Glycol)-Based Microgels: Insight into the Role of Internal Structure in Volume Phase Transitions and Loading of Magnetic Nanoparticles to Design Stable Thermoresponsive Hybrid Microgels. *Polym. Chem.* **2016**, *7* (2), 350–363. https://doi.org/10.1039/C5PY01078K.

25) Chen, J. Advanced Electron Microscopy of Nanophased Synthetic Polymers and Soft Complexes for Energy and Medicine Applications. *Nanomaterials* **2021**, *11* (9), 2405. https://doi.org/10.3390/nano11092405.

(26) Libera, M. R.; Egerton, R. F. Advances in the Transmission Electron Microscopy of Polymers. *Polym. Rev.* **2010**, *50* (3), 321–339. https://doi.org/10.1080/15583724.2010.493256.

(27) Acciaro, R.; Gilányi, T.; Varga, I. Preparation of Monodisperse Poly(N-Isopropylacrylamide) Microgel Particles with Homogenous Cross-Link Density Distribution. *Langmuir* **2011**, *27* (12), 7917–7925. https://doi.org/10.1021/la2010387.

(28) Meyer, S.; Richtering, W. Influence of Polymerization Conditions on the Structure of Temperature-Sensitive Poly(N-Isopropylacrylamide) Microgels. *Macromolecules* **2005**, *38* (4), 1517–1519. https://doi.org/10.1021/ma047776v.

(29) Varga, I.; Gilányi, T.; Mészáros, R.; Filipcsei, G.; Zrínyi, M. Effect of Cross-Link Density on the Internal Structure of Poly(N-Isopropylacrylamide) Microgels. *J. Phys. Chem. B* **2001**, *105* (38), 9071–9076. https://doi.org/10.1021/jp004600w.

(30) Alkan, C.; Günther, E.; Hiebler, S.; Ensari, Ö. F.; Kahraman, D. Polyethylene Glycol-Sugar Composites as Shape Stabilized Phase Change Materials for Thermal Energy Storage. *Polym. Compos.* **2012**, *33* (10), 1728–1736. https://doi.org/10.1002/pc.22307.

(31) Sawatari, C.; Kondo, T. Interchain Hydrogen Bonds in Blend Films of Poly(Vinyl Alcohol) and Its Derivatives with Poly(Ethylene Oxide). *Macromolecules* **1999**, *32* (6), 1949–1955. https://doi.org/10.1021/ma980900o.

(32) Zheng, H.; Zheng, S.; Guo, Q. Thermosetting Polymer Blends of Unsaturated Polyester Resin and Poly(Ethylene Oxide). II. Hydrogen-Bonding Interaction, Crystallization Kinetics, and Morphology. *J. Polym. Sci. Part Polym. Chem.* **1997**, *35* (15), 3169–3179. https://doi.org/10.1002/(SICI)1099-0518(19971115)35:15<3169::AID-POLA10>3.0.CO;2-9.

(33) Welsch, N.; Lyon, L. A. Oligo(Ethylene Glycol)-Sidechain Microgels Prepared in Absence of Cross-Linking Agent: Polymerization, Characterization and Variation of Particle Deformability. *PLoS ONE* **2017**, *12* (7). https://doi.org/10.1371/journal.pone.0181369.

Chapter 3

Sustained Release of Glucagon from an Injectable Glucose- and Thermo-responsive Hydrogel

3.1 Introduction

Diabetes is an autoimmune disorder that affects almost 10% of the worldwide population, with type I diabetes accounting for more than 400 million people.[1–5] Glucagon is an important hormone for the regulation of blood glucose levels.[6] In contrast to insulin, glucagon increases blood glucose levels to prevent hypoglycemia. Once glucagon binds to its receptor, a cascade of events catalyze glycogenolysis, gluconeogenesis, and even ketogenesis.[6] Regular insulin boluses are delivered throughout the day where glucagon is currently only used as an emergency injection for severe hypoglycemia.[7,8] Much of that reason can be attributed to the challenges that exist with glucagon formulation including low stability, low solubility at physiological pH, and its tendency to form toxic fibrils.[6,9–11]

Within the past number of years, new formulations of glucagon have been developed in industry with many such products being tested in clinical trials, with some receiving FDA approval. Eli Lilly unveiled the first nasal rescue glucagon, BAQSIMI™, which is formulated as a 3 mg dry powder.[12] Xeris Pharmaceuticals introduced the GVOKE™ hypopen which is formulated as a solution of glucagon in dimethyl sulfoxide in a ready-to-inject automatic injector.[13] Similarly, Zealand Pharma debuted their automatic injector ZEGALOGUE™ which contains an aqueous solution of a glucagon analog.[14] These new formulations have received much success, prompting Eli Lilly to announce the discontinuation of their original glucagon emergency rescue kit.[15] While these new hypoglycemia rescue kits are undoubtedly valuable, they are not intended for nighttime hypoglycemia. Almost 50% of all episodes of severe hypoglycemia occur at night during sleep.[16,17] When undetected and unmanaged, nocturnal hypoglycemia is associated with further impairment of counterregulatory responses to falling blood glucose levels and in the most extreme cases can lead to sudden death in bed syndrome.[16,17] A delivery system that allows for sustained and

controlled release of glucagon over a few hours span would greatly reduce the incidence of dangerous hypoglycemic states overnight. Since the embarkment of our experiments, there have been a handful of relevant publications that help solidify the need for sustained glucagon release models as well as our rationale behind the design of our system. A limited number of studies evaluate glucagon release models responsive to glucose levels. Yu et al reported the formulation of a glucose-responsive peptide-based hydrogel that releases dasiglucagon over a few hours.[18] Microneedle arrays have been explored as well with reports from Wu and coworkers of glucose-triggered native glucagon release at 0.5 mg/mL glucose.[19,20]

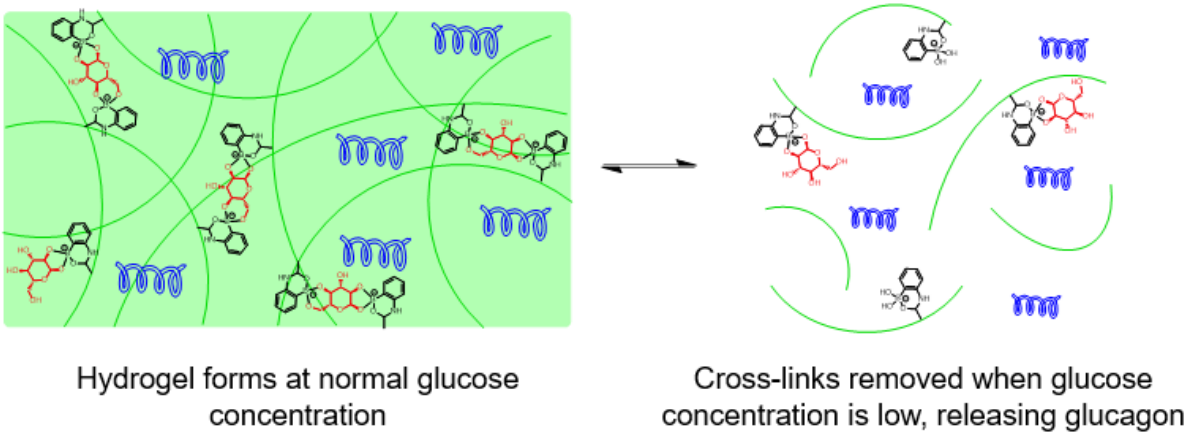

Figure 3.1 Hydrogel formation at normoglycemia followed by hydrogel dissolution and payload release at hypoglycemia. Blue helix = glucagon, green line = polymer, black molecule = boronic acid, red molecule = glucose

Here in this work, we present a hydrogel-mediated controlled delivery of native glucagon, formulated as an injectable, to combat nighttime hypoglycemia. Glucose- and thermo-responsive block co-polymer of polyethyleneglycol-block-poly(n-isopropylacrylamide-co-2-

aminophenylboronic acid) (PEG-*b*-p(NIPAM-co-2APBA)) was synthesized via reversible addition-fragmentation chain transfer (RAFT) polymerization followed by post-polymerization addition of the glucose responsive moiety 2-APBA.[21] Next, glucose was used as the crosslinker by taking advantage of the dynamic covalent bonds that phenylboronic acids promote. The use of 2-aminophenylboronic acid here is crucial to our mechanism as it forms a B-O dative bond with the carbonyl oxygen, inherently stabilizing a negative tetrahedral geometry which allows for glucose to act as an additive.[22] Glucose then structures water in its proximity and changes the hydration state of the pNIPAM chain to shift the lower critical solution temperature (LCST) of the polymer[23] and subsequently the gelation point of the hydrogel. With this mechanism, the 3D hydrogel network was formed by the addition of glucose at physiological temperature – encapsulating the glucagon within the hydrogel. As glucose levels decrease, the glucose crosslinks slowly dissolve and thereby release the glucagon (**Figure 3.1**). The effects of the polymer composition were investigated to optimize the sensitivity of the hydrogel. Then, the hydrogel was tested for glucagon release under hypoglycemic conditions. Lastly, rheological measurements demonstrated shear-thinning behavior and injection force was calculated for a wide range of needle gauges and flow rates.

3.2 Results and Discussion

Synthesis and Characterization of Block Copolymer Library

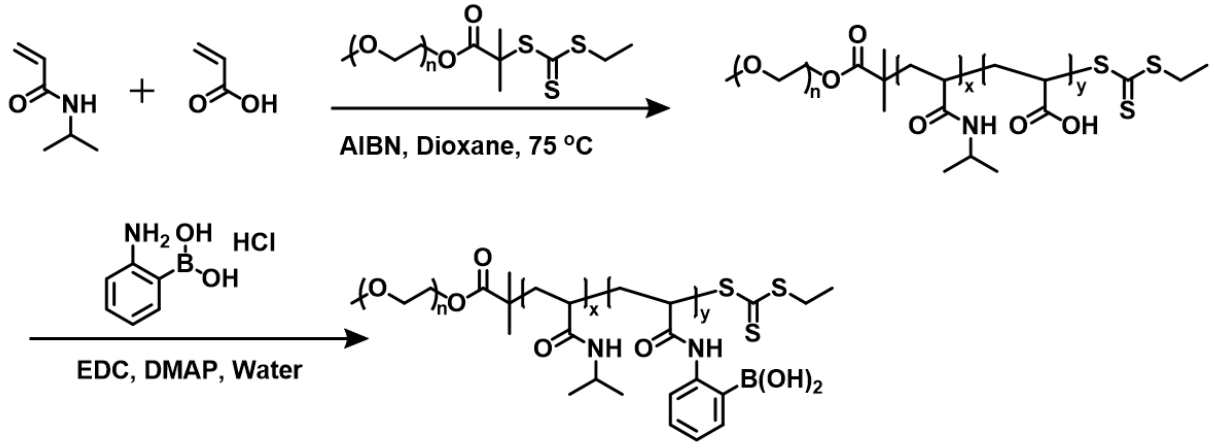

Figure 3.2 Synthesis of PEG-b-p(NIPAM-co-2APBA) via RAFT polymerization of NIPAM and AAc with PEG chain transfer agent followed by coupling of 2-APBA using carbodiimide chemistry

We designed a block copolymer-based hydrogel for a glucose-responsive glucagon delivery system. First, using a PEG chain transfer agent (CTA) (**Figure 3.9**), we employed RAFT to polymerize NIPAM and acrylic acid, followed by carbodiimide coupling to functionalize the acrylic acid with 2-amino phenyl boronic acid (**Figure 3.2,10-11**). This particular boronic acid was chosen because, unlike other commonly reported boronic acids, upon binding with glucose the charge remains unchanged because the B-O dative bond with the carbonyl oxygen inherently stabilizes the negative tetrahedral geometry. Several unsuccessful attempts to assess polymer size via gel permeation chromatography were made. A number of different solvents were screened including dimethylformamide, dimethylsulfoxide, tetrahydrofuran, and 200 mM Na_2SO_4 with 20% acetonitrile. The polymers were not reproducibly observed on the chromatograms, most likely due to some interaction of the boronic acids with the column. Therefore, the polymer molecular weight was calculated by ^{1}H NMR.

Table 3.1 Influence of relative PEG length on LCST determined by turbidity measurements via UV-Vis at 600 nm. Polymer was prepared at 10 wt % in 20 mM DPBS pH 7.4

Number	PEG (Da)	Total (Da)	mol % APBA	LCST (°C)
1	550	15400	20	42.6
2	550	8800	20	43.4
3	750	22000	19.5	42.9
4	750	5900	16	44.8
5	1000	16000	16.5	43.3
6	1000	6900	18.5	47.3
7	2000	38400	17.5	46.5
8	2000	6900	19.5	63.3
9	5000	36100	16	46.8
10	5000	13900	16	54.0

Using the well-known thermo-responsive polymer, p(NIPAM), along with different lengths of PEG, the effect of the lower critical solution temperature (LCST), and subsequently the gel point, based on the relative ratios of the two components was examined. Previous work by Zhang and co-workers demonstrated the influence of 2-APBA content on the LCST of the polymer. The influence of PEG on LCST was explored in the study summarized in this report.[21] The LCST for p(NIPAM) alone is 32 °C.[24] The addition of hydrophilic moieties to p(NIPAM), like 2-APBA, is known to increase the transition temperature.[25] As such, longer lengths of PEG, and higher overall ratios of PEG, increased the transition temperature. Comparing two different length polymers for each PEG size, the difference in the LCSTs exemplify this trend (**Table 3.1, Figure 3.31**). For each PEG length used, the LCSTs of two polymers, one longer and one shorter, are compared to demonstrate this point. As such, PEG5000 increased the LCST the most and required long chains of the NIPAM-2APBA block to tune the LCST back down to the physiological temperature range. In contrast, PEG550 and PEG750 affected the LCST minimally as the LCST difference between the two polymers for each PEG CTA length in each category is under 1 and 2

ºC, respectively. The minor differences in the mole percent of 2-APBA can subtly affect the LCST as well. From here, we decided to proceed with PEG2000 polymers as a middle ground as it allowed for a wide range of LCSTs based on modifications to polymer chain length.

Hydrogel Formation by Dynamic Glucose Crosslinking

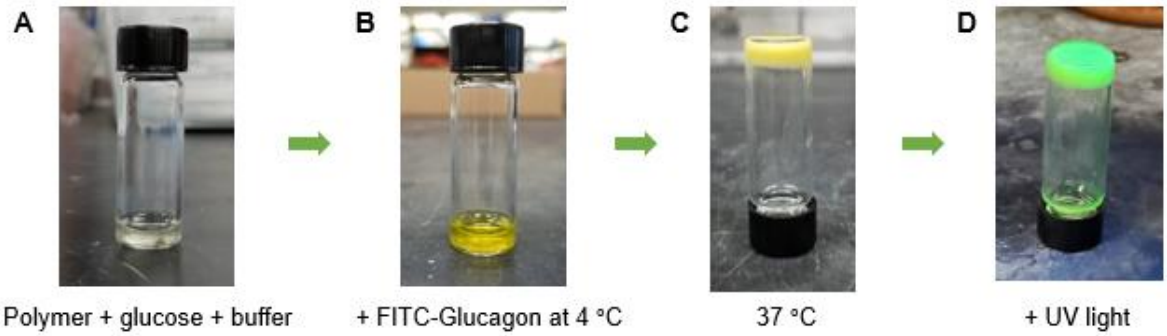

Figure 3.3 Hydrogel formation starting with A) a solution of polymer, glucose, and buffer dissolved at 4 ºC followed by B) the addition of FITC-glucagon as a visual guide. C) Hydrogel was formed at 37 ºC with D) UV light demonstrating the evenly distributed FITC-glucagon

There are many reports of using dynamic crosslinking in hydrogels.[26–32] Reversible covalent bonds are attractive design features in hydrogels because they allow an external stimulus to control the sol-gel transition. Another added advantage is that mesh size becomes much less important of an issue with regard to drug diffusion and release from the system. Some of the most commonly reported reversible crosslinking is based on chemistries utilizing imines, hydrazones, oximes, thiol-disulfides, and boronate esters.[29,33,34] In this work, glucose is utilized as the crosslinker due to the dynamic covalent bonds that phenylboronic acids form with 1,2 and 1,3 diols. The use of glucose alone as a crosslinker has been reported in literature.[35] Ideally, at normoglycemia levels, the hydrogel is intact due to the presence of glucose crosslinks and at hypoglycemia levels, the hydrogel crosslinks are slowly removed to release glucagon.

Crosslinking via bis-glucose boronic acid binding has been demonstrated numerous times in literature[26,27,36] and is one of two main mechanisms for the hydrogel formation herein. The second mechanism being that glucose also acts as an additive, structuring water in its proximity, changing the hydration state of the thermoresponsive pNIPAM chain to depress the LCST of the polymer and the gel point of the hydrogel.[23] The presence of the boronic acid moiety helps localize this effect closer to the pNIPAM chain.

To form the hydrogel, the polymer was dissolved in carbonate buffer with glucose under refrigeration, below the LCST, to aid the solubilization of the polymer. At 4 ºC, due to the thermoresponsive nature of the polymer, the solubility was higher and therefore aids in the dissolution of the polymer. Once the solution was homogeneous, the vial was placed into a 37 ºC incubator and the solution slowly solidified into an opaque gel. As a visual aid, the hydrogel formation and glucagon encapsulation process were demonstrated using glucagon labelled with fluorescein isothiocyanate (FITC) (**Figure 3.3**). Once the polymer, glucose, and buffer were a homogeneous solution at 4 ºC (**Figure 3.3A**), FITC-glucagon was added to the vial and allowed to mix on a rocker at 4 ºC for 10 min (**Figure 3.3B**). The vial was removed from refrigeration and allowed to solidify at 37 ºC. The vial inversion test confirmed the gelation (**Figure 3.3C**) and UV light was applied to demonstrate the encapsulation of the FITC-glucagon (**Figure 3.3D**).

Because of the various responsive components of this model, a number of formulations had to be examined to ensure that the gel point and glucose sensitivity were close to 37 ºC and 1 mg/mL, respectively. The gel point of the hydrogel was tuned based on the LCST of the polymer. Because glucose acts as an additive and lowers the LCST, the polymer alone should ideally have a LCST slightly higher than 37 ºC. Tuning the glucose sensitivity to a physiologically relevant level posed a bigger challenge. Initially, following commonly reported literature protocols,[37–39] the

Table 3.2 Glucose concentration to form hydrogel crosslinks at 10 wt % polymer in 20 mM DPBS pH 7.4

Number	PEG (Da)	Total (Da)	mol % APBA	Glucose sensitivity (mg/mL) at 37 °C	LCST°C
11	2000	15000	20	650	44°C
12	2000	22600	16.6	450	39.3°C
13	2000	38600	17.6	100	37.7°C
14	2000	48900	24.4	45	gel point >37°C
15	2000	53000	17.3	2 (36°C)	<36°C

hydrogel was formed with 10 wt % polymer and the glucose sensitivity was determined by slowly adding concentrated aliquots of glucose solution. This proved to be a rather time-consuming way to study and tune the glucose sensitivity because it would require that a new polymer be synthesized with each result. Using this method, we were able to successfully form a library of hydrogels in which the glucose sensitivity could be tuned with PEG content. However, it must be noted that the glucose sensitivity was often 10-600 fold of the physiological level (**Table 3.2**) which could be irrelevant for further clinical applications. With this set of experiments, we elucidated that the closer the LCST of the polymer was to 37 ºC, the greater the glucose sensitivity, likely because less glucose was required to depress the LCST to 37 ºC.

Influence of Polymer Weight Percent on Hydrogel Formation

At this point, the polymer concentration was varied to examine the effects on the glucose sensitivity and gel point. For the application of this system, the necessary working temperature, 37 ºC, and glucose sensitivity, 1 mg/mL, are already determined by physiological conditions. To demonstrate if the polymer wt % alone could shift the gel point, polymer solutions of 10 – 30 wt %

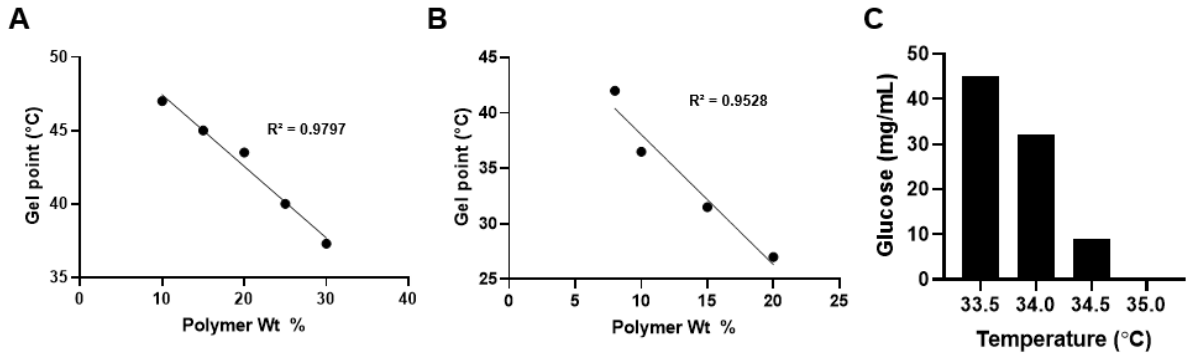

Figure 3.4 Dependence of polymer concentration (wt %) on the gelation temperature for A) polymer 16 and B) polymer 17 and C) the temperature dependent glucose concentration needed for gelation for polymer 5 at 30 wt %

were prepared in carbonate buffer. With these solutions, the temperature was incrementally increased and stabilized to determine the gel point. This shows the gel point is inversely related to the polymer wt % in a linear fashion (**Figure 3.4A,B**). Upon confirmation of these results, the polymer wt % was held constant and the temperature was varied to assess the necessary glucose concentration to form a hydrogel at a certain temperature (**Figure 3.4C**). After observing these trends, temperature and glucose concentration were kept constant at physiological levels and the polymer wt % was gradually increased to observe gelation. Interestingly, this confirmed that glucose sensitivity could be controlled and tuned to normoglycemia (or the desired glucose level) simply by varying the polymer concentration. A higher polymer wt % pushes the material to its saturation point so that a smaller glucose level will induce gelation. In addition, more polymer automatically translates to more boronic acid moieties in the vial, increasing the opportunity for glucose-boronic acid binding. Subsequently, two polymer formulations responsive to 1 mg/mL glucose at 37 ºC, polymer 18 and 19 (**Table 3.3**), were identified and prepared for glucagon release studies. A value of 1 mg/mL glucose was chosen as a middle range number for normoglycemia.

Glucagon Loading and Release from Hydrogel

Glucagon loaded hydrogels were prepared by dissolving the polymer in carbonate buffer pH 9.0 followed by the addition of glucose and glucagon as solutions. Polymer 18 was prepared at 19 wt % and polymer 19 at 32.5 wt % to allow for glucose responsivity at 1 mg/mL. The final glucagon concentration was 1 mg/mL. The contents were allowed to mix for 30 minutes at 4 ºC then pipetted into lo-bind centrifuge tubes (n = 3 control, n = 3 release) as a clear, thick liquid. The vials were placed in a 37 ºC incubator and allowed to gel for 30 minutes prior to the start of release. The clear viscous liquid turned into an off-white opaque gel. The vial inversion test was used to confirm the gelation. To initiate the release, 800 uL of 0 or 1 mg/mL glucose in 20 mM DPBS pH 7.4 was added to each vial with shaking at 250 rpm. Aliquots to determine glucagon release were taken at 5 min, 30 min, 1 h, 2 h, 4 h, 7 h, 16 h, 24 h, and 48 h. Polymer 18 shows statistical difference between the control and release starting at 7 h (**Figure 3.5A**) while polymer 19 shows statistical difference at 14 h (**Figure 3.5B**). At 48 h, polymer 18 shows release of up to 80% (240 ug) of glucagon and polymer 19 shows up to 40% (120 ug). Compared to their respective controls, polymer 18 released up to 40% (120 ug) and polymer 19 released up to 20% (60 ug) more glucagon when in hypoglycemic condition. The difference in the overall payload release between polymers 18 and 19 can be largely attributed to the final polymer wt % that was used. The higher polymer concentration that was used for polymer 19 creates a denser hydrogel network making it more difficult for the glucagon to diffuse out at low glucose concentrations. As is the case with many drug delivery systems,[40] some background release of glucagon was detected. Due to the methods and principles behind our hydrogel formation and release, some of the glucagon is reasonably expected to be on the surface of the gel and can be accounted for some of the payload, particularly in the initial timepoints. In addition, a macroscopic difference of the control and release vials can

be observed at the end of the 48-hour release study. The control group vials showed hydrogels that are largely intact with little dissolution (**Figure 3.5C**) while the release group vials showed

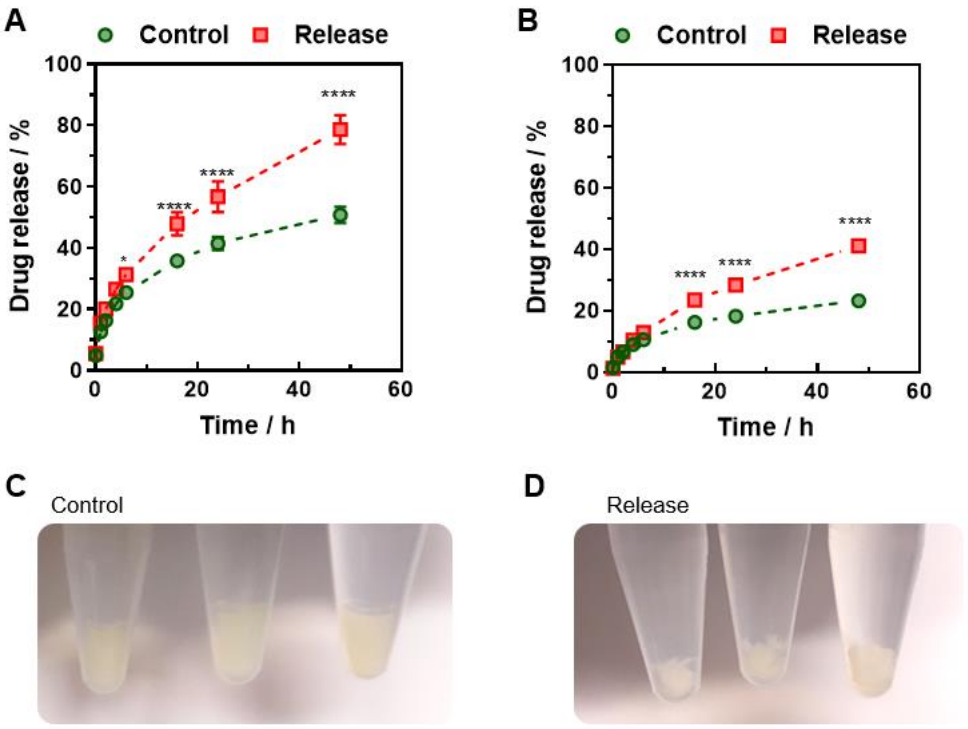

Figure 3.5 Glucagon release study using A) polymer 18 at 19 wt% and B) polymer 19 at 32.5 wt% over 48 hours. (*p < 0.5, **** p < 0.0001, two-way ANOVA with Sidak's multiple comparisons test) Representative images of hydrogels (n=3) post release study of C) the control group and D) the release group

considerably less remaining hydrogel, indicating that the hydrogel had dissolved and released glucagon in response to the hypoglycemic environment (**Figure 3.5D**).

Rheology and Injectability of Hydrogel

There is a growing interest in injectable hydrogels that can gelate *in situ* upon injection because it eliminates the need for complicated surgical procedures.[41,42] Shear-thinning properties are desirable as it will enable flow under modest pressure followed by self-healing gelation in a

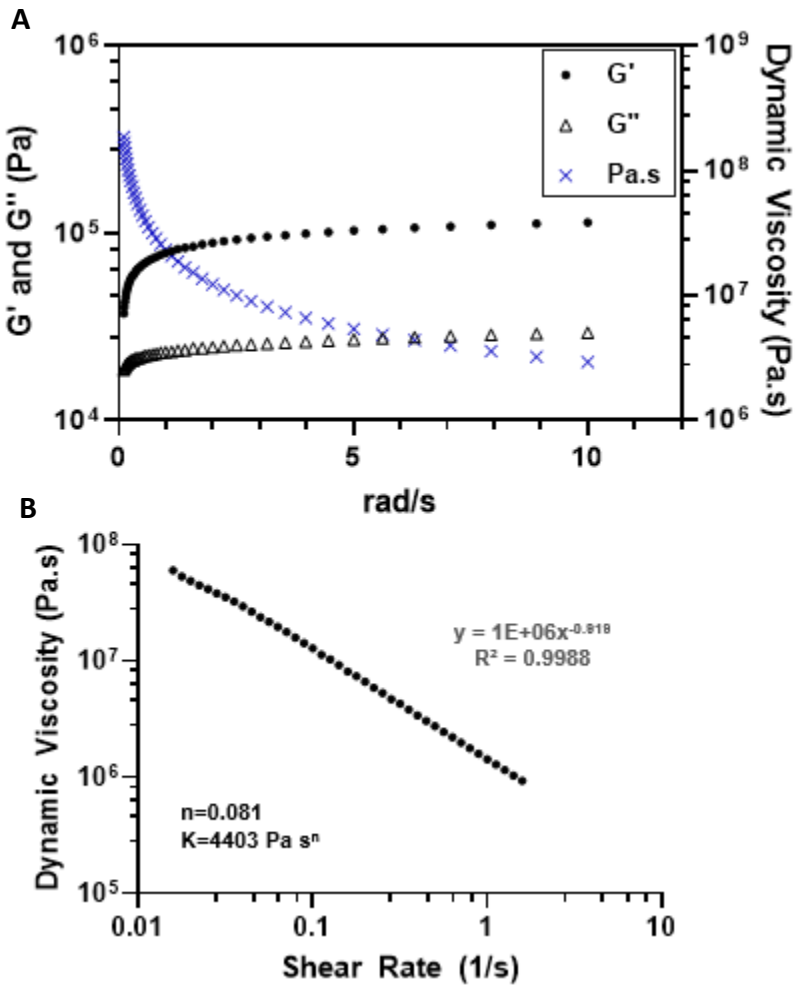

Figure 3.6 A) Rheological measurement of polymer 20 at a constant strain of 1%, and an angular frequency range of 0.1 to 10 rad s^{-1} plotted with **B)** Ostwald-de Waele power law

reasonable amount of time.[41,43–45] To assess the mechanical properties of our hydrogel, a frequency sweep with constant 1% strain was applied at 22 ºC to a preformed hydrogel of polymer 20 (**Table 3.3**) at 10 wt %. The storage modulus (G') values exceed the loss modulus (G") values which indicates that our formulation presents hydrogel characteristics (**Figure 3.6A**). Shear-thinning is supported by the decreasing dynamic viscosity. To further confirm this, the dynamic viscosity and shear rate were plotted according to the Ostwald-de Waele power law (**Figure 3.6B**). The flow behavior index, n, is a value below 1, indicating a shear-thinning pseudoplastic fluid. The flow

consistency index, K, was calculated to be 4403 Pa s^n. Next, to study the injection force of our hydrogel, the hydrogel formed from polymer 19 was loaded into a syringe as a liquid at 4 ºC and eluted through a viscometer at 25 ºC (**Table 3.4**). Many drugs, including injectables, are commonly administered at room temperature unless particular requirements are indicated so the viscosity was measured at 25 ºC. Due to the instrument limitations, the viscosity data was measured at 0.000192

A

$$F = \pi R_b{}^2 \left(\frac{2L_n}{R_n}\right)\eta\left(\frac{Q}{\pi R_n{}^3}\left(3+\frac{1}{n}\right)\right)$$

B

Needle	21 G	25 G	27 G	29 G
Force (N)	0.00289	0.0441	0.103	0.176
Force (mPa)	2.89	44.1	103	176

Flow rate = 0.000192 mL/sec

C

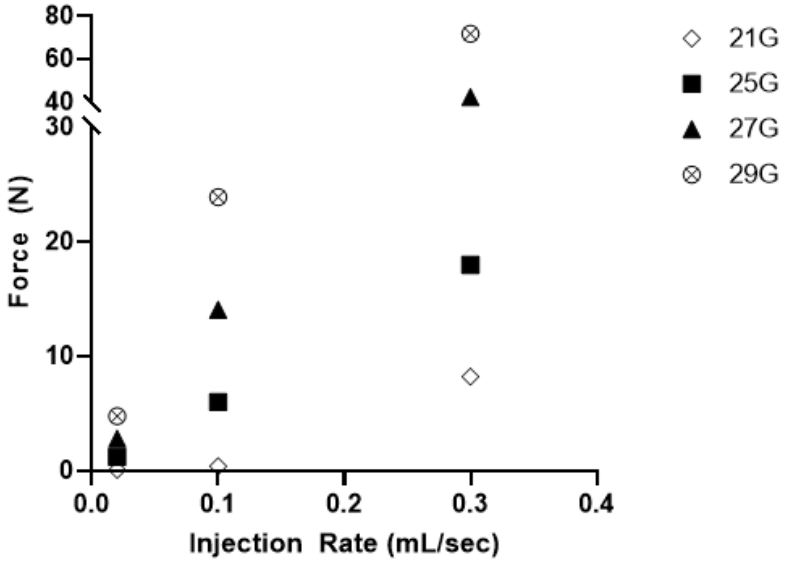

Figure 3.7 A) Simple shear-thinning fluid injection force equation. **B)** Injection force at assumed needle and barrel dimensions at measured flow rate of 0.000192 mL/sec. **C)** Injection force at assumed needle and barrel dimensions at hypothetical flow rates

mL/sec. Viscosity measurements from the viscometer as well as the power index, n, from the rheometer were applied to a simple shear thinning fluid equation to calculate the injection force (**Figure 3.7A**). Using assumed needle and barrel measurements for a typical 1 mL syringe and ½ inch needle (**Table 3.5**),[46] the injection force at various relevant gauges and injection rates were calculated. At the measured injection rate, the injection force ranged from 0.002 to 0.18 N (**Figure 3.7B, Table 3.6**). The measured injection rate, however, is three orders of magnitude smaller than typical used injection rates of 0.1 to 0.3 mL/sec.[47,48] At 0.1 mL/sec, 21G, 25G, and 27G were under 20 N which is the threshold for patient discomfort (**Table 3.7**).[49] At 0.3 mL/sec, 21G and 25G were under 20 N (**Figure 3.7C, Table 3.8**). For subcutaneous injections, 25G and 27G needles of ½ inch are most commonly used.[41,46] Taking all of this into account, a 25G needle at 0.1 and 0.3 mL/sec or a 27G needle at 0.1 mL/sec are most suitable for subcutaneous administration of our hydrogel models.

The hydrogel system described herein demonstrates a proof of concept sustained delivery of native glucagon targeted for nocturnal hypoglycemia. In order to bring this model forward, more optimization of the polymers and hydrogel will be necessary in order to ensure glucagon releases at 0.6 mg/mL glucose, an upper threshold for hypoglycemia, rather than the 0 mg/mL glucose concentration used in this work. In addition, glucagon leakage can lead to instabilities in blood glucose levels which, at normoglycemia, has the potential to cause hyperglycemia.

3.3 Conclusion

In conclusion, dual thermo- and glucose-responsive polymers of PEG-*b*-p(NIPAM-*co*-2-APBA) in conjunction with dynamic glucose crosslinking was used to formulate a hydrogel for sustained release of native glucagon. To optimize the system, the polymer size, block lengths, and

polymer concentration were screened to determine the effect of each parameter. In two separate formulations, the hydrogels released a total of 80 and 40% of the total loaded glucagon and 30 and 20% more than their respective controls. In addition, rheological measurements were used to assess the shear-thinning and injectable nature of our hydrogel, which showed that our hydrogel model is suitable for subcutaneous administration. Finally, to the best of our knowledge, this is the first demonstrated sustained release of native glucagon using a glucose responsive hydrogel with potential to combat nocturnal hypoglycemia.

Acknowledgements

The authors thank the Leona M. and Harry B. Helmsley Charitable Trust for the funding of these studies as well as Prof. Gaurav Sant at UCLA for the use of his AR 2000ex rheometer.

3.4 Appendix B

Materials

All chemicals were purchased from Sigma-Aldrich and Fisher Scientific and were used without purification unless noted otherwise. N-Isopropylacrylamide was recrystallized from n-hexane. α,α′-Azoisobutyronitrile was recrystallized from acetone. Acrylic acid was distilled under vacuum. Anhydrous dimethylsulfoxide was obtained by drying over molecular sieves. Glucagon was purchased from BioMatik at >90% purity.

Analytical Techniques

Nuclear magnetic resonance (NMR) spectra were recorded on a Bruker AV 400 MHz spectrometer. Nanogel turbidity was measured with 10 mg/mL solution in 20 mM DPBS pH 7.4 at 600 nm on a Tecan M1000 plate reader or SpectraMax iD3 plate reader. To determine hydrogel

mechanical properties, an AR 2000ex rheometer (TA instruments) in parallel plate geometry was used with an 8-mm diameter stainless steel, cross-hatched upper plate and 60 mm stainless steel, cross-hatched lower plate cover, at 22 °C, constant strain of 1%, and an angular frequency range of 0.1 to 10 rad s^{-1}. Viscosity was measured using a RheoSense microVisc.

Methods

Synthesis of CTA acid 2-(((ethylthio)carbonothioyl)thio)-2-methylpropanoic acid

Product was synthesized in accordance with previously reported literature.[50]

Representative Synthesis of PEG-CTA

In an oven-dried round bottom, methoxyPEG_x was added to a solution of 2-(((ethylthio)carbonothioyl)thio)-2-methylpropanoic acid, dimethylaminopyridine, and N,N'-dicyclohexylcarbodiimide in anhydrous DCM with a stir bar. The reaction was allowed to stir at 25 ºC for 20 h. The urea byproduct was filtered out and the supernatant was evaporated under reduced pressure and the product was purified by flash chromatography (DCM to DCM/MeOH 8/2 gradient). A yellow-colored solid was obtained as product (70.3% yield).

Representative RAFT Polymerization of PEG-b-p(NIPAM-AAc)

In an oven-dried Schlenk tube, stock solutions of NIPAM, PEG CTA, acrylic acid, and AIBN in dry DMSO were added with a stir bar. The tube was sealed off and subjected to three freeze, pump, thaw cycles. The polymerization was carried out at 75 °C for 2 h under argon. Polymerization was quenched by opening to air and submerging the tube into cold water. Crude reaction was carried forward directly. A small aliquot of the crude reaction was saved for ^{1}H NMR analysis in d-DMSO. NIPAM conversion was calculated by comparing the areas under the peak

of monomeric and polymeric amide peak at 7.9 ppm and 6.9-7.6 ppm, respectively. AAc mol% was calculated by comparing the area under the peak of AAc polymeric acidic peak at 11.8-12.1 ppm and NIPAM polymeric amide peak at 6.9-7.6 ppm. DP_{NIPAM} was calculated by comparing PEG glycolic peak at 3.4-3.5 ppm and NIPAM polymeric amide peak at 6.9-7.6 ppm. DP_{AAc} was calculated by comparing PEG glycolic peak at 3.4-3.5 ppm and AAc polymeric acidic peak at 11.8-12.1 ppm. $M_{n,NMR}$ was calculated according to the formula $M_{n,NMR} = MW_{PEG\text{-}CTA} + (DP_{NIPAM} * MW_{NIPAM}) + (DP_{AAc} * MW_{AAc})$.

Representative EDC Coupling of 2APBA to PEG-b-p(NIPAM-AAc)

EDC (4 eq.), DMAP (0.5 eq.), and PEG-b-p(NIPAM-AAc) (1 eq. of AAc), were dissolved in water in a round bottom flask and stirred for 20 min. Then, 2-APBA hydrochloride (2 eq.) was added and the reaction was allowed to stir for 24 hr. Afterwards, the solution was dialyzed using a 3.5 kDa MWCO membrane for 3 days against water and lyophilized to yield a fluffy white solid. Polymer molecular weight was determined by ^{1}H NMR. 2-APBA mol% was calculated by comparing the area under the peak of 2-APBA aromatic peak at 6.8-7.5 ppm and NIPAM tertiary isopropyl peak at 3.6-3.9 ppm. DP_{NIPAM} was calculated by comparing PEG glycolic peak at 3.5 ppm and NIPAM tertiary isopropyl peak at 3.6-3.9 ppm. $DP_{2\text{-}APBA}$ was calculated by comparing PEG glycolic peak at 3.5 ppm and 2-APBA aromatic peaks at 6.8-7.5 ppm. $M_{n,NMR}$ was calculated according to the formula $M_{n,NMR} = MW_{PEG\text{-}CTA} + (DP_{NIPAM} * MW_{NIPAM}) + (DP_{2\text{-}APBA} * MW_{2\text{-}APBA})$.

Hydrogel Formation

PEG-*b*-p(NIPAM-2APBA) was dissolved in carbonate buffer pH 9.0 at a specified weight % on a rocker at 4 ºC, for 16 h. Once the solution was homogeneous, it was pipetted into a 1.5 mL lo-bind tube along with a glucose solution in carbonate buffer pH 9.0. For glucagon release studies,

glucagon was added to the vial at this time as a solution in carbonate buffer pH 9.0. The vial was placed in an incubator at 37 °C. The contents of the vial turned opaque indicating hydrogel formation. The full formation of the hydrogel was confirmed by the inverted tube test.

Glucagon Release Studies

300 µL of pre-hydrogel solution was carefully pipetted into 1.5 mL lo-bind vials. Upon confirming full gelation, 800 uL of either 20 mM DPBS pH 7.4 (release) or 20 mM DPBS pH 7.4 with 1 mg/mL glucose (control) were added. Vials were placed on a thermoshaker at 37 °C and 250 rpm. Timepoints were taken by removing all of the supernatant and replenishing with 20 mM DPBS pH 7.4 (release) or 20 mM DPBS pH 7.4 with 1 mg/mL glucose (control). Timepoints were frozen at -20 ºC until ready for analysis. Glucagon was quantified via fluorescamine assay. 30 uL of fluorescamine (3 mg/mL in DMSO) was added to 120 uL of sample in a 96-well plate. The plate was shaken and incubated for 5 minutes, then scanned on the plate reader (λ_{ex} = 382 nm, λ_{em} = 480 nm).

Rheology

Hydrogel, without glucagon, was pre-formed in a 4 mL dram vial. The hydrogel disc was carefully removed from the dram vial using a spatula and placed onto the parallel plate for measurement.

Viscosity

The hydrogel solution, without glucagon, was allowed to homogenize at 4 ºC and then loaded into a Rheosense syringe. Air bubbles were carefully removed from the syringe. Syringe

was loaded into the viscometer and allowed to equilibrate at the measurement temperature for 20 minutes.

Table 3.3 Table of polymers in order of introduction in text with PEG size, polymer length, and mole percent of 2-APBA

Number	PEG (Da)	Total (Da)	mol % APBA
1	550	15400	20
2	550	8800	20
3	750	22000	19.5
4	750	5900	16
5	1000	16000	16.5
6	1000	6900	18.5
7	2000	38400	17.5
8	2000	6900	19.5
9	5000	36100	16
10	5000	13900	16
11	2000	15000	20
12	2000	22600	16.6
13	2000	38600	17.6
14	2000	48900	24.4
15	2000	53000	17.3
16	2000	15000	17
17	2000	48100	18
18	2000	34700	16.1
19	2000	15500	12.3
20	550	15000	15

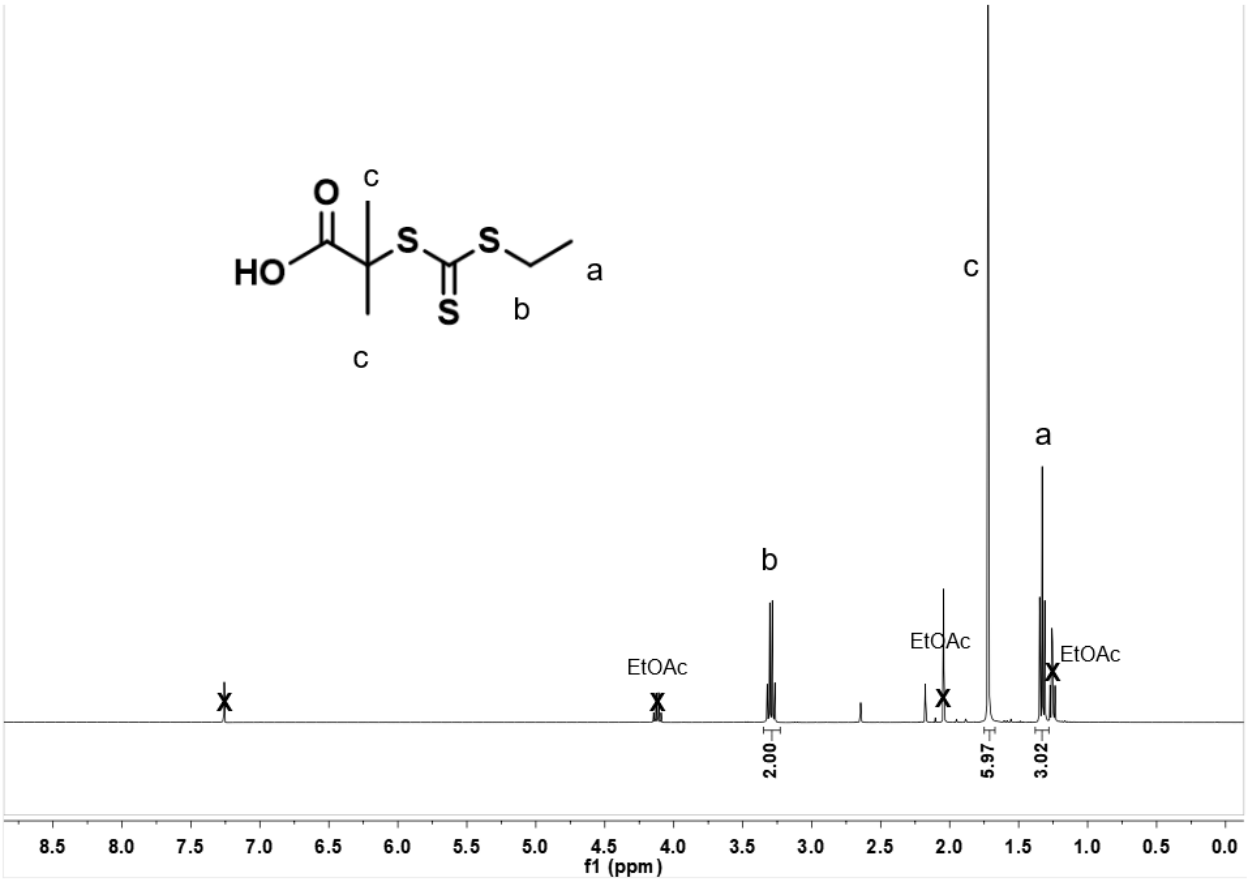

Figure 3.8 ^{1}H NMR of CTA acid. ^{1}H NMR of 2-(((ethylthio)carbonothioyl)thio)-2-methylpropanoic acid (400 MHz, $CDCl_3$).

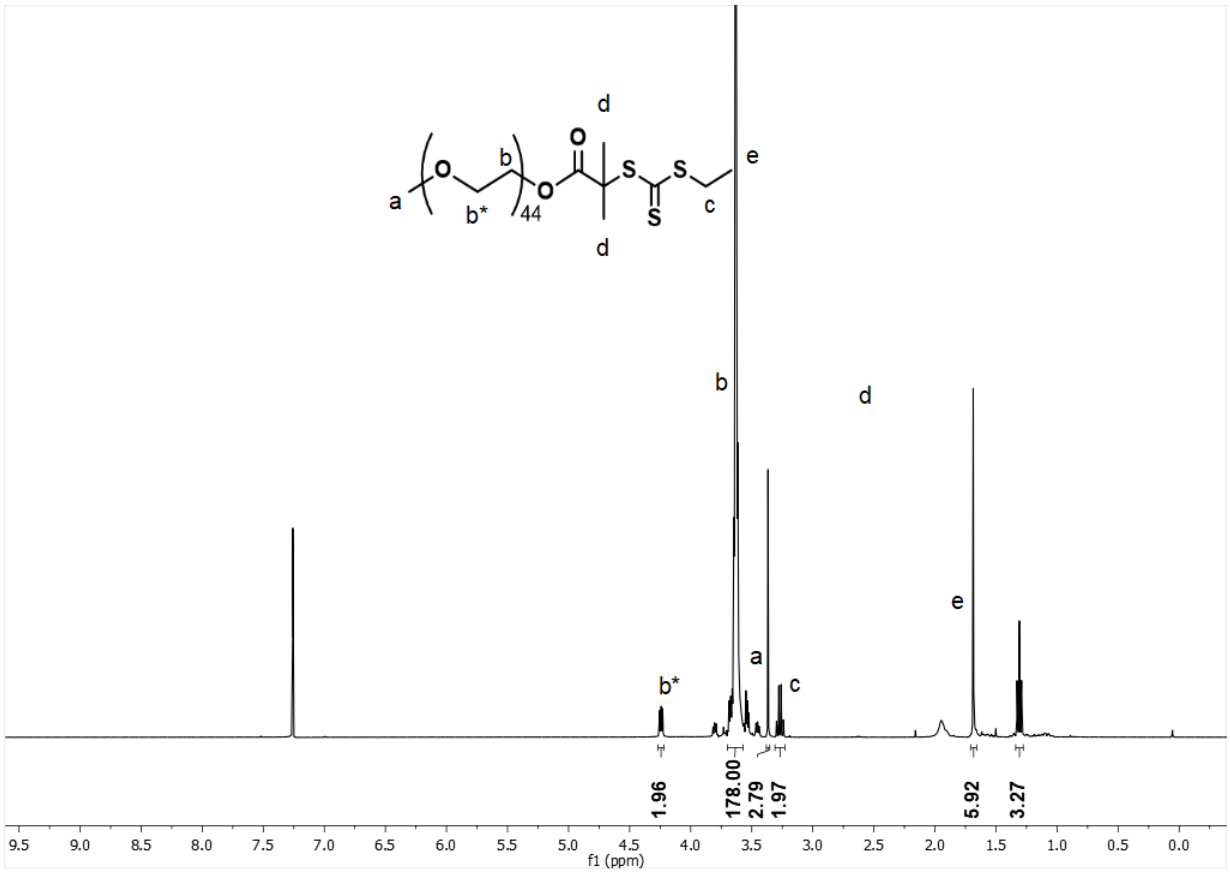

Figure 3.9. Representative ^{1}H NMR of PEG$_{2000}$-CTA. ^{1}H NMR of PEG$_{2000}$-CTA (400 MHz, $CDCl_3$). ^{1}H NMR (400 MHz, CDCl3) δ 4.27 – 4.22 (m, 2H), 3.70 – 3.57 (m, 178H), 3.37 (s, 3H), 3.27 (q, J = 7.4 Hz, 2H), 1.67 (d, J = 9.8 Hz, 6H), 1.31 (t, J = 7.4 Hz, 3H).

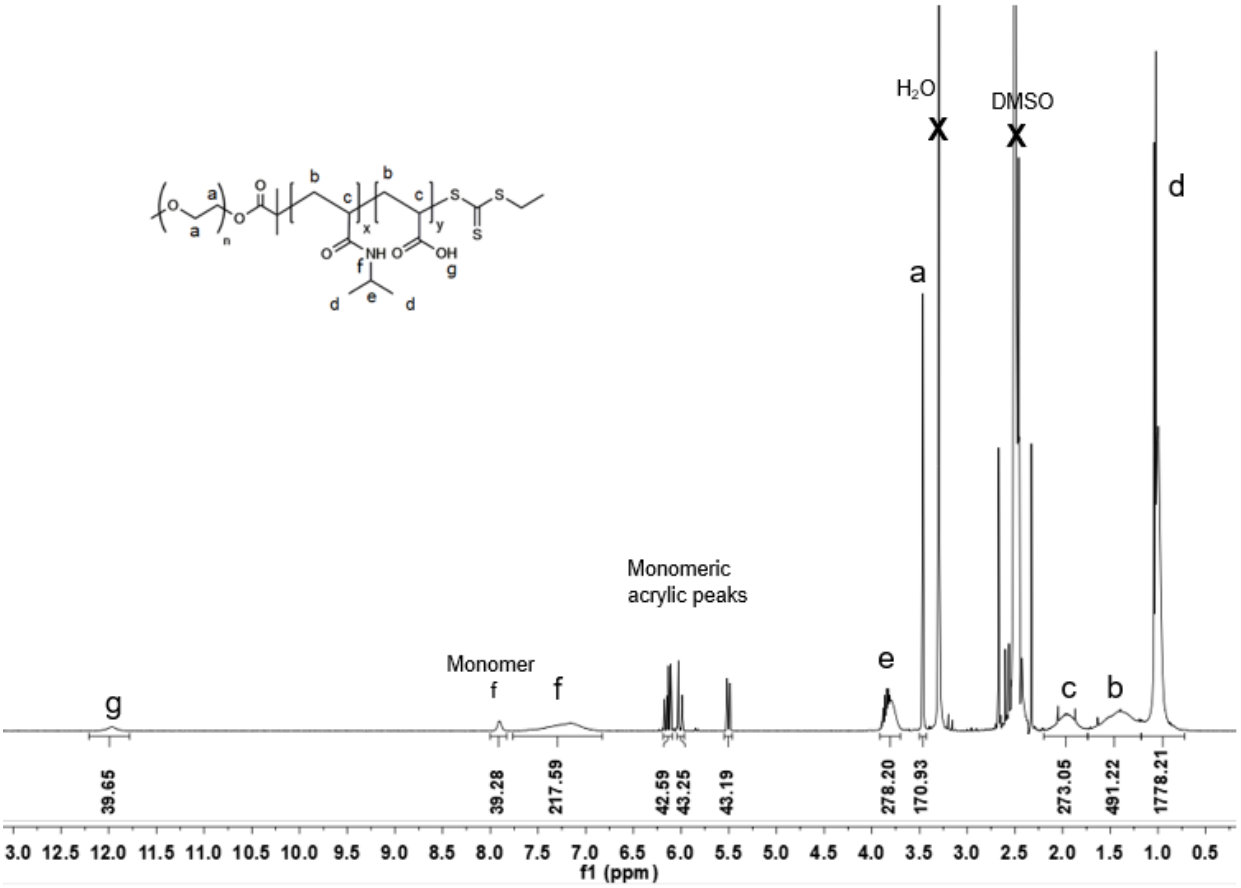

Figure 3.10 Representative ^{1}H NMR of crude PEG$_x$-*b*-(NIPAM-*co*-AAc). ^{1}H NMR of PEG$_{2000}$-*b*-(NIPAM-*co*-AAc) (400 MHz, DMSO). ^{1}H NMR (400 MHz, DMSO) δ 11.96 (s, 39H), 7.16 (s, 217H), 3.85 (m, 278H), 3.47 (s, 170H), 1.96 (m, 273H), 1.76 – 1.16 (m, 491H), 1.12 – 0.75 (m, 1778H).

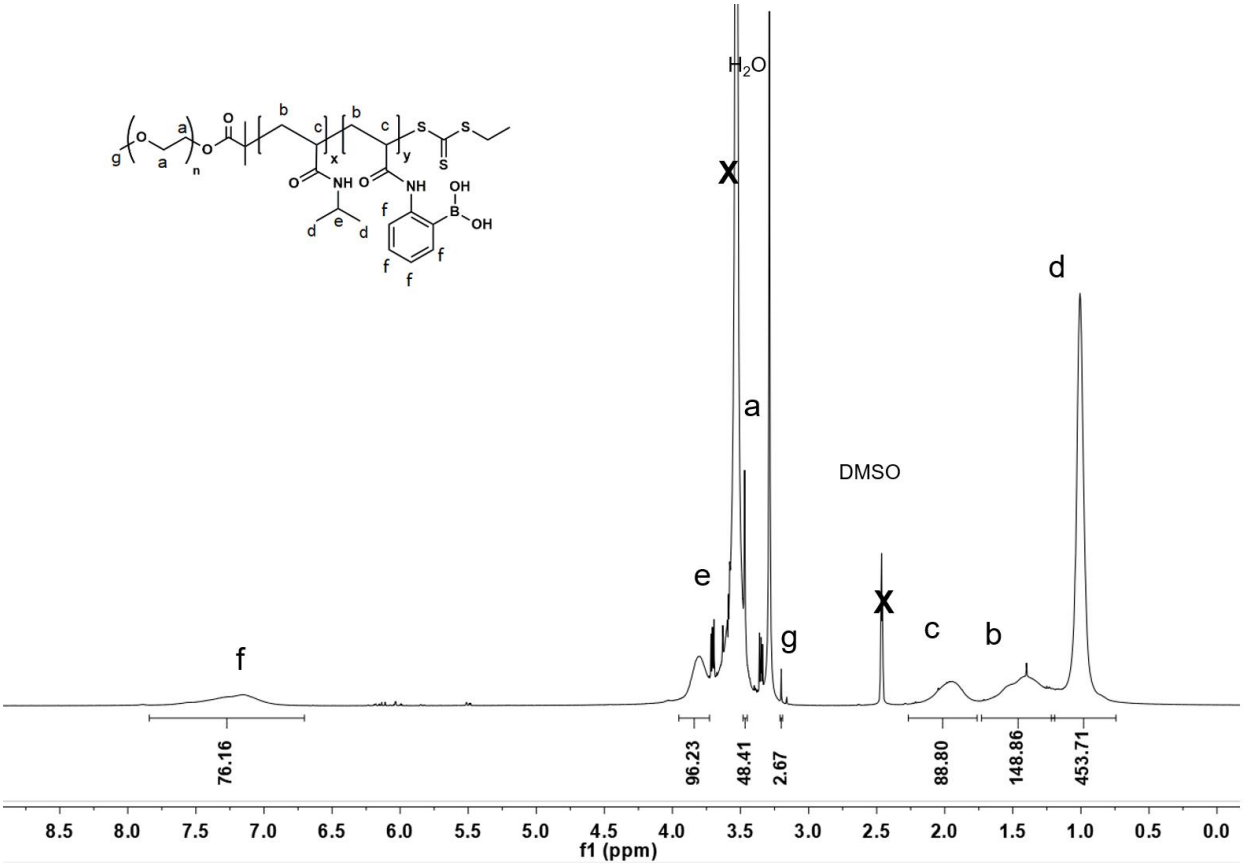

Figure 3.11 Polymer 1 ^{1}H NMR of PEG$_{2000}$-*b*-(NIPAM-*co*-APBA). ^{1}H NMR of PEG$_{2000}$- *b*-(NIPAM-*co*-APBA) (400 MHz, DMSO). ^{1}H NMR (400 MHz, DMSO) 7.16 (s, 76H), 3.85 (m, 96H), 3.47 (s, 48H), 1.96 (m, 88H), 1.76 – 1.16 (m, 148H), 1.12 – 0.75 (m, 453H).

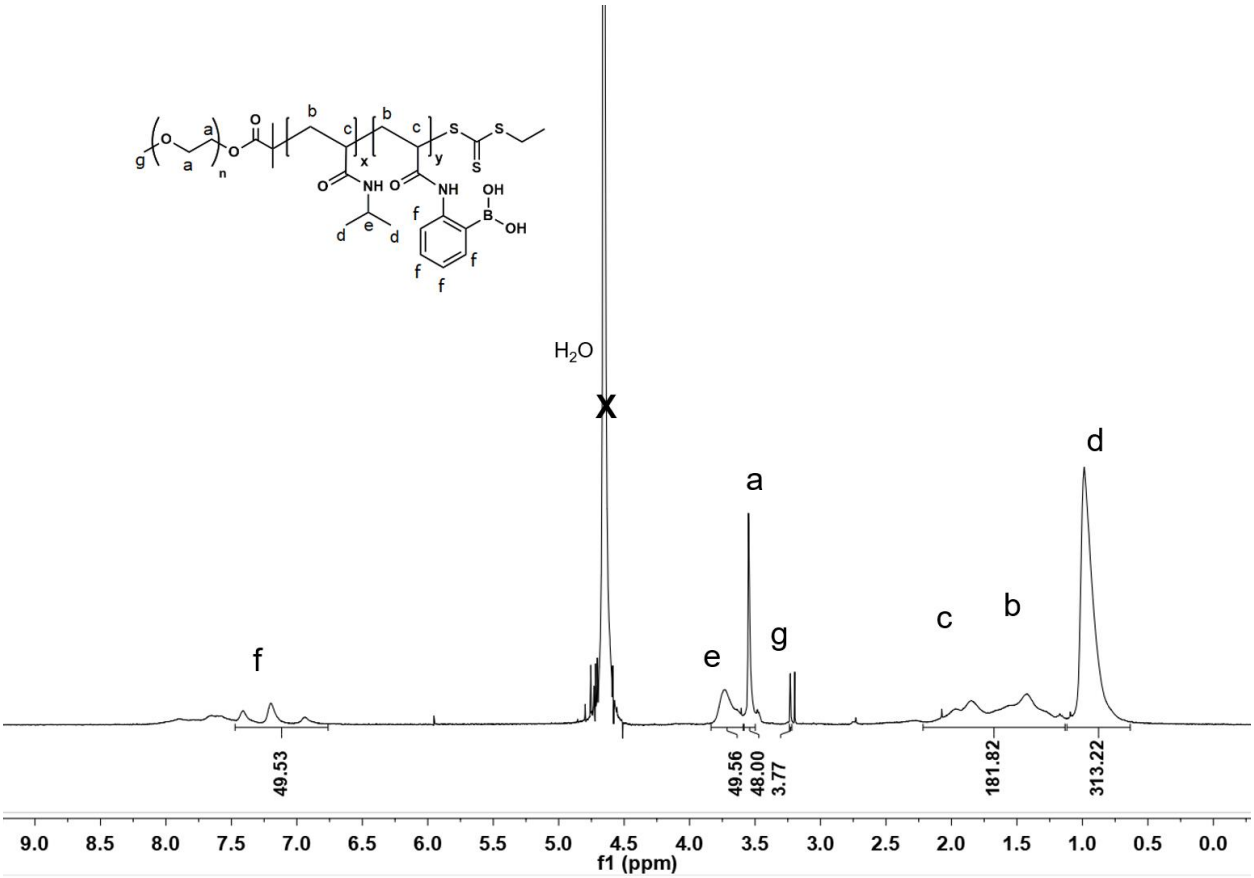

Figure 3.12 Polymer 2 ^{1}H NMR of PEG$_{550}$-*b*-(NIPAM-*co*-APBA). ^{1}H NMR of PEG$_{550}$- *b*-(NIPAM-*co*-APBA) (400 MHz, D_2O). ^{1}H NMR (400 MHz, D_2O) δ 7.20 (t, 49H), 3.74 (s, 49H), 3.57 (s, 48H), 3.30 (s, 3H), 2.18 – 1.15 (m, 181H), 1.00 (s, 1506H).

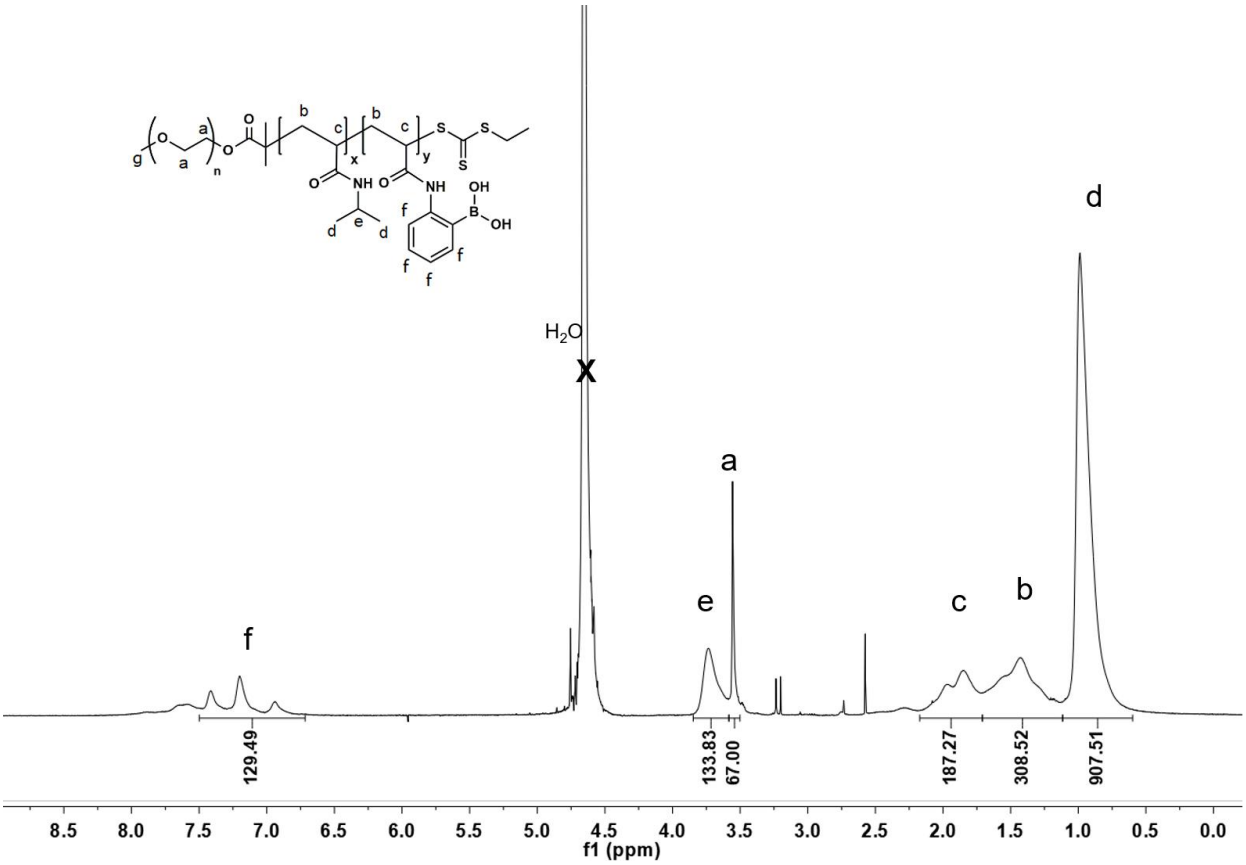

Figure 3.13. Polymer 3 ^{1}H NMR of PEG$_{750}$-*b*-(NIPAM-*co*-APBA). ^{1}H NMR of PEG$_{750}$- *b*-(NIPAM-*co*-APBA) (400 MHz, D_2O). ^{1}H NMR (400 MHz, D_2O) δ 7.20 (t, 129H), 3.74 (s, 133H), 3.57 (s, 67H), 2.18 – 1.74 (m, 187H), 1.74 - 1.25 (m, 308H), 1.00 (s, 907H).

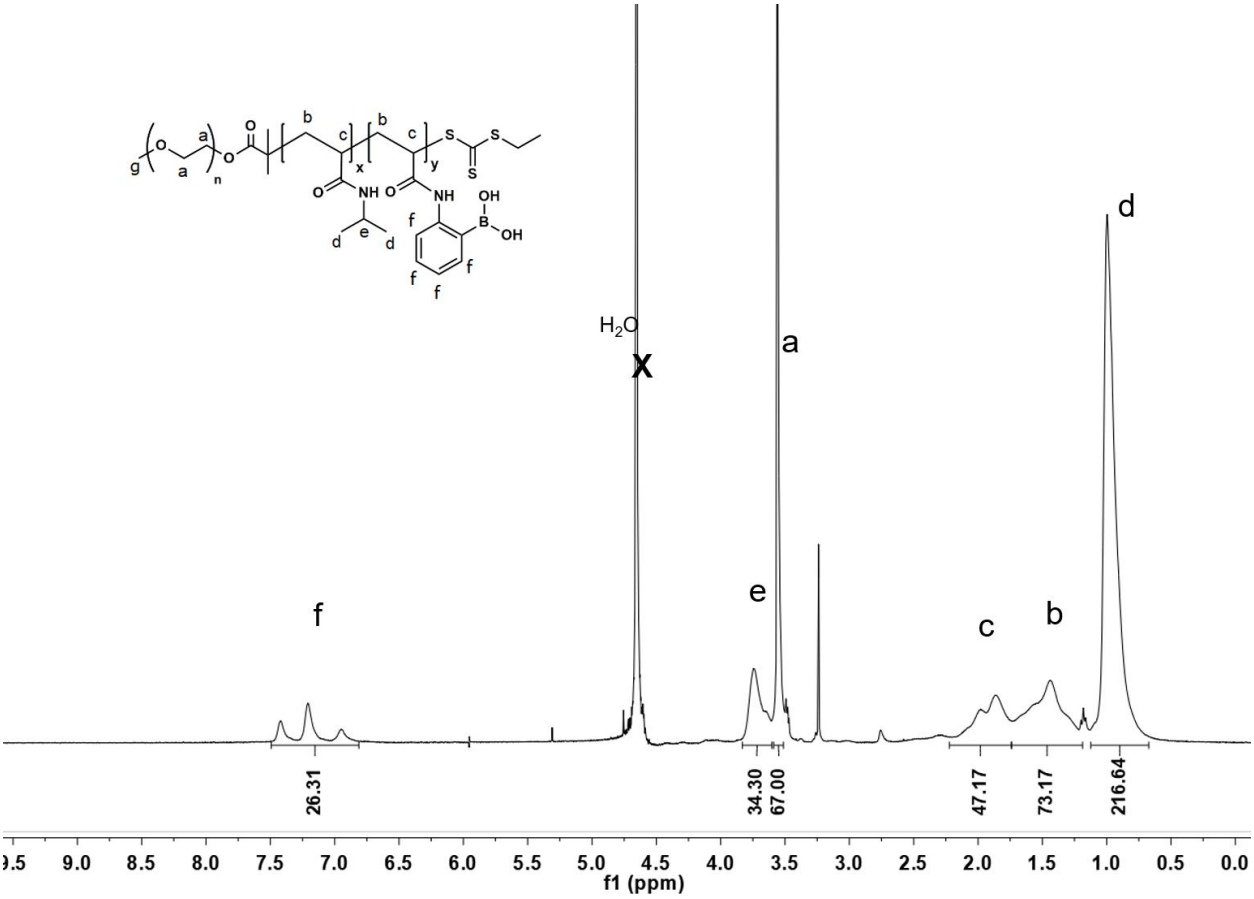

Figure 3.14. Polymer 4 ^{1}H NMR of PEG$_{1000}$-*b*-(NIPAM-*co*-APBA). ^{1}H NMR of PEG$_{1000}$- *b*-(NIPAM-*co*-APBA) (400 MHz, D_2O). ^{1}H NMR (400 MHz, D_2O) δ 7.20 (t, 26H), 3.74 (s, 34H), 3.57 (s, 67H), 2.18 – 1.74 (m, 47H), 1.74 - 1.25 (m, 73H), 1.00 (s, 216H).

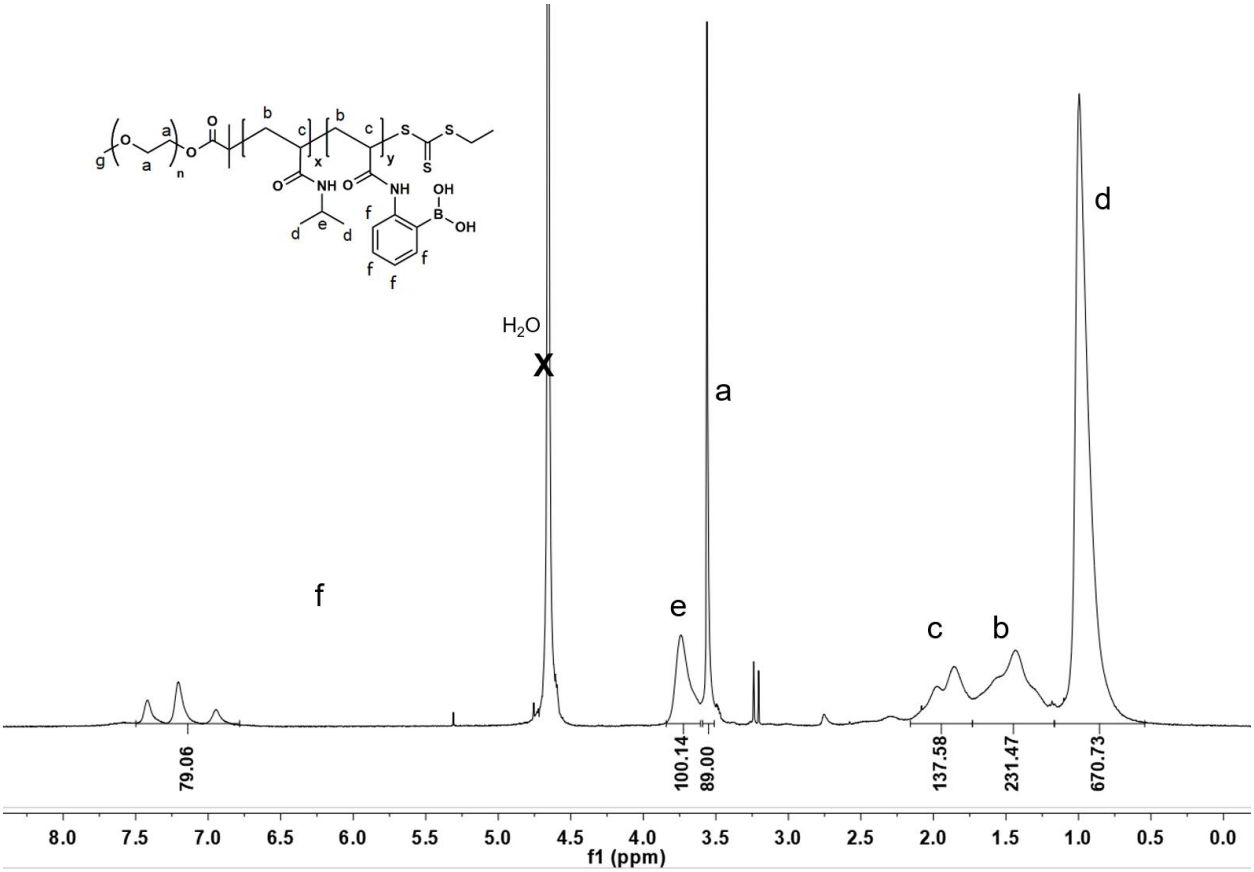

Figure 3.15. Polymer 5 ^{1}H NMR of PEG$_{1000}$-*b*-(NIPAM-*co*-APBA). ^{1}H NMR of PEG$_{1000}$- *b*-(NIPAM-*co*-APBA) (400 MHz, D_2O). ^{1}H NMR (400 MHz, D_2O) δ 7.20 (t, 79H), 3.74 (s, 34H), 3.57 (s, 67H), 2.18 – 1.74 (m, 47H), 1.74 - 1.25 (m, 73H), 1.00 (s, 216H).

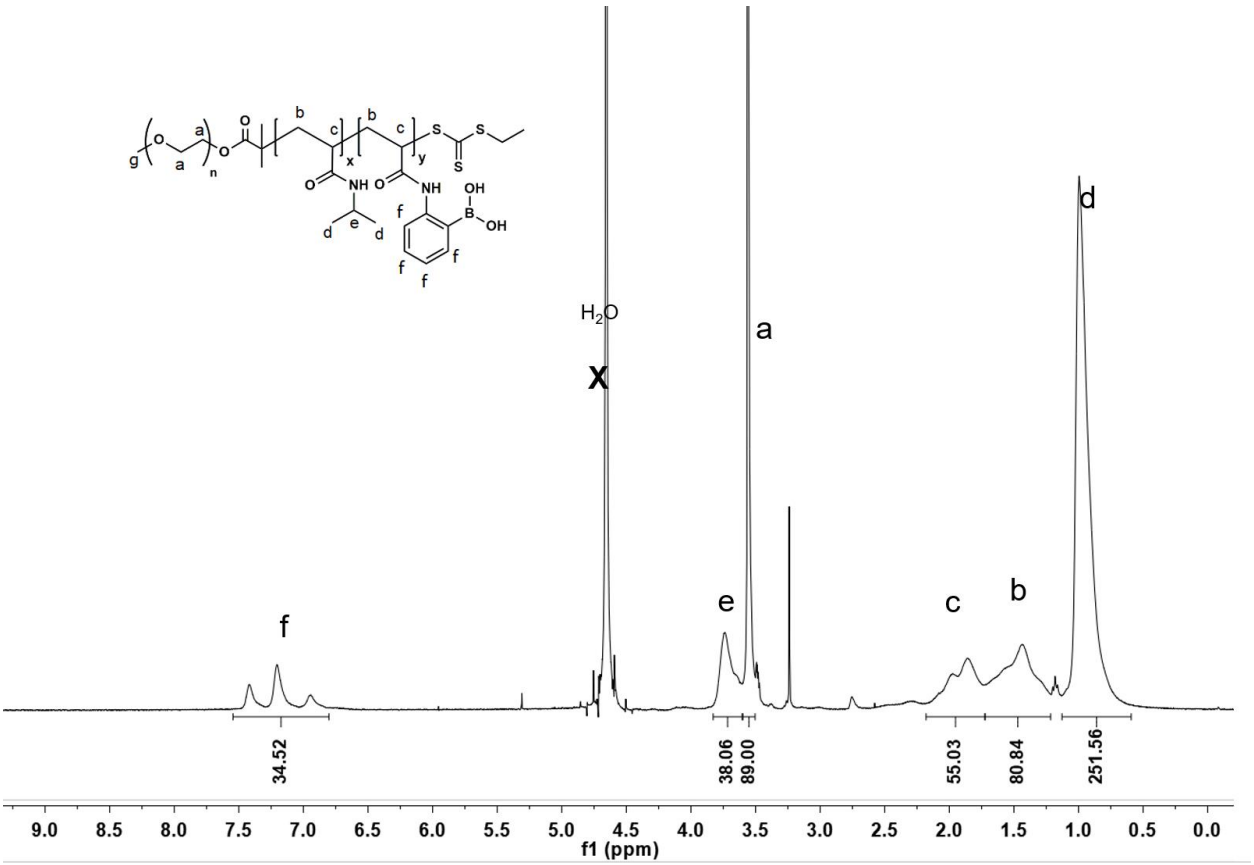

Figure 3.16. Polymer 6 ^{1}H NMR of PEG$_{1000}$-*b*-(NIPAM-*co*-APBA). ^{1}H NMR of PEG$_{1000}$- *b*-(NIPAM-*co*-APBA) (400 MHz, D_2O). ^{1}H NMR (400 MHz, D_2O) δ 7.20 (t, 34H), 3.74 (s, 38H), 3.57 (s, 89H), 2.18 – 1.74 (m, 55H), 1.74 - 1.25 (m, 80H), 1.00 (s, 252H).

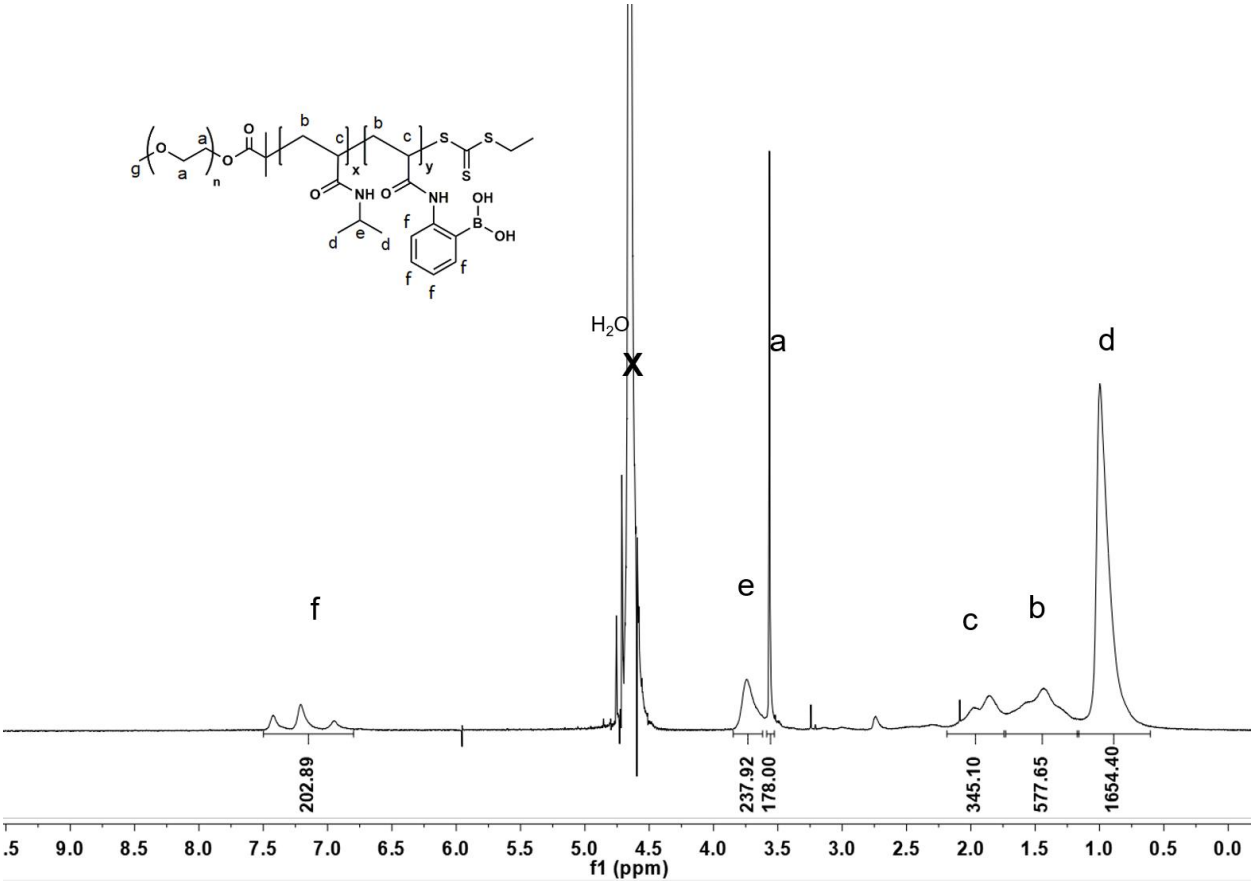

Figure 3.17. Polymer 7 ^{1}H NMR of PEG$_{2000}$-*b*-(NIPAM-*co*-APBA). ^{1}H NMR of PEG$_{2000}$- *b*-(NIPAM-*co*-APBA) (400 MHz, D_2O). ^{1}H NMR (400 MHz, D_2O) δ 7.20 (t, 202), 3.74 (s, 237H), 3.57 (s, 178H), 2.18 – 1.74 (m, 345H), 1.74 - 1.25 (m, 577H), 1.00 (s, 1654H).

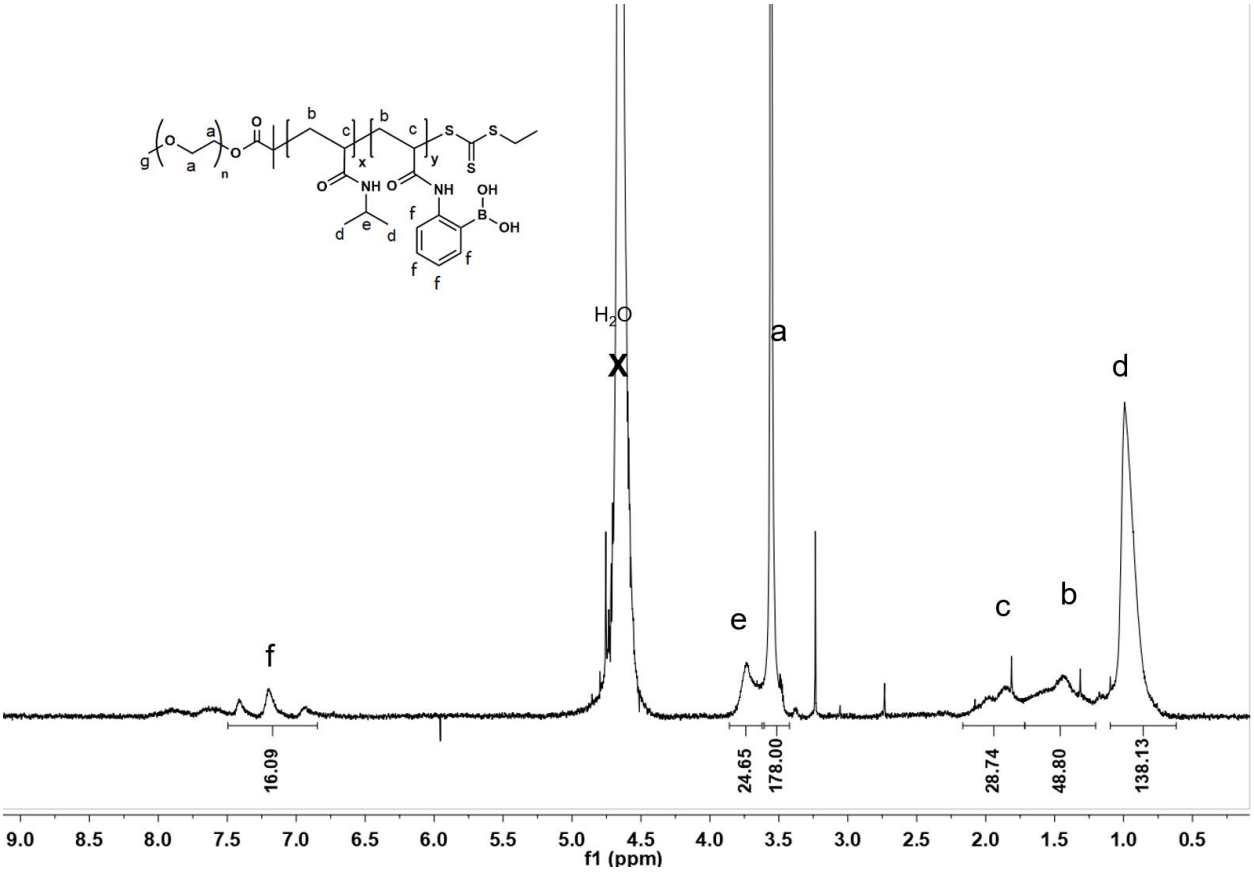

Figure 3.18. Polymer 8 ^{1}H NMR of PEG$_{2000}$-*b*-(NIPAM-*co*-APBA). ^{1}H NMR of PEG$_{2000}$- *b*-(NIPAM-*co*-APBA) (400 MHz, D_2O). ^{1}H NMR (400 MHz, D_2O) δ 7.20 (t, 16H), 3.74 (s, 24H), 3.57 (s, 178H), 2.18 – 1.74 (m, 28H), 1.74 - 1.25 (m, 48H), 1.00 (s, 138H).

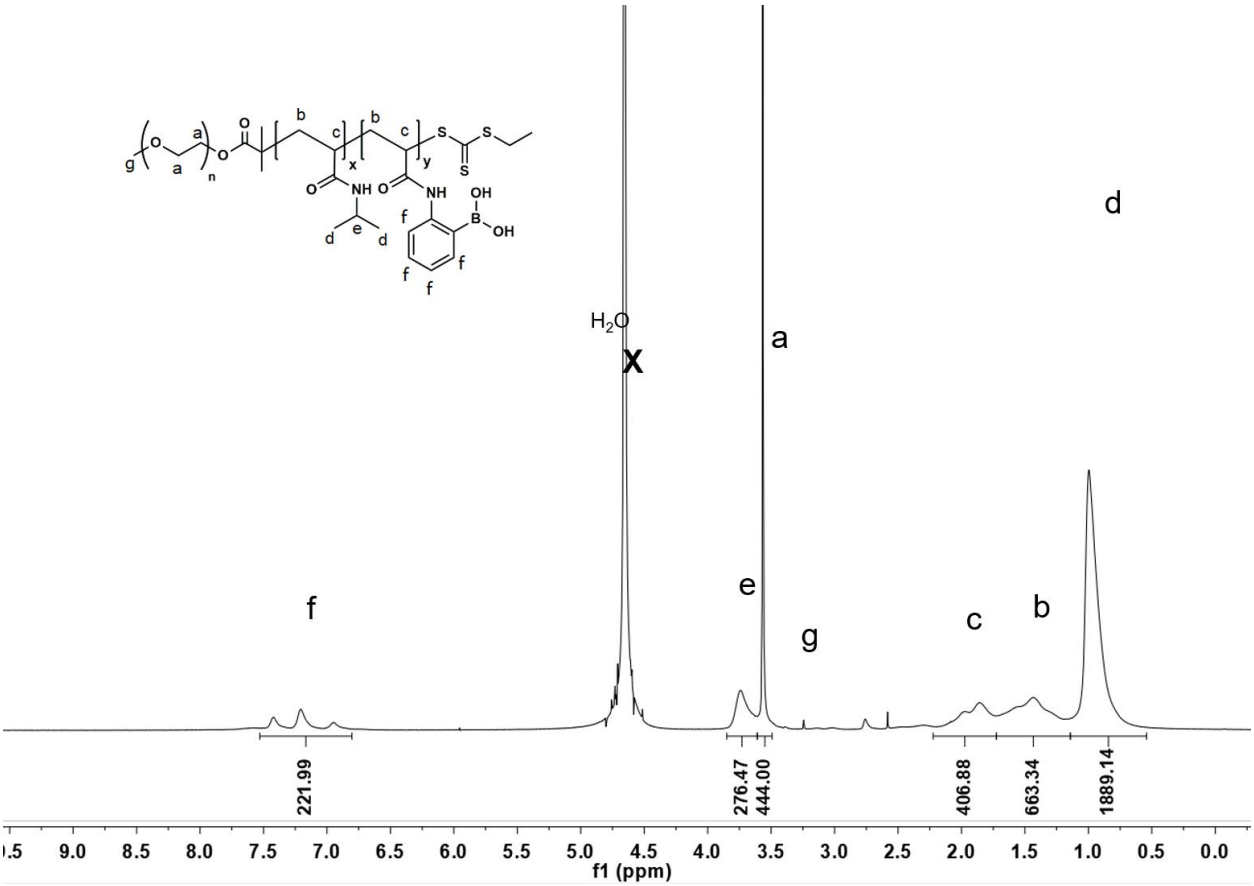

Figure 3.19. Polymer 9 ^{1}H NMR of PEG$_{5000}$-*b*-(NIPAM-*co*-APBA). ^{1}H NMR of PEG$_{5000}$- *b*-(NIPAM-*co*-APBA) (400 MHz, D_2O). ^{1}H NMR (400 MHz, D_2O) δ 7.20 (t, 221H), 3.74 (s, 276H), 3.57 (s, 444H), 2.18 – 1.74 (m, 406H), 1.74 - 1.25 (m, 663H), 1.00 (s, 1889H).

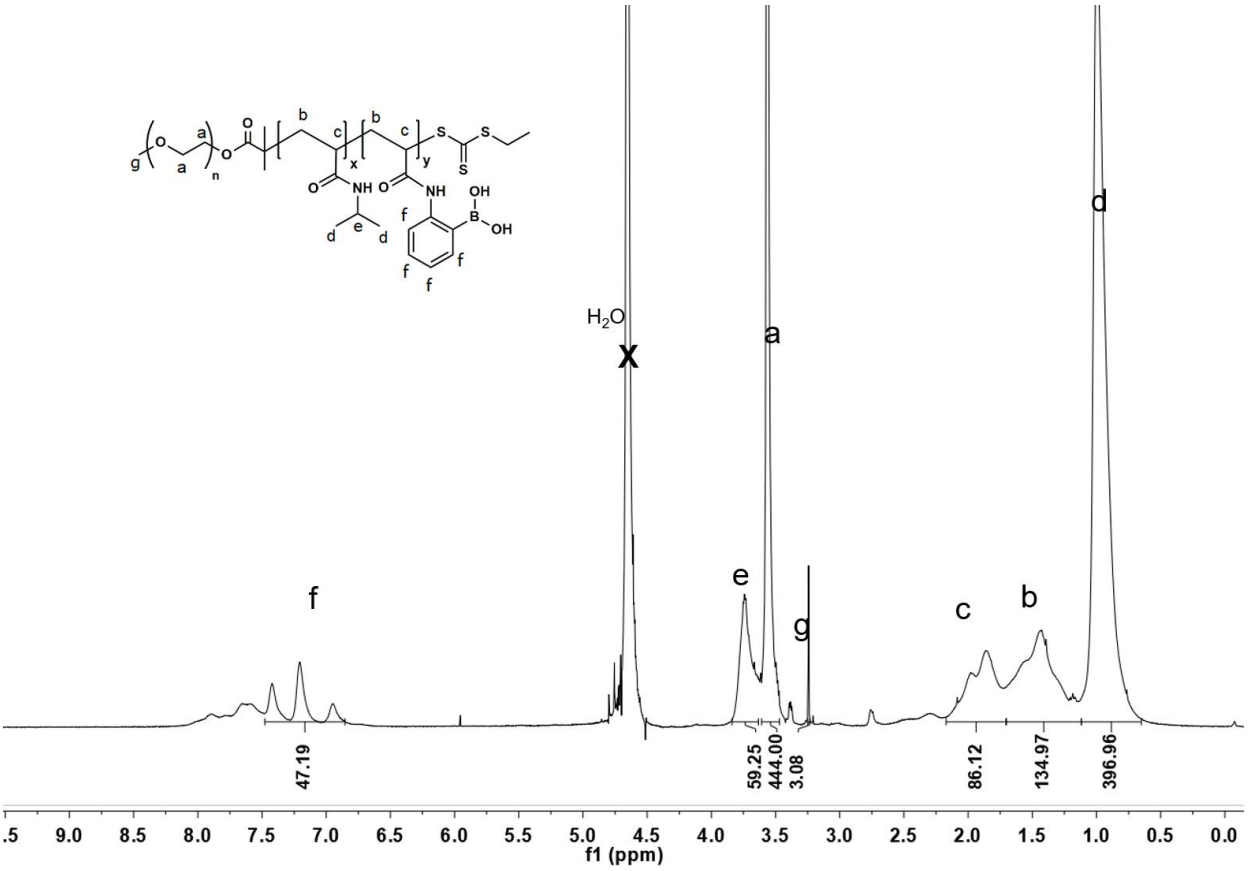

Figure 3.20. Polymer 10 ^{1}H NMR of PEG$_{5000}$-*b*-(NIPAM-*co*-APBA). ^{1}H NMR of PEG$_{5000}$- *b*-(NIPAM-*co*-APBA) (400 MHz, D_2O). ^{1}H NMR (400 MHz, D_2O) δ 7.20 (t, 47H), 3.74 (s, 59H), 3.57 (s, 444H), 3.30 (s, 3H), 2.18 – 1.74 (m, 86H), 1.74 - 1.25 (m, 134H), 1.00 (s, 396H).

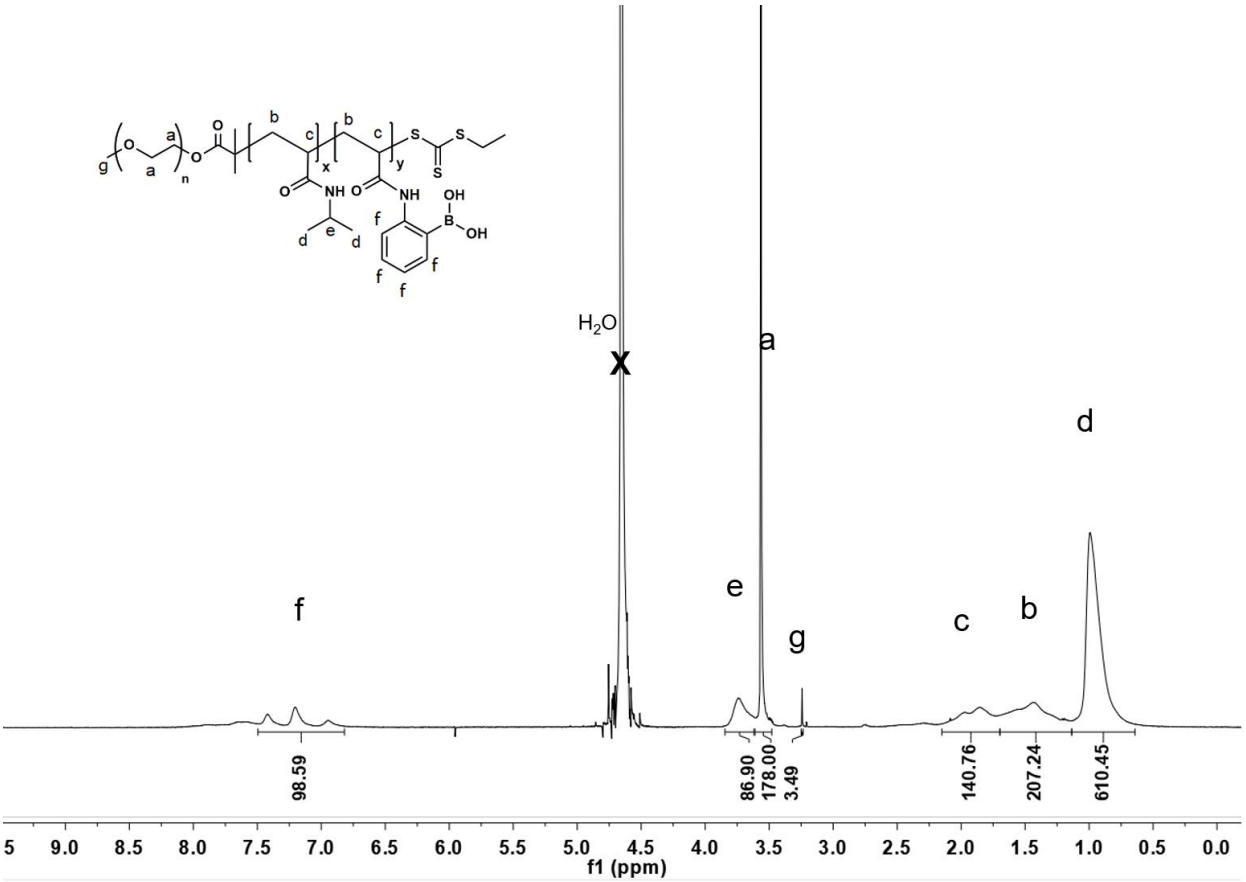

Figure 3.21. Polymer 11 ^{1}H NMR of pure PEG$_{2000}$-*b*-(NIPAM-*co*-APBA). ^{1}H NMR of PEG$_{2000}$-*b*-(NIPAM-*co*-APBA) (400 MHz, D_2O). ^{1}H NMR (400 MHz, D_2O) δ 7.20 (t, 98H), 3.74 (s, 86H), 3.57 (s, 178H), 2.18 – 1.74 (m, 140H), 1.74 – 1.23 (m, 207H), 1.00 (s, 610H).

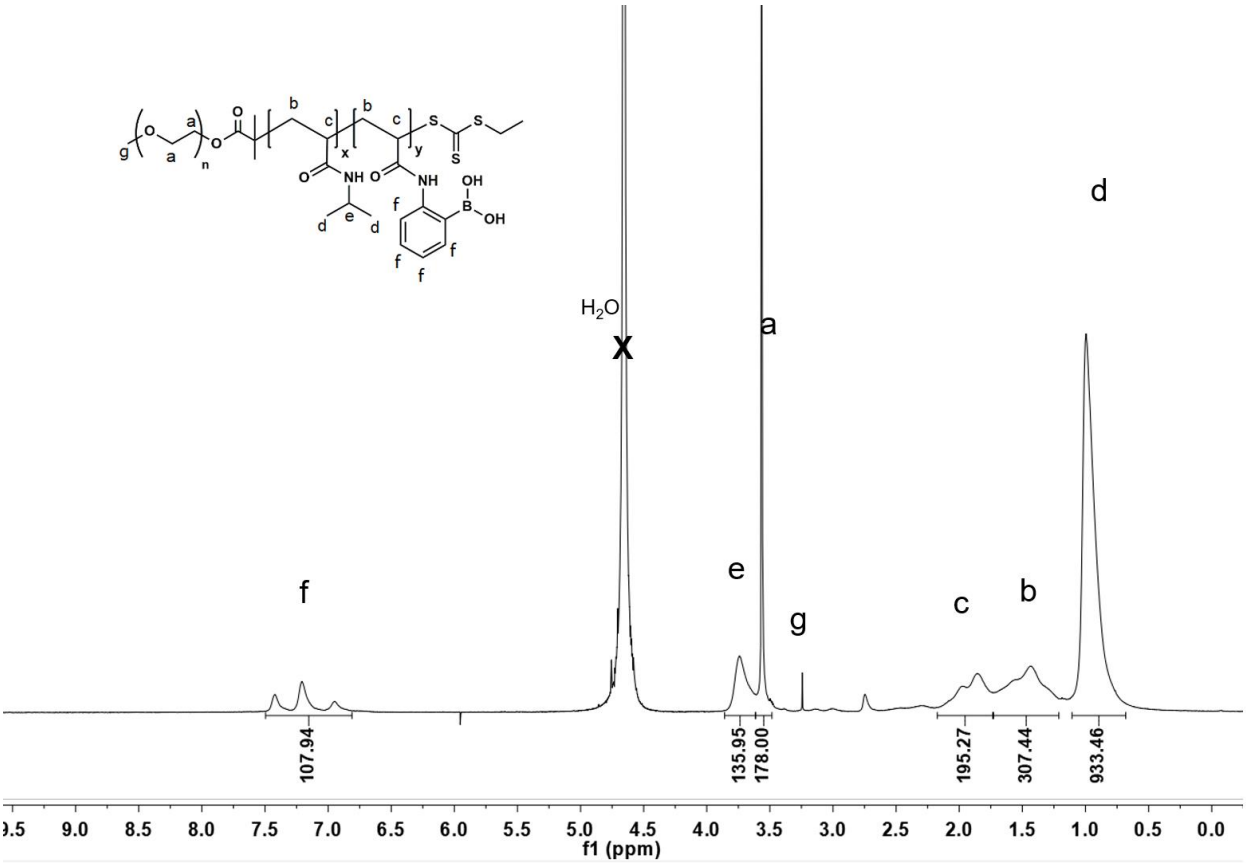

Figure 3.22. Polymer 12 ^{1}H NMR of pure PEG$_{2000}$-*b*-(NIPAM-*co*-APBA). ^{1}H NMR of PEG$_{2000}$-*b*-(NIPAM-*co*-APBA) (400 MHz, D_2O). ^{1}H NMR (400 MHz, D_2O) δ 7.20 (t, 100H), 3.74 (s, 135H), 3.57 (s, 178H), 2.18 – 1.74 (m, 195H), 1.74 – 1.23 (m, 307H), 1.00 (s, 933H).

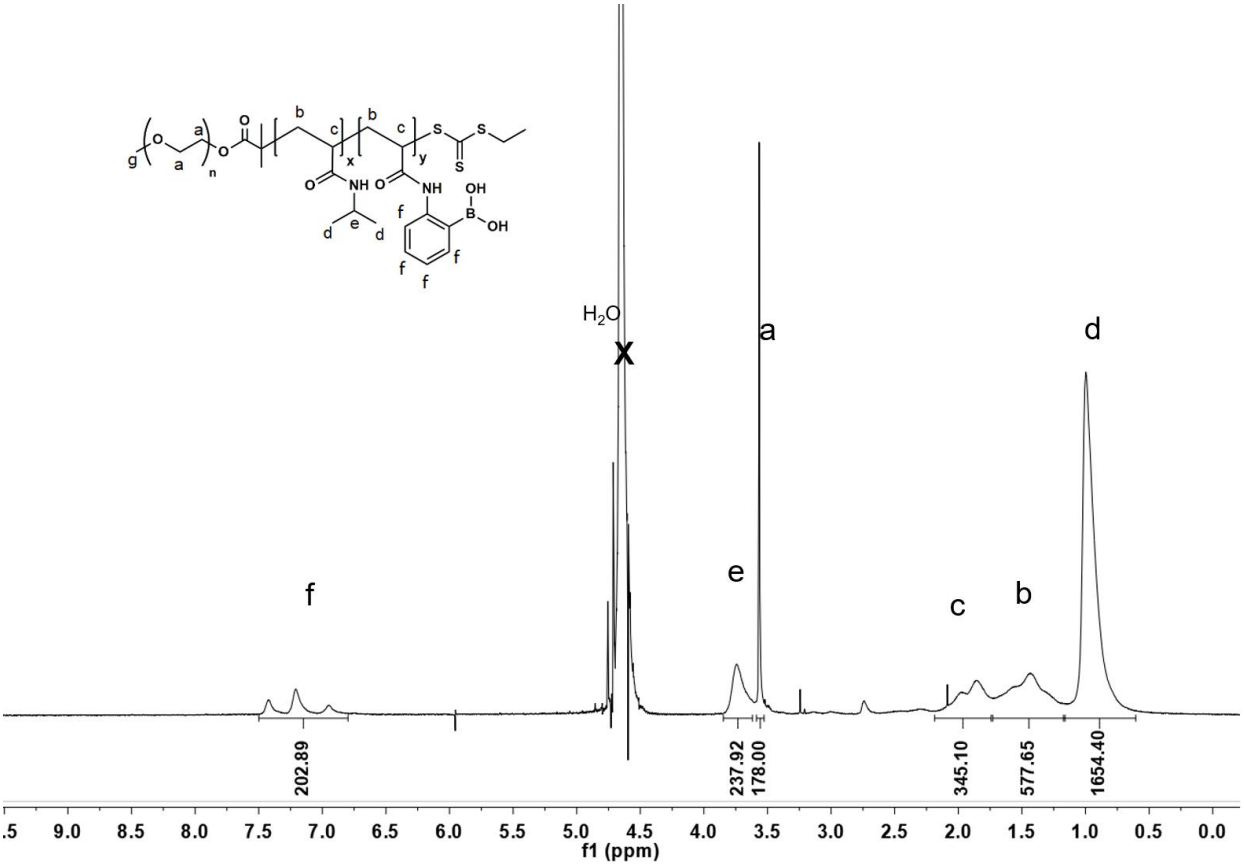

Figure 3.23. Polymer 13 ^{1}H NMR of pure PEG$_{2000}$-*b*-(NIPAM-*co*-APBA). ^{1}H NMR of PEG$_{2000}$-*b*-(NIPAM-*co*-APBA) (400 MHz, D_2O). ^{1}H NMR (400 MHz, D_2O) δ 7.20 (t, 203H), 3.74 (s, 238H), 3.57 (s, 178H), 2.18 – 1.74 (m, 345H), 1.74 – 1.23 (m, 577H), 1.00 (s, 1654H).

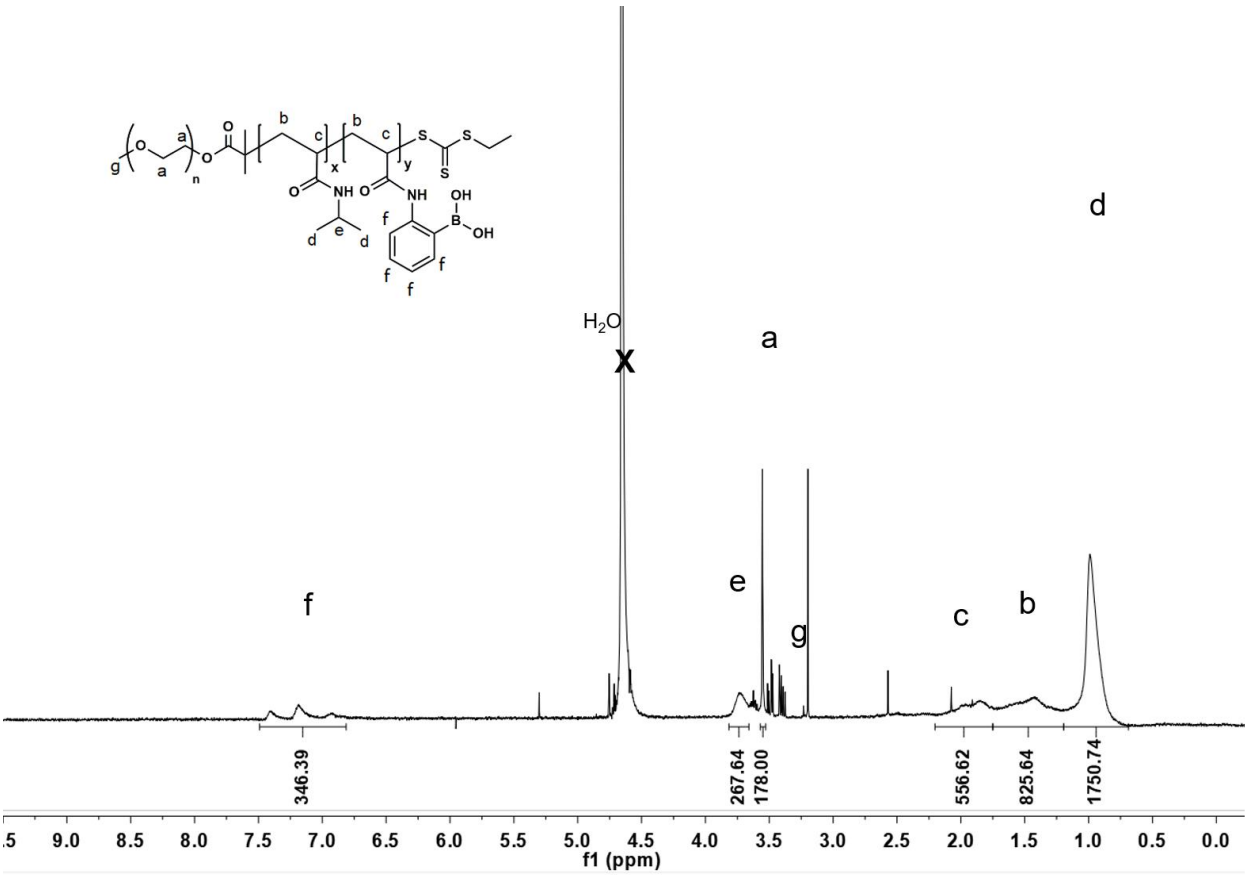

Figure 3.24. Polymer 14 ^{1}H NMR of pure PEG$_{2000}$-*b*-(NIPAM-*co*-APBA). ^{1}H NMR of PEG$_{2000}$-*b*-(NIPAM-*co*-APBA) (400 MHz, D_2O). ^{1}H NMR (400 MHz, D_2O) δ 7.20 (t, 346H), 3.74 (s, 267H), 3.57 (s, 178H), 2.18 – 1.74 (m, 556H), 1.74 – 1.23 (m, 825H), 1.00 (s, 1750H).

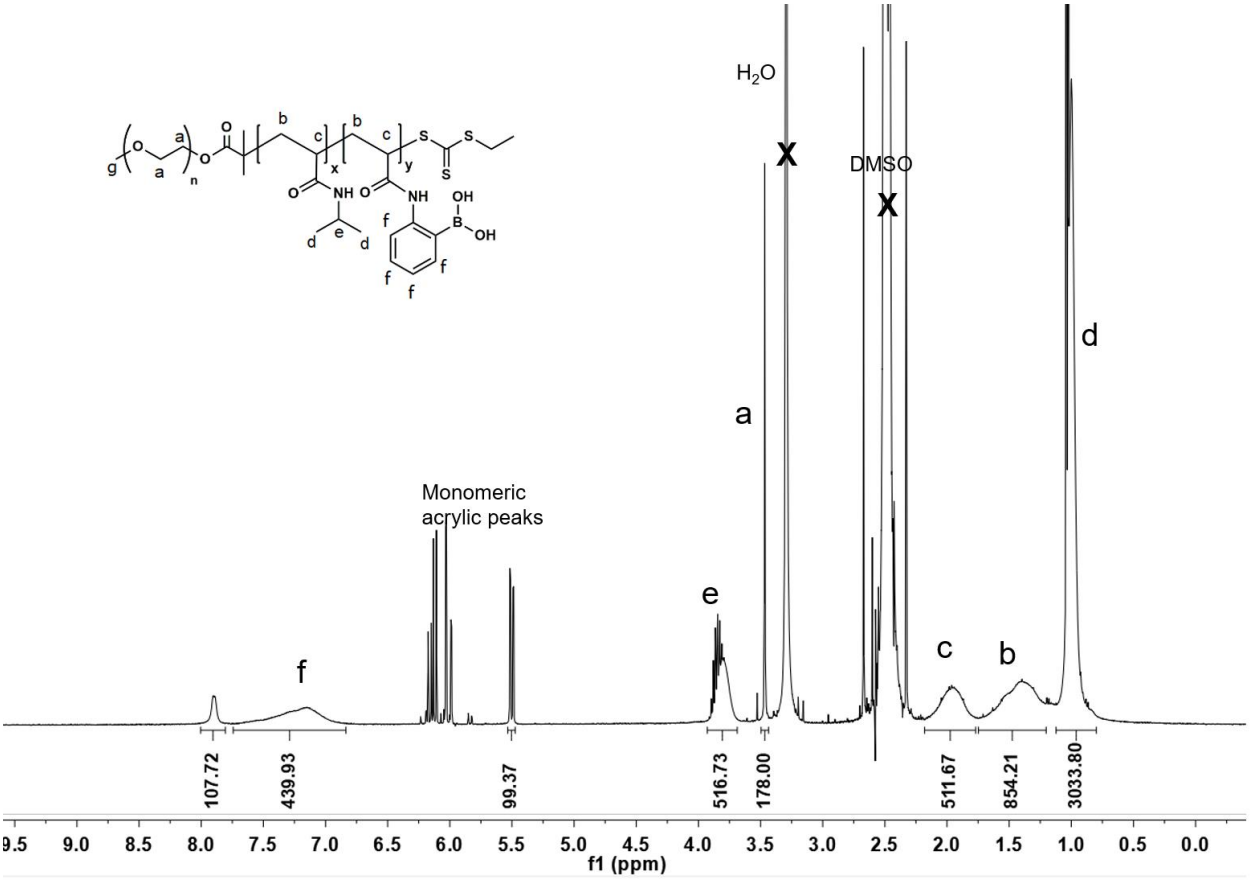

Figure 3.25 Polymer 15 ^{1}H NMR of crude PEG$_{2000}$-*b*-(NIPAM-*co*-APBA). ^{1}H NMR of PEG$_{2000}$- *b*-(NIPAM-*co*-APBA) (400 MHz, DMSO) 7.16 (s, 439H), 3.85 (m, 516H), 3.47 (s, 178H), 1.96 (m, 511H), 1.76 – 1.16 (m, 854H), 1.12 – 0.75 (m, 3033H).

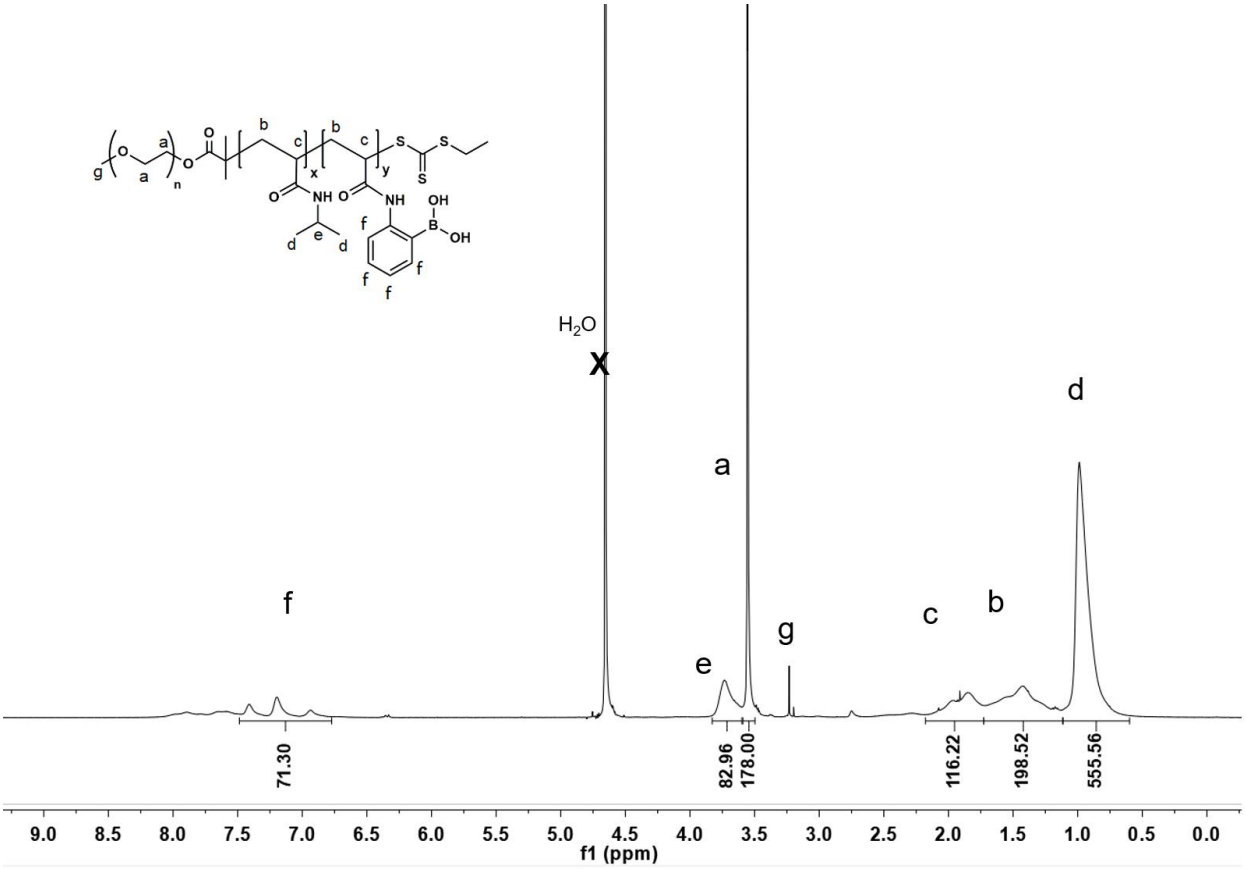

Figure 3.26. Polymer 16 ^{1}H NMR of pure PEG$_{2000}$-*b*-(NIPAM-*co*-APBA). ^{1}H NMR of PEG$_{2000}$-*b*-(NIPAM-*co*-APBA) (400 MHz, D_2O). ^{1}H NMR (400 MHz, D_2O) δ 7.20 (t, 71H), 3.74 (s, 83H), 3.57 (s, 178H), 2.18 – 1.74 (m, 116H), 1.74 – 1.23 (m, 198H), 1.00 (s, 555H).

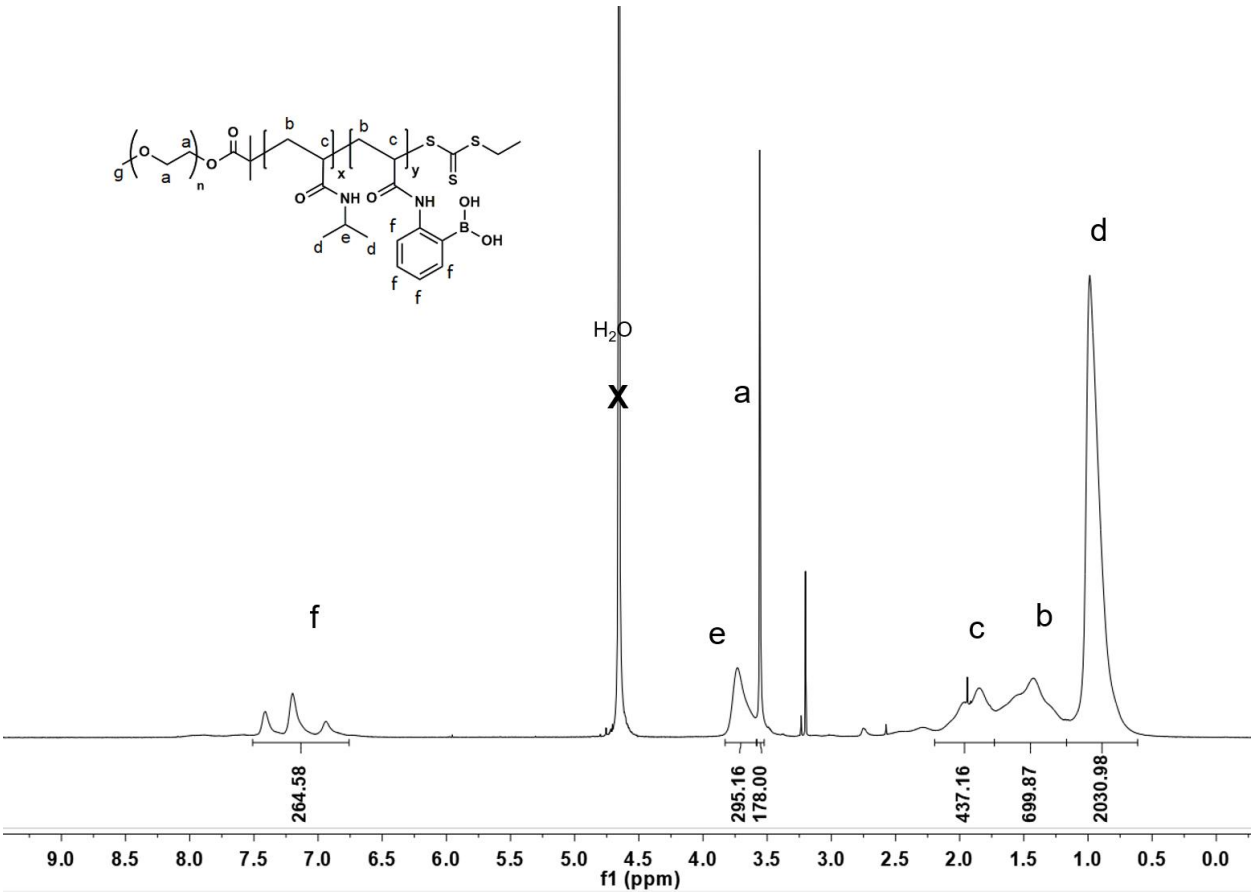

Figure 3.27. Polymer 17 ^{1}H NMR of pure PEG$_{2000}$-*b*-(NIPAM-*co*-APBA). ^{1}H NMR of PEG$_{2000}$-*b*-(NIPAM-*co*-APBA) (400 MHz, D_2O). ^{1}H NMR (400 MHz, D_2O) δ 7.20 (t, 264H), 3.74 (s, 295H), 3.57 (s, 178H), 2.18 – 1.74 (m, 437H), 1.74 – 1.23 (m, 699H), 1.00 (s, 2030H).

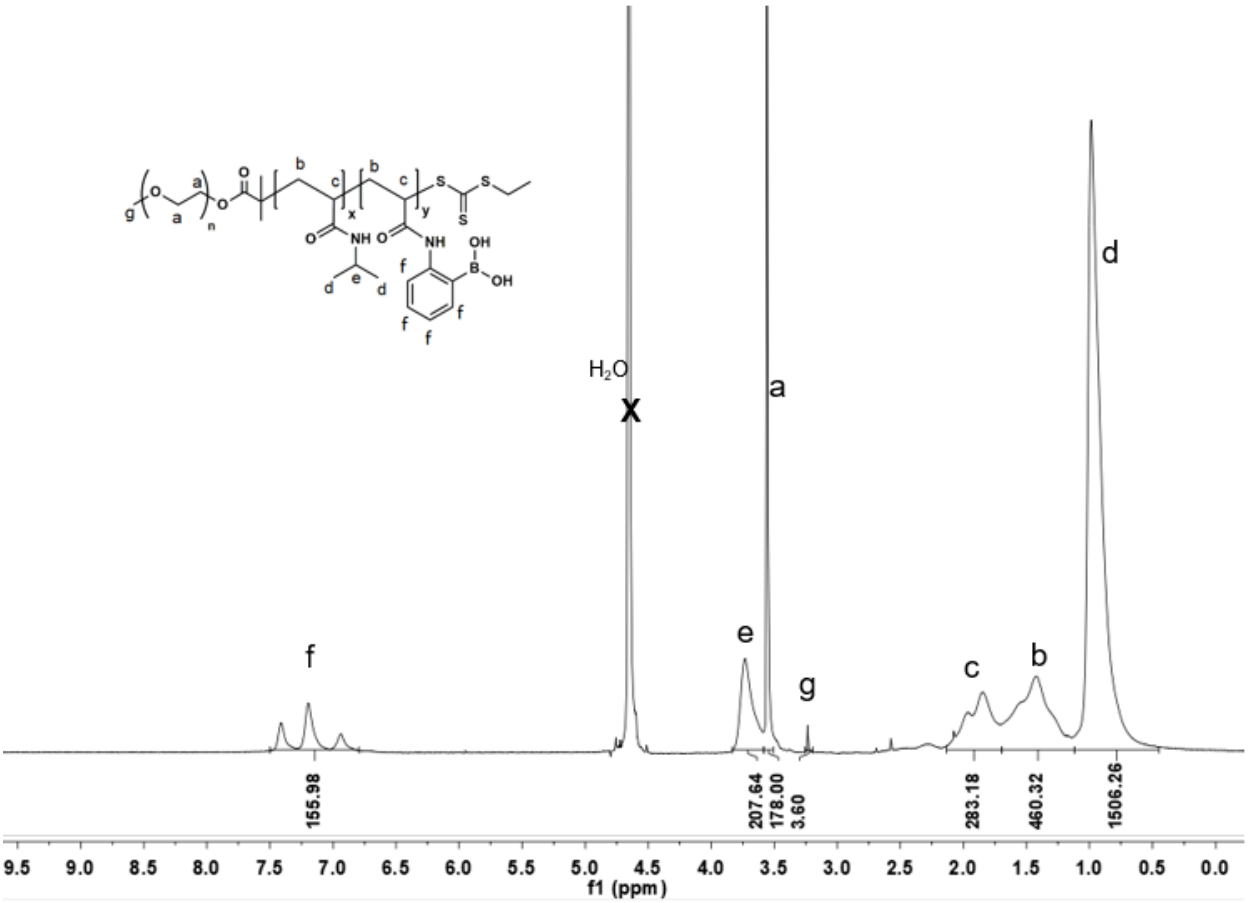

Figure 3.28. Polymer 18 ^{1}H NMR of pure PEG$_{2000}$-*b*-(NIPAM-*co*-APBA). ^{1}H NMR of PEG$_{2000}$-*b*-(NIPAM-*co*-APBA) (400 MHz, D_2O). ^{1}H NMR (400 MHz, D_2O) δ 7.20 (t, 156H), 3.74 (s, 208H), 3.57 (s, 178H), 2.18 – 1.74 (m, 283H), 1.43 (m, 460H), 1.00 (s, 1506H).

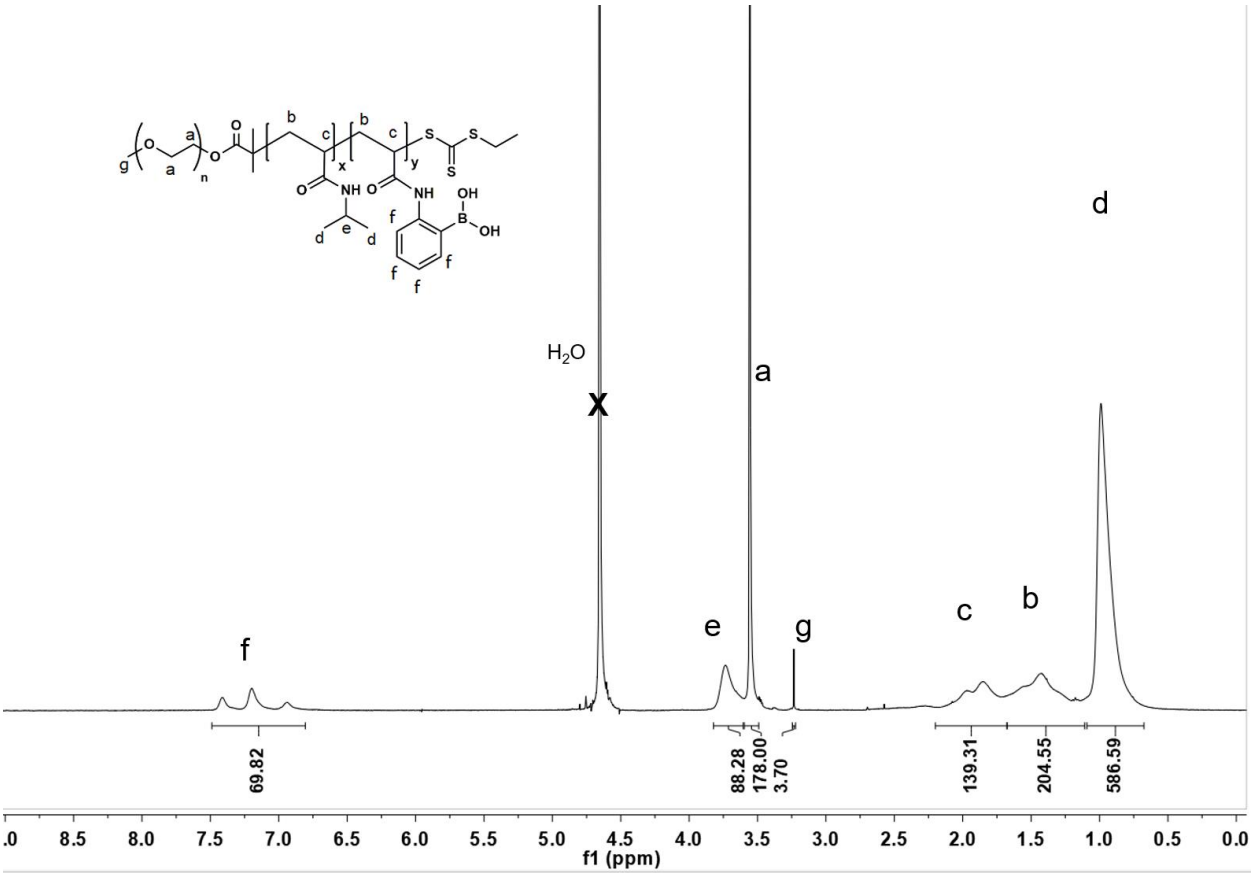

Figure 3.29. Polymer 19 ^{1}H NMR of pure PEG$_{2000}$-*b*-(NIPAM-*co*-APBA). ^{1}H NMR of PEG$_{2000}$-*b*-(NIPAM-*co*-APBA) (400 MHz, D_2O). ^{1}H NMR (400 MHz, D_2O) δ 7.20 (t, 69H), 3.74 (s, 86H), 3.57 (s, 178H), 3.30 (s, 3H), 2.18 – 1.74 (m, 139H), 1.74 – 1.23 (m, 204H), 1.00 (s, 586H).

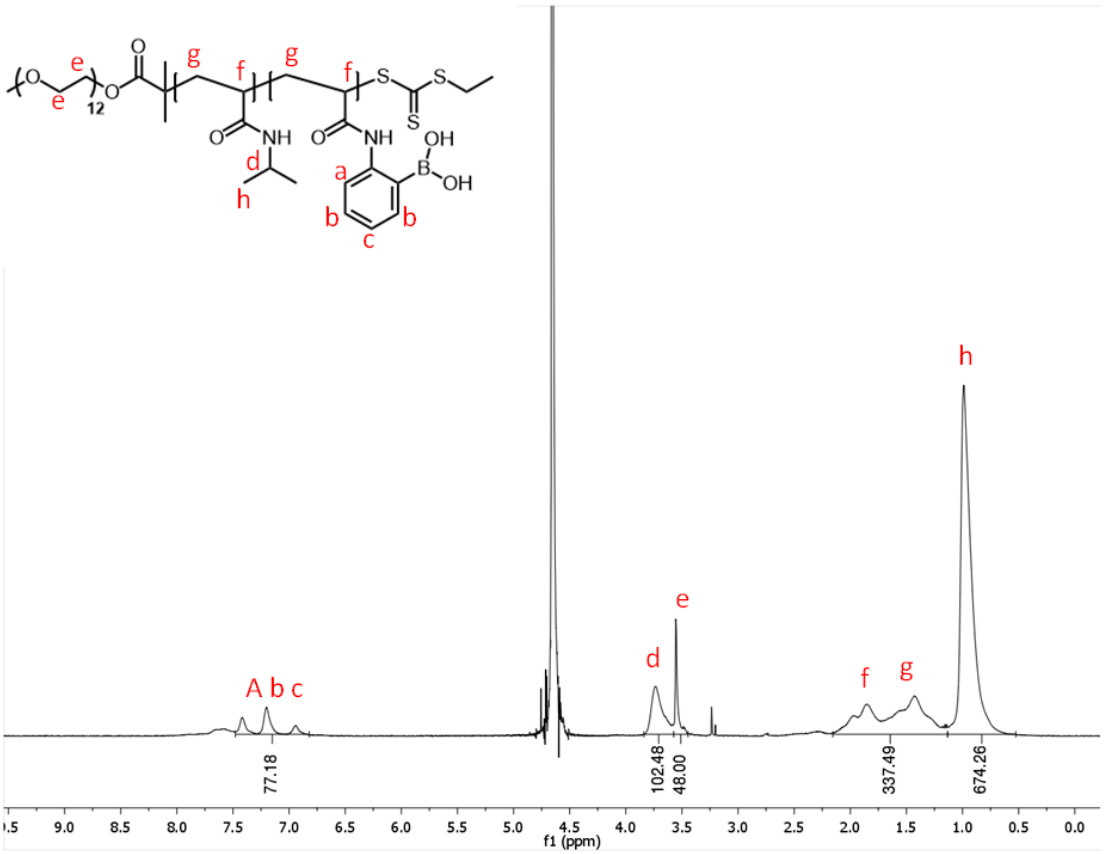

Figure 3.30. Polymer 20 ^{1}H NMR of PEG$_{550}$-*b*-(NIPAM-*co*-APBA). ^{1}H NMR of PEG$_{550}$- *b*-(NIPAM-*co*-APBA) (400 MHz, D_2O). ^{1}H NMR (400 MHz, D_2O) δ 7.20 (t, 77H), 3.74 (s, 102H), 3.57 (s, 8H), 2.18 – 1.12 (m, 337H), 1.00 (s, 674H).

Table 3.4 Viscosity Measurements using polymer 19 performed in triplicate.

Sample Name	Temp (C°)	Viscosity mPa-s	Flow Rate (ul/min)	P-Scale (%)	Shear Rate (1/s)	Shear Stress (Pa)	Volume (ul)	R^2
Trial 1	20.06	15.53	11.5	10.89	213.1	3.31	105.1	0.99
Trial 2	20.04	15.76	11.5	10.6	213.1	3.36	55	0.98
Trial 3	20.07	18.85	11.5	13.2	213.1	4.02	55	1
Average		16.71	11.5		213.1	3.56		

Table 3.5 Assumed measurements of 1 mL syringe and various needle gauges

Needle and Barrel assumptions:				
	21 G	**25 G**	**27 G**	**29 G**
Length (mm)	12.7	12.7	12.7	12.7
Diameter barrel (mm)	6.35	6.35	6.35	6.35
Inner Diameter Needle (mm)	0.514	0.26	0.21	0.184

Table 3.6 Injection force calculations based on assumed needle and barrel dimensions at 0.02 mL/sec flow rate

Flow rate of 0.02 mL/sec				
Needle	**21 G**	**25 G**	**27 G**	**29 G**
Force (N)	0.0784	1.19	2.81	4.77
Force (mPa)	78.4	1190	2810	4770

Table 3.7 Injection force calculations based on assumed needle and barrel dimensions at 0.1 mL/sec flow rate

Flow rate of 0.1 mL/sec				
Needle	**21 G**	**25 G**	**27 G**	**29 G**
Force (N)	0.392	5.99	14.1	23.9

Force (mPa)	392	5990	14100	23900

Table 3.8 Injection force calculations based on assumed needle and barrel dimensions at 0.02 mL/sec flow rate

Flow rate of 0.3 mL/sec				
Needle	**21 G**	**25 G**	**27 G**	**29 G**
Force (N)	8.22	17.9	42.2	71.7
Force (mPa)	8220	17900	42200	71700

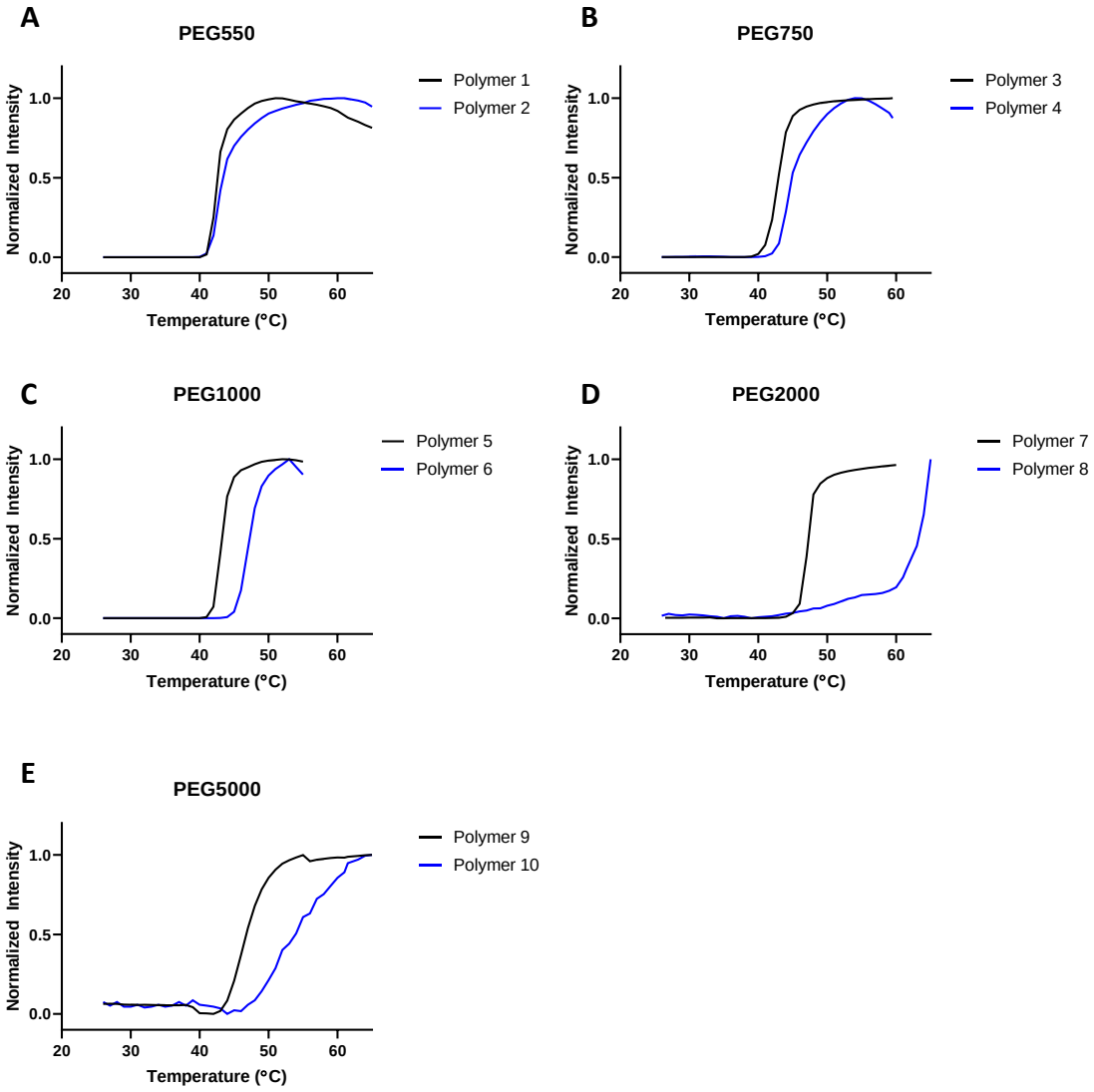

Figure 3.31. LCST determination of polymer library via UV-vis turbidity measurements at 600 nm

3.5 References

(1) CDC. *Diabetes Report Card*. Centers for Disease Control and Prevention. https://www.cdc.gov/diabetes/library/reports/reportcard.html (accessed 2022-08-15).

(2) *Global report on diabetes*. https://www.who.int/publications-detail-redirect/9789241565257 (accessed 2022-08-15).

(3) *National Diabetes Statistics Report | Diabetes | CDC*. https://www.cdc.gov/diabetes/data/statistics-report/index.html (accessed 2022-08-15).

(4) Xu, G.; Liu, B.; Sun, Y.; Du, Y.; Snetselaar, L. G.; Hu, F. B.; Bao, W. Prevalence of Diagnosed Type 1 and Type 2 Diabetes among US Adults in 2016 and 2017: Population Based Study. *The BMJ* **2018**, *362*, k1497. https://doi.org/10.1136/bmj.k1497.

(5) Lin, X.; Xu, Y.; Pan, X.; Xu, J.; Ding, Y.; Sun, X.; Song, X.; Ren, Y.; Shan, P.-F. Global, Regional, and National Burden and Trend of Diabetes in 195 Countries and Territories: An Analysis from 1990 to 2025. *Sci. Rep.* **2020**, *10* (1), 14790. https://doi.org/10.1038/s41598-020-71908-9.

(6) Rix, I.; Nexøe-Larsen, C.; Bergmann, N. C.; Lund, A.; Knop, F. K. Glucagon Physiology. In *Endotext*; Feingold, K. R., Anawalt, B., Boyce, A., Chrousos, G., de Herder, W. W., Dungan, K., Grossman, A., Hershman, J. M., Hofland, J., Kaltsas, G., Koch, C., Kopp, P., Korbonits, M., McLachlan, R., Morley, J. E., New, M., Purnell, J., Singer, F., Stratakis, C. A., Trence, D. L., Wilson, D. P., Eds.; MDText.com, Inc.: South Dartmouth (MA), 2000.

(7) Kedia, N. Treatment of Severe Diabetic Hypoglycemia with Glucagon: An Underutilized Therapeutic Approach. *Diabetes Metab. Syndr. Obes. Targets Ther.* **2011**, *4*, 337–346. https://doi.org/10.2147/DMSO.S20633.

(8) Pearson, T. Glucagon as a Treatment of Severe Hypoglycemia. *Diabetes Educ.* **2008**, *34* (1), 128–134. https://doi.org/10.1177/0145721707312400.

(9) Caputo, N.; Castle, J. R.; Bergstrom, C. P.; Carroll, J. M.; Bakhtiani, P. A.; Jackson, M. A.; Roberts, C. T.; David, L. L.; Ward, W. K. Mechanisms of Glucagon Degradation at Alkaline PH. *Peptides* **2013**, *45*, 40–47. https://doi.org/10.1016/j.peptides.2013.04.005.

(10) Caputo, N.; Jackson, M. A.; Castle, J. R.; El Youssef, J.; Bakhtiani, P. A.; Bergstrom, C. P.; Carroll, J. M.; Breen, M. E.; Leonard, G. L.; David, L. L.; Roberts, C. T.; Ward, W. K. Biochemical Stabilization of Glucagon at Alkaline PH. *Diabetes Technol. Ther.* **2014**, *16* (11), 747–758. https://doi.org/10.1089/dia.2014.0047.

(11) Onoue, S.; Ohshima, K.; Debari, K.; Koh, K.; Shioda, S.; Iwasa, S.; Kashimoto, K.; Yajima, T. Mishandling of the Therapeutic Peptide Glucagon Generates Cytotoxic Amyloidogenic Fibrils. *Pharm. Res.* **2004**, *21* (7), 1274–1283. https://doi.org/10.1023/b:pham.0000033016.36825.2c.

(12) Suico, J. G.; Hövelmann, U.; Zhang, S.; Shen, T.; Bergman, B.; Sherr, J.; Zijlstra, E.; Frier, B. M.; Plum-Mörschel, L. Glucagon Administration by Nasal and Intramuscular Routes in Adults With Type 1 Diabetes During Insulin-Induced Hypoglycaemia: A Randomised, Open-Label, Crossover Study. *Diabetes Ther.* **2020**, *11* (7), 1591–1603. https://doi.org/10.1007/s13300-020-00845-7.

(13) Christiansen, M. P.; Cummins, M.; Prestrelski, S.; Close, N. C.; Nguyen, A.; Junaidi, K. Comparison of a Ready-to-Use Liquid Glucagon Injection Administered by Autoinjector to Glucagon Emergency Kit for the Symptomatic Relief of Severe Hypoglycemia: Two Randomized Crossover Non-Inferiority Studies. *BMJ Open Diabetes Res. Care* **2021**, *9* (1), e002137. https://doi.org/10.1136/bmjdrc-2021-002137.

(14) Bailey, N. C.; Dimsits, J.; Hammer, M.; Kendall, D. M.; Bailey, T. S. A Comparative Study of Dasiglucagon Ready-to-Use Autoinjector and Glucagon Emergency Kit During Rescue from Simulated Severe Hypoglycemia. *Diabetes Technol. Ther.* **2022**, *24* (4), 231–240. https://doi.org/10.1089/dia.2021.0367.

(15) *PRODUCT DISCONTINUATION UPDATE: GLUCAGON EMERGENCY KIT (GLUCAGON FOR INJECTION, rDNA ORIGIN, DIN 02243297)*. https://www.lilly.ca/en-CA/news/press-releases/22.08.25-glucagon-discontinuation-update (accessed 2022-09-19).

(16) Siamashvili, M.; Davis, H. A.; Davis, S. N. Nocturnal Hypoglycemia in Type 1 and Type 2 Diabetes: An Update on Prevalence, Prevention, Pathophysiology and Patient Awareness. *Expert Rev. Endocrinol. Metab.* **2021**, *16* (6), 281–293. https://doi.org/10.1080/17446651.2021.1979391.

(17) Allen, K. V.; Frier, B. M. Nocturnal Hypoglycemia: Clinical Manifestations and Therapeutic Strategies Toward Prevention. *Endocr. Pract.* **2003**, *9* (6), 530–543. https://doi.org/10.4158/EP.9.6.530.

(18) Yu, S.; Xian, S.; Ye, Z.; Pramudya, I.; Webber, M. J. Glucose-Fueled Peptide Assembly: Glucagon Delivery via Enzymatic Actuation. *J. Am. Chem. Soc.* **2021**, *143* (32), 12578–12589. https://doi.org/10.1021/jacs.1c04570.

(19) GhavamiNejad, A.; Li, J.; Lu, B.; Zhou, L.; Lam, L.; Giacca, A.; Wu, X. Y. Glucose-Responsive Composite Microneedle Patch for Hypoglycemia-Triggered Delivery of Native Glucagon. *Adv. Mater.* **2019**, *31* (30), 1901051. https://doi.org/10.1002/adma.201901051.

(20) Lu, B.; GhavamiNejad, A.; Liu, J. F.; Li, J.; Mirzaie, S.; Giacca, A.; Wu, X. Y. "Smart" Composite Microneedle Patch Stabilizes Glucagon and Prevents Nocturnal Hypoglycemia:

Experimental Studies and Molecular Dynamics Simulation. *ACS Appl. Mater. Interfaces* **2022**, *14* (18), 20576–20590. https://doi.org/10.1021/acsami.1c24955.

(21) Wang, Q.; Wang, H.; Chen, Q.; Guan, Y.; Zhang, Y. Glucose-Triggered Micellization of Poly(Ethylene Glycol)-b-Poly(N-Isopropylacrylamide-Co-2-(Acrylamido)Phenylboronic Acid) Block Copolymer. *ACS Appl. Polym. Mater.* **2020**, *2* (9), 3966–3976. https://doi.org/10.1021/acsapm.0c00635.

(22) Tang, Z.; Guan, Y.; Zhang, Y. The Synthesis of a Contraction-Type Glucose-Sensitive Microgel Working at Physiological Temperature Guided by a New Glucose-Sensing Mechanism. *Polym. Chem.* **2018**, *9* (8), 1012–1021. https://doi.org/10.1039/C8PY00072G.

(23) Wang, Q.; Fu, M.; Guan, Y.; James, T. D.; Zhang, Y. Mechanistic Insights into the Novel Glucose-Sensitive Behavior of P(NIPAM-Co-2-AAPBA). *Sci. China Chem.* **2020**, *63* (3), 377–385. https://doi.org/10.1007/s11426-019-9680-6.

(24) Jain, K.; Vedarajan, R.; Watanabe, M.; Ishikiriyama, M.; Matsumi, N. Tunable LCST Behavior of Poly(N-Isopropylacrylamide/Ionic Liquid) Copolymers. *Polym. Chem.* **2015**, *6* (38), 6819–6825. https://doi.org/10.1039/C5PY00998G.

(25) Cook, M. T.; Haddow, P.; Kirton, S. B.; McAuley, W. J. Polymers Exhibiting Lower Critical Solution Temperatures as a Route to Thermoreversible Gelators for Healthcare. *Adv. Funct. Mater. n/a* (n/a), 2008123. https://doi.org/10.1002/adfm.202008123.

(26) Huang, Z.; Delparastan, P.; Burch, P.; Cheng, J.; Cao, Y.; Messersmith, P. B. Injectable Dynamic Covalent Hydrogels of Boronic Acid Polymers Cross-Linked by Bioactive Plant-Derived Polyphenols. *Biomater. Sci.* **2018**, *6* (9), 2487–2495. https://doi.org/10.1039/C8BM00453F.

(27) Cromwell, O. R.; Chung, J.; Guan, Z. Malleable and Self-Healing Covalent Polymer Networks through Tunable Dynamic Boronic Ester Bonds. *J. Am. Chem. Soc.* **2015**, *137* (20), 6492–6495. https://doi.org/10.1021/jacs.5b03551.

(28) Miwa, Y.; Kurachi, J.; Kohbara, Y.; Kutsumizu, S. Dynamic Ionic Crosslinks Enable High Strength and Ultrastretchability in a Single Elastomer. *Commun. Chem.* **2018**, *1* (1), 1–8. https://doi.org/10.1038/s42004-017-0004-9.

(29) Picchioni, F.; Muljana, H. Hydrogels Based on Dynamic Covalent and Non Covalent Bonds: A Chemistry Perspective. *Gels* **2018**, *4* (1), 21. https://doi.org/10.3390/gels4010021.

(30) Zheng, N.; Xu, Y.; Zhao, Q.; Xie, T. Dynamic Covalent Polymer Networks: A Molecular Platform for Designing Functions beyond Chemical Recycling and Self-Healing. *Chem. Rev.* **2021**, *121* (3), 1716–1745. https://doi.org/10.1021/acs.chemrev.0c00938.

(31) Ran, Y.; Zheng, L.-J.; Zeng, J.-B. Dynamic Crosslinking: An Efficient Approach to Fabricate Epoxy Vitrimer. *Materials* **2021**, *14* (4), 919. https://doi.org/10.3390/ma14040919.

(32) Winne, J. M.; Leibler, L.; Prez, F. E. D. Dynamic Covalent Chemistry in Polymer Networks: A Mechanistic Perspective. *Polym. Chem.* **2019**, *10* (45), 6091–6108. https://doi.org/10.1039/C9PY01260E.

(33) Li, J.; Mooney, D. J. Designing Hydrogels for Controlled Drug Delivery. *Nat. Rev. Mater.* **2016**, *1* (12). https://doi.org/10.1038/natrevmats.2016.71.

(34) Rizwan, M.; Baker, A. E. G.; Shoichet, M. S. Designing Hydrogels for 3D Cell Culture Using Dynamic Covalent Crosslinking. *Adv. Healthc. Mater.* **2021**, *10* (12), 2100234. https://doi.org/10.1002/adhm.202100234.

(35) Holz, E.; Rajagopal, K. In Situ-Forming Glucose-Responsive Hydrogel from Hyaluronic Acid Modified with a Boronic Acid Derivative. *Macromol. Chem. Phys.* **2020**, *221* (15), 2000055. https://doi.org/10.1002/macp.202000055.

(36) Xiang, Y.; Xian, S.; Ollier, R. C.; Yu, S.; Su, B.; Pramudya, I.; Webber, M. J. Diboronate Crosslinking: Introducing Glucose Specificity in Glucose-Responsive Dynamic-Covalent Networks. *J. Controlled Release* **2022**, *348*, 601–611. https://doi.org/10.1016/j.jconrel.2022.06.016.

(37) Nguyen, M. K.; Lee, D. S. Injectable Biodegradable Hydrogels. *Macromol. Biosci.* **2010**, *10* (6), 563–579. https://doi.org/10.1002/mabi.200900402.

(38) Nguyen, Q. V.; Huynh, D. P.; Park, J. H.; Lee, D. S. Injectable Polymeric Hydrogels for the Delivery of Therapeutic Agents: A Review. *Eur. Polym. J.* **2015**, *72*, 602–619. https://doi.org/10.1016/j.eurpolymj.2015.03.016.

(39) Jansen, L. E.; Negrón-Piñeiro, L. J.; Galarza, S.; Peyton, S. R. Control of Thiol-Maleimide Reaction Kinetics in PEG Hydrogel Networks. *Acta Biomater.* **2018**, *70*, 120–128. https://doi.org/10.1016/j.actbio.2018.01.043.

(40) Adepu, S.; Ramakrishna, S. Controlled Drug Delivery Systems: Current Status and Future Directions. *Molecules* **2021**, *26* (19), 5905. https://doi.org/10.3390/molecules26195905.

(41) Hyun Bae, K.; Wang, L.-S.; Kurisawa, M. Injectable Biodegradable Hydrogels: Progress and Challenges. *J. Mater. Chem. B* **2013**, *1* (40), 5371–5388. https://doi.org/10.1039/C3TB20940G.

(42) Mathew, A. P.; Uthaman, S.; Cho, K.-H.; Cho, C.-S.; Park, I.-K. Injectable Hydrogels for Delivering Biotherapeutic Molecules. *Int. J. Biol. Macromol.* **2018**, *110*, 17–29. https://doi.org/10.1016/j.ijbiomac.2017.11.113.

(43) Chen, M. H.; Wang, L. L.; Chung, J. J.; Kim, Y.-H.; Atluri, P.; Burdick, J. A. Methods To Assess Shear-Thinning Hydrogels for Application As Injectable Biomaterials. *ACS Biomater. Sci. Eng.* **2017**, *3* (12), 3146–3160. https://doi.org/10.1021/acsbiomaterials.7b00734.

(44) Guvendiren, M.; Lu, H. D.; Burdick, J. A. Shear-Thinning Hydrogels for Biomedical Applications. *Soft Matter* **2011**, *8* (2), 260–272. https://doi.org/10.1039/C1SM06513K.

(45) Loebel, C.; Rodell, C. B.; Chen, M. H.; Burdick, J. A. Shear-Thinning and Self-Healing Hydrogels as Injectable Therapeutics and for 3D-Printing. *Nat. Protoc.* **2017**, *12* (8), 1521–1541. https://doi.org/10.1038/nprot.2017.053.

(46) Usach, I.; Martinez, R.; Festini, T.; Peris, J.-E. Subcutaneous Injection of Drugs: Literature Review of Factors Influencing Pain Sensation at the Injection Site. *Adv. Ther.* **2019**, *36* (11), 2986–2996. https://doi.org/10.1007/s12325-019-01101-6.

(47) Berteau, C.; Filipe-Santos, O.; Wang, T.; Rojas, H. E.; Granger, C.; Schwarzenbach, F. Evaluation of the Impact of Viscosity, Injection Volume, and Injection Flow Rate on Subcutaneous Injection Tolerance. *Med. Devices Evid. Res.* **2015**, *8*, 473–484. https://doi.org/10.2147/MDER.S91019.

(48) Heise, T.; Nosek, L.; Dellweg, S.; Zijlstra, E.; Præstmark, K. A.; Kildegaard, J.; Nielsen, G.; Sparre, T. Impact of Injection Speed and Volume on Perceived Pain during Subcutaneous Injections into the Abdomen and Thigh: A Single-Centre, Randomized Controlled Trial. *Diabetes Obes. Metab.* **2014**, *16* (10), 971–976. https://doi.org/10.1111/dom.12304.

(49) Watt, R. P.; Khatri, H.; Dibble, A. R. G. Injectability as a Function of Viscosity and Dosing Materials for Subcutaneous Administration. *Int. J. Pharm.* **2019**, *554*, 376–386. https://doi.org/10.1016/j.ijpharm.2018.11.012.

(50) Belardi, B.; O'Donoghue, G. P.; Smith, A. W.; Groves, J. T.; Bertozzi, C. R. Investigating Cell Surface Galectin-Mediated Cross-Linking on Glycoengineered Cells. *J. Am. Chem. Soc*. **2012**, *134* (23), 9549–9552. https://doi.org/10.1021/ja301694s.

Chapter 4

Exploration of Degradable Zwitterionic Poly(caprolactone-carboxybetaine) as a PEG-alternative

4.1 Introduction

Protein therapeutics are highly effective for the treatment and management of numerous diseases. Despite this, their clinical potential is underutilized mainly due to drawbacks inherent to many native proteins such as poor stability, immunogenicity, and short pharmacokinetics. Currently, PEGylation is considered to be one of the hardiest routes to circumvent the aforementioned drawbacks of some native proteins. Upon covalent conjugation onto a protein, PEG has demonstrated the ability to prolong circulation time and increase stability of protein under storage conditions.[1] The half-life of PEGylated proteins is extended by protecting the protein from enzymatic degradation and immunogenic recognition, while the increased size also prevents filtration by the renal clearance pathway.[1–3] Though PEGylation has undoubtedly proven its utility, PEG-alternatives are an interesting field of research and will only help expand the toolset for stabilizing proteins and further the development and improvement of protein therapeutics.

As such, zwitterlation is an alternative strategy to PEGylation that has been studied in increasing frequency. Surface hydration and steric exclusion effect is considered to be the key properties that PEG exhibits in reducing nonspecific protein adsorption.[4] Zwitterionic materials have been applied to numerous biomedical and engineering materials for their non-fouling properties and have demonstrated the ability to reduce nonspecific protein adsorption.[5,6] Zwitterions bind water molecules through electrostatically induced hydration which results in much stronger interactions than that of the hydrogen bonding associated with PEG.[7] Previous studies from our group have shown that, when used as excipients, polyesters functionalized with a zwitterionic carboxybetaine side chains are able to stabilize insulin against agitation as well as granulocyte colony stimulating factor against thermal stress.[8,9] Inspired by this previous work, we sought to further explore the stabilizing effect of these polymers when covalently conjugated to a

therapeutic protein. The polyester backbone of our pCLZ renders our polymer biodegradable, alluding to fewer issues regarding organ and environmental accumulation.[10–12] Aliphatic polyesters are representative examples of environmentally relevant polymeric materials due to their hydrolysable ester bonds.[10,13]

To study the *in vitro* and *in vivo* effects of the covalent conjugation of our degradable zwitterionic polymer, we utilized a growth hormone receptor antagonist (GHA). GHAs are a class of recombinantly engineered protein therapeutics important for regulation of GH signaling in diseases such as acromegaly and insulin-like growth factor 1-dependent cancers.[14–20] The GHA B2036 variant has an FDA-approved multi-PEGylated formulation by the name Pegvisomant (Pfizer, Inc) which demonstrates an *in vivo* half life extension from 15 minutes for unmodified GHA B2036 to 74 h.[21] As with other non-specifically PEGylated proteins, unfortunately, PEGylation of 4-5 lysine residues of GHRA B2036 results in Pegvisomant having a reduced activity, and the PEGylation could elicit immunogenic responses in patients.[21–24] To address the bioactivity challenge, our group recently designed a modification to GHA B2036 whereby the tyrosine at the residue site 35 is replaced with the unnatural amino acid propargyl tyrosine (pgIY, T35pgIY) to function as a site-specific handle for bioconjugation.[25] This insertion site was selected based on research scanning a range of hGH residues for UAA incorporation to determine which sites could be modified without interfering with GHR binding[26–29] and later which could be used to site-specifically PEGylate hGH for increased peptide half-life without significantly reducing the bioactivity.[30,31] In that same work, we demonstrate the enhanced bioactivity of site-selectively PEGylated GHA B2036 and conclude that, compared to Pegvisomant, the half-maximal inhibitory concentrations (IC_{50}) are 12.5 to 23.8 fold lower, depending on the PEG size.

With these benchmarks in mind, we site-selectively conjugated azido-pCLZs of 5, 20, and

60 kDa to GHA-alkyne *via* copper-catalyzed cycloaddition. We hypothesized that site-specific protein-polymer conjugation with pCLZ to GHA-alkyne would improve the pharmacokinetics without decreasing the bioactivity or increasing the immunogenicity of the GHA. Evaluation of the *in vitro* bioactivity of these conjugates resulted in IC_{50} values to be 107 to 430 fold improved compared to Pegvisomant. Pharmacokinetics, studied *via* ^{18}F labelled PET/CT imaging, showed a significant, though short, increase in circulation time by 23 min. Finally, this is the first instance of a site-selective conjugation of a biodegradable, zwitterionic polymer to the best of our knowledge.

4.2 Results and Discussion

Design and Preparation of pCLZ

The initial synthetic scheme was to initiate ROP with PEG_4-azide and functionalize the poly(allyl-caprolactone) in two subsequent steps as reported.[8,9] While the polymerization itself was successful, the following steps introduced many variables to the polymers, including azide photodegradation, possible crosslinking leading to aqueous insolubility, and incomplete functionalization of the allyl side chain. Interestingly, the thiol-ene functionalization step under UV irradiation caused the degradation of the azide handle. While the photodegradation of aryl azides have been reported along with their use as photocrosslinkers,[32–36] alkyl azides are thought to be more stable against photolysis. To circumvent the aforementioned list of issues, a new initiator was synthesized to allow for post-polymerization incorporation of the azide. This new initiator was designed with the following parameters in mind: easily discernible peaks on ^1H NMR for monitoring polymerization, protected amino moiety allowing for post polymerization modification, and an overall structure resembling the caprolactone monomer. Ring opening polymerization of allyl-caprolactone using a N-Boc tyramine-O-hexanol was carried out under

inert conditions (**Figure 4.1A**) using the 3-O/MTBD co-catalyst system. Poly(allyl-caprolactone) polymers were prepared targeting sizes of 2.5, 10, and 30 kDa, designed to match the hydrodynamic radii of mPEG 5, 10, and 20 kDa. The poly(allyl-caprolactone) 30 kDa shows a broader peak, with a slight shoulder, which can likely be attributed to the occurrence of backbiting or co-catalyst degradation. For this particular polymer, an elevated temperature was necessary to achieve sizes past 15 kDa. Previous work by Kiesewetter and co-workers reported co-catalyst degradation at temperature ≥ 80 ºC in 60 min in toluene, therefore 50 ºC was chosen as an appropriate temperature for this reaction.[37] Further optimization of temperature, reaction time, and solvent may circumvent the broad tailing evidence on the GPC trace. However, overall polydispersity was still within the accepted range for controlled polymerizations, so the polymer was carried forward. Unfunctionalized polymers were characterized using gel permeation chromatography in DMF compared against poly(methyl methacrylate) standards (**Figure 4.1B-C**). The previously utilized two-step functionalization of the zwitterionic side chain, thiol-ene click with dimethylaminoethanthiol hydrochloride followed by amine quarternization with t-butyl bromoacetate, was modified to a single step of thiol-ene click with zwitterionic precursor (**Figure 4.2**). This modification proved to be key in ensuring full side chain functionalization. Additionally, the UV source was changed from a hand-held lamp irradiation for 4 h to a photosafety cabinet irradiation period of 10 min. The disappearance of the alkene protons and quantitative appearance of protons from the carboxybetaine moiety on ^{1}H NMR confirmed the successful thiol-ene reaction (**Figure 4.25-27**).

A

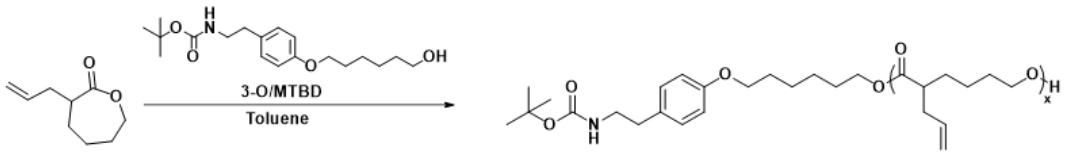

B

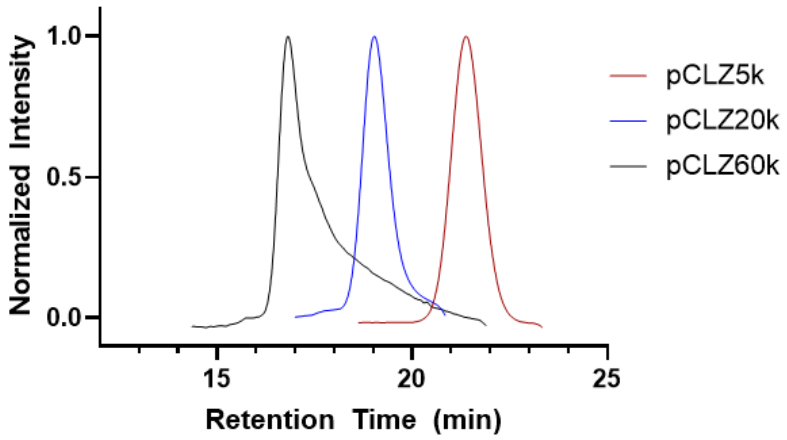

C

	Temp. (°C)	Time (h)	Conv. (%)	Mn	Mw	Đ
pCLZ 5k	20	1	92	2996	3159	1.05
pCLZ 20k	20	5	90	12076	12494	1.03
pCLZ 60k	50	5	82	30603	36852	1.20

Figure 4.1 A) Ring opening polymerization of poly(allyl-caprolactone) using 3-O/MTBD co-catalyst system **B**) DMF GPC traces detected by refractive index and **C**) polymerization conditions, size, and dispersity

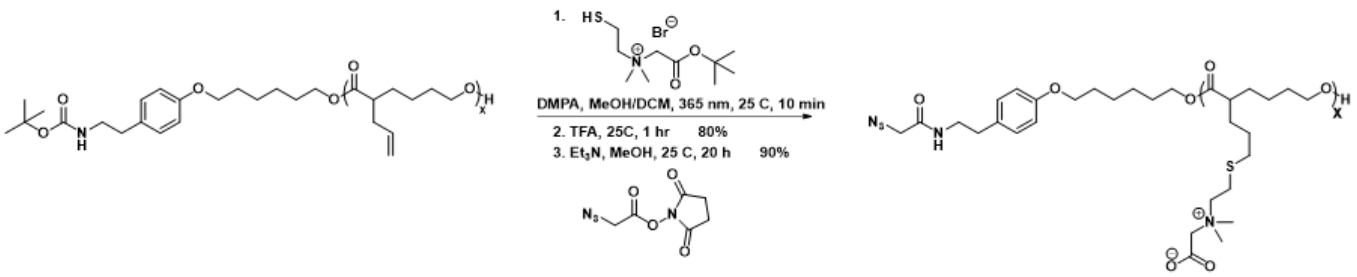

Figure 4.2 Scheme of functionalization of poly(allyl-caprolactone) and subsequent azidation

Site-Specific Conjugation of GHA-alkyne to Azido-pCLZ

Using a previously reported GHA-alkyne from our group,[25] standard copper catalyzed azide-alkyne cycloaddition (CuAAC) conditions were used to prepare the conjugates. For the conjugations using pCLZ 5 kDa and pCLZ 20 kDa, no modifications to this procedure were needed (70% conversion, 50% yield). For the conjugation using pCLZ 60 kDa, however, a number of different optimization conditions were explored, including the addition of organic co-solvents, modification of reaction temperature, and investigation of different catalyst concentrations (**Figure 4.29**). Due to the large size of the pCLZ 60 kDa polymer, the azide handle was thought to be less readily accessible to interact with the alkyne of the protein. The equivalents of protein to pCLZ 60 kDa were varied from 1:10 to 1:1. A higher equivalence of pCLZ 60 kDa, interestingly, did not increase conjugation efficiency and made subsequent FPLC purification more challenging. For this reason, the equivalents for the conjugation of GHA to pCLZ 60 kDa was set to 1:1. Using double the concentration of both $CuSO_4$ and BTTAA ligand, the CuAAC of GHA-pCLZ60k was carried out at 37 °C for 2 h, with a conversion of approximately 50%. Subsequent purification was carried out using FPLC on a Bio-Rad BioLogic

DuoFlow chromatography system equipped with two daisy-chained 1 mL GE Healthcare HiTrap Q HP columns using a method of 0-1 M NaCl in 10 mM PB, pH 7.4, 10% glycerol. Concentration of conjugates was determined *via* BCA assay and protein purity was assessed by SDS-PAGE (**Figure 4.3**). An overall 25% yield of pure GHA-pCLZ60k conjugate was obtained.

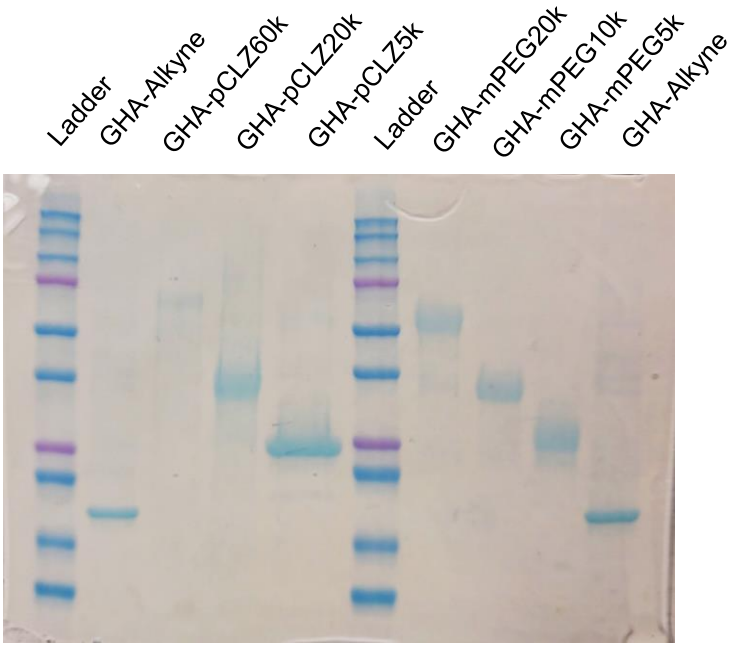

Figure 4.3 SDS-PAGE of GHA-Alkyne and purified conjugates visualized with Coomassie

Evaluation of Conjugate Activity *In Vitro* as a Function of pCLZ Molecular Weight

As previously performed in the literature and in our group, the efficacy of GHA-alkyne and the different conjugates was assessed by a cell viability assay with Ba/F3 cells engineered to stably express GHR and depend on hGH for proper growth.[25,38] For this assay, cells were incubated with different GHAs and hGH for 48 h before the cells were measured for viability with resazurin blue and the resulting GHA response was calculated from this measurement. As the efficacy of GHA-alkyne had already been found comparable to B2036 without the 35pgIY insertion, and the conjugation of mEG polymers was clearly shown to reduce bioactivity as a function of polymer size,[25] we decided to study a rnage of sizes of GHA-pCLZ and GHA-mPEG compared against GHA-alkyne. Despite larger polymer sizes detrimentally affecting conjugate bioactivity, it was reported that Pegvisomant, the non-site-specifically conjugated GHA-mPEG (totaling 20-25 kDa in mPEG), had an IC_{50} an order of magnitude larger (1289 nM) than the site-specific GHA-mPEG (20 kDa) (103.3 nM). By measuring the bioactivity of Ba/F3-GHR cells incubated with GHA-alkyne, GHA-pCLZ (60 kDa), GHA-pCLZ (20 kDa), GHA-pCLZ (5 kDa), GHA-mPEG (20 kDa), GHA-mPEG (10 kDa), and GHA-mPEG (5 kDa), the inhibitory efffect of the different polymers as well as the polymer chain lengths could be compared to determine the relationship between polymer, size, and bioactivity **(Figure 4.4**).

A

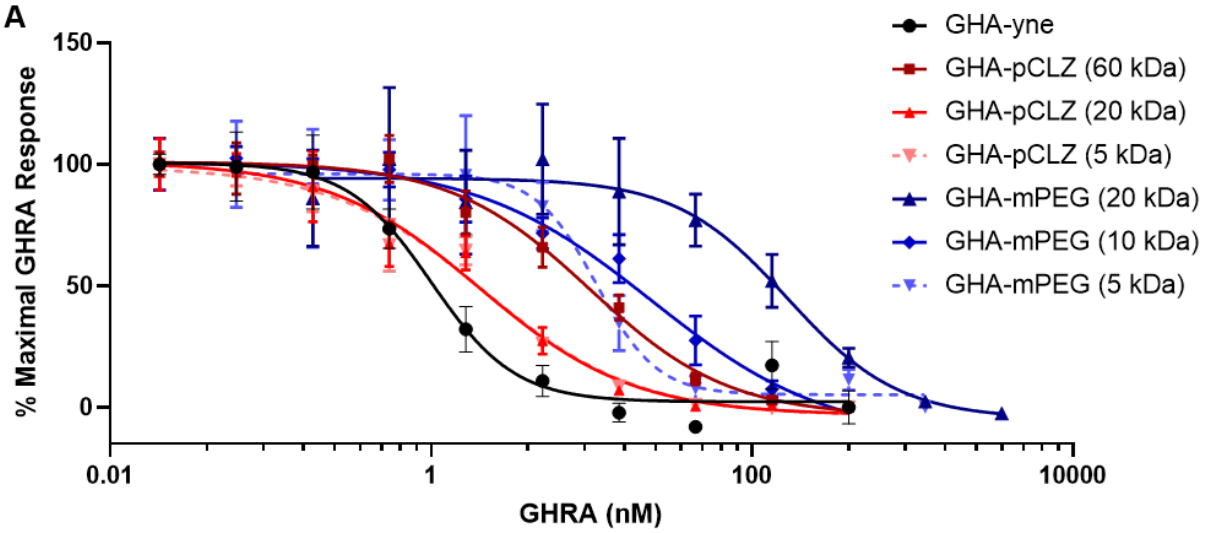

B

GHA	IC_{50} (nM)	95% CI (nM)
GHA-yne	2.679	1.265 – 4.228
GHA-pCLZ (60 kDa)	11.869	7.601 – 21.010
GHA-pCLZ (20 kDa)	3.307	2.258 – 4.875
GHA-pCLZ (5 kDa)	3.296	2.374 – 4.660
GHA-mPEG (20 kDa)	92.867	39.520 – 215.875
GHA-mPEG (10 kDa)	33.013	17.927 – 293.38
GHA-mPEG (5 kDa)	12.140	9.217 – 15.8167

Figure 4.4 A) GHA efficacy of GHA-alkyne, GHA-pCLZ conjugates (5-60 kDa), and GHA-mPEG conjugates (5-20 kDa) measured by inhibitory bioactivity dose response in Ba/F3-GHR cells. **B**) Averaged IC_{50} and 95% confidence interval (CI) results from three individual Ba/F3-GHR cell inhibitory experiments. All IC_{50} values are statistically different from each other ($p < 0.05$) except for the two smallest GHA-pCLZ conjugates (5 and 20 kDa, $p < 0.05$) according to ANOVA with subsequent Students' t-test.

In comparing the two different polymers, it is clear that conjugation of any polymer decreases the bioactivity of the conjugates, however this experiment showed that the pCLZ conjugates expereince a less of a decrease in bioactivity when compared to mPEG conjugates (**Figure 4.4**). Considering the earlier reported bioactivity of Pegvisomant and site-specific GHA-mPEG (20 kDa), all of these conjugates show 107 to 430 fold and 7 to 28 fold improved IC_{50} values compared to Pegvisomant and GHA-mPEG (20 kDa) reported here, respectively. This underlines the earlier finding that site-specifically conjugating polymers does not reduce the bioactivity of GHA-alkyne as much. This new data further expands our knowledge regarding the effect of different polymers as conjugates. The IC_{50} values of the mPEG conjugates, ranging in size from 5-20 kDa, were all higher than the IC_{50} values of the even larger pCLZ conjugates which ranged from 5-60 kDa (**Figure 4.4B**). In fact, the two smaller pCLZ conjugates (5 kDa and 20 kDa) were not statistically different from each other (3.3 nM), and very close to the inhbitory activity of GHA-alkyne (2.7 nM). Further, the largest GHA-pCLZ conjugate (60 kDa) (11.9 nM) has a bioactivity far closer to that of GHA-mPEG (5 kDa) (12.1 nM) than the largest GHA-mPEG (20 kDa). All together, this bioactivity data clearly indicates that the site-specific conjugation of pCLZ does not interfere with the GHA-alkyne bioactivity as much as the addition of mPEG and could allow the addition of larger polymer sizes without causing as dramatic of a decrease in bioactivity. This can be explained by the greater decrease in alpha-helicity of the protein shown by circular dichorism (CD) upon conjugation with mPEG compared to pCLZ and GHA-Alkyne alone(**Figure 4.30**). Loss of alpha-helicity indicates an unfolding of the tertiary structure which could impair the ability of the GHA conjugates to bind to GHR. In addition, it has been reported that PEGylation sterically reduces binding to growth hormone receptor.[24] These results imply that utilizing pCLZ could allow for the use of a potentially lower dose of therepeutic protein for

comparable efficacy.

Evaluation of Conjugate Immunogenicity *In Vivo*

The adaptive immune response can produce antibodies in response to perceived antigens that, in addition to the immune reaction, will remove the foreign material. The GHA-alkyne, GHA-pCLZ, and pCLZ were all studied for their potential to trigger the immune system to produce IgG and IgM antibodies, two of the most abundant types of antibody isotypes accounting for 75-95% of all antibodies.[39] Mice were challenged with intraperitoneal (i.p.) injections of GHA-alkyne, GHA-pCLZ, and pCLZ (2 mg/kg) at weeks 0 and 2. Enzyme-linked immunosorbent assay (ELISA) was used to measure IgGs and IgMs in serum specific to each potential antigen for each week.[40] As a negative control, naive mouse serum was added to the GHA-alkyne and GHA-pCLZ coated microplate. None of the possible antigens, modified protein, conjugate, or polymer elicited any measurable IgG or IgM response as compared to the naïve controls (**Figure 4.5**). These results are as expected as GHA-alkyne shares 182 of its 191 residues in common with hGH. GHA-alkyne does not instigate an immune reaction and both pCLZ alone and conjugated to GHA-alkyne are similarly benign with respect to the adaptive immune system. We would therefore expect that, without the production of antibodies in response to polymer, conjugate, or protein, the half-life in

circulation would not be cut short by antibody clearance mechanisms.

Pharmacokinetics and Biodistribution of [^{18}F] SFB-GHA-pCLZ 60 kDa Conjugate *In Vivo*

We then studied the pharmacokinetics and biodistribution of our most promising conjugate, GHA-pCLZ60k along with GHA B2036 and pCLZ 60 kDa as controls. GHA B2036, amino-pCLZ 60 kDa, and GHA-pCLZ60k were radiolabeled with [^{18}F] SFB (Figure 4.6) and injected at a radiochemical purity greater than 99% into mice (n=4, female, C57/BL6). Decay-corrected and attenuation corrected images from dynamic µPET suggest that the protein and the conjugate were

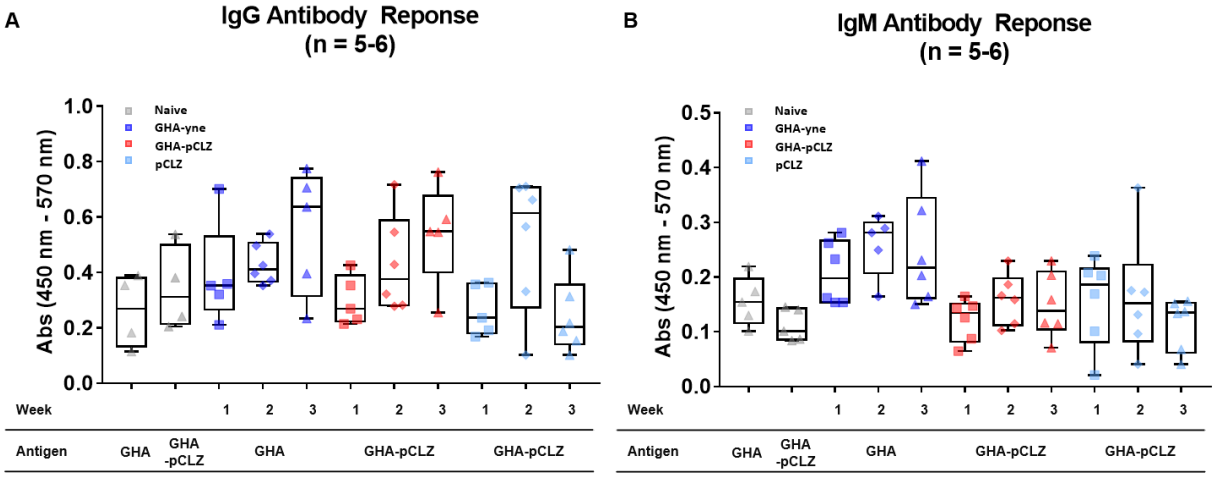

Figure 4.5 Antibody levels in mice specific to GHA-alkyne or GHA-pCLZ antigens over 3 weeks after i.p. injection of GHA, GHA-pCLZ, or azide-pCLZ at weeks 0 and 2 (n = 5 – 6). Levels measured by immune indirect ELISA for a. IgG and b. IgM specific antibody responses and compared to non-specific baseline antibody recognition in naïve mice

cleared predominantly through the kidneys while the polymer was cleared through the liver. Compared to the conjugate, the protein alone was cleared more rapidly through the kidney post-injection. The conjugate demonstrates a significant increase in circulation time, compared to the

protein alone, by measuring the μPET signal intensity in the blood pooled inside the heart (Figure 4.7A-B). Despite the presence of the large polymer on the conjugate, the GHA-pCLZ60k shows a much lower amount of uptake in the liver than the pCLZ 60 kDa does. The higher level of μPET signal intensity, in the liver and the lungs, of the conjugate than that of the protein alone is probably due to the higher activity in the blood in these organs. The blood half-life calculation is fit as a two-phase model (Graphpad Prism 9) – a rapid decrease phase followed by a slow decrease phase (Figure 4.35). In the slow decrease phase, the half-life of ^{18}F-SFB-GHA and ^{18}F-SFB-conjugate is 0.36 h and 0.74 h, respectively (Figure 4.8A). To our surprise, the half-life of the conjugate is much shorter than anticipated, though it is statistically significant compared to the protein alone. This can be attributed to a few possible explanations: considering the low liver uptake of the conjugate, the polymer may be degrading much faster by esterases *in vivo* than has been studied *in vitro*, and/or the pCLZ intrinsically does not extend circulation time at a meaningful scale. While the degradability of polyesters is well known and widely studied,[11,12] their degradation rate *in vivo* still exists as a challenging experiment due to the insoluble nature of polyesters and the lack of facile methods of detection, including soft ionization mass spectrometry. The zwitterionic moiety on our polyester makes the pCLZ readily soluble in aqueous solutions but unfortunately does not provide any added advantages in studying their degradation.

Ex Vivo Degradation in Plasma

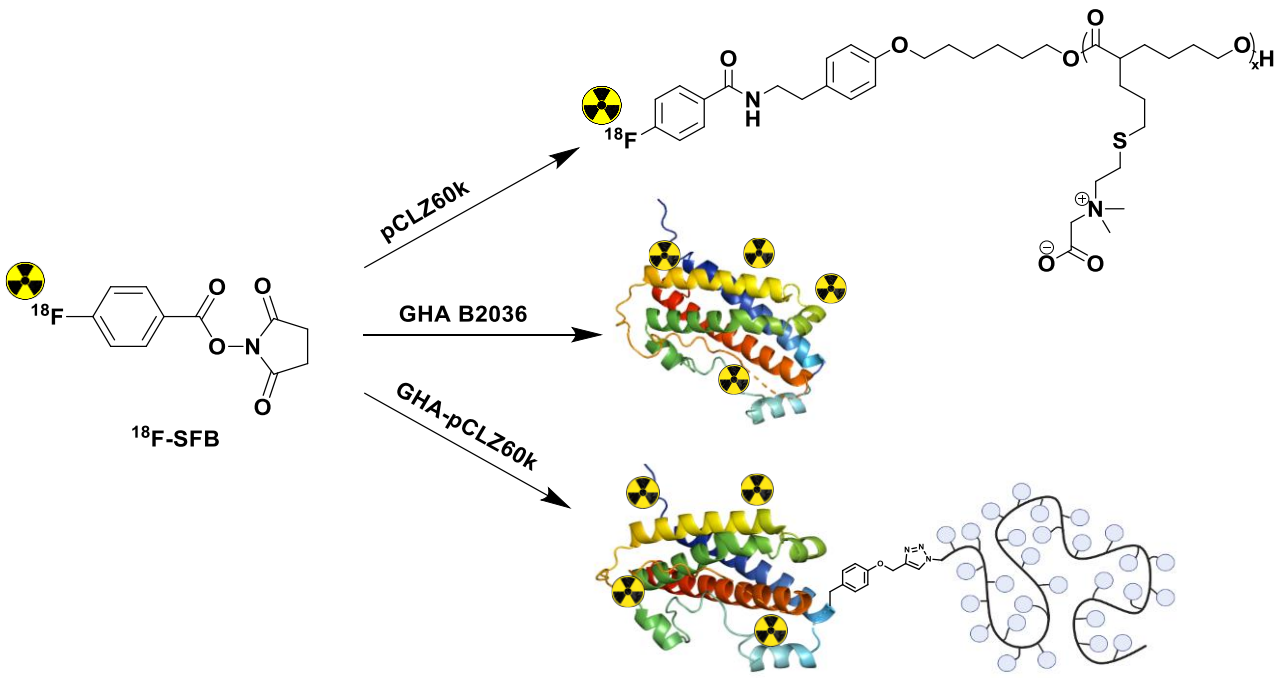

Figure 4.6 [^{18}F]SFB radiolabeling of amino-pCLZ60k, GHA B2036, and GHA-pCLZ60k

To further our understanding as to why the circulation time did not increase at a clinically meaningful scale, we examined the *ex vivo* degradability of the conjugate in mouse plasma. As a positive control to ensure the presence of esterases, fluorescein diacetate was mixed into plasma. Shortly after addition, the solution turned fluorescent, indicating that the esterases had hydrolyzed the fluorescein diacetate. A concentrated stock of GHA-pCLZ60k was added to plasma to a 1 mg/mL final concentration. The vial was mixed and placed in a 37 °C incubator and shaken at 250 rpm. Timepoints were taken at 0, 1, 2, 4, and 6 hours. Proteins were precipitated with isopropanol with 1% trichloroacetic acid. The supernatant was discarded while the protein pellet was dissolved and neutralized with ammonium bicarbonate. Timepoints were analyzed *via* Native PAGE followed by western blot. At t = 6 h, the presence of the GHA-pCLZ60k is clear(Figure 4.9). The absence of lower molecular weight conjugate species suggests that the polymer is intact against the esterases. It becomes apparent that the explanation for the shorter than anticipated extension

of *in vivo* circulation time is due to the nature of the polymer itself. The key difference between zwitterionic polymers that have been reported to extend circulation time and our pCLZ is the presence of a very hydrophobic polyester backbone in our model. The hydrophobic polyester backbone combined with the hydrophilic zwitterionic side chain could self-assemble into a micellar-type structure and reduce the overall hydrodynamic radii, an important property for circulation time extension. The presence of the polyester backbone could also interrupt the strong

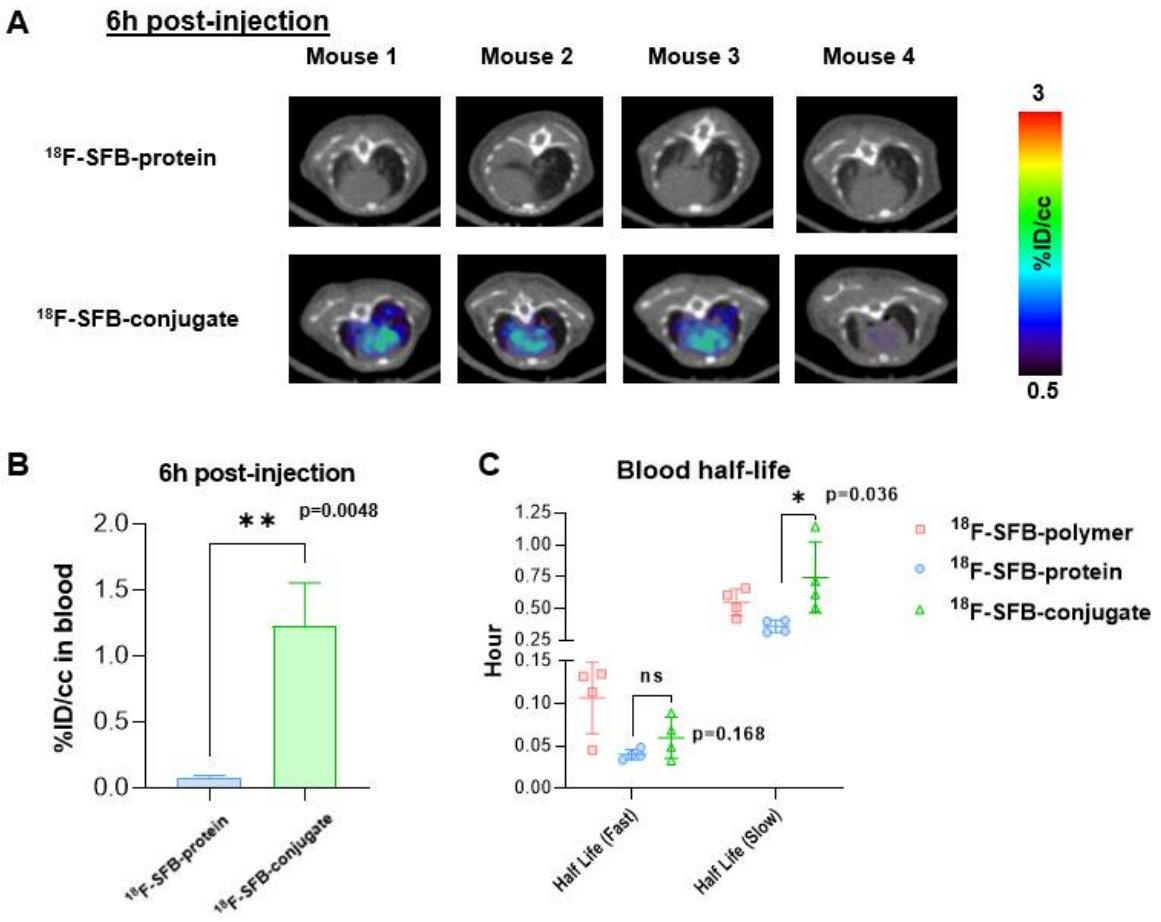

Figure 4.7 A) PET/CT images at 6 h post injection of [^{18}F]-SFB-GHA and [^{18}F]-SFB-GHA-pCLZ60k and **B**) %ID/cc in blood at 6 h post injection C) blood half-life analysis using two phase decay model

electrostatically induced hydration from the zwitterionic side chain and create hydrophobic pockets. Markedly, more hydrophobic polymers have demonstrated more destabilization of protein after conjugation while more hydrophilic polymers have resulted in higher protein activity.[41]

A

	^{18}F-SFB-protein	^{18}F-SFB-polymer	^{18}F-SFB-conjugate
Half Life (Fast)	0.03990	0.09476	0.05957
Half Life (Slow)	0.36083	0.57320	0.74318

B

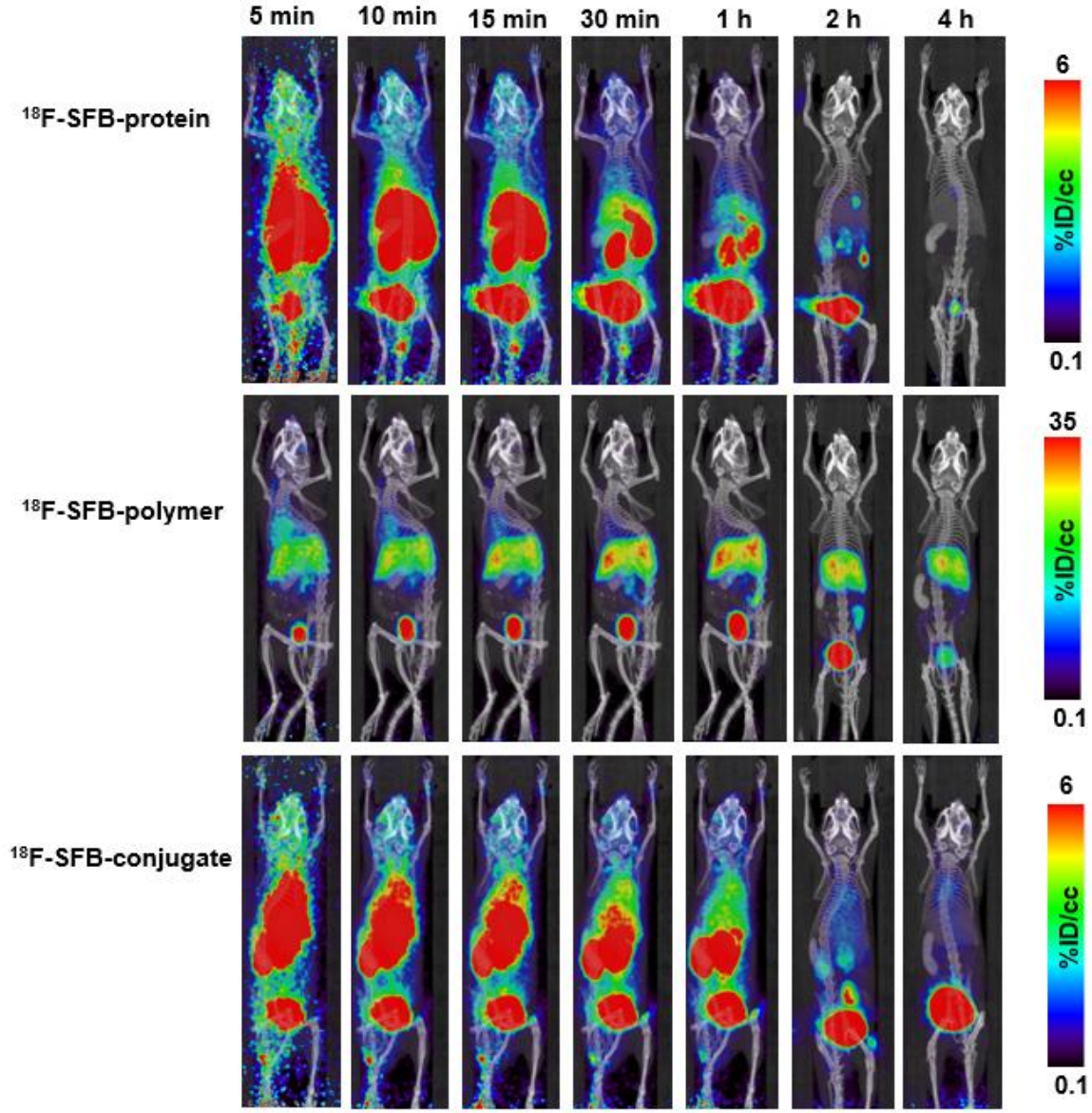

Figure 4.8 **A**) in vivo half lives in hours of [^{18}F]-SFB-GHA, [^{18}F]-SFB-pCLZ60k, and [^{18}F]-SFB-GHA-pCLZ60k and **B**) biodistribution over 4 h post-injection

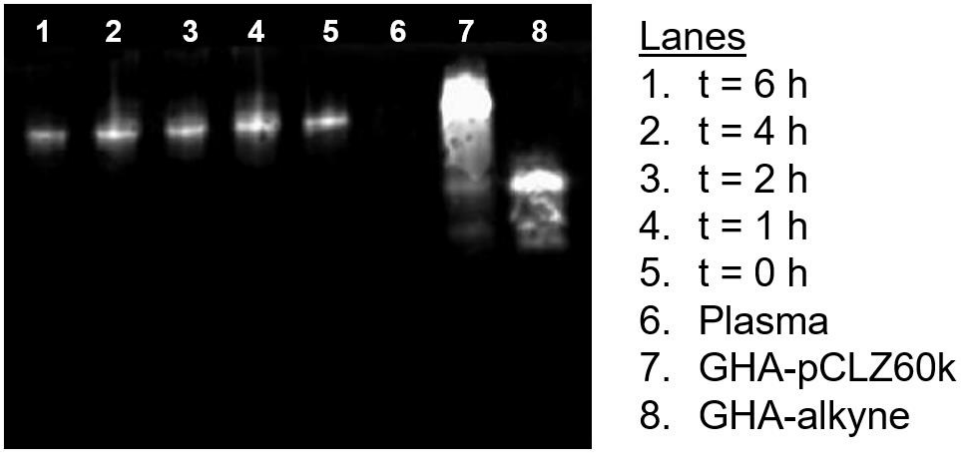

Figure 4.9 Western blot of *ex vivo* degradation of GHA-pCLZ60k in mouse plasma

4.3 Conclusion

Altogether GHA-alkyne, GHA-pCLZ, and pCLZ were all found to not elicit measurable antibody production, preserved bioactivity of the GHA *in vitro*, and demonstrated a measureable increase in *in vivo* circulation time. Because the pCLZ polymer is degradable, the conjugation of polymers over 40 kDa does not clearly pose a safety or *in vivo* attenuation risk,[42] as we expect any polymer not excreted as the conjugate would degrade over time. Despite this, the half-life was found to increase to 0.76 h compared to Pegvisomant with a half-life of 74 h. This result was particularly surprising as the net increase in MW with the GHA-pCLZ we studied is 60 kDa, and Pegvisomant has only a MW increase of ~20 kDa. We hypothesize that an explanation for this could be due to the hydrophobicity of the polyester backbone. PEG is an amphiphilic polymer in which the hydrophobic regions cause loss of bioactivity. Likewise, our pCLZs have a very hydrophobic backbone with a very hydrophilic side chain. To test this hypothesis, a zwitterionic

polymer with either a very hydrophilic backbone or a short traditional acrylate backbone could be site-selectively conjugated to GHA-alkyne.

In this work, GHA-pCLZ conjugates were investigated for immunogenicity, activity, and pharmacokinetics. Antibody production in response to GHA-alkyne, pCLZ, and GHA-pCLZ was measured, and no notable immunogenic response was measured through ELISA. The activity of GHA-pCLZ at a range of polymer sizes was measured *in vitro* with GHA-pCLZ conjugates providing better bioactivity than the GHA-mPEG conjugates. Finally, mice injected with the largest GHA-pCLZ conjugate (60kDa) and GHA B2036 were measured by μPET/μCT over time, and we found that the GHA-pCLZ conjugate did increase the half-life of the GHA by approximately 23 min.

Acknowledgements

The authors thank Crump Imaging Center staff (Mikayla Tamboline, Jeffrey Collins) and faculty (Mike van Dam, Shili Xu) for PET/CT imaging studies, JCCC Cancer Center Grant (NIH/NCI #2 P30 CA016042-44) that subsidizes JCCC members for imaging services, the CTSI award (NIH/NCATS #UL1TR001881), and the NIH S10 Shared Instrumentation for Animal Research (SIFAR) Grant (NIH #1 S10 OD026917-01A1) that funded the PET/CT scanner used in this study. NIH award S10OD028491 is acknowledged for providing funding for the circular dichroism spectrometer.

4.4 Appendix C

Materials

All materials and proteins were purchased from Sigma-Aldrich, Acros, or Fisher Scientific and were used without purification unless noted. Anhydrous toluene was distilled from CaH_2 and stored under argon prior to use. Anhydrous tetrahydrofuran (THF) was distilled from sodium benzophenone and stored under argon prior to use. Anhydrous dichloromethane (DCM) was distilled from CaH_2 and stored under argon prior to use. Polymerizations were performed in a Vacuum Atmospheres Genesis stainless steel glovebox under anhydrous nitrogen atmosphere. Spectra/Por3® regenerated cellulose membrane (MWCO 1 or 3.5 kDa) was purchased from Spectrum Chemical (New Brunswick, NJ) for polymer dialysis. Allyl-caprolactone was synthesized as previously described and purified by distillation under reduced pressure before use.[8,9] Bistristhiourea (3-O) was synthesized and purified according to literature precedent.[8,37,43] GHA B2036 and GHA-Alkyne were expressed and purified as previously described.[25] Spectra/Por3® regenerated cellulose membrane (MWCO 3.5 kDa or 1.0 kDa) used for polymer dialysis was purchased from Spectrum Chemical (New Brunswick, NJ). Amicon Centriprep™ tubes were purchased from Millipore. Any kD and 4-20% Mini-PROTEAN-TGX™ PAGE gels and SDS-PAGE protein standards (Precision Plus Protein™ Dual Color) were purchased from Bio-Rad. Murine Ba/F3 cells stably expressing human GHR (Ba/F3-GHR) were obtained from Professor Michael Waters (University of Queensland, Australia). RPMI 1640 media with L-glutamine and 25 mM HEPES buffer was purchased from Gibco, and recombinant hGH (rhGH) purchased from Dr. A.F. Parlow at the National Hormone and Peptide Program (Harbor-UCLA Medical Center, Torrance, CA) was resuspended at 0.5 mg/mL in 0.1 M PBS before being stored at -80 °C, following storage instructions. Goat anti-mouse IgG HRP conjugate and goat anti-mouse IgM HRP conjugate were both purchased from Abcam, reconstituted, diluted 2x with glycerol,

and stored at -80 °C following manufacturer's recommendations. Rabbit anti-hGH primary antibody (ab155276) and goat anti-rabbit IgG H&L (AF488) (ab150077) were purchased from Abcam. Pierce BCA assay kit and enzyme-linked immunosorbent assay (ELISA) TMB development solution was purchased from ThermoFisher Scientific. DuoSet hGH ELISA kit was purchased from R&D Systems (catalog #DY1067).

Analytical Techniques

NMR spectra were obtained on Bruker AV 500 and Bruker AV 400 MHz spectrometers. ^{1}H NMR spectra were acquired with a relaxation delay of 2 s for small molecules and 8 s for polymers. Infrared absorption spectra were recorded by using a PerkinElmer FT-IR equipped with an ATR accessory. Gel permeation chromatography (GPC) was conducted as follows: The allyl polymers were characterized on a Shimadzu high performance liquid chromatography (HPLC) system with a refractive index detector RID-10A, one Polymer Laboratories PLgel guard column, and two Polymer Laboratories PLgel 5 μm mixed D columns. Eluent was DMF with LiBr (0.1 M) at 50 °C (flow rate: 0.80 mL/min). Calibration was performed by using near-monodisperse PMMA standards from Polymer Laboratories. Ultraviolet irradiation was carried out in a Photochemical Safety Reaction Cabinet from Ace Glass Incorporated at 365 nm. Fast protein liquid chromatography (FPLC) was performed on a Bio-Rad BioLogic DuoFlow chromatography system equipped with two daisy-chained 1 mL GE Healthcare HiTrap Q HP column. Circular dichroism was performed on a Chirascan V-100 equipped with a Peltier at a temperature of 25 °C. Western blot was imaged on Pharos FX Gel Scanner (Bio-Rad).

Animal Usage

All animal experiments were conducted according to protocols approved by the UCLA

Animal Research Committee (ARC).

Methods

Polymer synthesis

In a nitrogen-filled glovebox, a dram vial was charged with a stir bar, 3-O, MTBD, toluene, and N-Boc tyramine O-hexanol. A solution of allyl-caprolactone in toluene was added to initiate the polymerization. Polymerization was allowed to proceed at 20 °C for pCL 2,5k and pCL 10k polymers. For the pCL 30k, the dram vial and its contents were fully assembled and sealed, then removed from the box and allowed to polymerize at 50 °C in an oil bath. Reaction was monitored by ^{1}H NMR. After 1 hr, 5 hr, and 5 hr, the polymerization was quenched with either acetic acid or benzoic acid in toluene for pCL 2.5k, pCL 10k, and pCL 30k, respectively. Polymers were purified *via* normal phase silica chromatography at 15% EtOAc/Hex to remove residual monomer and 50% EtOAc/Hex to elute polymer.

Thiol-Ene Modification

In a dram vial, poly(allyl-caprolactone), dimethoxyphenylacetophenone, zwitterion precursor, MeOH/DCM, and a stir bar were added. The mixture was sparged with argon for 5 min and then exposed to 365 nm UV light for 10 min. The solution was opened to air and volatiles were evaporated down to an oil. Trifluoroacetic acid was added to the crude oil to cleave the t-butyl protecting groups on the zwitterion precursor as well as the N-boc of the initiator to reveal a free amine. After 1 hour, the TFA was evaporated under vacuum and the crude mixture was diluted with 1:1 MeOH/water and dialyzed in a 1 kDa MWCO membrane against 1:1 MeOH/water, switching to 100% water after 24 h. The resulting solution was lyophilized to yield a white solid.

Azide functionalization of pCLZ

In a dram vial, amino-pCLZ (1 eq.), 2-azidoacetate succinimidyl ester (20 eq.), and triethylamine (20 eq.) were dissolved in a mixture of methanol and water. The reaction was allowed to proceed for 20 hours at 23 °C under vigorous stirring. Pure product was isolated by precipitating the mixture into 1:2 THF/diethyl ether twice.

Conjugation of Growth Hormone Antagonist-Alkyne with pCLZ

Conjugation was carried out according to standard copper-catalyzed azide-alkyne click (CuAAC) chemistry conditions.[44] $CuSO_4$ (20 mM), BTTAA (50 mM), aminoguanidine hydrochloride (100 mM), and sodium ascorbate were prepared as stock solutions in 100 mM phosphate buffer. Reactions were carried out at a final protein concentration of 1 mg/mL. In a 1.5 mL lo-bind tube, GHA-Alkyne, pCLZ, and phosphate buffer were added. In a separate vial, $CuSO_4$ and BTTAA were premixed in a 1:2 ratio and then added into the reaction vial. Aminoguanidine hydrochloride was added to the reaction vial to a final concentration of 5 mM. Sodium ascorbate was added at a final concentration of 5 mM to initiate the reaction. CuAAC of pCLZ 5 kDa and pCLZ 20 kDa were carried out at 25 °C for 2 h with rocking. CuAAC of pCLZ 60 kDa was carried out using twice the concentration of $CuSO_4$ and BTTAA at 37 °C for 2 h with rocking. Subsequently, the reaction mixtures were purified of small molecules *via* centrifugal filtration using a 10 kDa MWCO filter and replenishing with 10 mM phosphate buffer pH 7.4. Conjugates were furthur purified by FPLC on a Bio-Rad BioLogic DuoFlow chromatography system equipped with two daisy-chained 1 mL GE Healthcare HiTrap Q HP columns using a method of 0-1 M NaCl in 10 mM PB, pH 7.4, 10% glycerol. Fractions were analyzed by SDS-PAGE followed by coomassie or silver stain. Pure fractions were pooled together and concentrated down. Protein concentration was measured by BCA assay.

Antibody immunogenicity of GHA-alkyne, GHA-pCLZ, and pCLZ in Mice

CD-1 mice (8 weeks, female, n = 5 – 6, Charles River Laboratories) were used to study the immunogenicity of GHA-alkyne, GHA-pCLZ (6.56 kDa), and pCLZ (6.56 kDa). Protein, conjugate, and polymer were each administered *via* i.p. injection (2 mg/kg in sterile saline buffer). Mice were challenged again 2 weeks after inoculation with the same dosage for each condition. Blood was collected into serum separator centrifuge tubes (SSTs) *via* retro-orbital bleeding at 1, 2, and 3 weeks after administration. Blood was centrifuged at 2,000 rcf for 15 min to extract serum. Serum was stored at −80 ºC until ELISA could be run. Mice were sacrificed after 4 weeks and a final time point was collected *via* cardiac puncture. Blood was treated the same as prior time points.

Antibody IgG and IgM immunogenicity ELISA

Sterile-filtered 0.1 M PBS buffer + 0.3% n-dodecyl-β-D-maltoside was used to wash the wells four times between each step, making sure to remove solution by hitting the plates against paper towels after each wash. Antigen solutions of GHA-alkyne or GHA-pCLZ conjugate (total 0.02 mg/mL, 100 µL/well) were plated on 96-well plates. After incubating at room temperature (21 °C) for 13 h, antigen was removed, the wells washed and blocked with sterile filtered 3% BSA in 0.1 M PBS (300 µL) for 2 h at 37 °C. After washing out the BSA blocking solution, serum from the mice was diluted 100, 500, 2,500, and 12,500-fold with filtered 3% BSA in 0.1 M PBS (100 µL/well) was then incubated with the respective antigen for 2 h at 37 °C (GHA-alkyne antigen with GHA-alkyne exposed mice, GHA-pCLZ antigen GHA-pCLZ exposed mice, and GHA-pCLZ antigen with pCLZ exposed mice). After washing the wells, goat anti-mouse IgG or IgM HRP-conjugate antibody diluted 2,000 × with filtered 1% BSA in 0.1 M PBS (100 µL/well) was incubated for 1 h at 37 °C. The secondary detection antibody HRP conjugate was removed and the wells washed. In the dark, TMB substrate solution was added (100 µL/well), and the plate was incubated at room temperature (21 °C). After 5 – 10 min when color had developed in positive

control wells, reaction was quenched by adding 2 M H_2SO_4 (50 µL/well) stop solution. Absorbance was measured at 450 nm and background was subtracted at 570 nm. Controls included ovalbumin (OVA) antigen with OVA exposed mouse serum (positive control), OVA antigen with naïve mouse serum (negative control), GHA-alkyne antigen with naïve mouse serum (negative control), and GHA-pCLZ antigen with naive mouse serum (negative control and check on non-specific binding).

Cell viability assay measure of GHA-pCLZ conjugate activity

Ba/F3-GHR cells were cultured at 37 ºC and 5% CO_2 in RPMI 1640 media completed with 100 U/mL penicillin, 100 U/mL streptomycin, 1% Glutamax, 5% fetal bovine serum (FBS), and 25 ng/mL rhGH (added fresh at least every 7 days). After thawing out, Ba/F3-GHR cells were cultured every 2-4 days with fresh media to stay within a cell concentration of 10,000-200,000 cells/mL; a common splitting ratio was 1:10 to maintain appropriate concentrations of cells.

After the cells had grown to sufficient density for the assay, cells were serum starved overnight for up to 16 h. To replace the serum with complete media sans 25 ng/mL rhGH, cells were spun down, media was removed, and cells were resuspended in the incomplete serum media two times. Cells were then diluted and plated at 20,000 cells/well (80 µL) in the interior wells of a standard, clear, 96-well plate. The outer wells were filled with media to prevent edge effects, and plates were incubated for 20 min at room temperature before being returned to the incubator (37 ºC and 5% CO_2) while serial dilutions of the GHA-alkyne and conjugates were made. The dilutions ranged from 0 to 36,000 nM depending on the antagonist, and, upon completion, they were added to the wells (10 µL) (n = 4 replicates per dilution). Finally, rhGH was added to the wells (10 µL) for a concentration of 20 ng/mL and the cells were incubated for 48 h (37 ºC and 5% CO_2). Final cell viability after incubation with GHA-alkyne or a conjugate was measured by adding resazurin

sodium salt (0.5 mg/mL) to each well (5 µL), incubating for 2 h (37 ºC and 5% CO_2), and taking fluorescence measurements (λ_{excite} = 530 nm, λ_{emit} = 585 nm). *In vitro* assays were repeated at least two times on cells of different generations, and a representative figure of these is shown in the text. The half-maximal inhibitory concentration (IC_{50}) for GHA-alkyne and each GHA conjugate was calculated by fitting a sigmoidal dose-response model.

[^{18}F] SFB radiolabeling onto GHA B2036, pCLZ 60 kDa, and GHA-pCLZ60k

[^{18}F] SFB was re-suspended in sodium borate buffer (~300 MBq in 100 µL SBB 50 µmol/L, pH 8.0) and incubated with protein, polymer, and conjugate molecules (100–200 µg in 200 µL SBB) for 10 min at 40 °C. Excess prosthetic group was separated from the conjugate using Amicon Ultra (0.5 mL, Ultracel 10 kDa) centrifugal filters. The centrifuge tubes were spun at 8000 RPM for 3 min after loading the crude reaction material. The column was then rinsed by adding 0.5 mL of PBS (pH 7.4) and spinning for an additional 3 min at 8000 RPM. The rinse procedure was repeated 3 times (or as many times needed until the radioactivity level remained constant on the filter of the column). The activity remaining on the filter was removed by adding 0.5 mL of PBS and pipetting it out to an Eppendorf tube. Labeling efficiency and radiochemical purity were analyzed using ITLC strips with saline as solvent. [^{18}F] SFB-GHA-B2036 and [^{18}F] SFB-pCLZ 60 kDa were produced at 4% radiolabeling efficiency with > 99% radiochemical purity. [^{18}F] SFB-GHA-pCLZ60k was produced at 10% radiolabeling efficiency with > 99% radiochemical purity.

Pharmacokinetics and Biodistribution studies of [^{18}F] SFB radiolabeled GHA B2036, pCLZ 60 kDa, and GHA-pCLZ60k

Four C57BL/6 mice (15 weeks, female, from Jackson Laboratory) were anesthetized with 1.5%

vaporized isoflurane and were injected *via* i.v. injection (tail vein) with 18F-labeled SFB-Protein , 18 F-labeled SFB-polymer, and 18 F-labeled SFB-conjugate of the protein and polymer (20-80 µCi). Each group was scanned immediately after injection for a 1 h dynamic µPET followed by a 1 min µCT scan with or without contrast agent, Exitron Nano 12000 (Miltenyi Biotec). Mice were imaged by µPET/µCT again at 2 h and 4 h (static µPET, 20-50 minutes) post tracer injection. All µPET images were acquired with an energy window of 350-650 keV, followed by 3D histographic analysis and reconstruction using the 3D-OSEM/MAP methods.Data was decay- and attenuation-corrected, and scaled by initial imaging. All µCT images were acquired at 80 kVp and a 200 µm resolution. Amide software was used to analyze co-registered µPET/µCT images, and MIPs were generated.

***Ex Vivo* Degradation of GHA-pCLZ60k in mouse plasma**

One C57BL/6 mouse used for µPET/µCT imaging experiment was sacrificed and plasma was collected. Plasma was stored in -80 °C until ready to use. A stock solution of fluorescein diacetate was prepared as 1 mg/mL of which 1 µL of stock was added to 1 µL of plasma. A bright fluorescent color indicated the presence of esterases in plasma, serving as a positive control. Degradation was studied at 37 ºC with shaking at 250 rpm. Timepoints were taken at 0, 1, 2, 4, and 6 h. Proteins were precipitated out by adding isopropanol with 1% trichloroacetic acid at a 1:10 ratio. The solution was vortexed and then centrifuged down at 4 °C at 13200 rpm for 5 min. The protein pellet was dissolved and neutralized with 100 mM ammonium bicarbonate pH 7.2, and prepared for Native-PAGE by adding 2x Native loading buffer. Native-PAGE (4-20% Mini-PROTEAN TGX) was run at 200 V for 35 min. Proteins were wet-transferred to a nitrocellulose blot at 100V for 1 h. Non-specific proteins were blocked in 5% milk for 2 h at 25 °C. Blot was rinsed twice in TBST followed by incubation in primary antibody (recombinant rabbit anti-hGH) for 18 h at 4 °C.

Blot was rinsed twice in TBST followed by incubation secondary antibody (goat anti-rabbit IgG AF488) for 2 h at 25 °C in the dark. Blot was rinsed twice in TBST and imaged.

Statistical Analysis

All experimental values are reported as the average ± SEM. Graph Pad Prism 7-9 (GraphPad Software, San Diego, USA) was used for the statistical analyses. Results were considered significantly different if $p < 0.05$ (*); results are also reported with $p < 0.01$ (**), and $p < 0.001$ (***). Cell viability assay was analyzed with a nonlinear regression analysis also in GraphPad Prism 7 with data expressed as means with 95% CI and compared using Student's t-tests or one-way ANOVA as necessary.

Synthesis of N-Boc Tyramine

Scheme 4.1

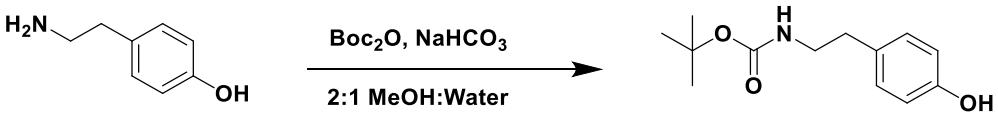

Adapted from previously reported protocol.[45]

To a 1-neck 300 ml round bottom flask equipped with a stir bar was added tyramine (2 g, 14.6 mmol, 1 eq.), $NaHCO_3$ (3.7 g, 43.7 mmol, 3 eq.), Boc anhydride (4.7 g, 21.8 mmol, 1.5 eq), and 90 ml of 2:1 MeOH:H_2O solution. The solution was stirred at 22 ºC for 15 hours, then methanol was removed under vacuum and the resulting slurry was partitioned with EtOAc (100 ml). The aqueous layer was removed and the organic layer was washed once with 50 ml 1 M HCl solution, then once with 50 ml brine. Organics were dried over anhydrous magnesium sulfate, filtered, and dried under vacuum with 5 grams of silica gel in preparation for flash chromatography using a 8-66% EtOAc/Hexane gradient. TLC indicated that the resulting material was mostly pure using a

solvent system of 2:1 Hexanes:EtOAc (Rf=0.83; 0.63; Boc_2O, product). Pure fractions were combined and concentrated under vacuum to yield an orange oil (2.1 g, 62% yield).

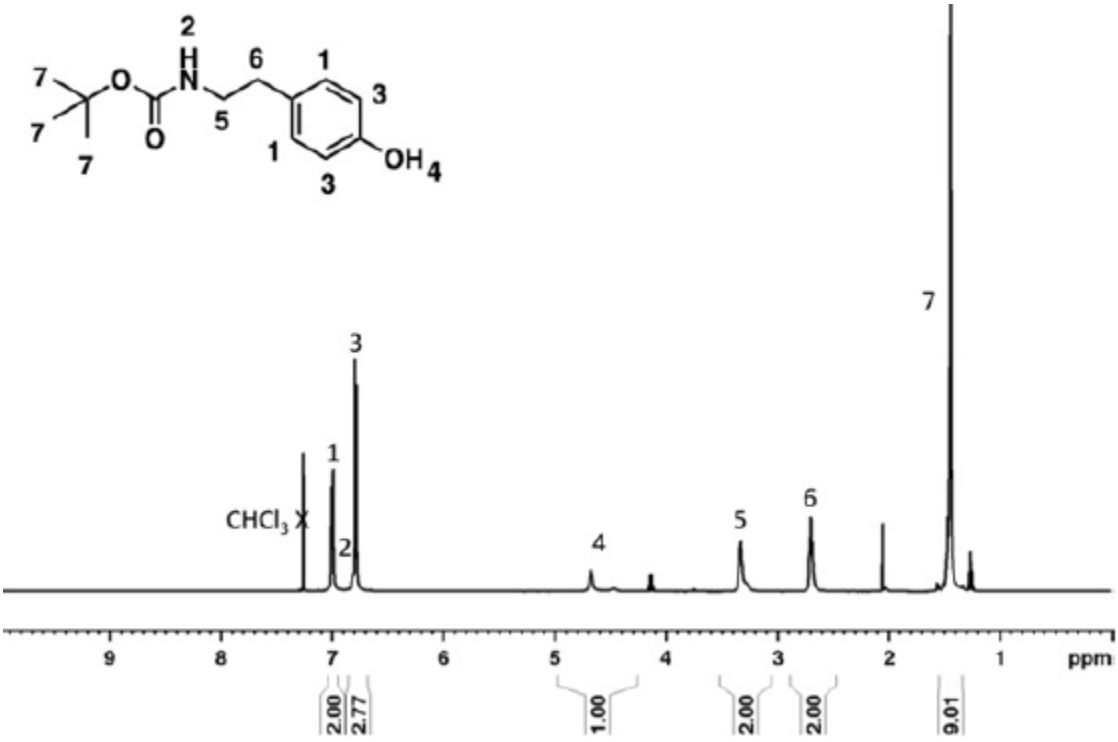

Figure 4.10 ^1H NMR of N-Boc Tyramine ($CDCl_3$)

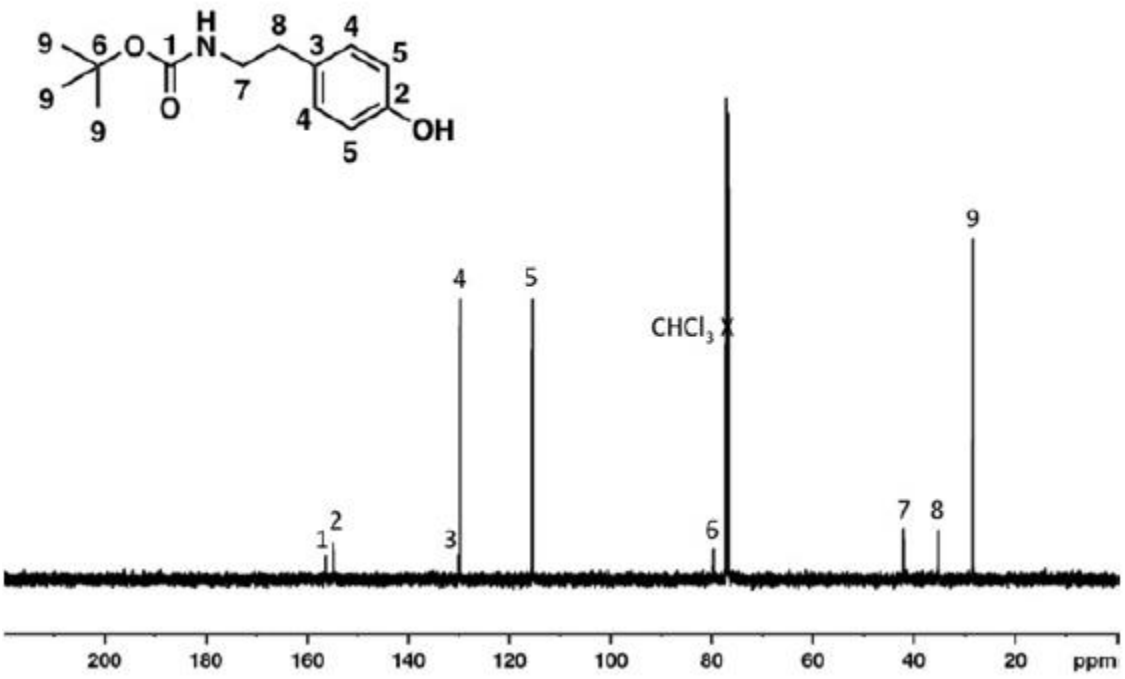

Figure 4.11 ^{13}C NMR of N-Boc Tyramine ($CDCl_3$)

Synthesis of 1-Tosyl-6-hexanol

Scheme 4.2

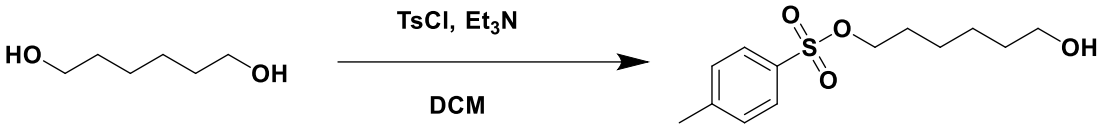

To a 250 ml 2-neck round bottom flask equipped with a stir bar was added 1,6-hexanediol (15.5 g, 131 mmol, 5 eq.), DCM (100 mL), and triethylamine (7.3 mL, 52.5 mmol, 2 eq.). Once fully dissolved, tosyl chloride (5 g, 26.2 mmol, 1 eq.) was added and the reaction was stirred under argon for 15 hours. The reaction was monitored by TLC using a solvent system of 2:1 EtOAc:Hex (Rf= 0.90, 0.79, 0.49, 0.19; TsCl, double addition product, desired product, hexanediol/TEA). The reaction appeared to be complete as all TsCl had been consumed. The reaction mixture was then diluted with DCM and washed twice with 1 M HCl then once with saturated sodium bicarbonate solution before the organic layer was dried over anhydrous magnesium sulfate, filtered, and dried

under vacuum with 5 grams of silica gel for flash chromatography using a 10-100% EtOAc/Hex gradient. Pure fractions were combined and concentrated to yield a yellow liquid (5.7 g, 80.0% yield).

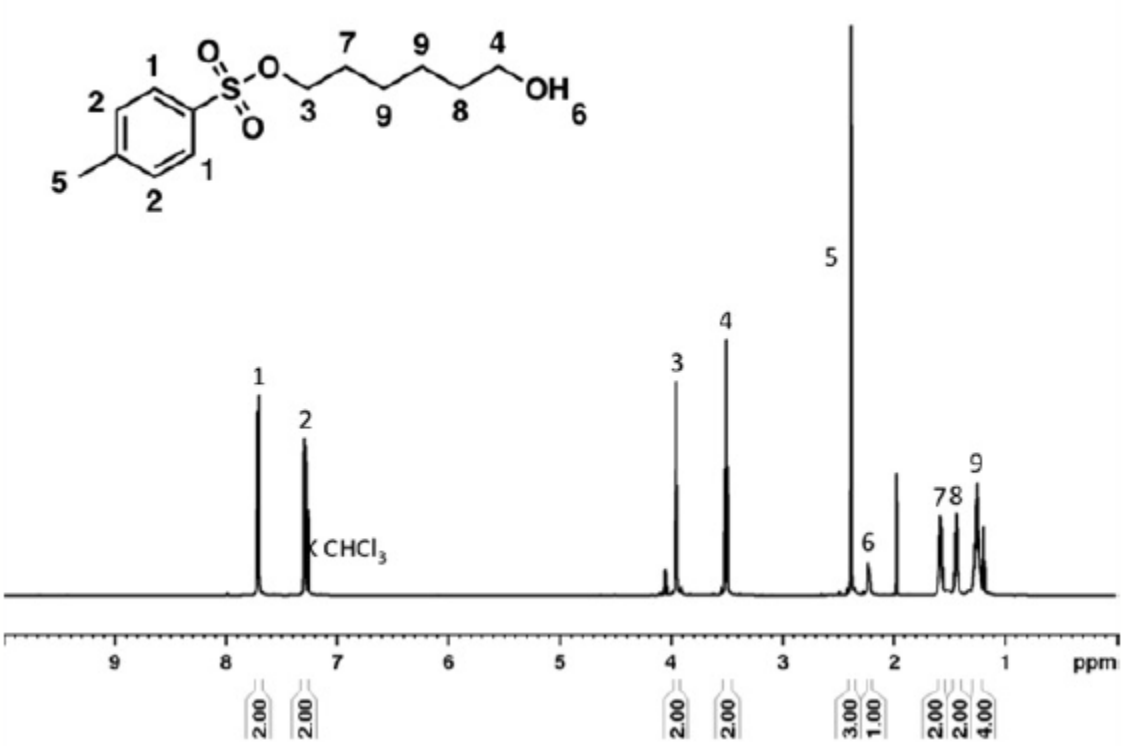

Figure 4.12 ^{1}H NMR of 1-Tosyl-6-Hexanol ($CDCl_3$)

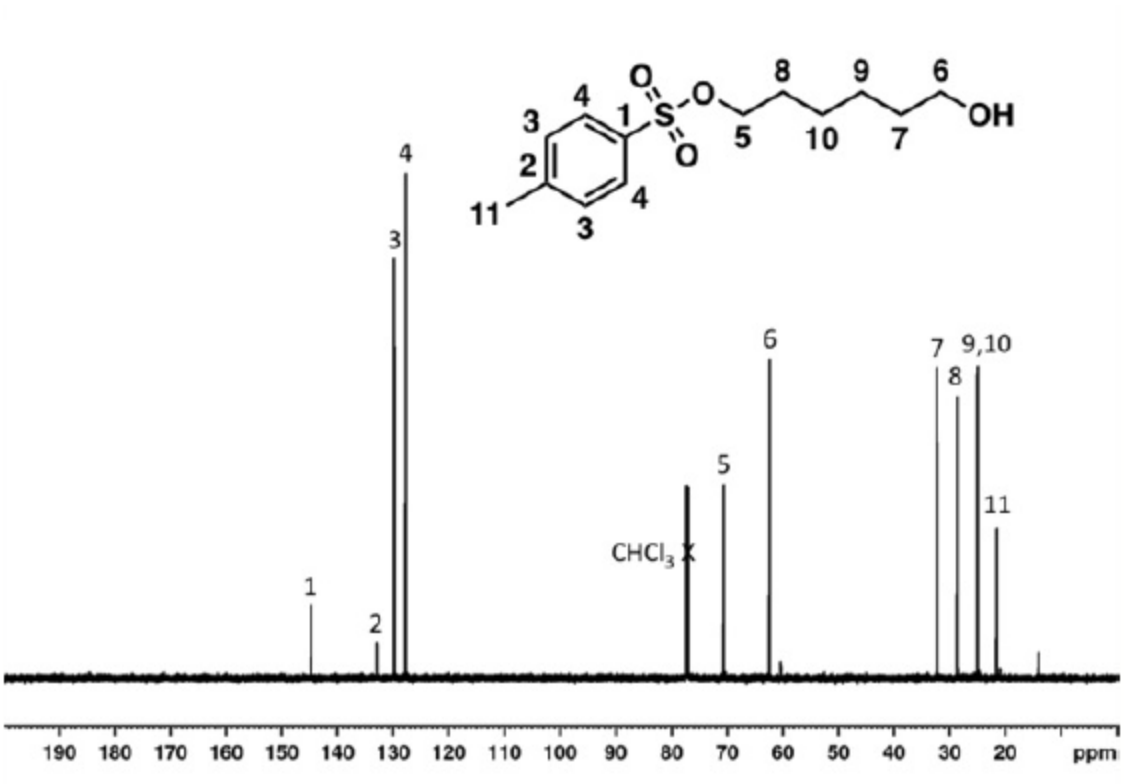

Figure 4.13^{13}C NMR of 1-Tosyl-6-Hexanol ($CDCl_3$)

Synthesis of N-Boc Tyramine O-hexanol

Scheme 4.3

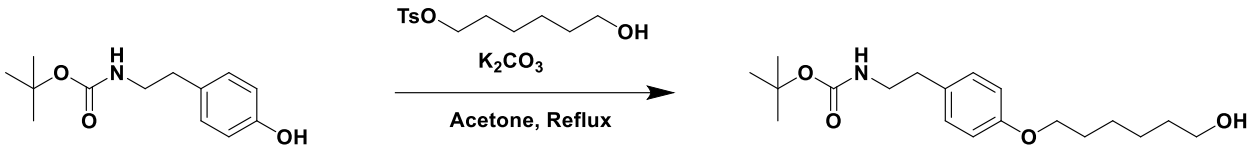

To a 100 ml 1-neck round bottom flask equipped with a stir bar and water condenser was added N-boc Tyramine (1.0 g, 4.2 mmol, 1 eq.) , K_2CO_3 (0.5 g, 5 mmol, 1.2 eq.), and 1-Tosyl-6-hexanol (1.7 g, 6.3 mmol, 1.5 eq.) with 40 ml acetone. The reaction was heated to a gentle reflux (55°C) and stirred for 15 hours at which point the reaction was evaluated by TLC and did not proceed to completion (only about 50% conversion), so the temperature was increased to 75°C for an

additional 7 hours. The reaction was monitored by TLC using a solvent system of 1:1 Hexanes:EtOAc (Rf=0.79, 0.71, 0.5, 0.39; impurity, N-Boc tyramine, Product, 1-tosyl-6-hexanol). Upon assessment of nearly full conversion by TLC, the reaction was cooled, filtered, and concentrated under vacuum with 5 grams of silica gel in preparation for flash chromatography using a 10-100% EtOAc/Hex gradient. Pure product was obtained as a white solid (490 mg, 35% yield) and cycled into glovebox.

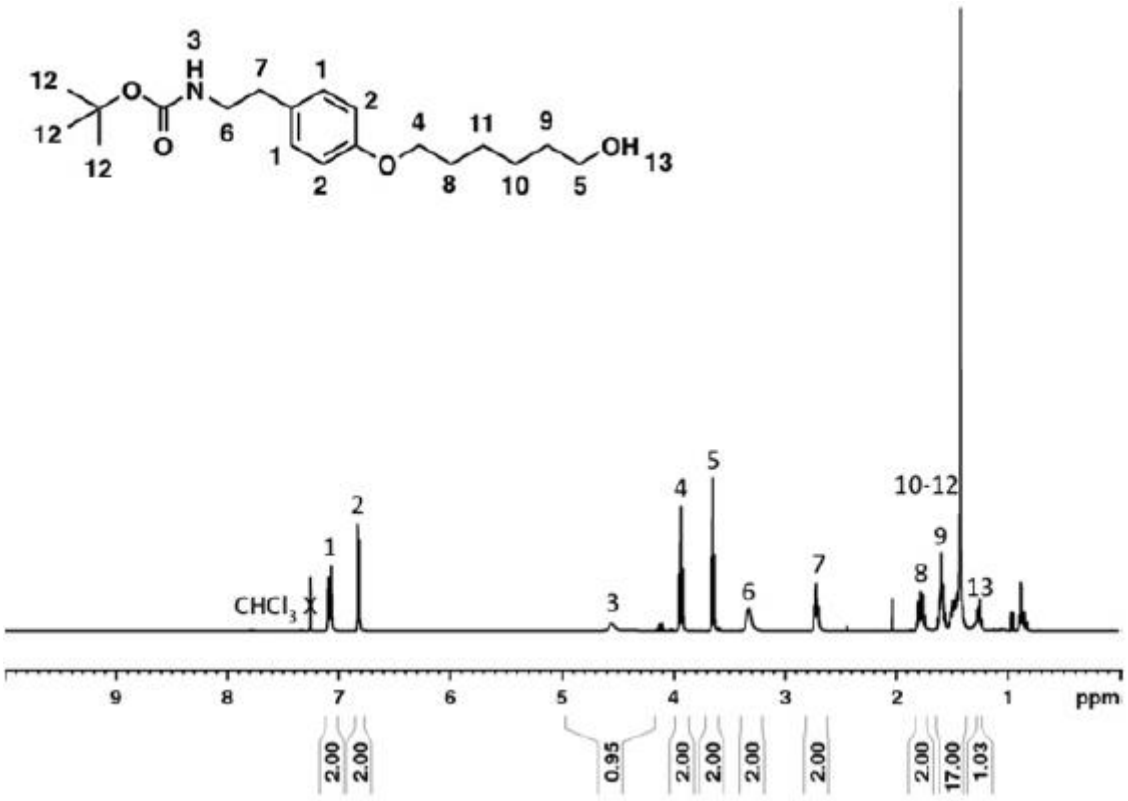

Figure 4.14 ^{1}H NMR of N-Boc Tyramine-O-hexanol ($CDCl_3$)

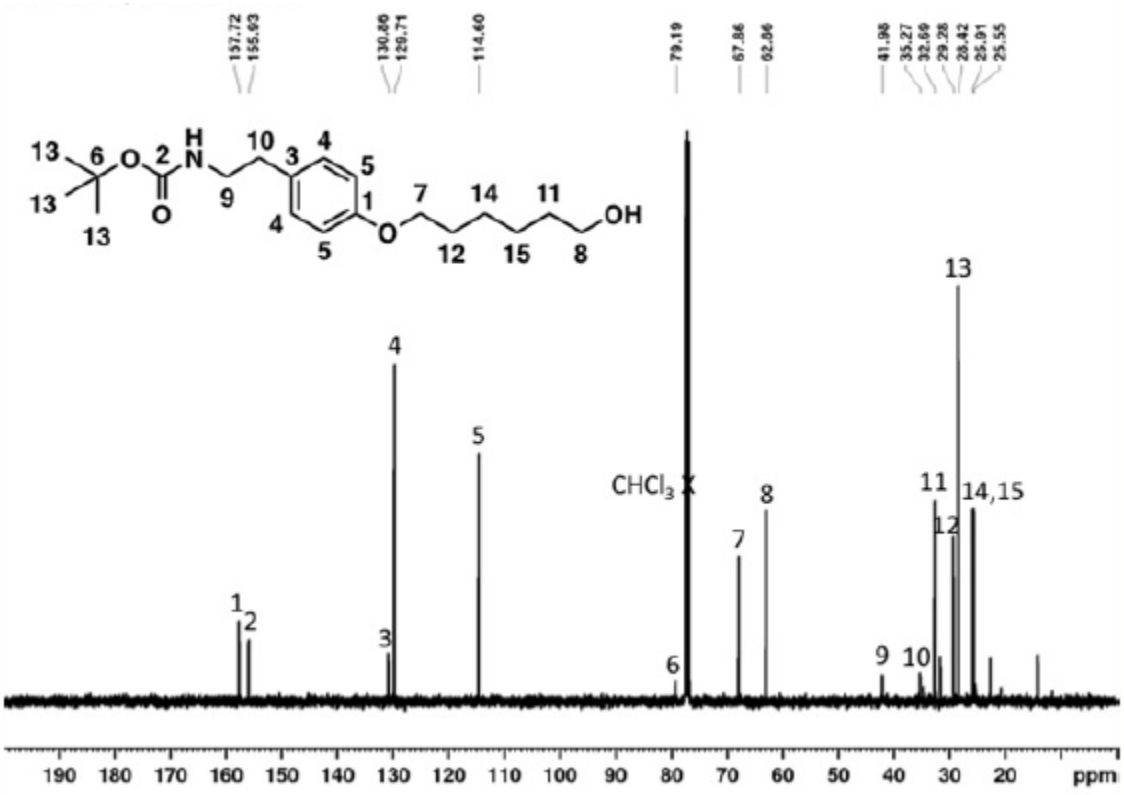

Figure 4.15 ^{13}C NMR of N-Boc Tyramine-O-hexanol ($CDCl_3$)

Synthesis of T-butylazidoacetate

Scheme 4.4

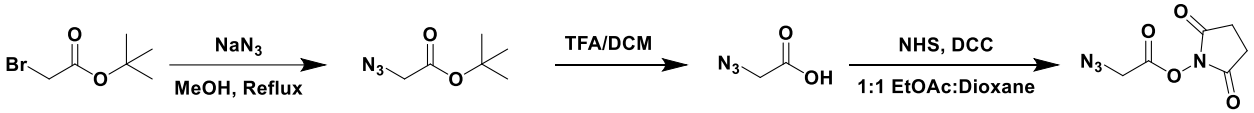

To a 100 ml 1-neck round bottom flask equipped with a stir bar was added sodium azide (2.4 g, 37.2 mmol, 1.1 eq.), methanol, and t-butylbromoacetate (5.0 mL, 33.9 mmol, 1 eq.). The reaction was heated to reflux (75°C) and stirred for 22 hours and monitored by TLC using a solvent system of 9:1 Hexanes:EtOAc stained with $KMnO_4$ (Rf=0.62; product). Conversion was also initially assessed after 22 hours by NMR and the reaction was determined to be complete. Solvent was then removed under vacuum and the resultant slurry was partitioned between EtOAc (150 ml) and water (50 ml). The organic layer was collected and the aqueous layer was extracted with EtOAc (2 x 150 ml) and the combined organics were dried over anhydrous magnesium sulphate, filtered, and dried under vacuum to yield an orange oil (4.5 g, 84 % yield).

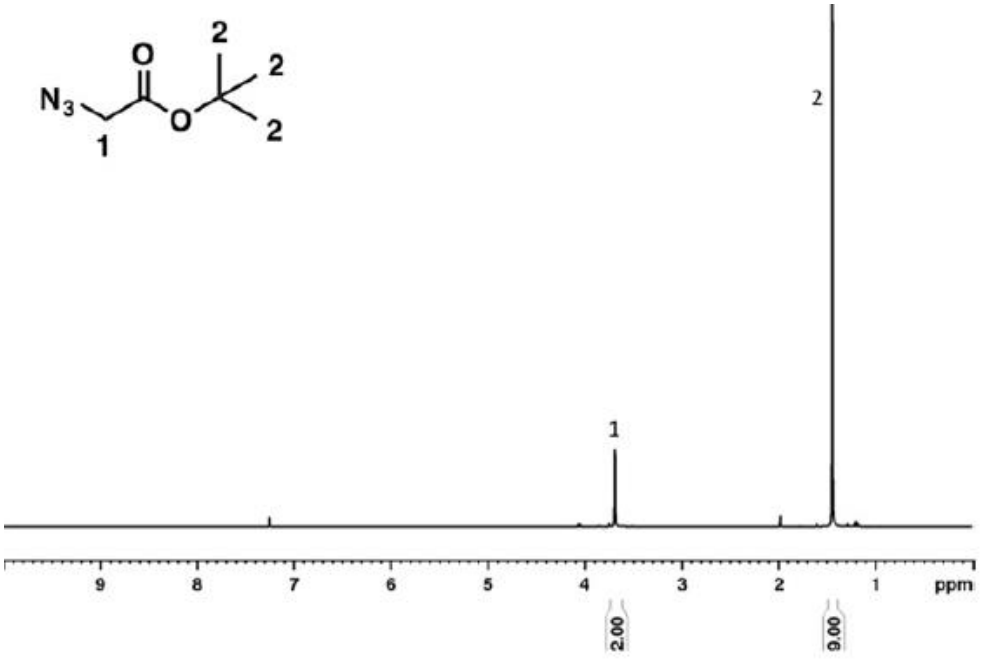

Figure 4.16 ^1H NMR of T-butylazidoacetate ($CDCl_3$)

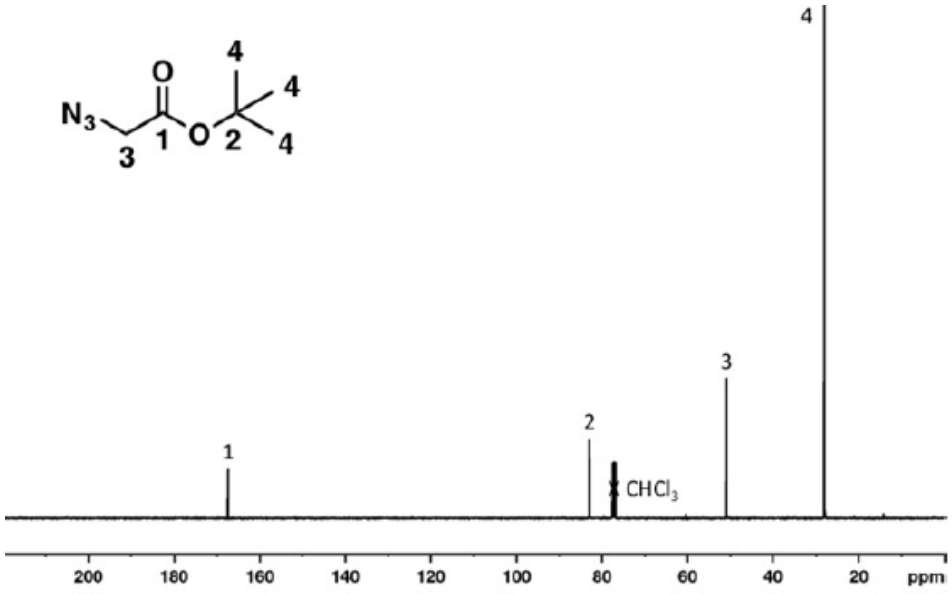

Figure 4.17 ^{13}C NMR of T-butylazidoacetate ($CDCl_3$)

Synthesis of Azidoacetic acid

To a 40 ml scintillation vial equipped with a stir bar was added t-butylazidoacetate (4.5 g, 37.7 mmol, 1 eq.) in minimal DCM, then an 8 ml solution of 1:1 TFA:DCM was added dropwise followed by 1 ml water. The reaction was stirred for 18 hours then dried under vacuum to yield an orange liquid (3.5 g, 91% yield). The material was used without further purification.

Synthesis of 2-azidoacetate succinimidyl ester

Adapted from previously reported protocol.[46]

To a stirred solution of azidoacetic acid (3.4 g, 33.6 mmol, 1 eq.) and N-hydroxysuccinimide (3.8 g, 33.6 mmol, 1 eq.) in 1:1 ethyl acetate:1,4-dioxane was added DCC (6.9 g, 33.6 mmol, 1 eq.) in

one portion. The resulting mixture was stirred at room temperature for 17 hours. The formed urea byproduct was then filtered off and the filtrate concentrated under vacuum with 5 grams of silica gel in preparation for flash chromatography using a 10-100% EtOAc/Hex gradient. TLC solvent system was 2:1 Hex:EtOAc (Rf=0.5, 0.0; product, NHS). Pure fractions were combined and concentrated under vacuum to yield a white solid (2.9 g, 44.4% yield).

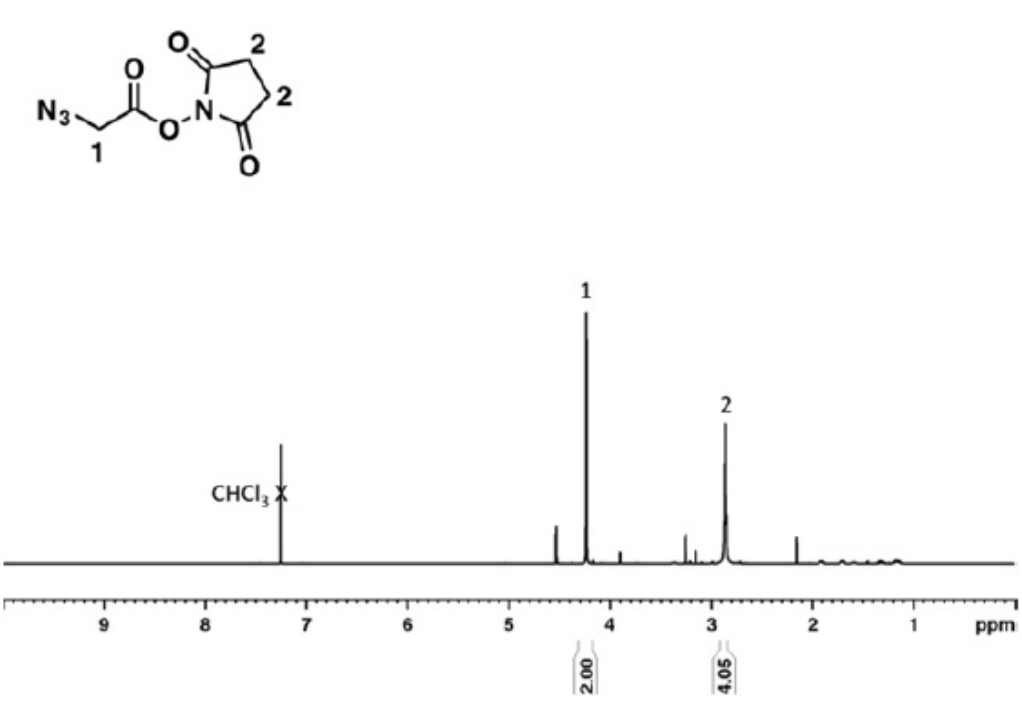

Figure 4.18 ^{1}H NMR of 2-azidoacetate succinimidyl ester ($CDCl_3$)

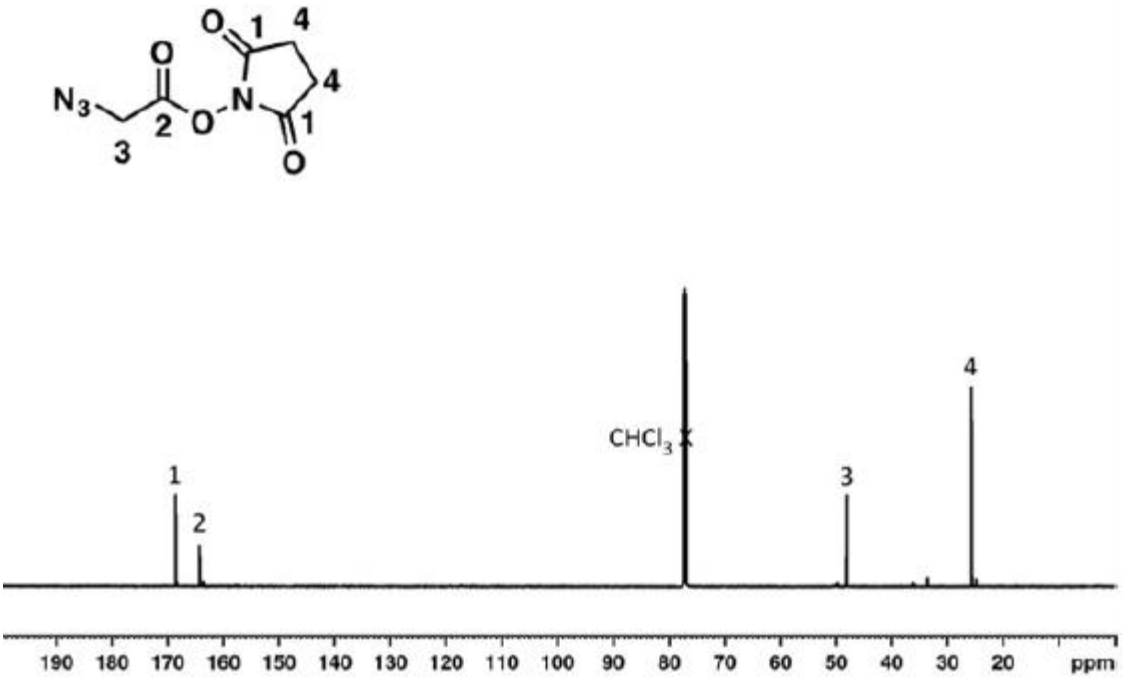

Figure 4.19 ^{13}C NMR of 2-azidoacetate succinimidyl ester ($CDCl_3$)

Synthesis of Zwitterion Precursor

Scheme 4.5

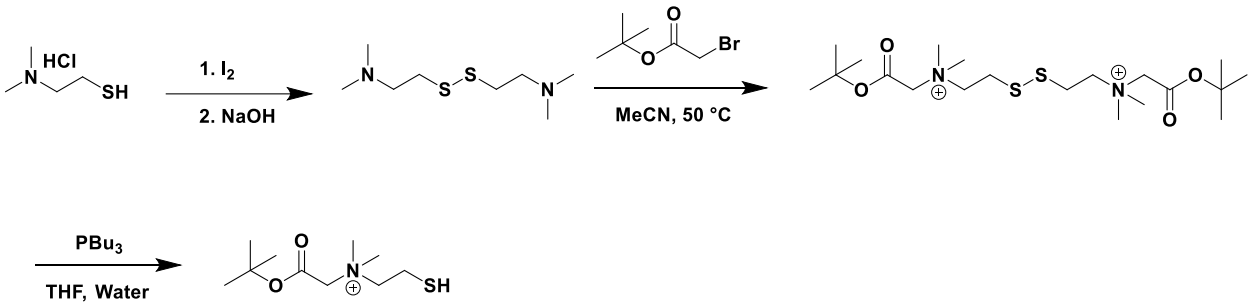

A previously reported protocol was followed.[8]

Figure 4.20 ^{1}H NMR of zwitterion precursor (MeOD)

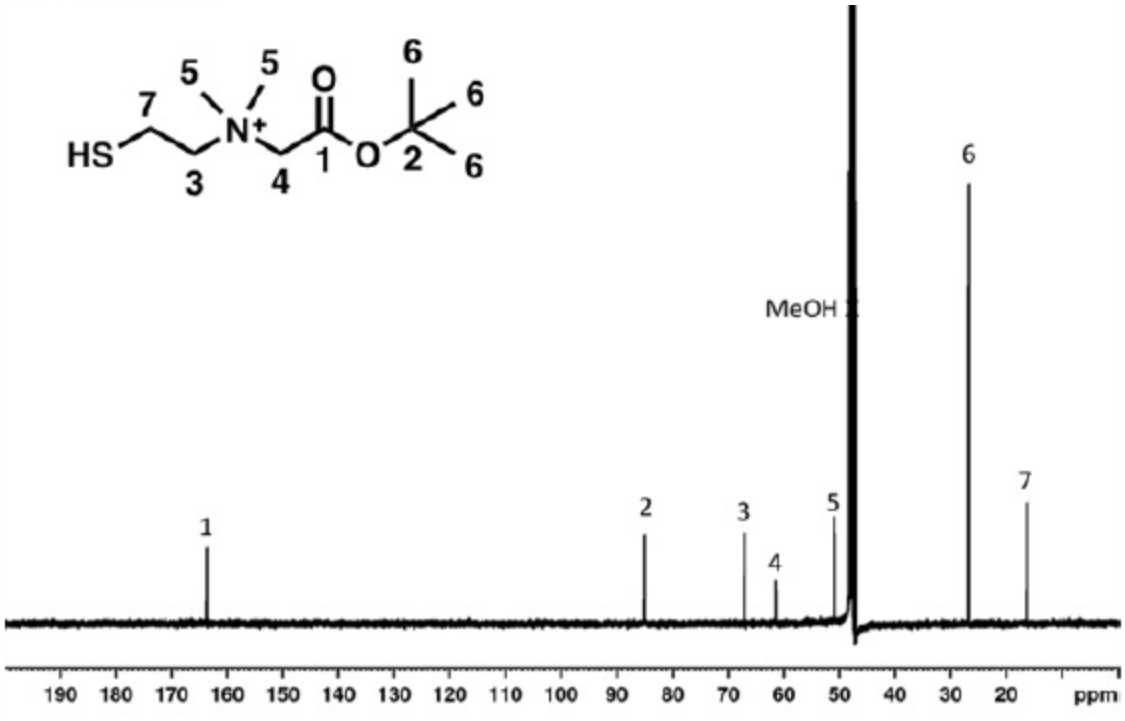

Figure 4.21 ^{13}C NMR of zwitterion precursor (MeOD)

Characterization of pCL-allyl$_x$ Polymers

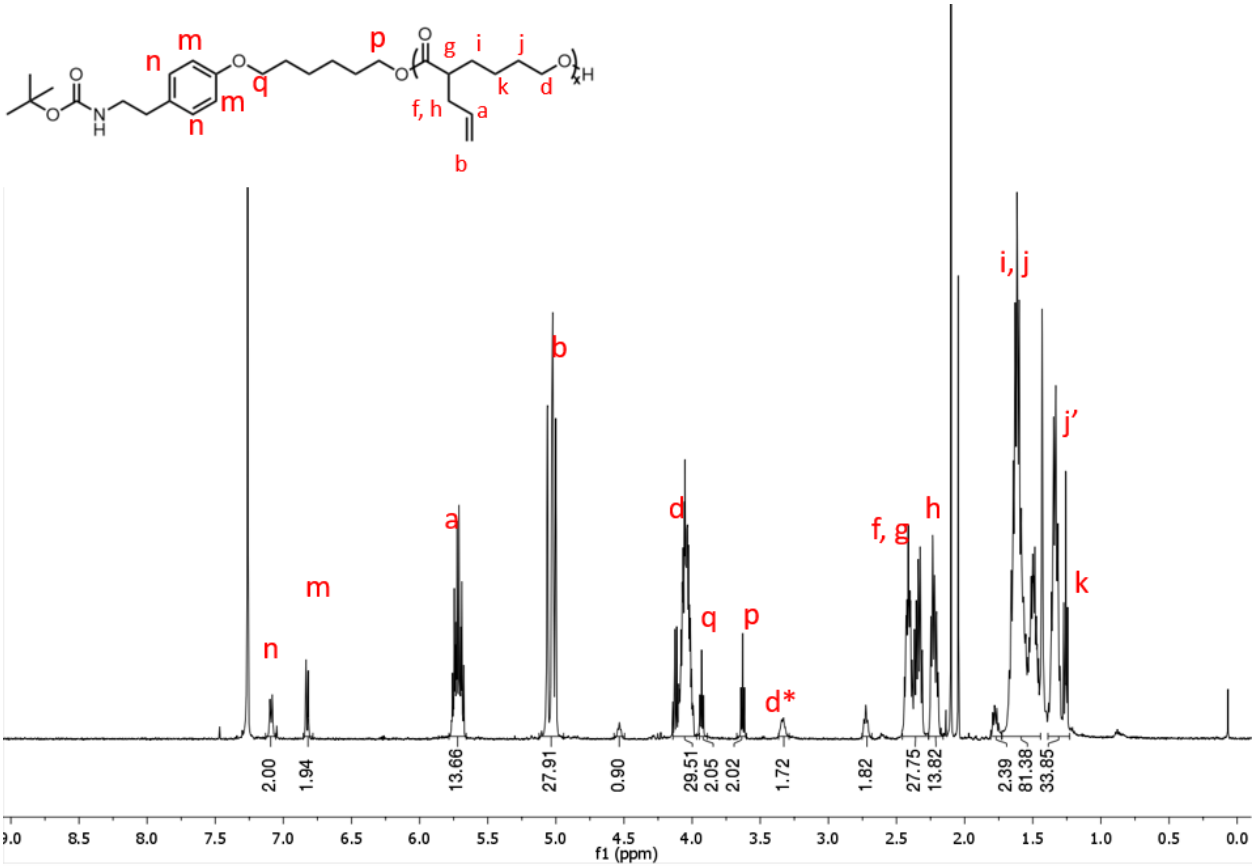

Figure 4.22 ^{1}H-NMR spectrum of pCL-allyl$_{13}$ ($CDCl_3$, 400 MHz). * = protons from terminal repeat unit on polymer

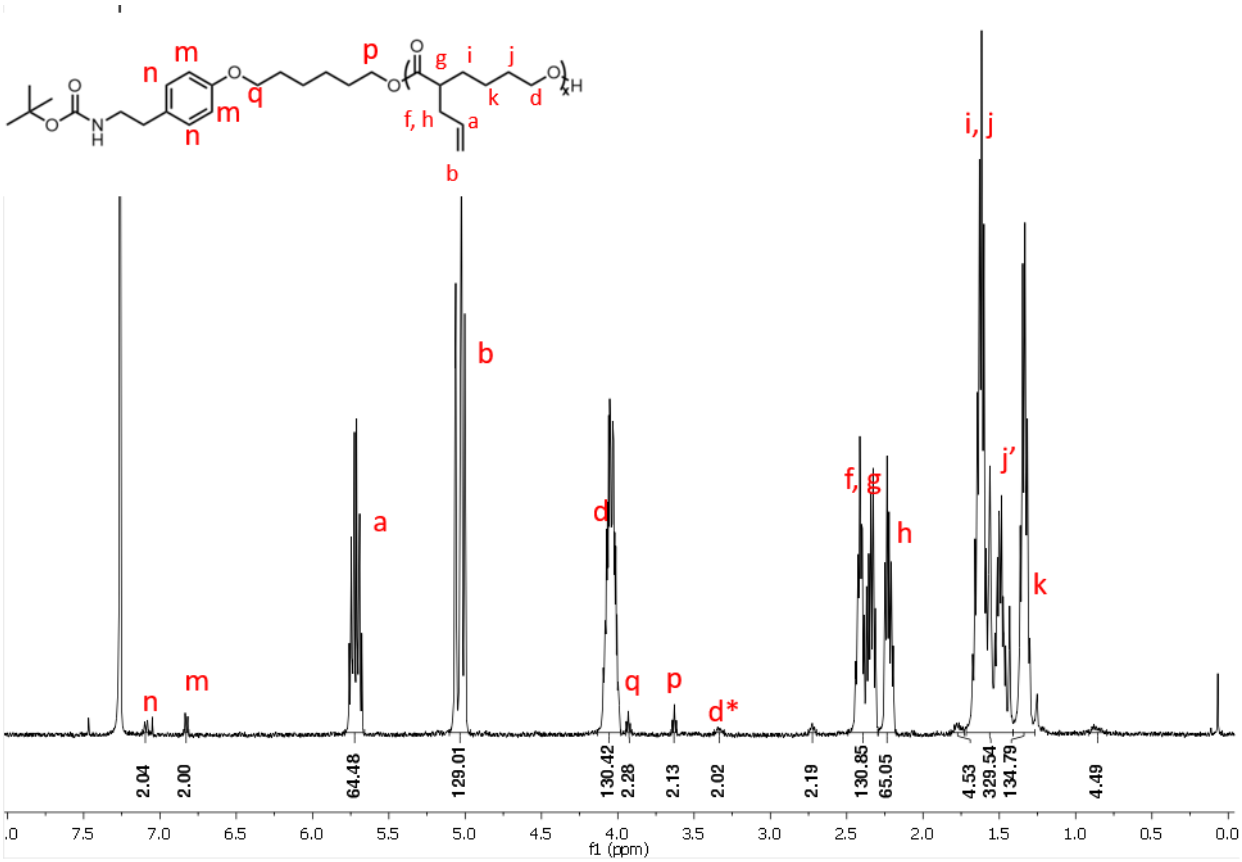

Figure 4.23 ^{1}H-NMR spectrum of pCL-allyl$_{64}$ ($CDCl_3$, 500 MHz). * = protons from terminal repeat unit on polymer

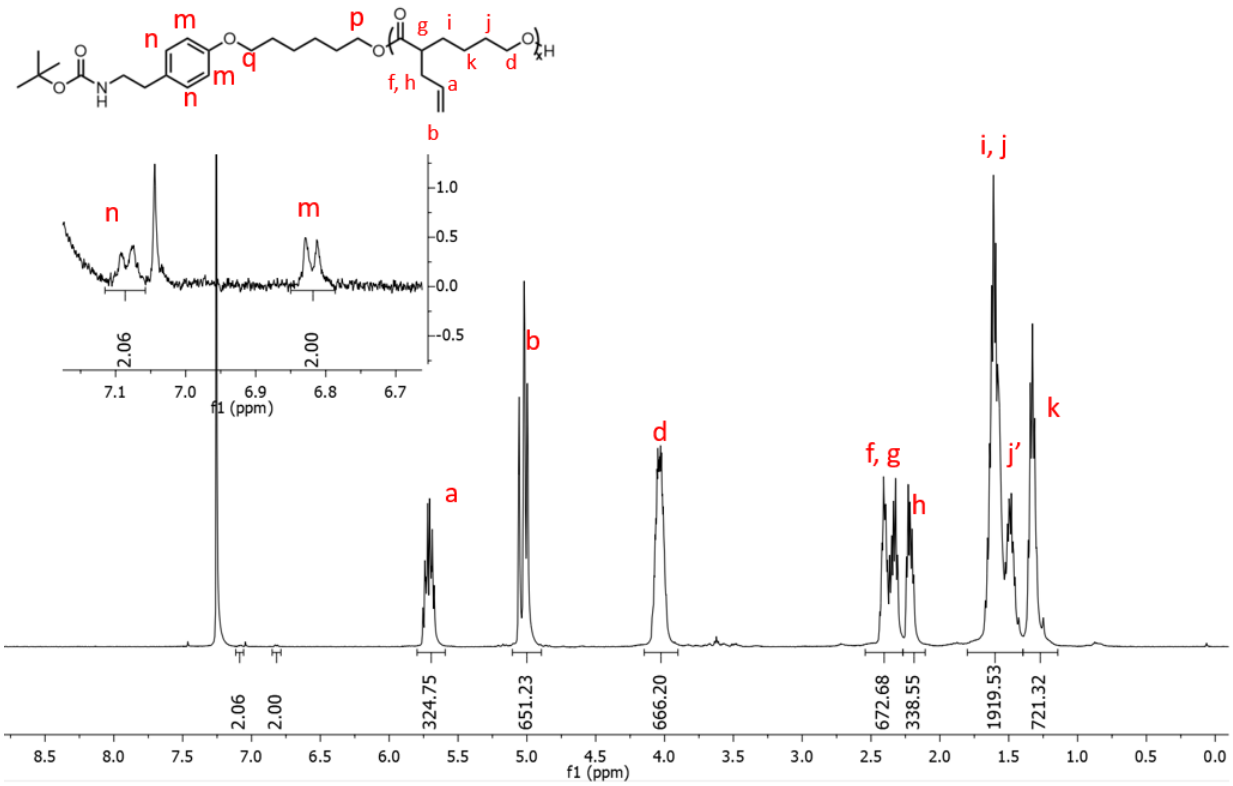

Figure 4.24 ^{1}H-NMR spectrum of pCL-allyl$_{324}$ ($CDCl_3$, 500 MHz).

Characterization of pCLZ polymers

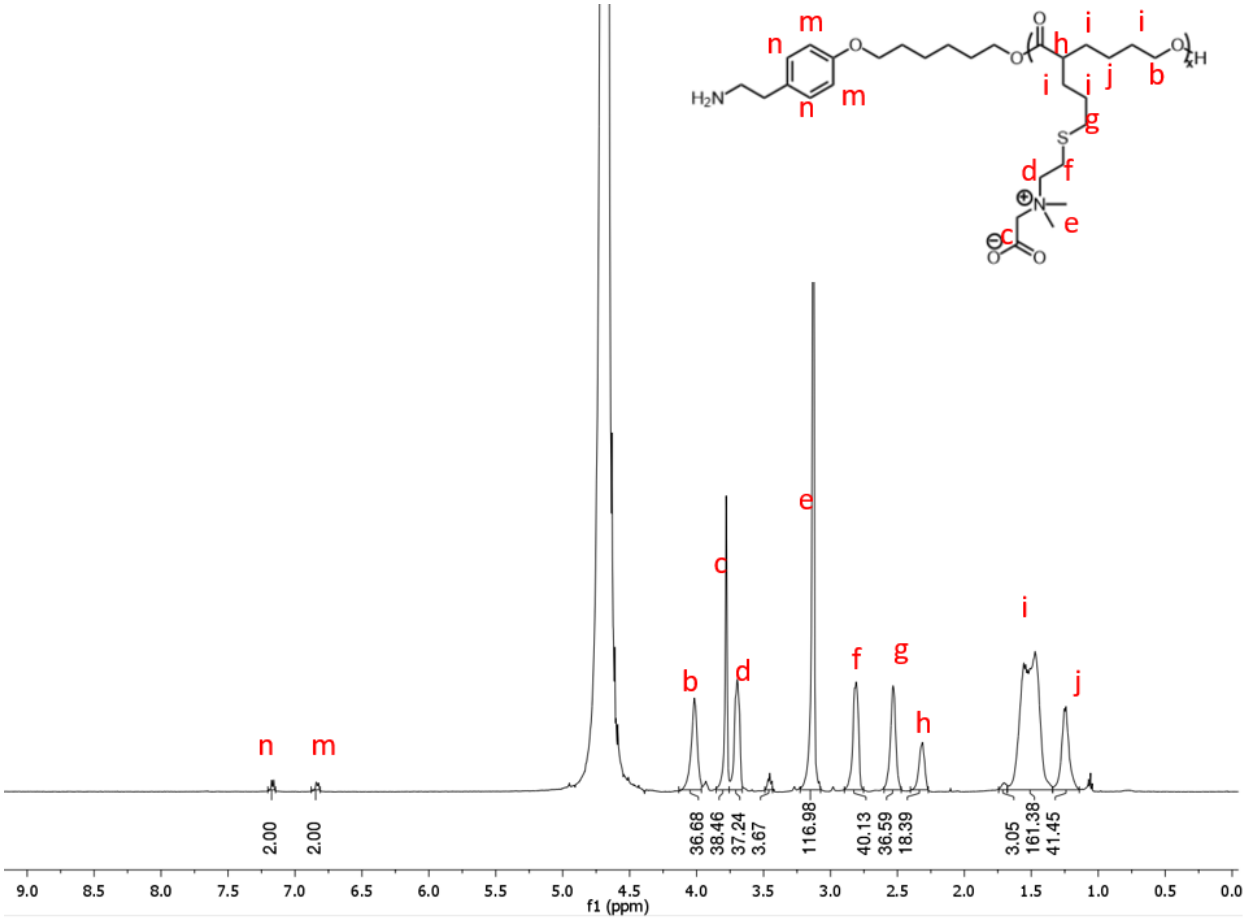

Figure 4.25 ^{1}H-NMR spectrum of pCLZ 5 kDa (D_2O, 500 MHz).

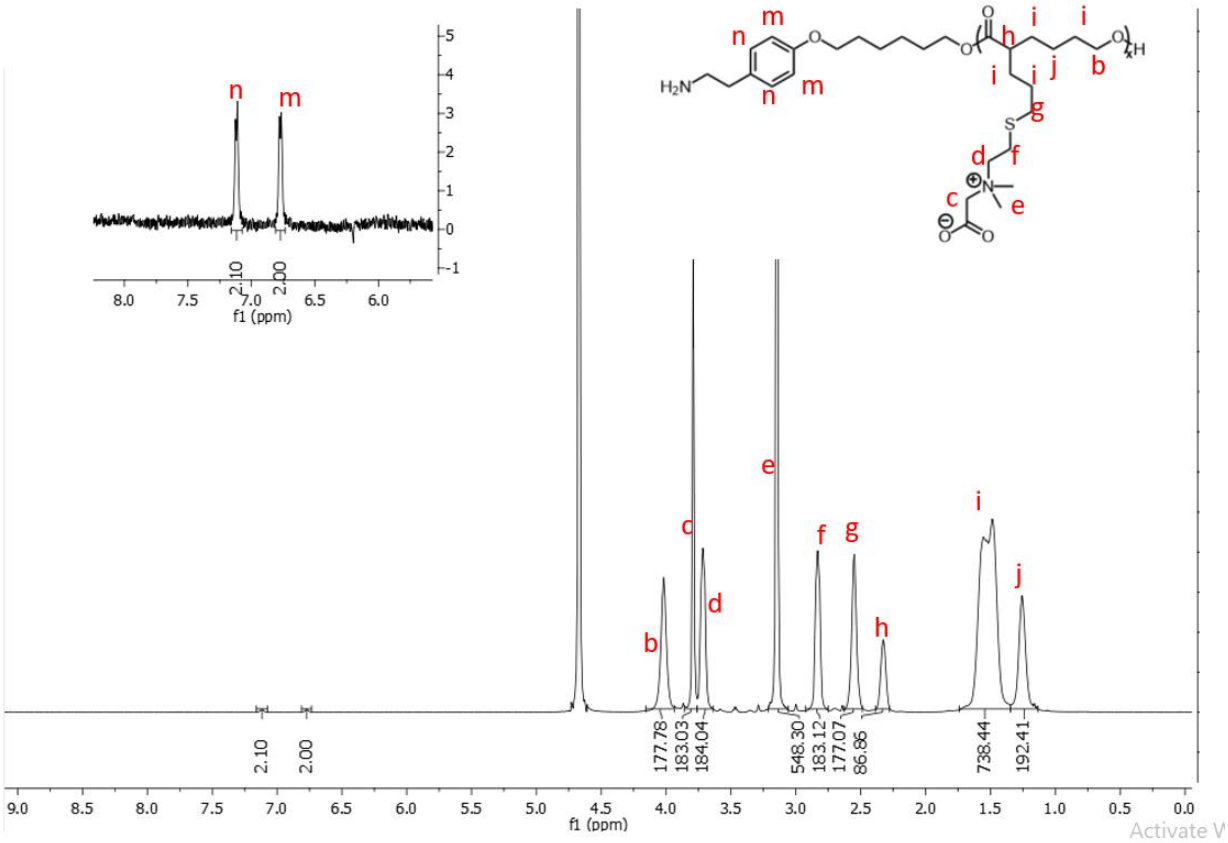

Figure 4.26 ^{1}H-NMR spectrum of pCLZ 20 kDa (D_2O, 500 MHz).

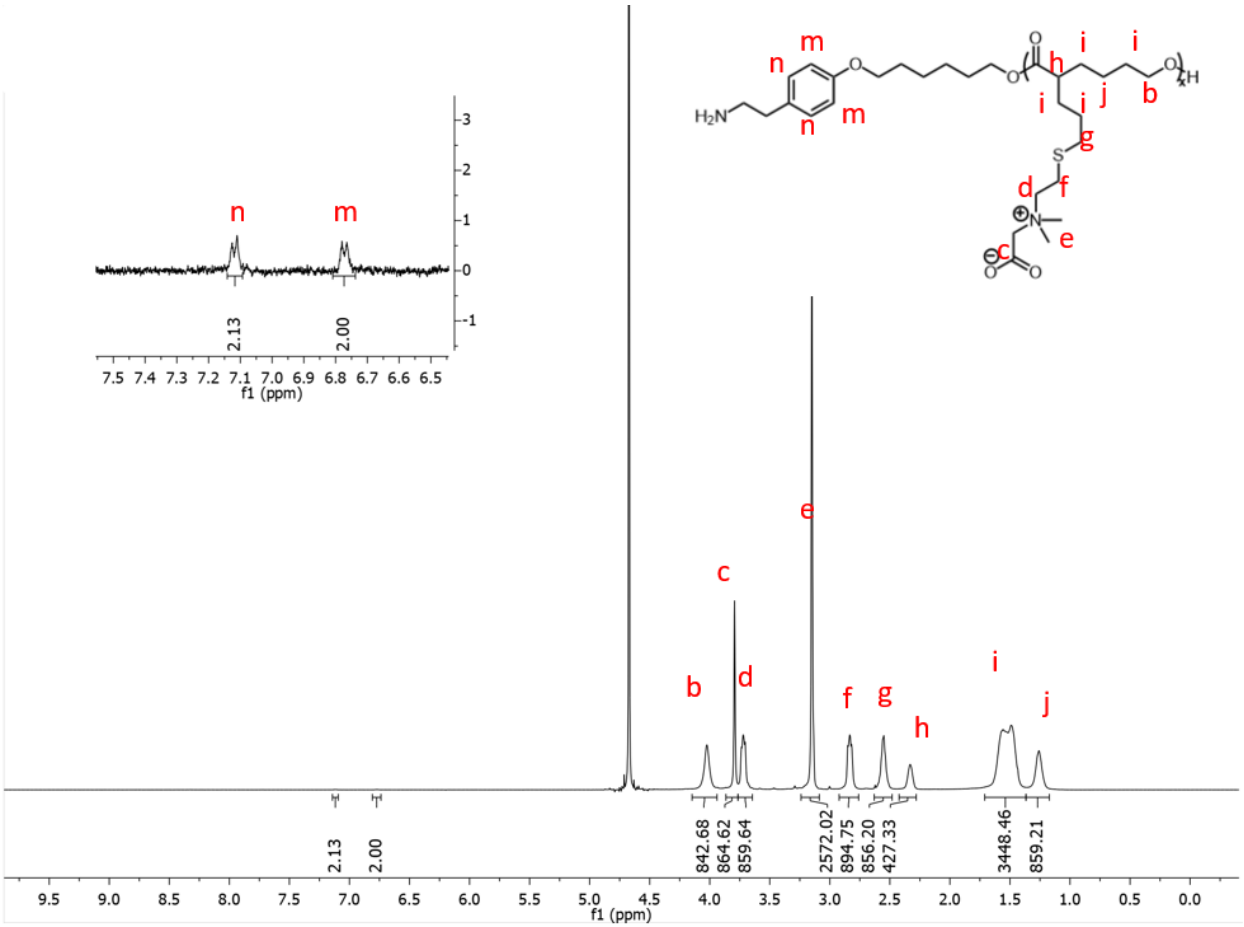

Figure 4.27 ^{1}H-NMR spectrum of pCLZ 60 kDa (D_2O, 500 MHz).

PEGylation of GHA B2036-Alkyne

A previously reported protocol was followed.[25]

FPLC chromatograms of crude site-specific B2036-pCLZ conjugates

In general, first peak corresponds to free polymer, second peak corresponds to free GHA, and the third peak is conjugate. Fractions were collected in 0.5 mL increments.

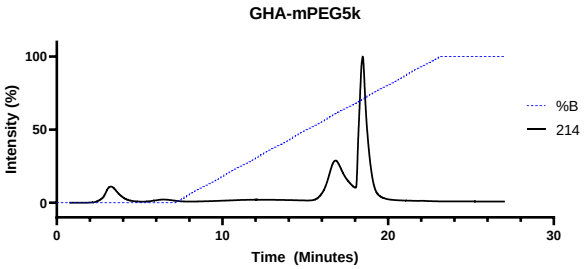
GHA-mPEG5k
Intensity (%)
100
50
0
0
10
20
30
Time (Minutes)
%B
214

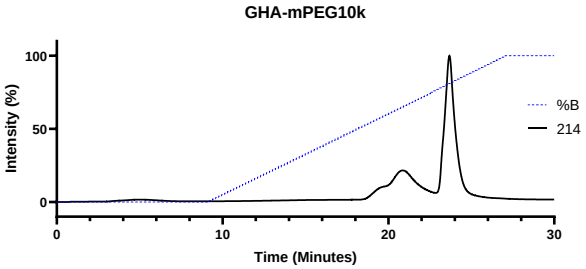
GHA-mPEG10k
Intensity (%)
100
50
0
0
10
20
30
Time (Minutes)
%B
214

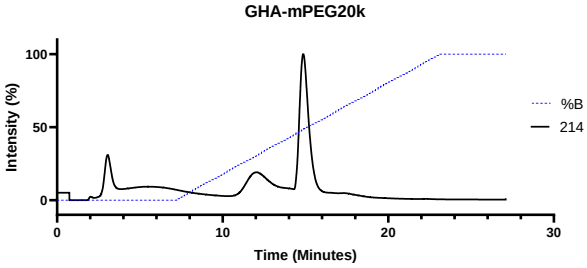
GHA-mPEG20k
Intensity (%)
100
50
0
0
10
20
30
Time (Minutes)
%B
214

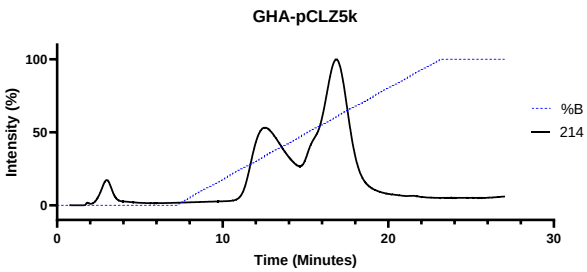
GHA-pCLZ5k
Intensity (%)
100
50
0
0
10
20
30
Time (Minutes)
%B
214

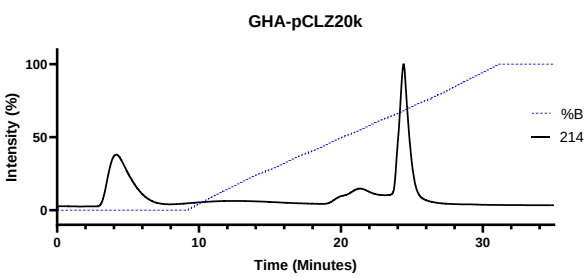
GHA-pCLZ20k
Intensity (%)
100
50
0
0
10
20
30
Time (Minutes)
%B
214

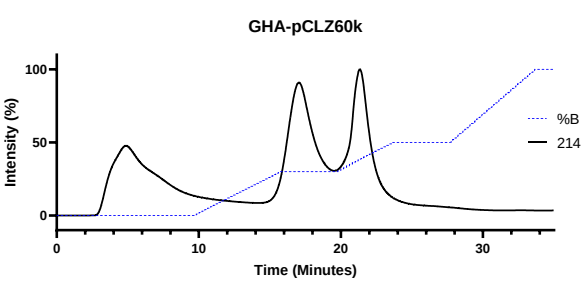
GHA-pCLZ60k
Intensity (%)
100
50
0
0
10
20
30
Time (Minutes)
%B
214

Figure 4.28 FPLC chromatograms of the purification of site-specific GHA-conjugates

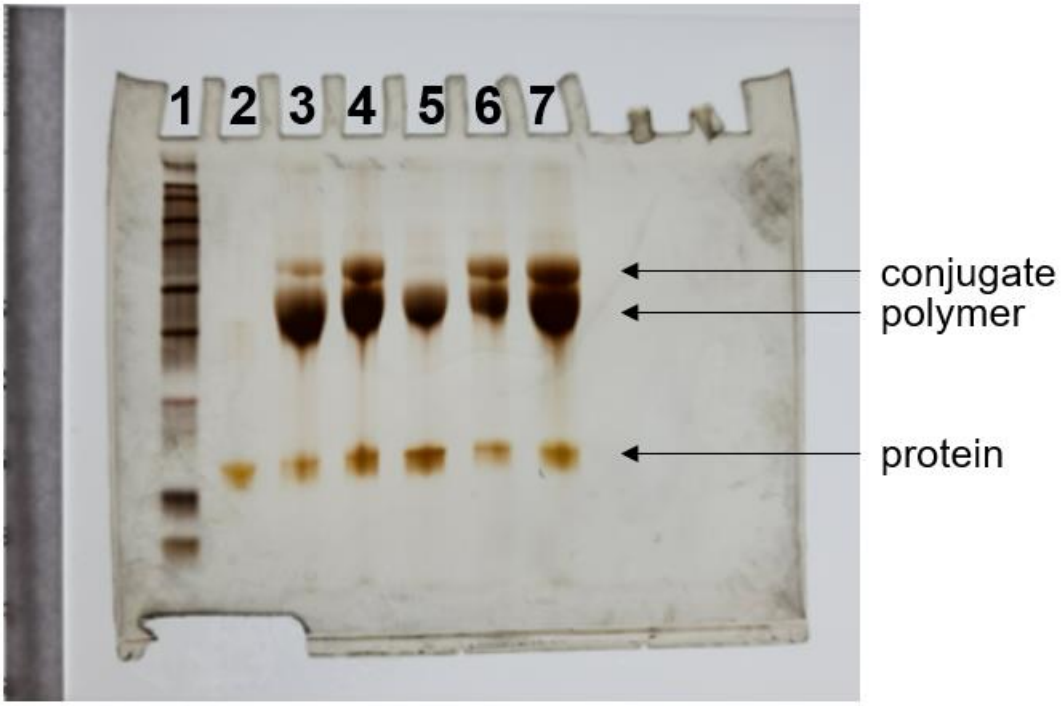

Figure 4.29 CuAAC condition screening for the conjugation of GHA-alkyne to pCLZ60k

Optimization of CuAAC conditions for GHA-pCLZ60k

SDS-PAGE of crude GHA-pCLZ60k conjugation reactions with 1:1 equivalents of GHA to pCLZ60k visualized with silver stain. Lane 1: protein standards; Lane 2: GHA B2036-Alkyne; Lane 3: magnetic stirring at 20 ºC for 2 h; Lane 4: 50% DMSO co-solvent at 20 ºC for 2 h; Lane 5: 20% MeCN co-solvent at 20 ºC for 2 h; Lane 6: 2x concentration of $CuSO_4$ and BTTAA at 20 ºC for 2 h; Lane 7: 37 ºC for 2h;

Circular Dichroism

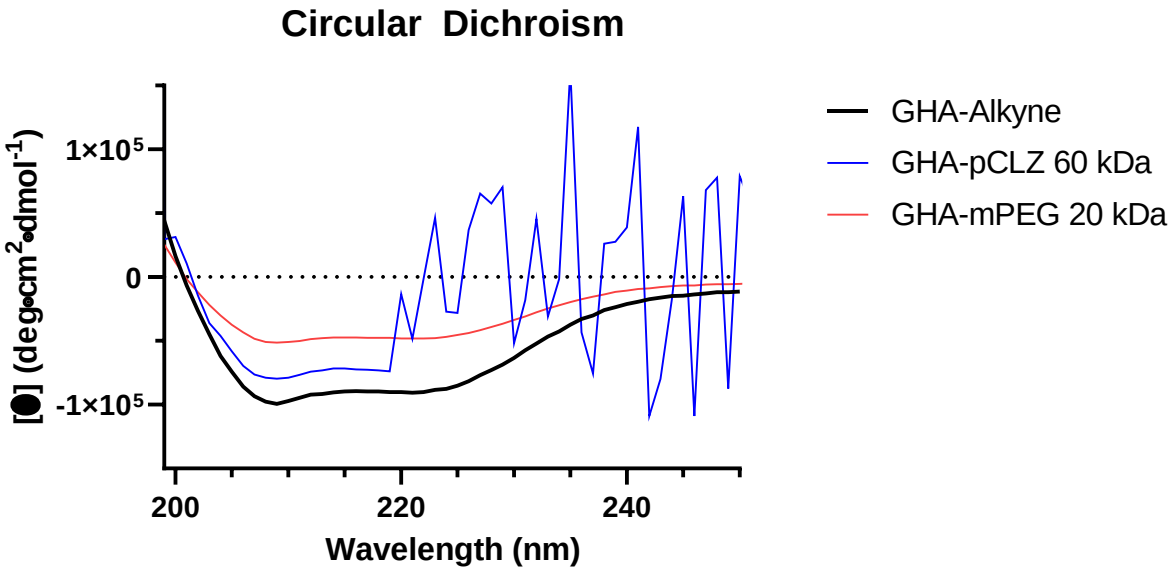

Figure 4.30 Circular Dichroism of GHA-Alkyne, GHA-pCLZ60k, and GHA-mPEG20k in 20 mM DPBS pH 7.4

Ellipticities were normalized by conversion to molar ellipticities.

Immunogenicity ELISA serum dilutions

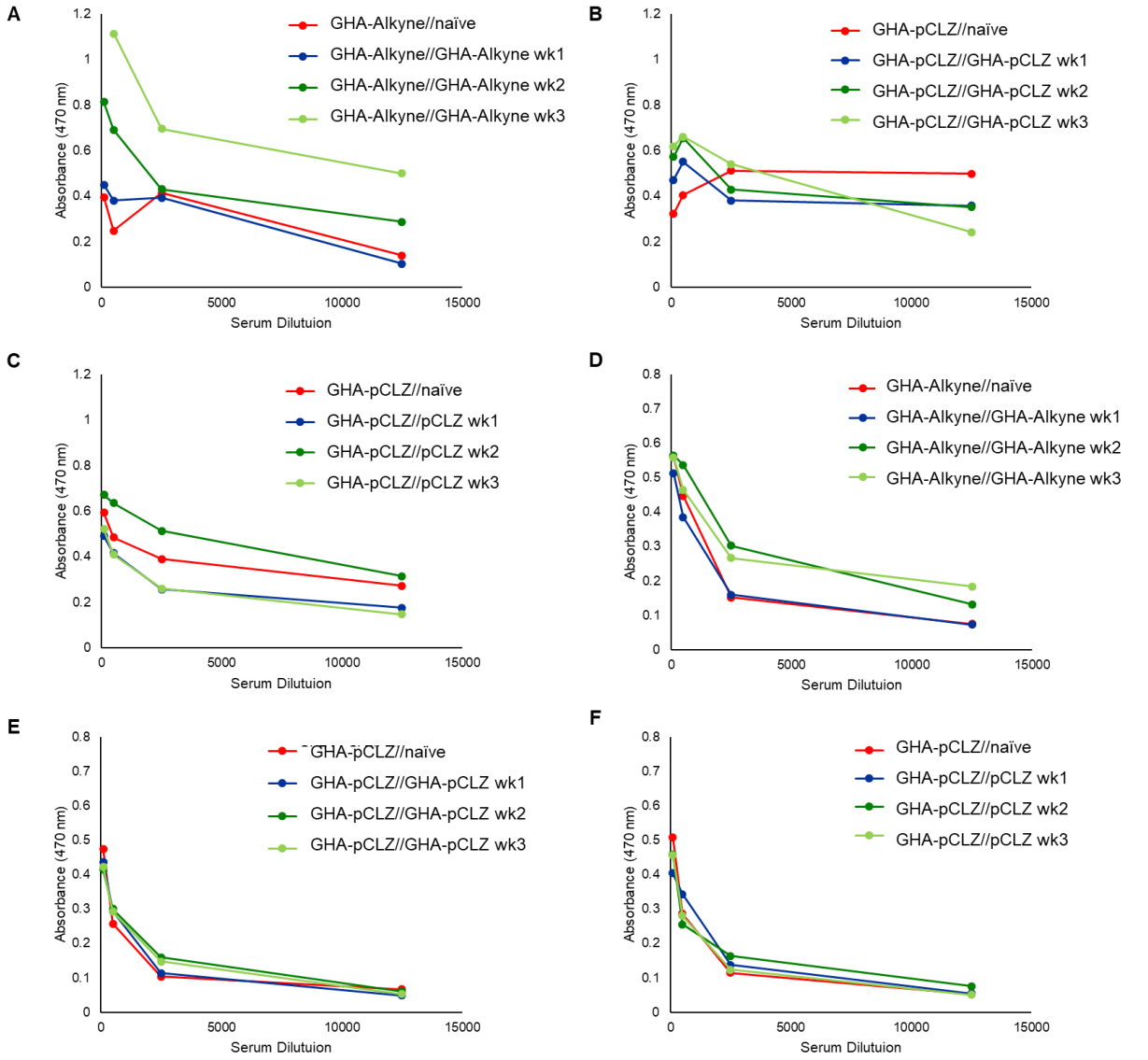

Figure 4.31 A) IgG week 1, B) IgG week 2, C) IgG week 3, D) IgM week 1, E) IgM week 2, and F) IgM week for I. Naïve GHA-yne [naïve mouse serum with GHA-yne antigen], II. Naïve GHA-pCLZ [naïve mouse serum with GHA-pCLZ antigen], III. GHA-yne GHA-yne [mouse serum from mice injected with GHA-yne with GHA-yne antigen], IV. GHA-pCLZ GHA-pCLZ [mouse serum from mice injected with GHA-pCLZ with GHA-pCLZ antigen], and V. pCLZ GHA-pCLZ [mouse serum from mice injected with pCLZ with GHA-pCLZ antigen].

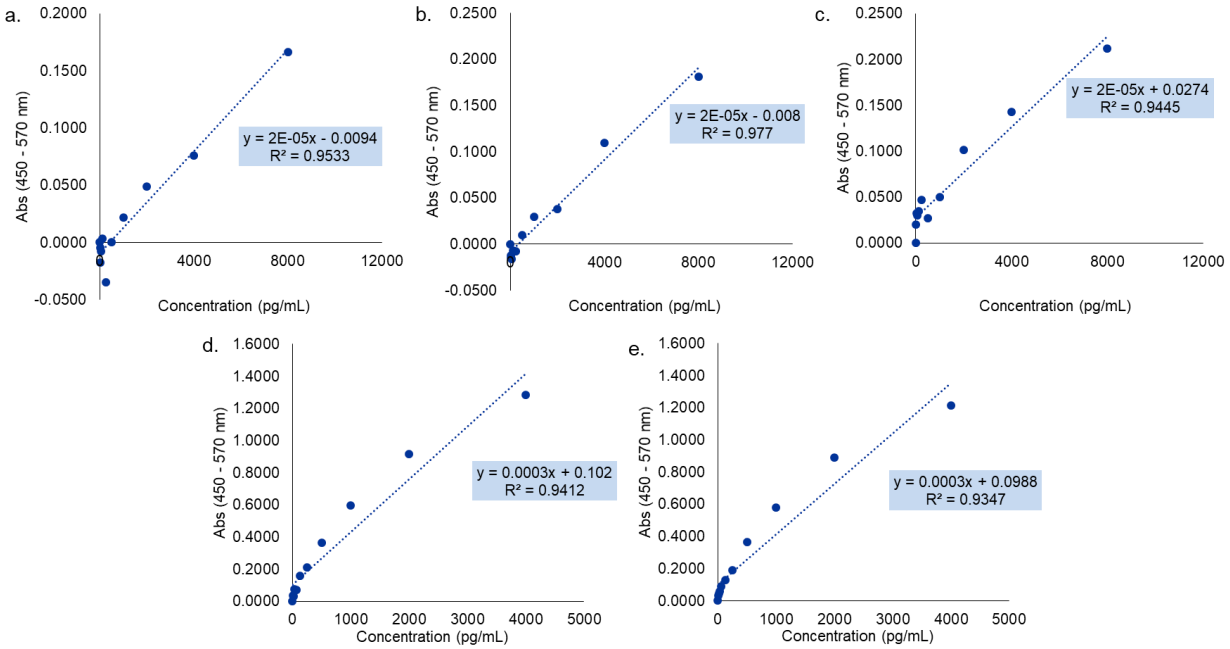

Figure 4.32 A-C) GHA-pCLZ and D-E) GHA-alkyne used in the calculation of plasma concentration for the corresponding conjugate or protein at the time points at a. 0.5 h and 1 h, b. 2 h and 4 h, c. 8 h and 24 h, d. 0.5 h,1 h, and 2 h, and e. 4 h, 8 h, and 24 h.

[^{18}F] SFB radiolabeling

^{18}F fluoride was trapped on the QMA cartridge and released into reactor 1 with a solution of potassium carbonate and kryptofix. This solution is evaporated and azeotropically dried using acetonitrile before adding the precursor and performing the fluorination reaction at 110°C for 15 min. After the fluorination, 25 µLTMAOH in 1 mL of MeCN is added to the reactor and the contents are evaporated at 110°C for 4 min. An additional 2 mL of MeCN is added to the reactor

and the contents are once again evaporated at 110°C for 3 min. After the solvents have been removed, TSTU is added and the contents are reacted in the sealed vial at 110°C for 5 min.
The crude product was diluted with HPLC mobile phase and transferred to the HPLC loop for purification. Decay-corrected yield was 40.3%. Chemical and radiochemical purity were > 95%.

Pharmacokinetics of GHA-alkyne and GHA-pCLZ conjugate in mice

CD-1 mice (8 weeks, female, n = 5 – 6, Charles River Laboratories) were used to study the blood clearance rate of GHA-alkyne and GHA-pCLZ (60 kDa). Protein and conjugate were each administered via i.v. tail injection (2 mg/kg of GHA-alkyne and 0.75 mg/kg of GHA-pCLZ in sterile saline buffer). Blood was collected by saphenous vein bleeding at 0.5, 2, 4, and 8 h using EDTA-coated pipette tips and LoBind tubes and tubes were rotated to prevent clotting. A time point was taken after the mice were sacrificed at 24 h, and the final time point was collected via cardiac puncture and the blood was treated the same as the earlier time points. After each time point was taken, blood was centrifuged at 2,000 rcf for 15 min to extract plasma. Plasma was transferred to a fresh LoBind tube (not EDTA coated) and stored at -80 ºC until the pharmacokinetics ELISA could be run.

Biodistribution studies of [^{18}F] SFB radiolabeled GHA B2036, pCLZ60k, and GHA-pCLZ60k

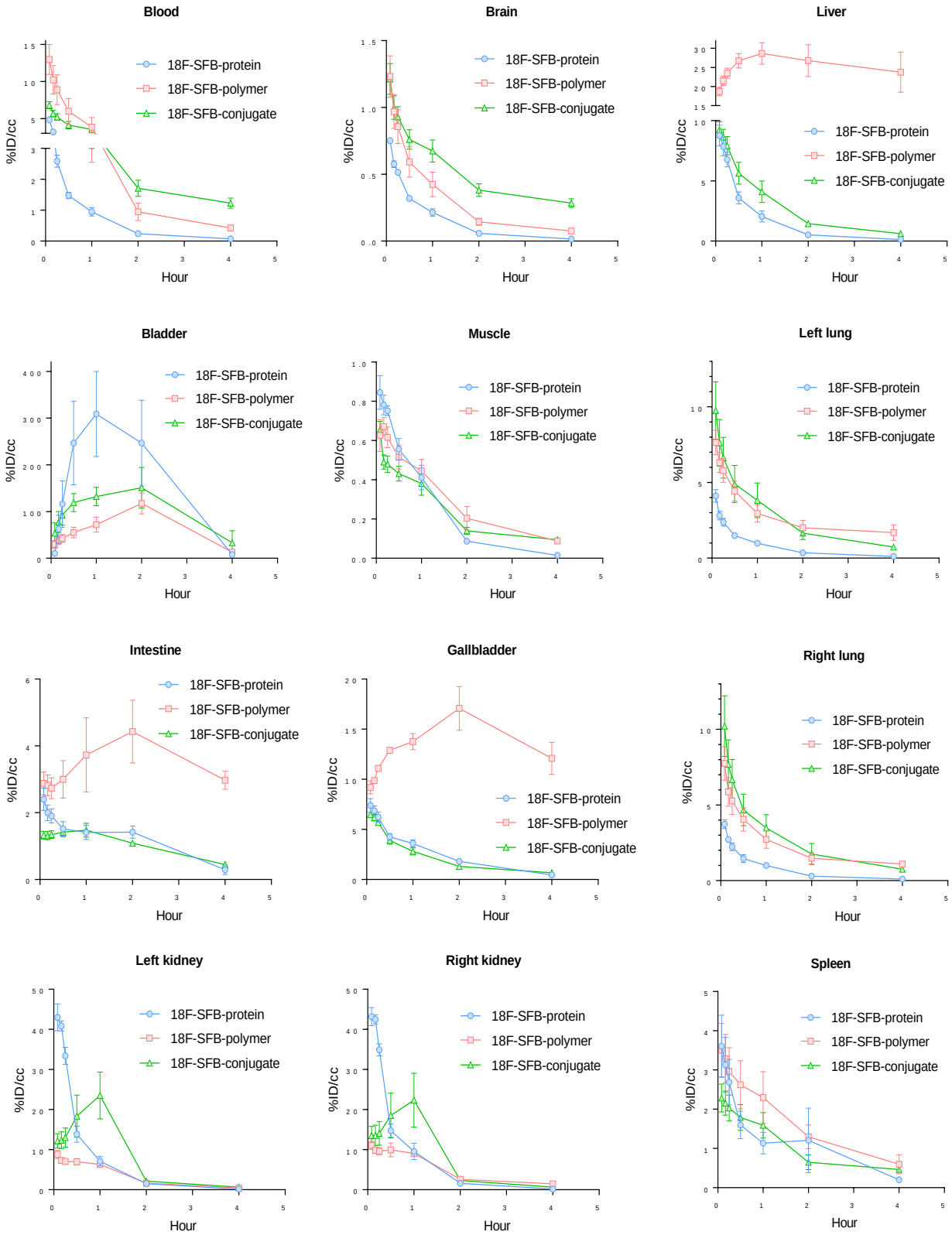

Figure 4.33 Biodistribution organized by %ID/cc over time in each specific organ

Standard and Contrast CT images of mouse liver with of [^{18}F] SFB-GHA B2036

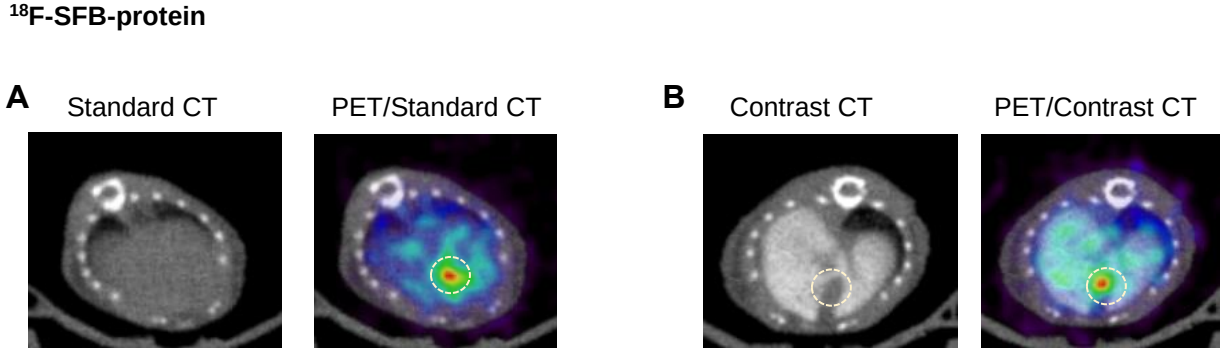

Figure 4.34 Signal intensity inside the liver A. without and B. with liver/speen specific CT contrast agent (ExiTron 12000) depicting high intensity signal from within the gallbladder

Individual Regression Curves for Two-phase Decay Model for Blood Half-life

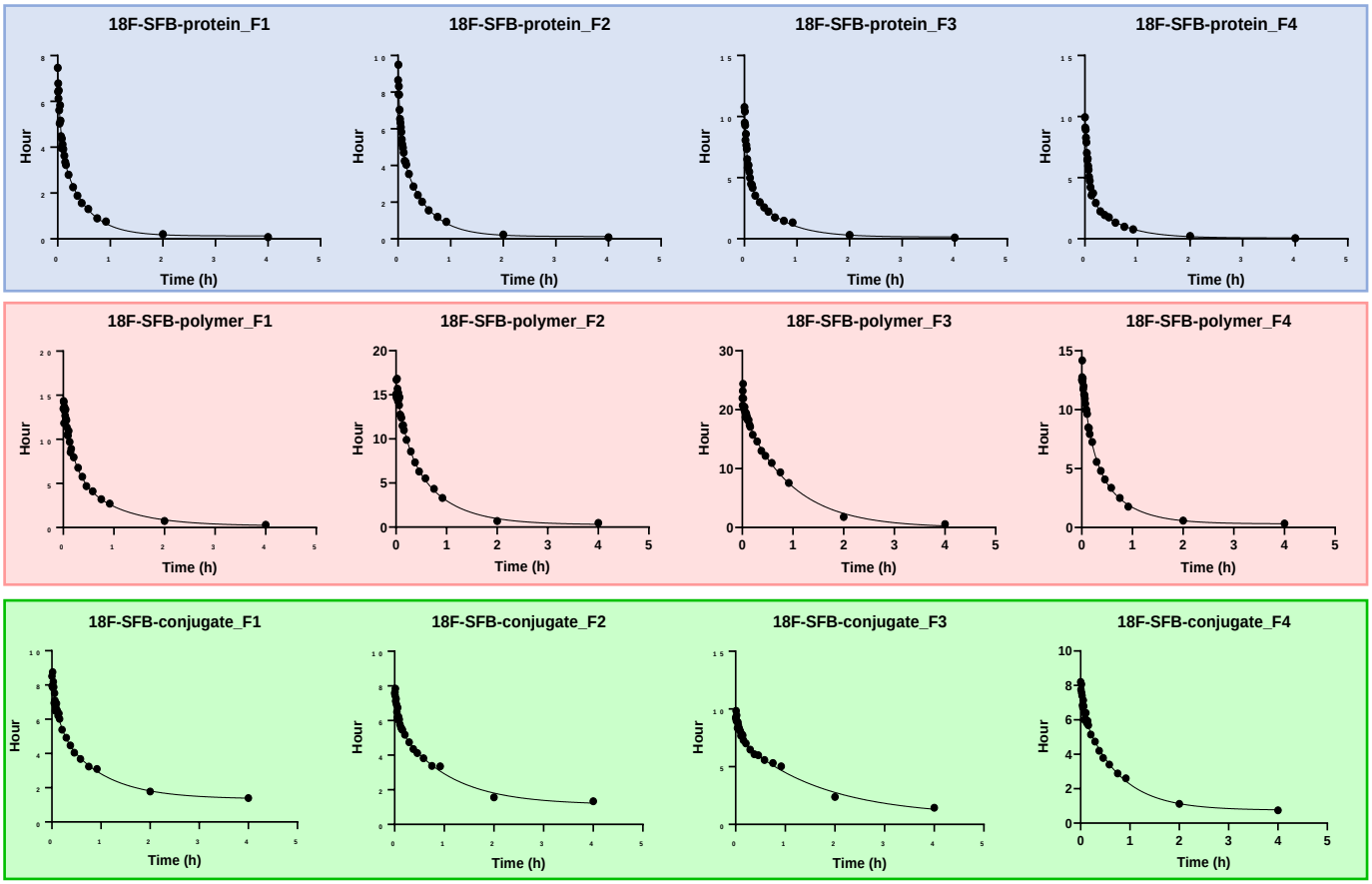

Figure 4.35 Individual regression curves for two-phase decay model for blood half-life for ^{18}F-SFB-protein, ^{18}F-SFB-polymer, and ^{18}F-SFB-conjugate

Pharmacokinetics of GHA-pCLZ 60 kDa Conjugate *In Vivo* via ELISA

Plasma collected as part of the pharmacokinetic study of GHA-alkyne and GHA-pCLZ was analyzed by hGH DuoSet ELISA. To accommodate the many time points and dilutions, the samples were split up over five different 96-well plates with space dedicated to the necessary standard curve on each plate. The same sterile filtered 0.1 M PBS buffer + 0.05% Tween-20 was used to wash the wells four times between each step, making sure to remove solution by hitting the plates against paper towels after each wash. First, hGH capture antibody was diluted 180 fold with 0.1 M PBS (2 µg/mL) and added to each well (100 µL) and incubated at room temperature

(21 °C) for 18 h. Afterwards, capture antibody was removed, the wells washed, and finally cells were blocked with sterile filtered 3% BSA in 0.1 M PBS (300 µL) for 1 h at room temperature. After washing out the BSA blocking solution, standards of GHA-alkyne or GHA-pCLZ conjugate (60 kDa) were plated on 96-well plates (100 µL/well) at nine concentrations (8,000, 4,000, 2,000, 1,000, 500, 250, 125, 62.5, 31.25, 15.625, and 0 pg/mL). The collected plasma was diluted 20, 200, 2,000, and 20,000 fold before being plated (100 µL/well) and incubating both the plasma and standards at room temperature (21 °C) for 18 h, samples were removed, the wells washed and blocked with sterile filtered 3% BSA in 0.1 M PBS (300 µL) for 1 h at room temperature. The hGH detection antibody was diluted 360x with sterile filtered 1% BSA in 0.1 M PBS (100 ng/mL), and, after washing out the BSA blocking solution, the detection antibody was added (100 µL/well). The plates were then incubated at room temperature for 2 h. After washing the wells, streptavidin-HRP conjugate was diluted 200× with filtered 1% BSA in 0.1 M PBS and, in the dark, added to the wells (100 µL/well) before incubating the plates in the dark for 20 min at room temperature. Still in the near-complete dark, the HRP conjugate was washed from the wells and TMB substrate solution was added (100 µL/well) and the wells were allowed to develop for approximately 30 min. When color had developed appropriately according to the standard curve wells, the reaction was quenched by adding 2 M H_2SO_4 (50 µL/well). The absorbance was measured at 450 nm and background at 570 nm.

GHA levels in mice over 24 h after i.v. injection of GHA-yne or GHA-pCLZ (60 kDa) (n = 5 – 6). GHA levels were measured by sandwich ELISA compared to GHA-yne or GHA-pCLZ (60 kDa) standard curves.

Plasmsa levels in mice injected with GHA-pCLZ (60 kDa) and GHA-yne were measured by ELISA over time to measure the half-life of the GHA-yne and conjugate. For these

measurements, mice were injected by i.v. with GHA-yne (2 mg/kg) or the largest size of GHA-pCLZ (60 kDa) (0.75 mg/kg), concentration of conjugate reduced from the planed 2 mg/kg due to insufficient materials. Subsequently time points were taken at 0.5, 2, 4, and 8 h were taken by saphenous vein collection and a final time point at 24 h was taken post-mortem. Plasma from each time point was diluted four times, requiring samples be split up over 3 and 2 plates for GHA-pCLZ (60 kDa) and GHA-yne, respectively. For each plate, the corresponding GHA-pCLZ or GHA-yne standard was used to make a standard curve.

Due to limitations in how quickly the first time point (0.5 h) could be taken after administration, the measurements of GHA-yne are best used as a baseline for the conjugate as the literature reports a half-life for hGH of 15-30 min.[1, 7-8, 13] The half-life of GHA-pCLZ (60 kDa) was calculated to be 2.28 ± 0.5 h, and clearly has extended the circulation time *in vivo* as compared to the GHA-yne. This increase in half-life resulted in measureable levels of GHA in blood circulation as far out as 8 h, although nowhere near as long as the half-life of Pegvisomant (~74 h).

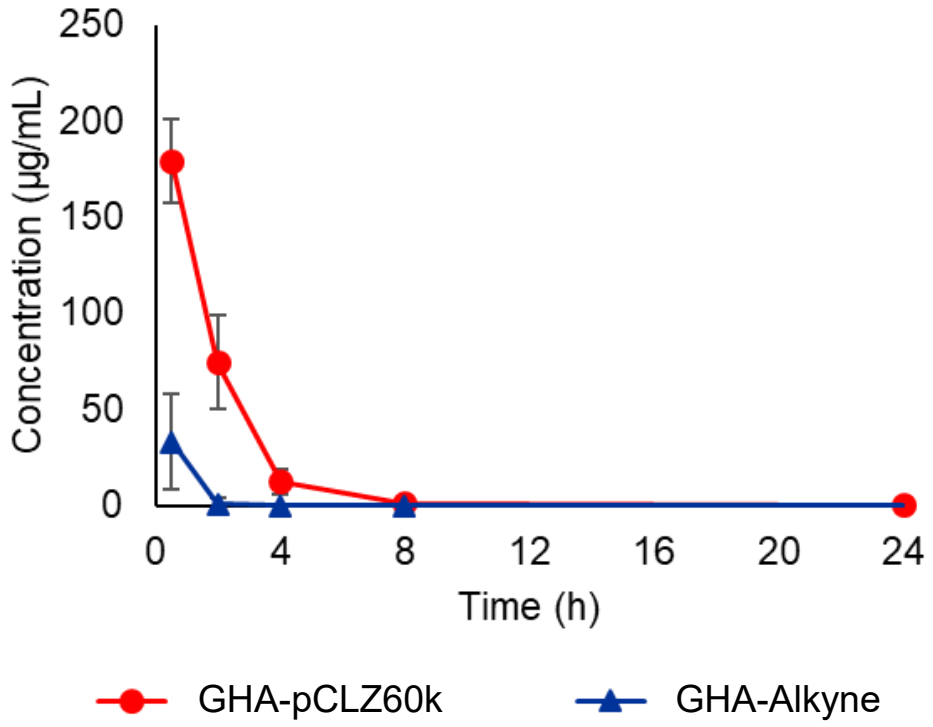

Figure 4.36 Pharmacokinetics data of GHA-pCLZ60k via ELISA

4.5 References

(1) Alconcel, S. N. S.; Baas, A. S.; Maynard, H. D. FDA-Approved Poly(Ethylene Glycol)–Protein Conjugate Drugs. *Polym. Chem.* **2011**, *2* (7), 1442–1448. https://doi.org/10.1039/C1PY00034A.

(2) Ganson, N. J.; Kelly, S. J.; Scarlett, E.; Sundy, J. S.; Hershfield, M. S. Control of Hyperuricemia in Subjects with Refractory Gout, and Induction of Antibody against Poly(Ethylene Glycol) (PEG), in a Phase I Trial of Subcutaneous PEGylated Urate Oxidase. *Arthritis Res. Ther.* **2006**, *8* (1), R12. https://doi.org/10.1186/ar1861.

(3) Hershfield, M. S.; Ganson, N. J.; Kelly, S. J.; Scarlett, E. L.; Jaggers, D. A.; Sundy, J. S.

Induced and Pre-Existing Anti-Polyethylene Glycol Antibody in a Trial of Every 3-Week Dosing of Pegloticase for Refractory Gout, Including in Organ Transplant Recipients. *Arthritis Res. Ther.* **2014**, *16* (2), R63. https://doi.org/10.1186/ar4500.

(4) Chao, S.-H.; Matthews, S. S.; Paxman, R.; Aksimentiev, A.; Gruebele, M.; Price, J. L. Two Structural Scenarios for Protein Stabilization by PEG. *J. Phys. Chem. B* **2014**, *118* (28), 8388–8395. https://doi.org/10.1021/jp502234s.

(5) Han, Y.; Yuan, Z.; Zhang, P.; Jiang, S. Zwitterlation Mitigates Protein Bioactivity Loss in Vitro over PEGylation. *Chem. Sci.* **2018**, *9* (45), 8561–8566. https://doi.org/10.1039/C8SC01777H.

(6) Keefe, A. J.; Jiang, S. Poly(Zwitterionic)Protein Conjugates Offer Increased Stability without Sacrificing Binding Affinity or Bioactivity. *Nat. Chem.* **2012**, *4* (1), 59–63. https://doi.org/10.1038/nchem.1213.

(7) Shao, Q.; Jiang, S. Molecular Understanding and Design of Zwitterionic Materials. *Adv. Mater.* **2015**, *27* (1), 15–26. https://doi.org/10.1002/adma.201404059.

(8) Pelegri-O'Day, E. M.; Bhattacharya, A.; Theopold, N.; Ko, J. H.; Maynard, H. D. Synthesis of Zwitterionic and Trehalose Polymers with Variable Degradation Rates and Stabilization of Insulin. *Biomacromolecules* **2020**, *21* (6), 2147–2154. https://doi.org/10.1021/acs.biomac.0c00133.

(9) Pelegri-O'Day, E. M.; Paluck, S. J.; Maynard, H. D. Substituted Polyesters by Thiol–Ene Modification: Rapid Diversification for Therapeutic Protein Stabilization. *J. Am. Chem. Soc.* **2017**, *139* (3), 1145–1154. https://doi.org/10.1021/jacs.6b10776.

(10) Rydz, J.; Sikorska, W.; Kyulavska, M.; Christova, D. Polyester-Based (Bio)Degradable Polymers as Environmentally Friendly Materials for Sustainable Development. *Int. J. Mol.*

Sci. **2014**, *16* (1), 564–596. https://doi.org/10.3390/ijms16010564.

(11) Woodard, L. N.; Grunlan, M. A. Hydrolytic Degradation and Erosion of Polyester Biomaterials. *ACS Macro Lett.* **2018**, *7* (8), 976–982. https://doi.org/10.1021/acsmacrolett.8b00424.

(12) Mueller, R.-J. Biological Degradation of Synthetic Polyesters—Enzymes as Potential Catalysts for Polyester Recycling. *Process Biochem.* **2006**, *41* (10), 2124–2128. https://doi.org/10.1016/j.procbio.2006.05.018.

(13) Vert, M. Aliphatic Polyesters: Great Degradable Polymers That Cannot Do Everything. *Biomacromolecules* **2005**, *6* (2), 538–546. https://doi.org/10.1021/bm0494702.

(14) Kopchick, J. J.; Parkinson, C.; Stevens, E. C.; Trainer, P. J. Growth Hormone Receptor Antagonists: Discovery, Development, and Use in Patients with Acromegaly. *Endocr. Rev.* **2002**, *23* (5), 623–646. https://doi.org/10.1210/er.2001-0022.

(15) Muller, A. F.; Kopchick, J. J.; Flyvbjerg, A.; van der Lely, A. J. Growth Hormone Receptor Antagonists. *J. Clin. Endocrinol. Metab.* **2004**, *89* (4), 1503–1511. https://doi.org/10.1210/jc.2002-022049.

(16) McCutcheon, I. E.; Flyvbjerg, A.; Hill, H.; Li, J.; Bennett, W. F.; Scarlett, J. A.; Friend, K. E. Antitumor Activity of the Growth Hormone Receptor Antagonist Pegvisomant against Human Meningiomas in Nude Mice. *J. Neurosurg.* **2001**, *94* (3), 487–492. https://doi.org/10.3171/jns.2001.94.3.0487.

(17) Dagnaes-Hansen, F.; Duan, H.; Rasmussen, L. M.; Friend, K. E.; Flyvbjerg, A. Growth Hormone Receptor Antagonist Administration Inhibits Growth of Human Colorectal Carcinoma in Nude Mice. *Anticancer Res.* **2004**, *24* (6), 3735–3742.

(18) Divisova, J.; Kuiatse, I.; Lazard, Z.; Weiss, H.; Vreeland, F.; Hadsell, D. L.; Schiff, R.;

Osborne, C. K.; Lee, A. V. The Growth Hormone Receptor Antagonist Pegvisomant Blocks Both Mammary Gland Development and MCF-7 Breast Cancer Xenograft Growth. *Breast Cancer Res. Treat.* **2006**, *98* (3), 315–327. https://doi.org/10.1007/s10549-006-9168-1.

(19) Yin, D.; Vreeland, F.; Schaaf, L. J.; Millham, R.; Duncan, B. A.; Sharma, A. Clinical Pharmacodynamic Effects of the Growth Hormone Receptor Antagonist Pegvisomant: Implications for Cancer Therapy. *Clin. Cancer Res.* **2007**, *13* (3), 1000–1009. https://doi.org/10.1158/1078-0432.CCR-06-1910.

(20) Evans, A.; Jamieson, S. M. F.; Liu, D.-X.; Wilson, W. R.; Perry, J. K. Growth Hormone Receptor Antagonism Suppresses Tumour Regrowth after Radiotherapy in an Endometrial Cancer Xenograft Model. *Cancer Lett.* **2016**, *379* (1), 117–123. https://doi.org/10.1016/j.canlet.2016.05.031.

(21) Pradhananga, S.; Wilkinson, I.; Ross, R. J. M. Pegvisomant: Structure and Function. *J. Mol. Endocrinol.* **2002**, *29* (1), 11–14. https://doi.org/10.1677/jme.0.0290011.

(22) Kopchick, J. J. Discovery and Mechanism of Action of Pegvisomant. *Eur. J. Endocrinol.* **2003**, *148 Suppl 2*, S21-25. https://doi.org/10.1530/eje.0.148s021.

(23) van der Lely, A. J.; Hutson, R. K.; Trainer, P. J.; Besser, G. M.; Barkan, A. L.; Katznelson, L.; Klibanski, A.; Herman-Bonert, V.; Melmed, S.; Vance, M. L.; Freda, P. U.; Stewart, P. M.; Friend, K. E.; Clemmons, D. R.; Johannsson, G.; Stavrou, S.; Cook, D. M.; Phillips, L. S.; Strasburger, C. J.; Hackett, S.; Zib, K. A.; Davis, R. J.; Scarlett, J. A.; Thorner, M. O. Long-Term Treatment of Acromegaly with Pegvisomant, a Growth Hormone Receptor Antagonist. *Lancet Lond. Engl.* **2001**, *358* (9295), 1754–1759. https://doi.org/10.1016/s0140-6736(01)06844-1.

(24) Ross, R. J. M.; Leung, K. C.; Maamra, M.; Bennett, W.; Doyle, N.; Waters, M. J.; Ho, K.

K. Y. Binding and Functional Studies with the Growth Hormone Receptor Antagonist, B2036-PEG (Pegvisomant), Reveal Effects of Pegylation and Evidence That It Binds to a Receptor Dimer1. *J. Clin. Endocrinol. Metab.* **2001**, *86* (4), 1716–1723. https://doi.org/10.1210/jcem.86.4.7403.

(25) Tamshen, K.; Wang, Y.; Jamieson, S. M. F.; Perry, J. K.; Maynard, H. D. Genetic Code Expansion Enables Site-Specific PEGylation of a Human Growth Hormone Receptor Antagonist through Click Chemistry. *Bioconjug. Chem.* **2020**, *31* (9), 2179–2190. https://doi.org/10.1021/acs.bioconjchem.0c00365.

(26) Cunningham, B. C.; Wells, J. A. Rational Design of Receptor-Specific Variants of Human Growth Hormone. *Proc. Natl. Acad. Sci. U. S. A.* **1991**, *88* (8), 3407–3411. https://doi.org/10.1073/pnas.88.8.3407.

(27) Cunningham, B. C.; Wells, J. A. Comparison of a Structural and a Functional Epitope. *J. Mol. Biol.* **1993**, *234* (3), 554–563. https://doi.org/10.1006/jmbi.1993.1611.

(28) de Vos, A. M.; Ultsch, M.; Kossiakoff, A. A. Human Growth Hormone and Extracellular Domain of Its Receptor: Crystal Structure of the Complex. *Science* **1992**, *255* (5042), 306–312. https://doi.org/10.1126/science.1549776.

(29) Cunningham, B. C.; Wells, J. A. High-Resolution Epitope Mapping of HGH-Receptor Interactions by Alanine-Scanning Mutagenesis. *Science* **1989**, *244* (4908), 1081–1085. https://doi.org/10.1126/science.2471267.

(30) Cho, H.; Daniel, T.; Buechler, Y. J.; Litzinger, D. C.; Maio, Z.; Putnam, A.-M. H.; Kraynov, V. S.; Sim, B.-C.; Bussell, S.; Javahishvili, T.; Kaphle, S.; Viramontes, G.; Ong, M.; Chu, S.; GC, B.; Lieu, R.; Knudsen, N.; Castiglioni, P.; Norman, T. C.; Axelrod, D. W.; Hoffman, A. R.; Schultz, P. G.; DiMarchi, R. D.; Kimmel, B. E. Optimized Clinical Performance of

Growth Hormone with an Expanded Genetic Code. *Proc. Natl. Acad. Sci.* **2011**, *108* (22), 9060–9065. https://doi.org/10.1073/pnas.1100387108.

(31) Wu, L.; Chen, J.; Wu, Y.; Zhang, B.; Cai, X.; Zhang, Z.; Wang, Y.; Si, L.; Xu, H.; Zheng, Y.; Zhang, C.; Liang, C.; Li, J.; Zhang, L.; Zhang, Q.; Zhou, D. Precise and Combinatorial PEGylation Generates a Low-Immunogenic and Stable Form of Human Growth Hormone. *J. Control. Release Off. J. Control. Release Soc.* **2017**, *249*, 84–93. https://doi.org/10.1016/j.jconrel.2017.01.029.

(32) Chin, J. W.; Santoro, S. W.; Martin, A. B.; King, D. S.; Wang, L.; Schultz, P. G. Addition of P-Azido-l-Phenylalanine to the Genetic Code of Escherichia Coli. *J. Am. Chem. Soc.* **2002**, *124* (31), 9026–9027. https://doi.org/10.1021/ja027007w.

(33) Nguyen, D. P.; Lusic, H.; Neumann, H.; Kapadnis, P. B.; Deiters, A.; Chin, J. W. Genetic Encoding and Labeling of Aliphatic Azides and Alkynes in Recombinant Proteins via a Pyrrolysyl-TRNA Synthetase/TRNACUA Pair and Click Chemistry. *J. Am. Chem. Soc.* **2009**, *131* (25), 8720–8721. https://doi.org/10.1021/ja900553w.

(34) Murale, D. P.; Hong, S. C.; Haque, Md. M.; Lee, J.-S. Photo-Affinity Labeling (PAL) in Chemical Proteomics: A Handy Tool to Investigate Protein-Protein Interactions (PPIs). *Proteome Sci.* **2017**, *15* (1), 14. https://doi.org/10.1186/s12953-017-0123-3.

(35) Merrill, S. H.; Unruh, C. C. Photosensitive Azide Polymers. *J. Appl. Polym. Sci.* **1963**, *7* (1), 273–279. https://doi.org/10.1002/app.1963.070070124.

(36) Leyshon, L. J.; Reiser, A. Sensitized Photodecomposition of Phenyl Azide and α-Naphthyl Azide. *J. Chem. Soc. Faraday Trans. 2 Mol. Chem. Phys.* **1972**, *68* (0), 1918–1927. https://doi.org/10.1039/F29726801918.

(37) Coderre, D. N.; Fastnacht, K. V.; Wright, T. J.; Dharmaratne, N. U.; Kiesewetter, M. K. H-

Bonding Organocatalysts for Ring-Opening Polymerization at Elevated Temperatures. *Macromolecules* **2018**, *51* (24), 10121–10126. https://doi.org/10.1021/acs.macromol.8b02219.

(38) Conway-Campbell, B. L.; Brooks, A. J.; Robinson, P. J.; Perani, M.; Waters, M. J. The Extracellular Domain of the Growth Hormone Receptor Interacts with Coactivator Activator to Promote Cell Proliferation. *Mol. Endocrinol.* **2008**, *22* (9), 2190–2202. https://doi.org/10.1210/me.2008-0128.

(39) Schroeder, H. W.; Cavacini, L. Structure and Function of Immunoglobulins. *J. Allergy Clin. Immunol.* **2010**, *125* (2 0 2), S41–S52. https://doi.org/10.1016/j.jaci.2009.09.046.

(40) Kozma, G. T.; Shimizu, T.; Ishida, T.; Szebeni, J. Anti-PEG Antibodies: Properties, Formation, Testing and Role in Adverse Immune Reactions to PEGylated Nano-Biopharmaceuticals. *Adv. Drug Deliv. Rev.* **2020**, *154–155*, 163–175. https://doi.org/10.1016/j.addr.2020.07.024.

(41) Pelosi, C.; Duce, C.; Wurm, F. R.; Tinè, M. R. Effect of Polymer Hydrophilicity and Molar Mass on the Properties of the Protein in Protein–Polymer Conjugates: The Case of PPEylated Myoglobin. *Biomacromolecules* **2021**, *22* (5), 1932–1943. https://doi.org/10.1021/acs.biomac.1c00058.

(42) Fox, M. E.; Szoka, F. C.; Fréchet, J. M. J. Soluble Polymer Carriers for the Treatment of Cancer: The Importance of Molecular Architecture. *Acc. Chem. Res.* **2009**, *42* (8), 1141–1151. https://doi.org/10.1021/ar900035f.

(43) Fastnacht, K. V.; Spink, S. S.; Dharmaratne, N. U.; Pothupitiya, J. U.; Datta, P. P.; Kiesewetter, E. T.; Kiesewetter, M. K. Bis- and Tris-Urea H-Bond Donors for Ring-Opening Polymerization: Unprecedented Activity and Control from an Organocatalyst. *ACS*

Macro Lett. **2016**, *5* (8), 982–986. https://doi.org/10.1021/acsmacrolett.6b00527.

(44) Presolski, S. I.; Hong, V. P.; Finn, M. G. Copper-Catalyzed Azide–Alkyne Click Chemistry for Bioconjugation. *Curr. Protoc. Chem. Biol.* **2011**, *3* (4), 153–162. https://doi.org/10.1002/9780470559277.ch110148.

(45) Bernini, R.; Crisante, F.; Barontini, M.; Fabrizi, G. A New and Efficient Route for the Synthesis of Naturally Occurring Catecholamines. *Synthesis* **2009**, *2009* (22), 3838–3842. https://doi.org/10.1055/s-0029-1217027.

(46) Munneke, S.; Kodar, K.; Painter, G. F.; Stocker, B. L.; Timmer, M. S. M. The Modular Synthesis of Multivalent Functionalised Glycodendrons for the Detection of Lectins Including DC-SIGN. *RSC Adv.* **2017**, *7* (72), 45260–45268. https://doi.org/10.1039/C7RA08872H.

Chapter 5

Uniform Polymer-Protein Conjugates for Evaluating the Impact of Molecular Features of Conjugated Polymers on the Activity of Growth Hormone Antagonist

5.1 Introduction

Protein therapeutics show their benefits of efficiency and specificity due to their low off-target effect as modern therapeutical medicines.[1] However, owing to issues such as fast clearance *in vivo*, and poor stability during cold-chain transport, biological activities of proteins are compromised as therapeutics.[2] Polymer-protein conjugation has been one effective way to address the aforementioned limitations through covalently attaching polymer chains with proteins.[3,4] Amongst various conjugation systems, polyethylene glycol (PEG) is the most widely used polymers for this purpose. The hydrophilicity and low immunogenicity of PEG offered great opportunities for them to be applied in physiological conditions.[5] Meanwhile, the conjugation of polymers onto a protein increases their overall sizes and provides shielding to prevent proteins from aggregation and degradation.[6] Numerous work based on PEGylation have shown advantages on enhanced stability *in vitro* and improved circulation time *in vivo* of PEGylated conjugates. However, despite constructing various polymeric architectures with branched or grafted PEG,[7,8] a lack of tunable molecular features of polymer structures to explore their impact on protein activities remains. In addition, alternative polymers to PEG as conjugates in therapeutic treatments have become a topic of interest owing to the more recently reported immunogenicity of PEG.[9–11]

Various systems beyond PEGylation with linear PEG have been explored to elucidate their impact of polymer structures on the protein activities and stability in the format of polymer-protein conjugates.[12] For instance, Maynard and coworkers generated a series of various glycopolymers to conjugate to proteins, and proved the polymers stabiliized proteins under different environment stresses (*e.g.* freeze-thaw process,[13] heat,[14,15] mechanical agitation,[16] etc). Jiang and coworkers applied a zwitterionic polymer to conjugate with proteins that showed similar improvement of protein stability as PEGylated proteins. These zwitterionic protein-polymer conjugates

demonstrated significantly enhanced binding affinity, compared to PEGylated proteins, due to the hydrophobic interactions between zwitterionic polymers and proteins. [17] These different systems played important roles of understanding the relationship between polymer structures and protein behaviors. Nevertheless, due to the disperse nature of synthetic polymers used in these works, a systematic evaluation would be difficult to achieve.

Synthesis of a uniform conjugation system with structurally complex polymers has been attempted by alternative methodologies and various synthetic polymers. Stemmer and coworkers designed a plasmid expression system to directly encode a sequence-defined polypeptide attached at the C-terminus of a protein drug and was shown successfully increase half-life.[18] Despite this success, the attached polymers were restricted to a polypeptide. Recently, Johnson and coworkers applied a series of discrete polymers synthesized via an iterative exponential growth strategy to conjugate with insulin. Due to the existence of various molecular features of conjugated IEG polymers (*i.e.* stereochemistry and backbone rigidity), the evaluations of insulin activities *in vivo* revealed that the different combinations of polymers with alternative features resulted in a significant difference in the response time of diabetic mice to administrate their blood glucose level. This system has shown great potential in terms of exploring the structure-activity relationship of polymer-protein conjugates; however, it remained to be a heterogenous mixture for the final conjugates due to the existence of regioisomers using strain-promoted azide-alkyne cycloaddition (SPAAC) reactions.[19]

In this work, we constructed a fully uniform platform of polymer-protein conjugates with more diverse structural features of conjugated polymers compared to the previously reported work. Human growth hormone receptor antagonists are a class of recombinantly engineered protein therapeutics designed to block human growth hormone signaling which has been investigated for

use against diseases such as acromegaly and certain cancers. Recently, Maynard and coworkers reported a new construct of the growth hormone antagonist (GHA) B2036-Alkyne through the use of genetic code expansion.[20] Tyrosine at position 35 was substituted with the unnatural amino acid propargyl tyrosine to enable an alkyne handle to facilitate azide-alkyne cycloadditions.[21] Additionally, the incorporation of trehalose into the side chains of polymers has stabilized proteins by preventing aggregation, reducing crystallization, and serving as chaperones.[22–24] Leveraging allyl-IEG$^+$ systems that the Johnson lab reported before,[25,26] in collaboration with the Johnson group, we synthesized various IEG octamers with allyl groups on the side chains for further trehalose functionalizations using thiol-ene reactions. Furthermore, through a copper-catalyzed azide-alkyne cycloaddition (CuAAC), we achieved a site-specific modification of these IEG polymers onto a genetically site-specific modified GHA with one determined structure of the final conjugates. Using these conjugates, we can evaluate the impact of stereochemistry, rigidity, and side-chain functionalities of conjugated polymers on the delivered proteins regarding to their biological activities and stability *in vitro*. We believe that this could broader understanding of lengths and stereochemistry of polymers in protein conjugation systems in order to gain full control over their biological performances.

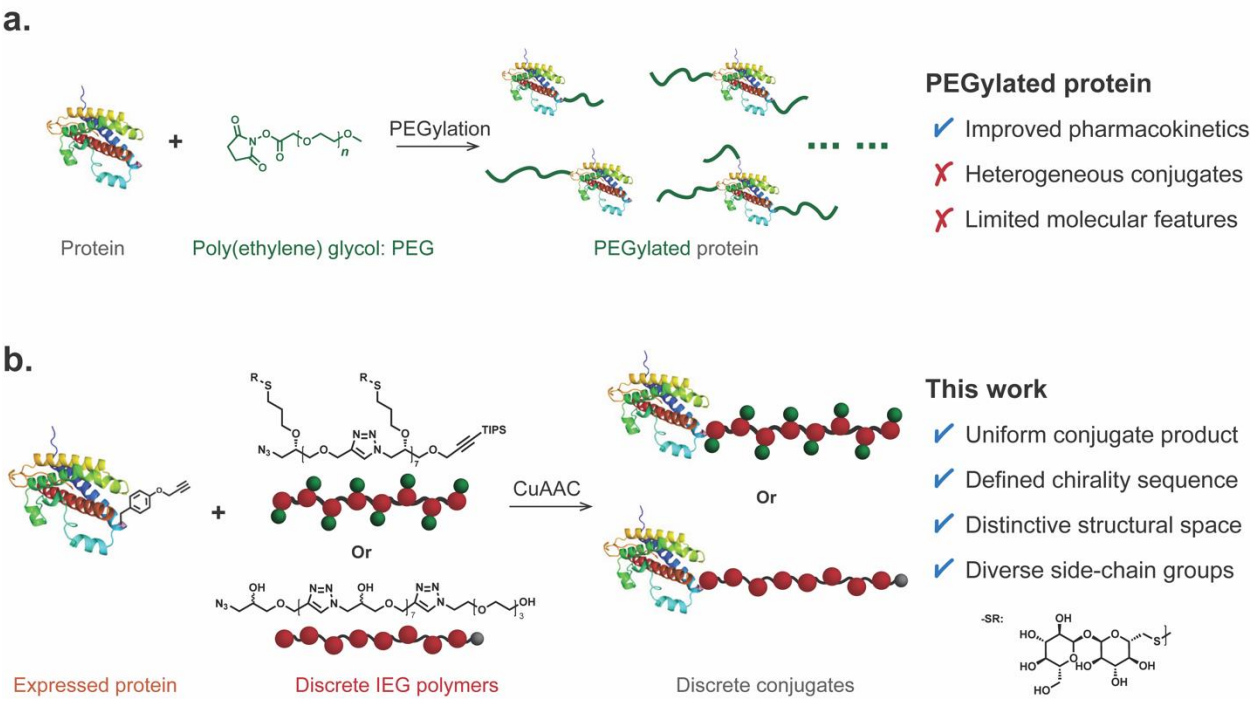

Figure 5.1. Representative protein delivery systems and their distinctive characteristics. A) Conventional PEGylation of proteins leads to a heterogeneous mixture of conjugates with limited control over their structures. **B)** In this work, we fully eliminated the heterogeneity problem meanwhile offered more molecular features for studying the structure-property relationship in polymer-protein conjugates.

5.2 Results and discussion

Preparation of IEG macromolecule library for conjugation.

In order to create a library of discrete macromolecules with diverse molecular features, we first applied the previously reported IEG systems to synthesize two series of discrete polymers: one flexible system with 5 atoms between each triazole repeating unit (5A-IEG) and one relatively rigid version with 2 atoms (2A-IEG).[25–28] Starting from allyl-IEG^{+} systems, we first ran thiol-ene reactions to modify the side chains with trehalose, followed by an azidation reaction to anchor a reactive, azide group, on the end for further conjugation reaction (Fig. 5.2a-b). Therefore, we

introduced two IEG macromolecules with trehalose-modified side chains with defined chemical composition sequence, and stereochemistry.

MALDI-TOF data confirmed the molecular weight of the synthesized polymers (Fig. 5.2c-d). For **N_3-5A-*S*-Tre**, an exact molecular weight plus one potassium ion was observed on MALDI-TOF, which correlated to the MW of the synthesized macromolecule (Fig. 5.2c). For **N_3-2A-*S*-Tre**, the major peak aligned with its exact molecular weight plus one potassium ion. Another small peak that appeared to the left of the desirable molecular weight correlated to the cleavage of one ester from the side chain of the final product (Fig. 5.2c). Furthermore, purification of these two trehalose-modified polymers on FPLC further revealed their relative size. Due to the lower flexibility of the backbone of **N_3-2A-*S*-Tre**, it showed a shorter elution time on the FPLC, which indicated a larger hydrodynamic volume compared to **N_3-5A-*S*-Tre** (Fig. 5.2d). After purification on FPLC, pure fraction peaks were collected for conjugation.

Beside these newly made discrete polymers with defined amounts of trehalose side chains, we also utilized the same six IEG macromolecules with different backbone rigidity and stereochemistries as previously reported with insulin as comparison. Therefore, in order to fully study the impact of various molecular features on protein activity, we created a library of 8 azide-terminated water-soluble IEG octamers for examinations: **N_3-5A-*R*-OH**, **N_3-5A-*S*-OH**, **N_3-5A-*Alt*-OH**, **N_3-2A-*R*-OH**, **N_3-2A-*S*-OH**, **N_3-2A-*Alt*-OH**, **N_3-5A-*S*-Tre**, and **N_3-2A-*S*-Tre** (Scheme 5.1).

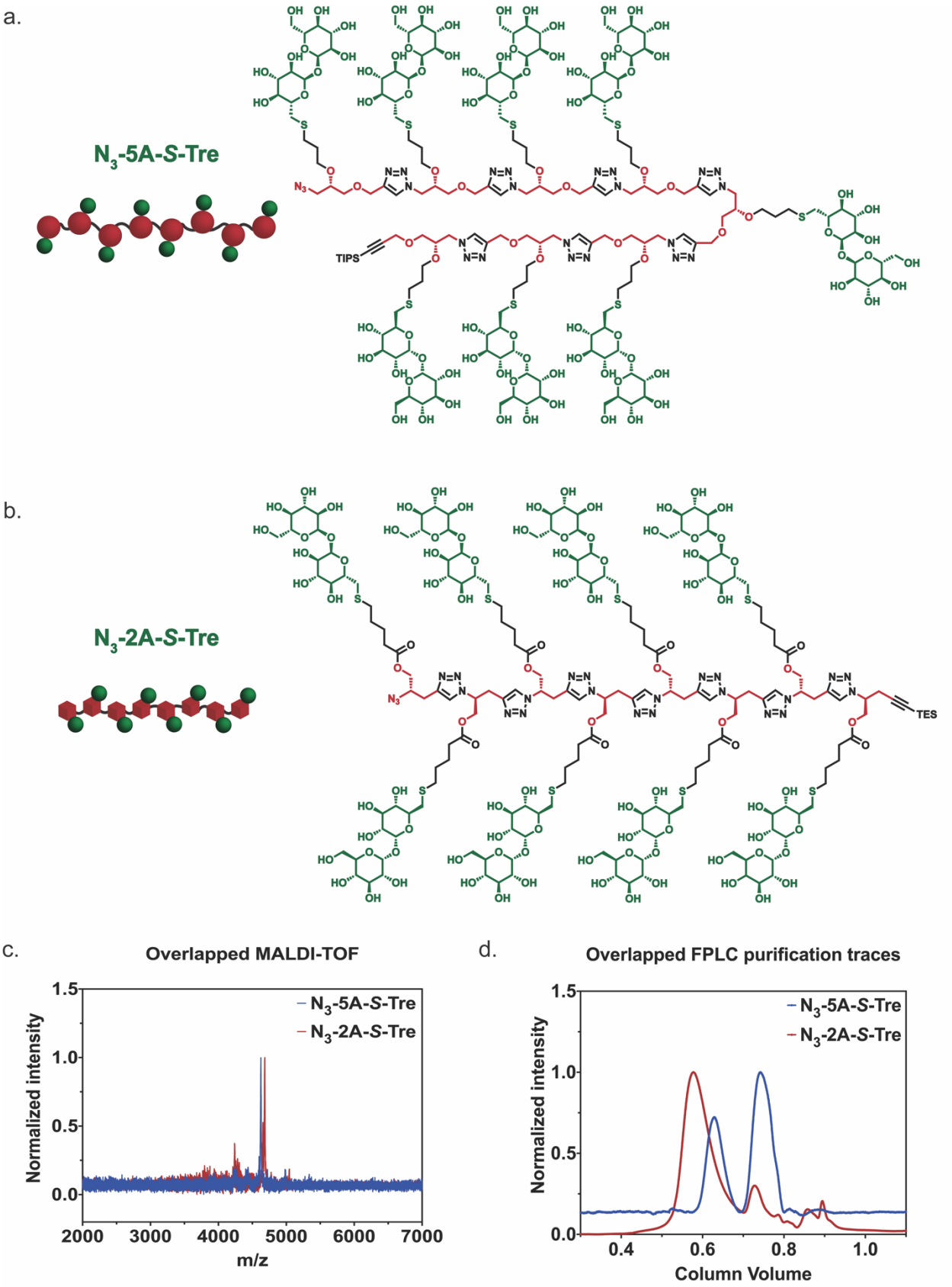
a.
N3-5A-S-Tre
TIPS
b.
N3-2A-S-Tre
TES
c.
Overlapped MALDI-TOF
N3-5A-S-Tre
N3-2A-S-Tre
Normalized intensity
m/z
d.
Overlapped FPLC purification traces
N3-5A-S-Tre
N3-2A-S-Tre
Normalized intensity
Column Volume

Figure 5.2 Structures and characterizations of N_3-*S*-IEG-Tre polymers. A. Chemical structure of trehalose-modified 5A-IEG octamer, **N_3-5A-*S*-Tre**; **B.** Chemical structure of trehalose-modified 2A-IEG octamer, **N_3-2A-*S*-Tre**; **C.** Overlapped MALDI-TOF of trehalose-modified octamer: 1) **N_3-5A-*S*-Tre** (blue trace): observed m/z at 4624.6 [M + K]+ ; calcd m/z = 4624.1 [M + K] + ; 2) **N_3-2A-*S*-Tre** (red trace): observed m/z at 4678.9 [M + K]+ ; calcd m/z = 4678.0 [M + K] +; **D.** Overlapped purification traces of trehalose-modified octamer on FPLC at 280 nm: 1) **N_3-5A-*S*-Tre** (blue trace): elution peak was around column volume; 2) **N_3-2A-*S*-Tre** (red trace): elution peak was around column volume.

Conjugation and characterizations of GHA-alkyne with azide-terminated IEG polymers

In order to prepare our conjugates, the GHA B2036-Alkyne variant was expressed and purified as previously reported.[20,21] Subsequently, the conjugates were prepared through CuAAC between various azide-terminated IEG polymers and **GHA-Alkyne** (Fig. 5.3a). SDS-PAGE was first used to identify and collect pure conjugate fractions after purification of reaction mixtures using fast protein liquid chromatography. After combining pure fractions based on gel electrophoresis, LC-MS was further used to assess purity of the conjugates and showed desirable products as we designed. Q-TOF of the final conjugates revealed the MW of final conjugates (Fig. 5.3b-c). All products showed the MW of various synthesized GHA conjugates; whereas, the Q-TOF peaks of **2A-*S*-Tre-GHA** showed extra peaks that correlated to the cleavage of ester side chains that was observed in previous MALDI-TOF characterization as well. The concentration of various conjugates was measured by bicinchoninic acid assay (BCA) and stored in the -80 °C freezer for later biological assay.

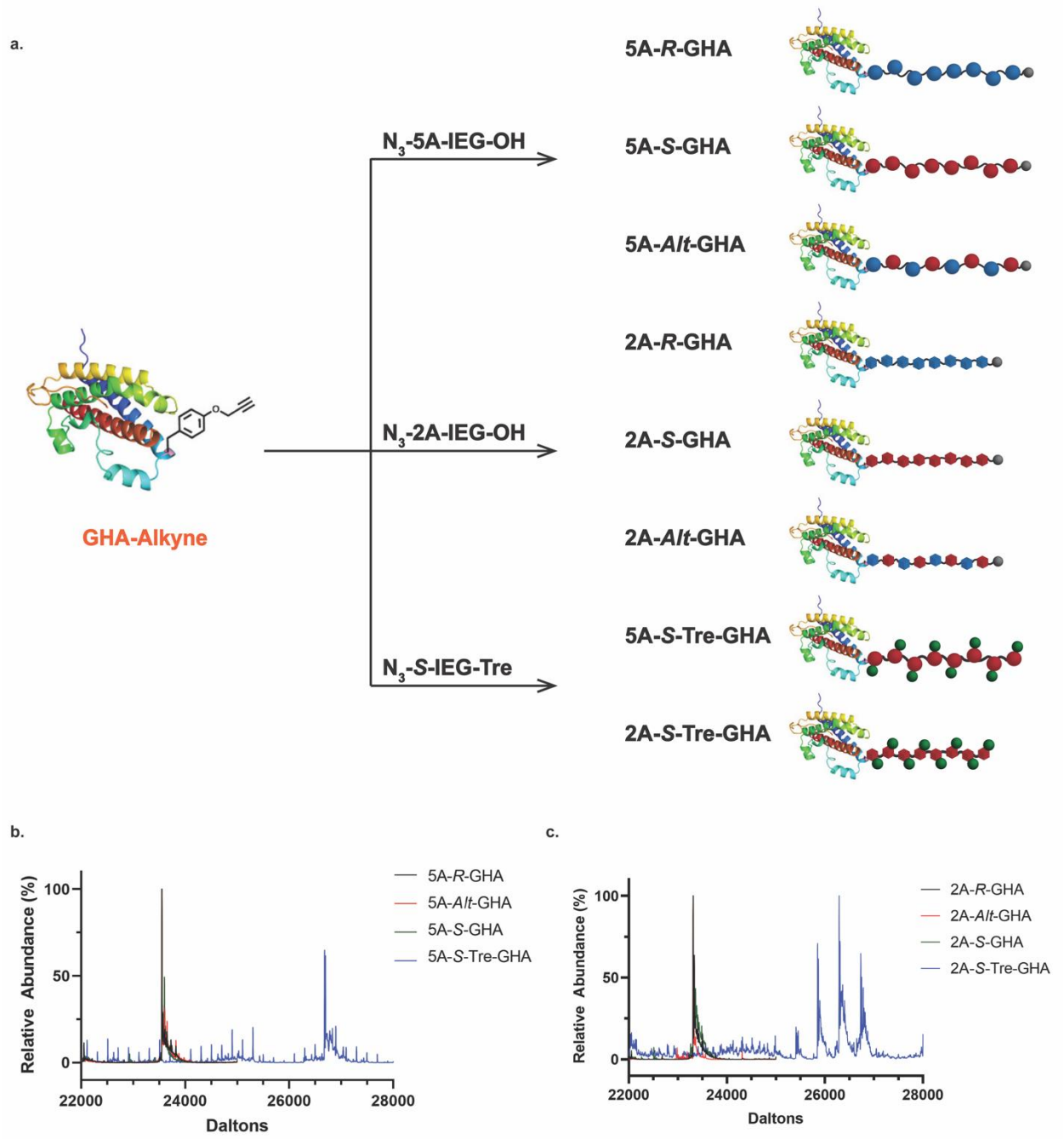

Figure 5.3. Conjugations and characterizations of various GHA conjugates. A) schematic figure of final conjugate library, including **5A-*R*-GHA**, **5A-*S*-GHA**, **5A-*Alt*-GHA**, **2A-*R*-GHA**, **2A-*S*-GHA**, **2A-*Alt*-GHA**, **5A-*S*-Tre-GHA**, and **2A-*S*-Tre-GHA**; **B)** LC/Q-TOF of 5A-IEG-GHA: 5A-IEG-GHA with hydroxyl groups as side chains: observed 23553.34 m/z at [M + K]+ ; calcd 23539.43 m/z = [M + K] +; 5A-IEG-GHA with trehalose as side chains (**N_3-5A-*S*-Tre**):

observed 26697.67 m/z at [M + K]+ ; calcd 26703.1m/z = [M + K] + ; **C)** LC/Q-TOF of 2A-IEG-GHA: 2A-IEG-GHA with hydroxyl groups as side chains: observed 23313.65 m/z at [M + K]+ ; calcd 23299.22 m/z = [M + K] +; 2A-IEG-GHA with trehalose as side chains (**N_3-2A-*S*-Tre**): observed 26732.82 m/z at [M + K]+ ; calcd 26757.0 m/z = [M + K] +.

In vitro protein activity study of discrete GHA conjugates

Cell viability was assessed using Ba/F3-GHR cells. Serial dilutions of each conjugate, ranging from 0 to 900 nM, were made and plated to serum starved cells. Following the subsequent addition of GH solution, the cells were incubated at 37 °C with 5% CO_2 for 48 h. To visualize the cell viability, a solution of resazurin sodium salt was added and further incubated for 2 h.

In Fig. 5.4a, the half maximal inhibitory concentrations of each conjugate are reported with confidence intervals. Within the 5A-GHA conjugates, the IC50 values reflect the inverse relationship between bioactivity and conjugate size. The **5A-*S*-Tre-GHA** conjugate exhibits the highest IC50 value followed by the **5A-*R*-GHA**, **5A-*S*-GHA**, and **5A-*Alt*-GHA.** One-way ANOVA with Tukey's post hoc analysis showed that only GHA and **5A-*Alt*-GHA** show statistical significance ($p < 0.05$). Fig. 5.4b demonstrates the same trend with the 2A-GHA conjugates under the current conditions. One-way ANOVA with Tukey's post hoc analysis showed that 2**A-*Alt*-GHA** and **5A-*S*-Tre-GHA** statistically differ from GHA ($p < 0.05$).

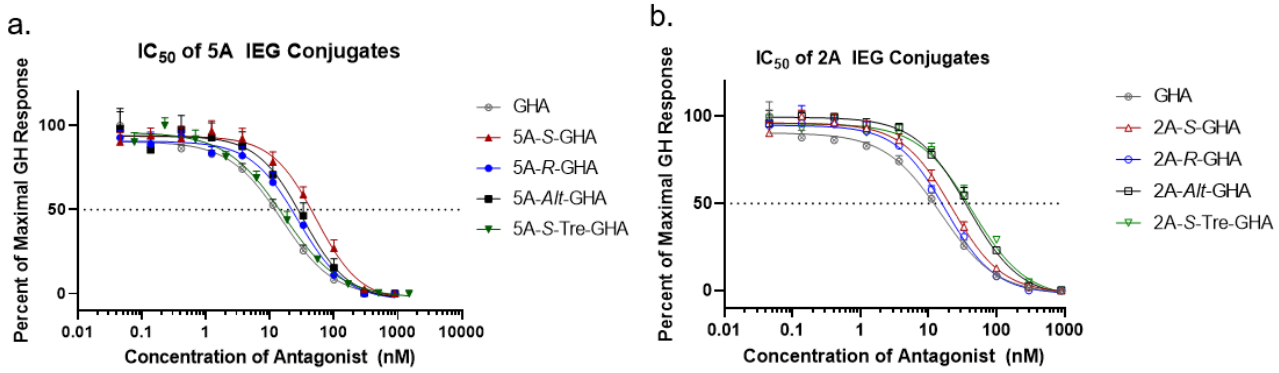

Figure 5.4. Cell viability studies of all GHA conjugates. A) IC50 of 5A-IEG-GHA conjugates; **B)** IC50 of 2A-IEG-GHA conjugates.

Antagonist	IC_{50} (nM)	95% CI (nM)
GHA-Alkyne	15.20	13.79 – 17.28
5A-S-GHA	52.54	42.42 – 63.05
5A-R-GHA	27.79	21.75 – 32.10
5A-Alt-GHA	32.33	24.46 – 41.13
5A-S-Tre-GHA	23.11	16.28 – 26.98
2A-S-GHA	22.17	19.47 – 25.76
2A-R-GHA	17.83	15.29 – 19.54
2A-Alt-GHA	40.64	37.00 – 44.72
2A-S-Tre-GHA	50.21	42.29 – 59.37

Table 5.1 IC50 values of all GHA conjugates with 95% confidence intervals

HPLC Stability of Conjugates

Upon confirming the activity of the conjugates, the stability of the conjugates in DPBS at 37 ºC was measured. Owing to the known stabilization properties of trehalose, we were interested in comparing the stability of the unconjugated protein and the trehalose-modified conjugates. Following literature precedent,[29] GHA-Alkyne, GHA B2036, 5A-STre-GHA, and 2A-STre-GHA were prepared as 25 ug/mL in 20 mM DPBS pH 7.4 with a detectable amount of vanillin as an internal standard. Timepoints were taken at days 0, 13, 20, 27, 35, 42, 56, 70, and 84 and analyzed via HPLC. For conjugates 5A-STre-GHA and 2A-STre-GHA (Fig. 5.5c,d) , day 20 to 27 appear to be the time period at which instability becomes visible by peak shape. Conjugate elutes at 11.8 min and comparing chromatograms from day 20 and day 27, new peaks arise at 10.4 and 11.4 min. From day 35, a shoulder on the tail end of the conjugate appears at 12.0 min and continues to

increase in size as the days progress. For unmodified proteins GHA-Alkyne and GHA B2036 (Fig. 5.5a,b), the peak shape is well retained until day 56 when a shoulder appears on the tail end of the protein peak at 12.1 min. Similarly to the two conjugates studied, the two unmodified proteins also developed a new peak at 11.4 min at day 27. The appearance of new peaks is, however, inconclusive in determining conjugate instability because the internal standard, vanillin, at 5.9 min used to compare the AUC changes begins to show peak shape changes as well(**Fig. 5.5F**). At day 56, the peak shape of the internal standard changed to include a shoulder at the tail end of the peak at 6.2 min. From day 56 to day 84, the AUC shifts from the original compound peak at 5.9 to the shoulder peak at 6.2 min. Though the peak shape of the two conjugates begins to broaden and exhibit shoulder peaks approximately three weeks before the shoulder develops on the two unmodified protein peaks, GHA B2036 and GHA-Alkyne, the stability of the conjugates is inconclusive because of the instability of the internal standard.

To analyze the effect of the trehalose more closely, 5A-*S*-GHA and 2A-S-GHA were also studied for stability under the same conditions above. The 5A-S-GHA sample ended up being too low in concentration and could not be studied due to shortage of material. Looking at the 2A-S-GHA (Fig. 5.5e) chromatograms, the changes in the chromatogram and peak shape align with that of the 2A-S-Tre-GHA sample. A new peak appears at 11.4 min at day 27 and a shoulder appears on the tail end of the conjugate at day 35. No stabilizing effect from the trehalose modified macromolecule was thus observed. This could be because the oligomers were too small to stabilize the protein or that the protein is not stabilized by trehalose itself as the latter was never tested. Future stability studies could be improved with a large abundance of conjugates and proteins, addition of internal standard directly before analysis of each timepoint, and careful analysis via mass spectrometry.

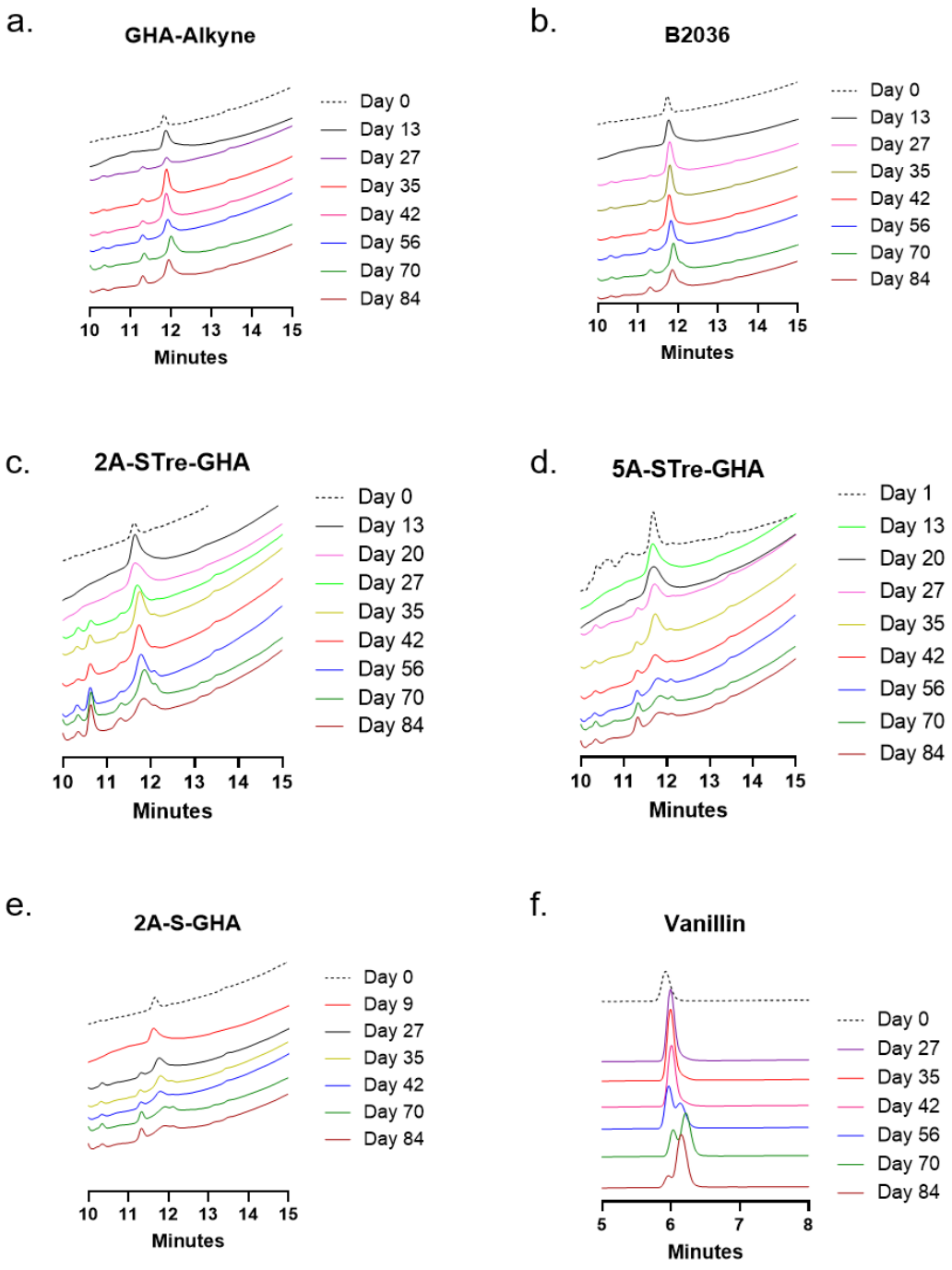

Figure 5.5. HPLC stability of GHA and conjugates over 84 days A. GHA-Alkyne **B.** GHA B2036 **C.** 2A-STre-GHA. **D.** 5A-STre-GHA. **E.** 2A-S-GHA. **F**. Vanillin (Internal Standard). Proteins and conjugates were incubated as 25 ug/mL in 20 mM DPBS pH 7.4 at 37 ºC with a detectable amount of vanillin as an internal standard. Timepoints were taken at days 0, 13, 20, 27, 35, 42, 56, 70, and 84 and analyzed via HPLC.

X-Ray Crystallography

Leveraging new methodologies in elucidating structures of macromolecules, we set out to image the first uniform protein-polymer conjugate using micro electron diffraction (microED). This was done in collaboration with the BiopacificMIP. With the services of the Institute for Genomics and Proteomics X-ray and Electromagnetic Structure Determination core, a wide number of crystallization conditions were screened. In order to narrow down conditions, the crystallization was attempted with the GHA-Alkyne protein alone. The following commercial plates were set up: JCSG+, MPDs, PEG, ProPlexEco, Structure Screen, Wizard, Midas Plus, and

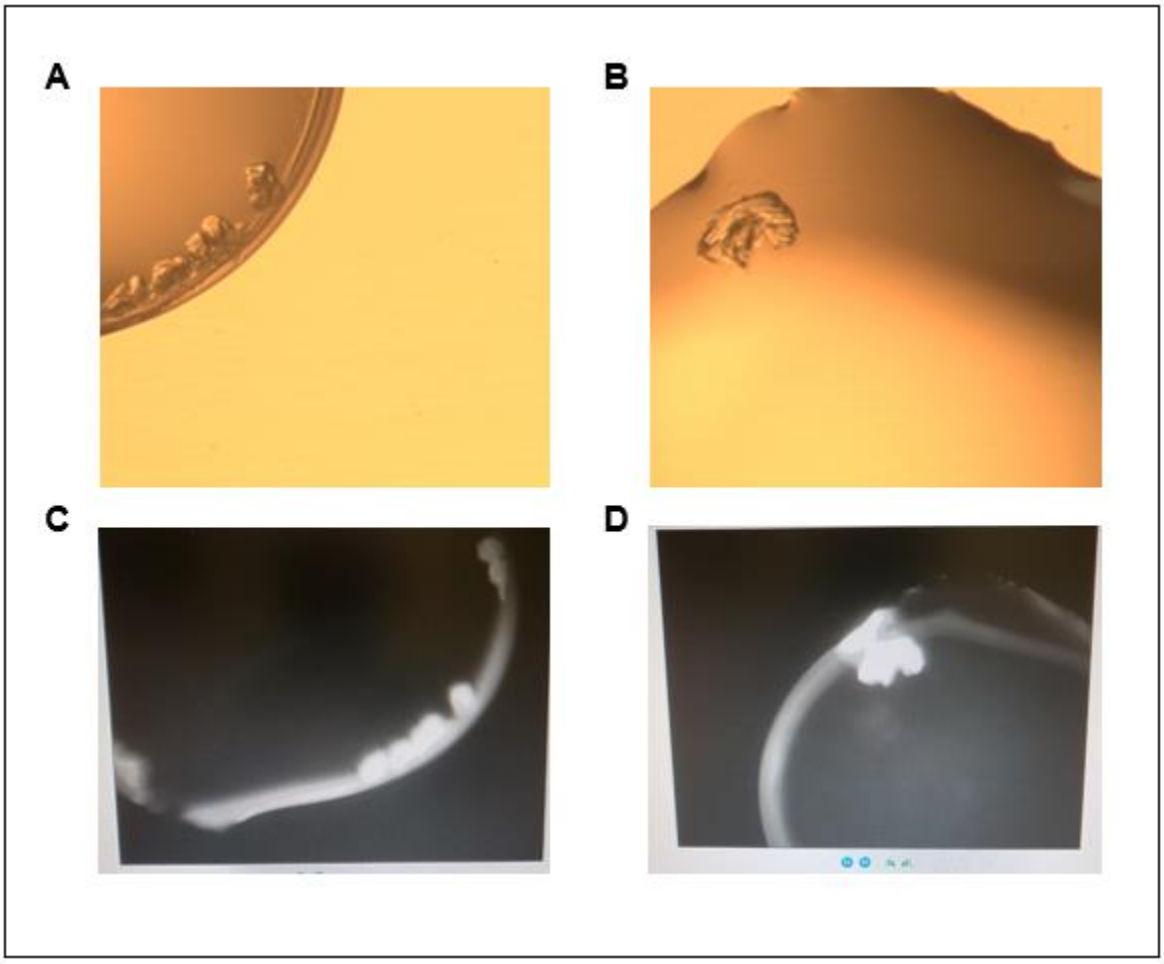

Figure 5.6. Crystals of GHA-Alkyne from PEG commercial plate. Light microscope images of **A.** well A10 and **B.** well A11. Fluorescent microscope images of **C.** well A10 and **D.** well A11

Index. As a starting point, protein was prepared as 10 mg/mL in 20 mM Tris buffer pH 7.2. No promising candidates were observed. Thus, protein concentration was increased to 15 mg/mL in order to favor the supersaturation state for crystal formation.

Upon increasing the protein concentration, the PEG commercial plate yielded crude crystals by the eighth day. Specifically, wells A10 and A11 had large crystals that could be seen via light microscope (Fig. 5.6a,b). In order to confirm that these structures were protein crystals, the wells were examined under an ultraviolet microscope (Fig.5.6.c,d) and the structures were positively identified to be protein. Protein crystals with UV active residues such as tryptophan and tyrosine will fluoresce and this approach is a quick way to confirm that the crystals are protein rather than salt or aggregates. The conditions for wells A10 and A11 are 20 w/v % PEG3350 with 0.2 M sodium iodide and 20 w/v% PEG3350 with 0.2 M potassium iodide, respectively.

Crystals from wells A10 and A11 were isolated and stored in a cryotank until ready to characterize. Initial x-ray diffraction using an in-house FRE+ x-ray diffractometer resulted in low

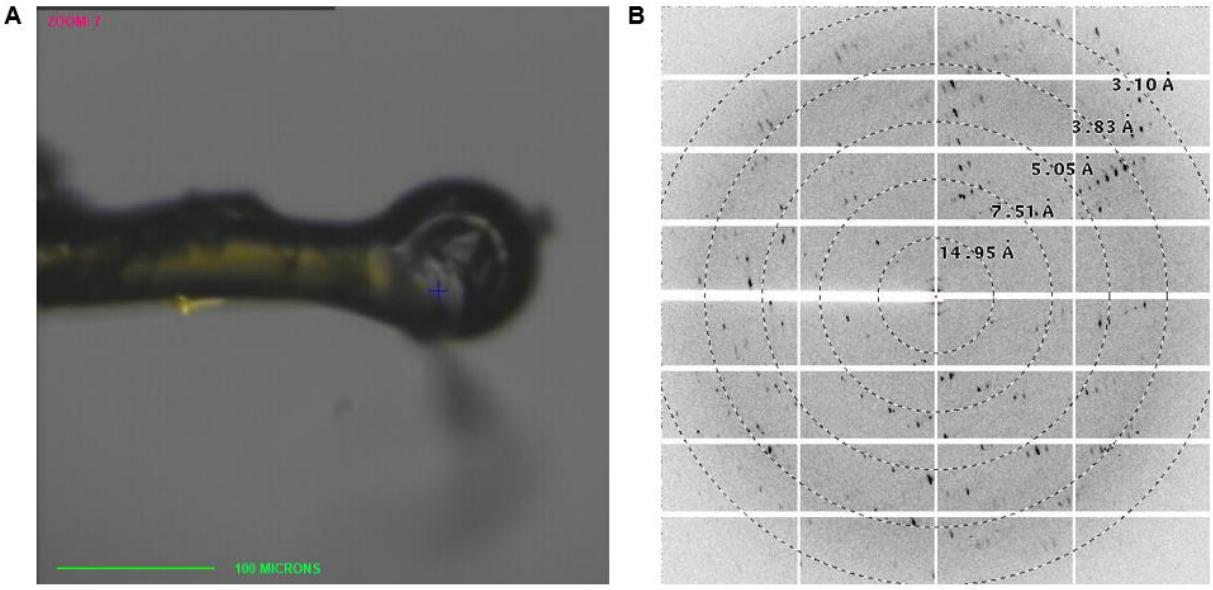

Figure 5.7. Images of GHA-Alkyne Crystal. A. Microscope images of the crystal used for data collection **B.** Diffraction images with rings indicating resolution

resolution data that could not be used for structure elucidation. Remaining crystals (Fig. 5.7a) were sent to Argonne National Laboratory to be analyzed using the Advanced Photon Source synchrotron. Diffraction data (Fig. 5.7b) was analyzed by Dr. Michael Sawaya and transformed into an electron density map (Fig. 5.8). Data collection statistics are reported in Table 5.2. Despite the stronger beamline, the data obtained could only account for 91.1% of the protein structure. Higher quality crystals are necessary to obtain the complete structure.

Table 5.2 Data collection statistics of diffracted GHA-Alkyne crystal

Data Collection	
Beamline	APS 24-ID-C
Space group	$P2_1$
Resolution (Å)	2.80 (2.87-2.80)*
Unit cell dimensions: a,b,c (Å)	35.0,47.0, 41.1
Unit cell angles: α,β,γ (°)	90.0,109.7,90.0
Measured reflections	20135 (1108)
Unique reflections	6511 (432)
Overall completeness (%)	91.1 (83.6)
Overall redundancy	3.0 (2.6)
Overall R_{merge}	0.135 (2.86)
$CC_{1/2}$	99.0 (21.8)
Overall I/δ	5.2 (0.7)
Refinement	
R_{work} / R_{free}	0.344 / 0.371
RMSD bond length (Å)	0.012
RMSD angle (°)	1.9
Number of protein atoms	2459
Number of water atoms	0
Number of other solvent atoms	0
Average B-factor of peptide (Å²)	110.9
Average B-factor of water (Å²)	N/A
Average B-factor other solvent (Å²)	N/A

*Numbers in parentheses report statistics in highest resolution shell.

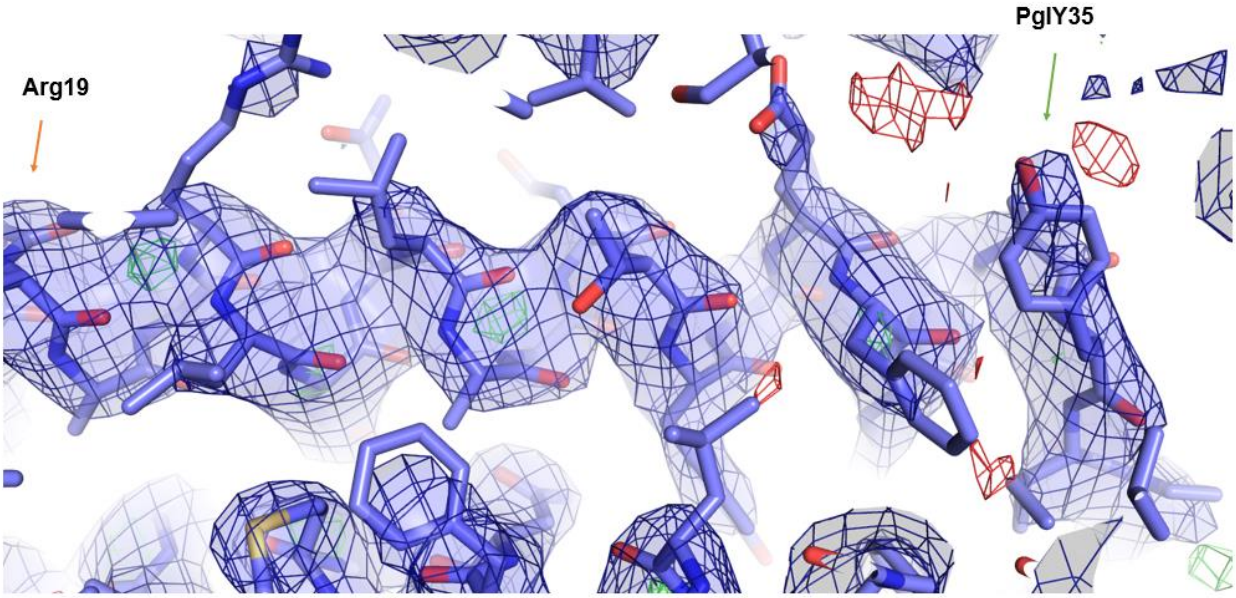

Figure 5.8. Image of best refined model from Arg19 to pgIY35 with electron density map

At this point, the protein crystallization was attempted again. Using the conditions from wells A10 and A11 from the PEG commercial plate, two optimization plates were created. Potassium iodide and sodium iodide was varied across the row from 0.15 M to 0.26 M and PEG3350 was varied across the column from 10 % to 25 %. Two different attempts at setting up these custom trays did not yield any crystals. The PEG commercial plate was set up once again but unfortunately did not produce crystals. Since the other commercial plates previously did not show any promising conditions, a published crystallization condition based on GHA B2036 was set up. GHA-Alkyne differs by one residue compared to GHA B2036 in that Y35 is modified to pgIY35. Following the irreproducibility of these protein crystals, the project was concluded.

5.3 Conclusion

In this work, we further expanded the structural parameters of polymers with diverse side-chain functionalities to study the structure-property relationship of polymer-protein conjugates. With this platform in hand, it offered us a system with full control over the dispersity, stereochemistry, rigidity, and side-chain functionalities of the IEG polymers and precise design of the final polymer-protein conjugates. We believe that it could lead to a precision design and optimization of properties of final protein therapeutics.

5.4 Appendix D

Materials

All reagents were purchased from commercial suppliers and used without further purification unless stated otherwise. Five-atom iterative exponential growth (5AIEG) octamer precursor **5A-*R*-Allyl-8mer**, **5A-*S*-Allyl-8mer**, and **5A-*Alt*-*(S,R)*-Allyl-8mer** were prepared according to literature procedures using glycidal propargyl ether (**GPE**) monomers by Wencong Wang. **2A-*R*-OPe**, **2A-*S*-OPe**, and **2A-*Alt*-*(S,R)*-OPe** were synthesized following literature procedures starting from stereopure epichlorohydrin by Wencong Wang. **N_3-5A-*R*-OH**, **N_3-5A-*S*-OH**, **N_3-5A-*Alt*-OH**, **N_3-2A-*R*-OH**, **N_3-2A-*S*-OH**, and **N_3-2A-*Alt*-OH** were prepared by Wencong Wang according to previous work. Thiolated trehalose was prepared according to previous work.[30] Growth hormone antagonist – alkyne (GHA-Alkyne) was expressed according to previous work.[31] Mouse Ba/F3 cells stably expressing human GHR (Ba/F3-GHR) were obtained from Professor Michael Waters (University of Queensland, Australia).

Analytical Techniques

Nuclear magnetic resonance (NMR) spectra were recorded on Bruker AVANCE III-400 spectrometers, and Bruker Avance Neo-600 with working frequencies of 400 (^{1}H) and 100 (^{13}C)

MHz, and 600 (^{1}H) and 125 (^{13}C) MHz, respectively. Chemical shifts are reported in ppm relative to the signals corresponding to the residual non-deuterated solvents: $CDCl_3$: δ_H = 7.26 ppm and δ_C = 77.16 ppm, MeOD: δ_H = 3.31 ppm and δ_C = 49.30 ppm; D_2O: δ_H = 4.79 ppm.

Fast protein liquid chromatography (FPLC) analyses were performed on a BioRad NGC Quest10 Plus system with a BioRad ENrich SEC 70 column at a flow rate of 1 mL/min, which utilizes 1× PBS buffer as mobile phases. Column chromatography was carried out on silica gel 60F (EMD Millipore, 0.040–0.063 mm) or on aluminum oxide (Sigma-Aldrich, activated, neutral, Brockmann Activity I). Liquid chromatography mass spectrometry (LC/MS) was performed on an Agilent 1260 Infinity LC system equipped with a Zorbax SB-C18 rapid resolution HT column using a binary solvent system (acetonitrile and water with 0.1% trifluoroacetic acid). Matrix-assisted laser desorption/ionization-time of flight (MALDI-TOF) mass spectra were measured on a Bruker model MicroFlex instrument using α-cyano-4-hydroxycinnamic acid as the matrix.

Size exclusion chromatography (SEC) analyses were performed on an Agilent 1260 Infinity setup with two Agilent PL1110-6500 columns in tandem and a 0.025 M LiBr DMF mobile phase run at 60 °C. The differential refractive index (dRI) of each compound was monitored using a Wyatt Optilab T-rEX detector. Gel permeation chromatography (GPC) analyses were carried out on an Agilent 1260 Infinity system with dual Agilent PL1110-6500 columns using a chloroform mobile phase at a flow rate of 1 mL/min.

SDS-PAGE was performed using Bio-Rad Any kD Mini-PROTEAN-TGX gels, and gels were stained with silver for visualization. SDS-PAGE protein standards were obtained from Bio-Rad (Precision Plus Protein Prestained Standards). Semi-preparatory high performance liquid chromatography was performed on an Agilent 1290 Infinity II LC system equipped with a Zorbax SB-C18 semi-preparatory column using a binary solvent system (acetonitrile and water

with 0.1% trifluoroacetic acid). High resolution mass spectra of protein and protein-polymer conjugates were acquired using an Agilent 6530 Q-TOF LC/MS equipped with 1260 Infinity LC. Conjugates were purified on a Bio-Rad BioLogic DuoFlow fast protein liquid chromatography (FPLC) system equipped with a GE Healthcare Life Sciences Q HP (1 mL) column. Protein concentrations were determined using the Pierce BCA Protein Assay kit from Thermo Fisher and read on a Molecular Devices SpectraMax iD3 Multi-Mode Microplate Reader.

Experimental

1) Synthesis of Trehalose modified IEG octamers

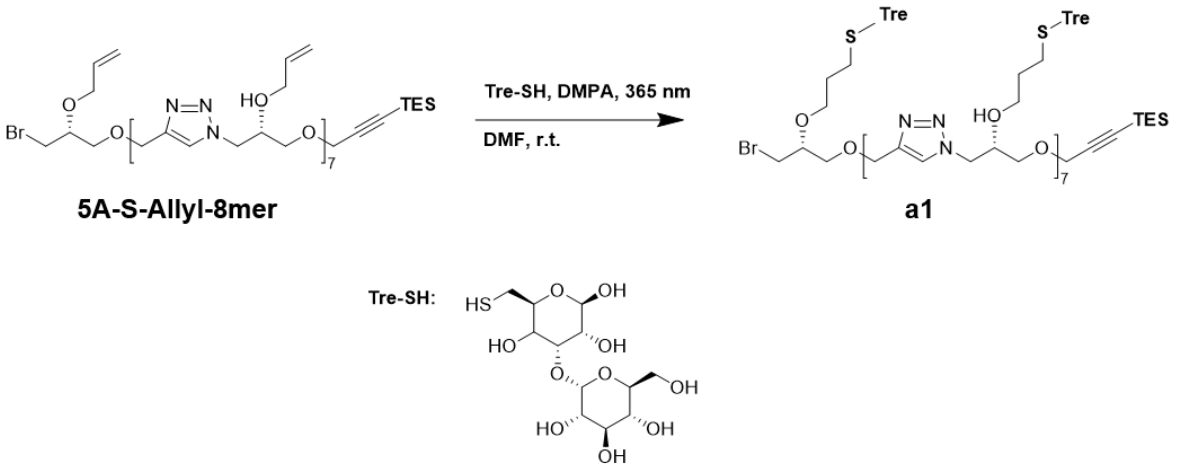

Scheme 5.1. Synthesis of **a1** from **5A-*S*-Allyl-8mer**.

a1: DMPA (640 mg, 5.2 mmol), Tre-SH (3.2 g, 4.4 mL, 31.4 mmol), and **5A-*S*-Allyl-8mer** (200 mL) were mixed together in DMF and degassed under nitrogen. Then the reaction was left stirring in a UV reactor with a wavelength of 365 nm for 30 minutes. Crude NMR was taken before working up the reaction to ensure that all allyl groups on the side chain of IEG octamers were fully reacted. After completion of the reaction, Amicon® Ultra-4 3 kDa centrifugal tubes were used to exchange the solvent from DMF to PBS before loading on to fast protein liquid chromatography

(FPLC). Through purification on SEC-70 column, pure product was obtained in PBS buffer. Water was then removed via lyophilization and product was obtained as a white solid (5.6 g, 17.2 mmol, 82% yield). ^{1}H NMR (600 MHz, $CDCl_3$, ppm) δ_H 5.85 (ddt, J = 16.7, 10.3, 6.4 Hz, 1H), 5.07 (m, 2H), 4.33 (dd, J = 11.5, 4.0 Hz, 1H), 4.17 (dd, J = 11.2 Hz, 1H), 3.75 (qd, J = 6.8, 4.0 Hz, 1H), 2.56 (t, J = 6.7 Hz, 2H), 2.50 (t, J = 5.6 Hz, 2H), 2.43 (p, J = 7.5 Hz, 2H), 1.00 (t, J = 7.9 Hz, 9H), 0.61 (q, J = 7.9 Hz, 6H).

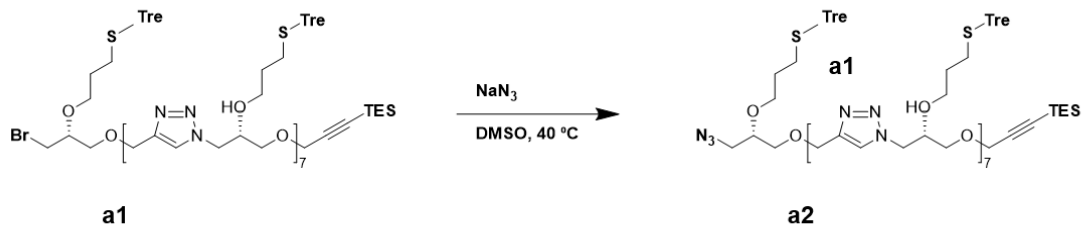

Scheme 5.2. Synthesis of **a2** from **a1**.

a2: Sodium azide (640 mg, 5.2 mmol) was added into **a1** (640 mg, 5.2 mmol) dissolved in DMSO (5.2 mL). The reaction was left stirring at 40 °C overnight. After the completion of reaction, Amicon® Ultra-4 3 kDa centrifugal tubes were used to wash out the unreacted salt and exchange the solvent from DMSO to water before usage. After lyophilization, product was obtained as white powder (5.6 g, 17.2 mmol, 82% yield). ^{1}H NMR (600 MHz, D_2O, ppm) δ_H 5.85 (ddt, J = 16.7, 10.3, 6.4 Hz, 1H), 5.07 (m, 2H), 4.33 (dd, J = 11.5, 4.0 Hz, 1H), 4.17 (dd, J = 11.2 Hz, 1H), 3.75 (qd, J = 6.8, 4.0 Hz, 1H), 2.56 (t, J = 6.7 Hz, 2H), 2.50 (t, J = 5.6 Hz, 2H), 2.43 (p, J = 7.5 Hz, 2H), 1.00 (t, J = 7.9 Hz, 9H), 0.61 (q, J = 7.9 Hz, 6H).

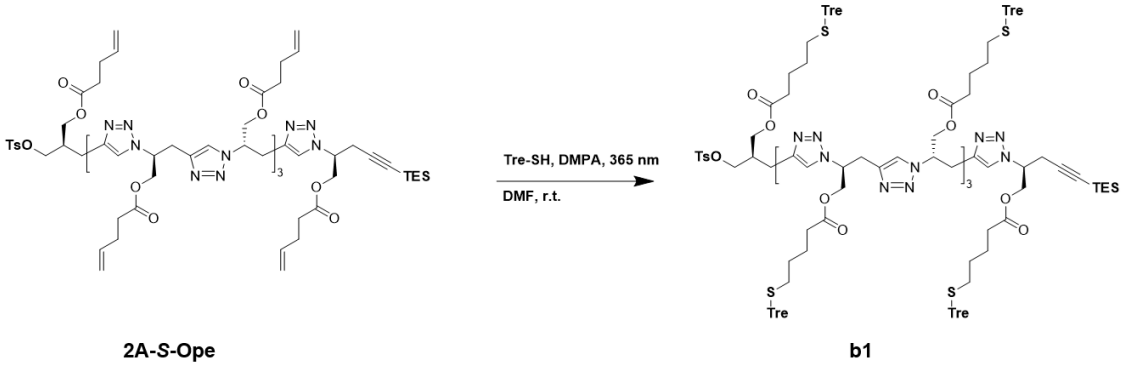

Scheme 5.3. Synthesis of **b1** from **2A-*S*-OPe**.

b1: DMPA (640 mg, 5.2 mmol), Tre-SH (3.2 g, 4.4 mL, 31.4 mmol), and **2A-*S*-OPe** (640 mg, 5.2 mmol) were mixed together in DMF (200 mL) and degassed under nitrogen. Then the reaction was left stirring in a UV reactor with a wavelength of 365 nm for 30 minutes. Crude NMR was taken before working up the reaction to ensure that all allyl groups on the side chain of IEG octamers were fully reacted. After completion of the reaction, Amicon® Ultra-4 3 kDa centrifugal tubes were used to exchange the solvent from DMF to PBS before loading on to fast protein liquid chromatography (FPLC). Through purification on SEC-70 column, pure product was obtained in PBS buffer. Water was then removed via lyophilization, and product was obtained as a white solid (5.6 g, 17.2 mmol, 82% yield). ^{1}H NMR (600 MHz, $CDCl_3$, ppm) δ_H 5.85 (ddt, J = 16.7, 10.3, 6.4 Hz, 1H), 5.07 (m, 2H), 4.33 (dd, J = 11.5, 4.0 Hz, 1H), 4.17 (dd, J = 11.2 Hz, 1H), 3.75 (qd, J = 6.8, 4.0 Hz, 1H), 2.56 (t, J = 6.7 Hz, 2H), 2.50 (t, J = 5.6 Hz, 2H), 2.43 (p, J = 7.5 Hz, 2H), 1.00 (t, J = 7.9 Hz, 9H), 0.61 (q, J = 7.9 Hz, 6H).

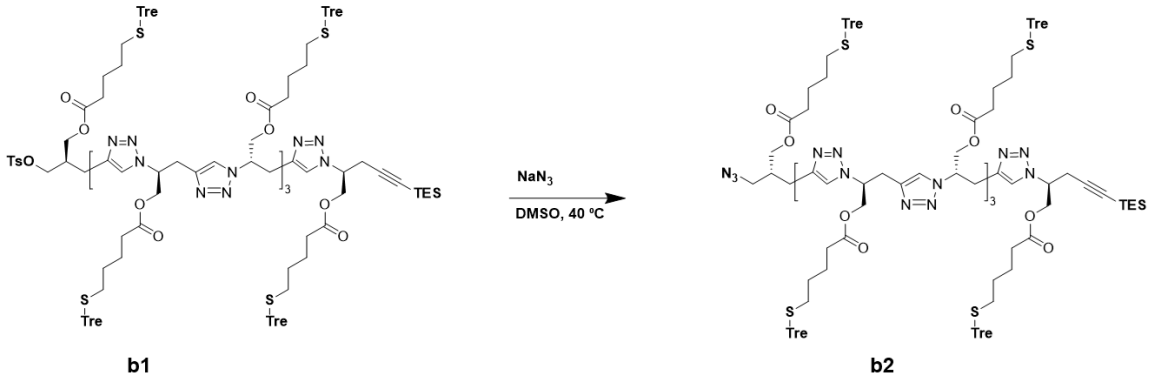

Scheme 5.4. Synthesis of **b2** from **b1**.

b2: Sodium azide (640 mg, 5.2 mmol) was added into **b1** (640 mg, 5.2 mmol) dissolved in DMSO (5.2 mL). The reaction was left stirring at 40 °C overnight. After the completion of reaction, Amicon® Ultra-4 3 kDa centrifugal tubes were used to wash out the unreacted salt and exchange the solvent from DMSO to water before usage. After lyophilization, product was obtained as white powder (5.6 g, 17.2 mmol, 82% yield). ^{1}H NMR (600 MHz, D_2O, ppm) δ_H 5.85 (ddt, J = 16.7, 10.3, 6.4 Hz, 1H), 5.07 (m, 2H), 4.33 (dd, J = 11.5, 4.0 Hz, 1H), 4.17 (dd, J = 11.2 Hz, 1H), 3.75 (qd, J = 6.8, 4.0 Hz, 1H), 2.56 (t, J = 6.7 Hz, 2H), 2.50 (t, J = 5.6 Hz, 2H), 2.43 (p, J = 7.5 Hz, 2H), 1.00 (t, J = 7.9 Hz, 9H), 0.61 (q, J = 7.9 Hz, 6H).

GHA-IEG MM Conjugation

Conjugation of IEG macromolecules to GHA-Alkyne was carried out under standard copper-catalyzed click reaction conditions. BTTAA (50 mM), CuSO4 (20 mM), aminoguanidine HCl (100 mM), and sodium ascorbate (100 mM) were prepared as stock solutions. To a Lo-bind tube, GHA-Alkyne (1 mg, 45 nmol), IEG macromolecule (2 mg, 452 nmol), and enough 100 mM phosphate buffer to reach a final volume of 1 mL were pipetted. BTTAA (20 uL, 1 mmol) and

$CuSO_4$ (10 uL, 0.2 mmol) were pre-mixed and then added to the reaction vial followed by aminoguanidine HCl (50 uL, 5 mmol). Finally, to initiate the reaction, freshly prepared sodium ascorbate (50 uL, 5 mmol) was added. The reaction was allowed to rock at 20 ºC for 2 hours.

GHA-IEG Purification

Crude conjugate solutions were purified of unreacted small molecules via centrifugal filtration using a 10 kDa molecule weight cut off filter. Next, crude conjugate solutions were purified via FPLC. Using a 1 mL GE Healthcare HiTrap Q HP column, the conjugates were purified using a 0-0.5 M NaCl in 10 mM phosphate buffer, pH 7.4, 10% glycerol gradient. Unreacted IEG macromolecule was eluted in the first five minutes with 0 M NaCl. After confirming the elution of unreacted IEG macromolecule, the salt concentration was slowly raised. The conjugate eluted next, followed by the unreacted GHA-alkyne. Due to the small molecular weight of the macromolecules, high conversions of 90-95% were achieved. Fractions were analyzed via SDS-PAGE followed by silver stain. The fractions containing conjugate were pooled together.

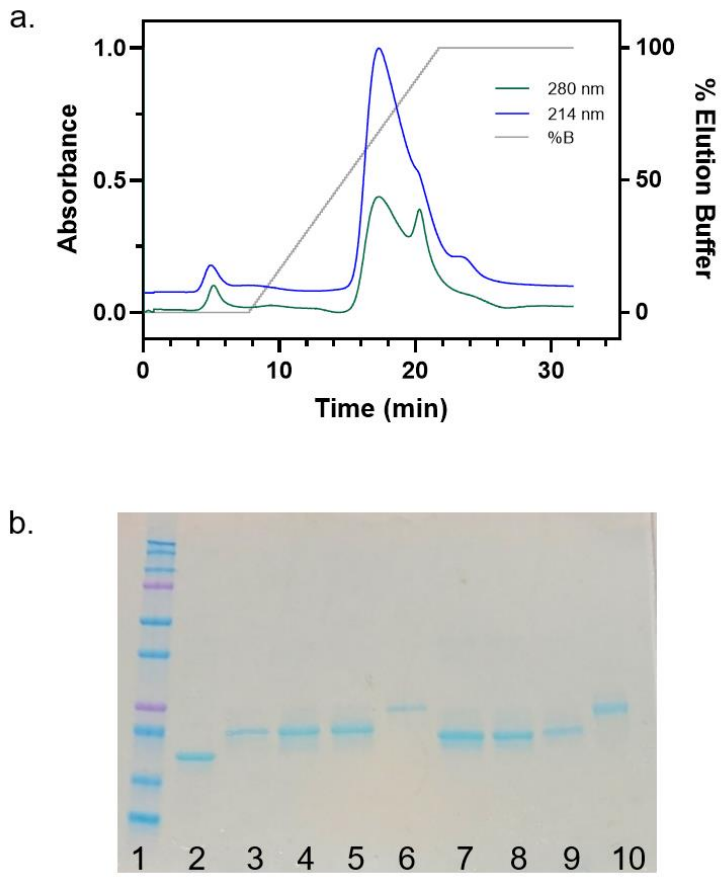

Figure 5.8 a. Representative FPLC chromatogram of GHA-IEG conjugate purification with %B denoting amount of buffer B (0.5 M NaCl). **B.** SDS-PAGE of all conjugates visualized with Coomassie. Lane 1: Ladder, Lane 2: GHA-Alkyne, Lane 3: 5A-*R*-GHA, Lane 4: 5A-*S*-GHA, Lane 5: 5A-*Alt*-GHA, Lane 6: 5A-*STre*-GHA, Lane 7: 2A-*R*-GHA, Lane 8: 2A-*S*-GHA, Lane 9: 2A-*Alt*-GHA, Lane 10: 2A-*STre*-GHA.

HPLC Stability of Proteins and Conjugates

Proteins and conjugates were prepared at 25 ug/mL in 20 mM DPBS pH 7.4 at a total volume ranging from 1.5 to 2 mL depending on availability of sample. The samples were place in 5 mL lo-bind tubes and placed in a water bath at 37 ºC. At each timepoint, 80 uL of sample was pipetted out and filtered through a 0.2 um PTFE syringe filter prior to injecting on the HPLC. A

Zorbax 300 SB-C3 column with a gradient method of 5-95% acetonitrile in water + 0.1% trifluoroacetic acid over 17 minutes was used. Peaks were analyzed at 280 nm.

Crystallographic Structure Determination.

A beamline 24-ID-C of the Advanced Photon Source located at Argonne National Laboratory was used. Crystals were cooled to a temperature of 100 K. Diffraction data were indexed, integrated, scaled, and merged using the programs XDS and XSCALE (Kabsch, 2010). Data collection statistics are reported in Table 1. Initial phases were obtained by molecular replacement with the program Phaser (McCoy et al. 2007) using a complex of human growth hormone with its soluble binding protein (PDB ID 1hwg) as a search model. Refinement was performed using the programs Phenix (Liebschner, 2019) abd Refmac (Murshudov et al., 2011). Model building was performed using the graphics program Coot (Emsley et al., 2010). Structure illustrations were created using PyMOL (Schrödinger, LLC). All crystallographic structure determination was done by Michael Sawaya.

5.5 References

(1) Duncan, R. The Dawning Era of Polymer Therapeutics. *Nat. Rev. Drug Discov.* **2003**, *2* (5), 347–360. https://doi.org/10.1038/nrd1088.

(2) Leader, B.; Baca, Q. J.; Golan, D. E. Protein Therapeutics: A Summary and Pharmacological Classification. *Nat. Rev. Drug Discov.* **2008**, *7* (1), 21–39. https://doi.org/10.1038/nrd2399.

(3) Gauthier, M. A.; Klok, H. A. Polymer-Protein Conjugates: An Enzymatic Activity Perspective. *Polym. Chem.* **2010**, *1* (9), 1352–1373. https://doi.org/10.1039/c0py90001j.

(4) Ko, J. H.; Maynard, H. D. A Guide to Maximizing the Therapeutic Potential of Protein-Polymer Conjugates by Rational Design. *Chem. Soc. Rev.* **2018**, *47* (24), 8998–9014. https://doi.org/10.1039/c8cs00606g.

(5) Alconcel, S. N. S.; Baas, A. S.; Maynard, H. D. FDA-Approved Poly(Ethylene Glycol)-Protein Conjugate Drugs. *Polym. Chem.* **2011**, *2* (7), 1442–1448. https://doi.org/10.1039/c1py00034a.

(6) Ekladious, I.; Colson, Y. L.; Grinstaff, M. W. Polymer–Drug Conjugate Therapeutics: Advances, Insights and Prospects. *Nat. Rev. Drug Discov.* **2019**, *18* (4), 273–294. https://doi.org/10.1038/s41573-018-0005-0.

(7) Nguyen, T. H.; Kim, S. H.; Decker, C. G.; Wong, D. Y.; Loo, J. A.; Maynard, H. D. A Heparin-Mimicking Polymer Conjugate Stabilizes Basic Fibroblast Growth Factor. *Nat. Chem.* **2013**, *5* (3), 221–227. https://doi.org/10.1038/nchem.1573.

(8) Kochendoerfer, G. G.; Chen, S. Y.; Mao, F.; Cressman, S.; Traviglia, S.; Shao, H.; Hunter, C. L.; Low, D. W.; Cagle, E. N.; Carnevali, M.; Gueriguian, V.; Keogh, P. J.; Porter, H.; Stratton, S. M.; Con Wiedeke, M.; Wilken, J.; Tang, J.; Levy, J. J.; Miranda, L. P.; Crnogorac, M. M.; Kalbag, S.; Botti, P.; Schindler-Horvat, J.; Savatski, L.; Adamson, J. W.; Kung, A.; Kent, S. B. H.; Bradburne, J. A. Design and Chemical Synthesis of a Homogeneous Polymer-Modified Erythropoiesis Protein. *Science* **2003**, *299* (5608), 884–887. https://doi.org/10.1126/science.1079085.

(9) Ekladious, I.; Colson, Y. L.; Grinstaff, M. W. Polymer–Drug Conjugate Therapeutics: Advances, Insights and Prospects. *Nat. Rev. Drug Discov.* **2019**, *18* (4), 273–294. https://doi.org/10.1038/s41573-018-0005-0.

(10) Chang, C. J.; Chen, C. H.; Chen, B. M.; Su, Y. C.; Chen, Y. T.; Hershfield, M. S.; Lee, M. T. M.; Cheng, T. L.; Chen, Y. T.; Roffler, S. R.; Wu, J. Y. A Genome-Wide Association Study Identifies a Novel Susceptibility Locus for the Immunogenicity of Polyethylene Glycol. *Nat. Commun.* **2017**, *8* (1), 1–7. https://doi.org/10.1038/s41467-017-00622-4.

(11) Chen, B. M.; Cheng, T. L.; Roffler, S. R. Polyethylene Glycol Immunogenicity: Theoretical, Clinical, and Practical Aspects of Anti-Polyethylene Glycol Antibodies. *ACS Nano* **2021**. https://doi.org/10.1021/acsnano.1c05922.

(12) Pelegri-Oday, E. M.; Lin, E. W.; Maynard, H. D. Therapeutic Protein-Polymer Conjugates: Advancing beyond Pegylation. *J. Am. Chem. Soc.* **2014**, *136* (41), 14323–14332. https://doi.org/10.1021/ja504390x.

(13) Mancini, R. J.; Lee, J.; Maynard, H. D. Trehalose Glycopolymers for Stabilization of Protein Conjugates to Environmental Stressors. *J. Am. Chem. Soc.* **2012**, *134* (20), 8474–8479. https://doi.org/10.1021/ja2120234.

(14) Mancini, R. J.; Lee, J.; Maynard, H. D. Trehalose Glycopolymers for Stabilization of Protein Conjugates to Environmental Stressors. *J. Am. Chem. Soc.* **2012**, *134* (20), 8474–8479. https://doi.org/10.1021/ja2120234.

(15) Forsythe, N. L.; Maynard, H. D. Synthesis of Disulfide-Bridging Trehalose Polymers for Antibody and Fab Conjugation Using a Bis-Sulfone ATRP Initiator. *Polym. Chem.* **2021**, *12* (9), 1217–1223. https://doi.org/10.1039/d0py01579b.

(16) Liu, Y.; Lee, J.; Mansfield, K. M.; Ko, J. H.; Sallam, S.; Wesdemiotis, C.; Maynard, H. D. Trehalose Glycopolymer Enhances Both Solution Stability and Pharmacokinetics of a Therapeutic Protein. *Bioconjug. Chem.* **2017**, *28* (3), 836–845. https://doi.org/10.1021/acs.bioconjchem.6b00659.

(17) Keefe, A. J.; Jiang, S. Poly(Zwitterionic)Protein Conjugates Offer Increased Stability without Sacrificing Binding Affinity or Bioactivity. *Nat. Chem.* **2012**, *4* (1), 59–63. https://doi.org/10.1038/nchem.1213.

(18) Schellenberger, V.; Wang, C. W.; Geething, N. C.; Spink, B. J.; Campbell, A.; To, W.; Scholle, M. D.; Yin, Y.; Yao, Y.; Bogin, O.; Cleland, J. L.; Silverman, J.; Stemmer, W. P. C. A Recombinant Polypeptide Extends the in Vivo Half-Life of Peptides and Proteins in a Tunable Manner. *Nat. Biotechnol.* **2009**, *27* (12), 1186–1190. https://doi.org/10.1038/nbt.1588.

(19) Jewett, J. C.; Sletten, E. M.; Bertozzi, C. R. Rapid Cu-Free Click Chemistry with Readily Synthesized Biarylazacyclooctynones. *J. Am. Chem. Soc.* **2010**, *132* (11), 3688–3690. https://doi.org/10.1021/ja100014q.

(20) Tamshen, K.; Wang, Y.; Jamieson, S. M. F.; Perry, J. K.; Maynard, H. D. Genetic Code Expansion Enables Site-Specific PEGylation of a Human Growth Hormone Receptor Antagonist through Click Chemistry. *Bioconjug. Chem.* **2020**, *31* (9), 2179–2190. https://doi.org/10.1021/acs.bioconjchem.0c00365.

(21) Wang, Y.; Langley, R. J.; Tamshen, K.; Jamieson, S. M.; Lu, M.; Maynard, H. D.; Perry, J. K. Long-Acting Human Growth Hormone Receptor Antagonists Produced in E. Coli and Conjugated with Polyethylene Glycol. *Bioconjug. Chem.* **2020**, *31* (6), 1651–1660. https://doi.org/10.1021/acs.bioconjchem.0c00208.

(22) Mancini, R. J.; Lee, J.; Maynard, H. D. Trehalose Glycopolymers for Stabilization of Protein Conjugates to Environmental Stressors. *J. Am. Chem. Soc.* **2012**, *134* (20), 8474–8479. https://doi.org/10.1021/ja2120234.

(23) Liu, Y.; Lee, J.; Mansfield, K. M.; Ko, J. H.; Sallam, S.; Wesdemiotis, C.; Maynard, H. D. Trehalose Glycopolymer Enhances Both Solution Stability and Pharmacokinetics of a Therapeutic Protein. *Bioconjug. Chem.* **2017**, *28* (3), 836–845. https://doi.org/10.1021/acs.bioconjchem.6b00659.

(24) Lee, J.; Lin, E. W.; Lau, U. Y.; Hedrick, J. L.; Bat, E.; Maynard, H. D. Trehalose Glycopolymers as Excipients for Protein Stabilization. *Biomacromolecules* **2013**, *14* (8), 2561–2569. https://doi.org/10.1021/bm4003046.

(25) Jiang, Y.; Golder, M. R.; Nguyen, H. V. T.; Wang, Y.; Zhong, M.; Barnes, J. C.; Ehrlich, D. J. C.; Johnson, J. A. Iterative Exponential Growth Synthesis and Assembly of Uniform Diblock Copolymers. *J. Am. Chem. Soc.* **2016**, *138* (30), 9369–9372. https://doi.org/10.1021/jacs.6b04964.

(26) Golder, M. R.; Jiang, Y.; Teichen, P. E.; Nguyen, H. V. T.; Wang, W.; Milos, N.; Freedman, S. A.; Willard, A. P.; Johnson, J. A. Stereochemical Sequence Dictates Unimolecular Diblock Copolymer Assembly. *J. Am. Chem. Soc.* **2018**, *140* (5), 1596–1599. https://doi.org/10.1021/jacs.7b12696.

(27) Barnes, J. C.; Ehrlich, D. J. C.; Gao, A. X.; Leibfarth, F. A.; Jiang, Y.; Zhou, E.; Jamison, T. F.; Johnson, J. A. Iterative Exponential Growth of Stereo- and Sequence-Controlled Polymers. *Nat. Chem.* **2015**, *7* (10), 810–815. https://doi.org/10.1038/nchem.2346.

(28) Nguyen, H. V. T.; Jiang, Y.; Mohapatra, S.; Wang, W.; Barnes, J. C.; Oldenhuis, N. J.; Chen, K. K.; Axelrod, S.; Huang, Z.; Chen, Q.; Golder, M. R.; Young, K.; Suvlu, D.; Shen, Y.; Willard, A. P.; Hore, M. J. A.; Gómez-Bombarelli, R.; Johnson, J. A. Bottlebrush Polymers with Flexible Enantiomeric Side Chains Display Differential Biological Properties. *Nat. Chem.* **2021**. https://doi.org/10.1038/s41557-021-00826-8.

(29) Basu, R.; Nahar, K.; Kulkarni, P.; Kerekes, O.; Sattler, M.; Hall, Z.; Neggers, S.; Holub, J. M.; Kopchick, J. J. A Novel Peptide Antagonist of the Human Growth Hormone Receptor. *J. Biol. Chem.* **2021**, *296*, 100588. https://doi.org/10.1016/j.jbc.2021.100588.

(30) Pelegri-O'Day, E. M.; Bhattacharya, A.; Theopold, N.; Ko, J. H.; Maynard, H. D. Synthesis of Zwitterionic and Trehalose Polymers with Variable Degradation Rates and Stabilization of Insulin. *Biomacromolecules* **2020**, *21* (6), 2147–2154. https://doi.org/10.1021/acs.biomac.0c00133.

(31) Tamshen, K.; Wang, Y.; Jamieson, S. M. F.; Perry, J. K.; Maynard, H. D. Genetic Code Expansion Enables Site-Specific PEGylation of a Human Growth Hormone Receptor Antagonist through Click Chemistry. *Bioconjug. Chem.* **2020**, *31* (9), 2179–2190. https://doi.org/10.1021/acs.bioconjchem.0c00365.